THÈSE

présentée pour obtenir le grade de

DOCTEUR DE L'UNIVERSITÉ DE STRASBOURG

Discipline : Chimie des matériaux et catalyse

par Luca DI FELICE

Captage de CO_2 et reformage catalytique des hydrocarbures produits pendant la vapogazéification de la biomasse en lit fluidisé.

Soutenue publiquement le 28 avril 2010 devant la commission d'examen :

Pr. Colomba DI BLASI (Université de Naples)	Rapporteur externe
Pr. Sergio RAPAGNA (Université de Teramo)	Rapporteur externe
Dr. Barbara ERNST (Université de Strasbourg)	Examinateur
Dr. Claire COURSON (Université de Strasbourg)	Examinateur
Pr. Bruno RUBINO (Université de L'Aquila)	Examinateur
Pr. Alain KIENNEMANN (Université de Strasbourg)	Directeur de thèse
Pr. Pier Ugo Foscolo (Université de L'Aquila)	Directeur de thèse Rapporteur interne

CHAPTER 3: HYDROCARBON STEAM REFORMING AND CO_2 CAPTURE IN A FLUIDIZED BED……………………….. 66

CHAPTER 4: IRON AND NICKEL SUPPORTED ON CALCINED DOLOMITE, CaO AND MgO : A STUDY ON CHARACTERIZATION………………………………………… 96

Résumé de thèse

Luca Di Felice

Le travail de doctorat avait pour objectifs d'améliorer les performances de la gazéification de la biomasse en se focalisant plus particulièrement sur deux aspects:

- la qualité des gaz obtenus lors de la gazéification (élimination des goudrons pour une valorisation chimique en plus de la valorisation énergétique) ;
- le captage de CO2 formé au cours de la gazéification pour une valorisation chimique ultérieure.

Le travail de thèse a été divisé en quatre parties principales.

1) Tests de laboratoire sur la gazéification de la biomasse dans des conditions proches d'une utilisation effective avec la mise en place d'un élément catalytique filtrant dans la partie disponible du réacteur de gazéification en lit fluidisé. La présence de goudrons (hydrocarbures aromatiques lourds) est le principal obstacle à une valorisation autre que énergétique des gaz formés.

2) Etude couplée du reformage d'hydrocarbures (méthane,aromatiques) et de la capture de CO_2 avec de la dolomite (CaO, MgO) plus un catalyseur à base de nickel. Les hydrocarbures testés sont représentatifs des goudrons produits lors de la gazéification de la biomasse.

3) Optimisation du solide minéral (dolomite) pour un système catalytique à double fonction : vaporeformage et captage de CO_2 pour une meilleure efficacité de la dolomite modifiée pour les réactions de reformage. Etude de l'addition d'oxyde de fer et de nickel à la structure dolomite.

4) Etude du captage de CO_2 par la dolomite dans un réacteur lit fluidisé à l'échelle du laboratoire. La cinétique de l'adsorption de CO_2 par CaO dans les conditions réelles a été déterminée et un modèle réactionnel proposé.

Chacun de ces quatre points sera maintenant discuté en détail dans ce résumé.

Point 1

Pour accroître le potentiel d'utilisation du gaz produit par la gazéification de la biomasse (utilisation énergétique ou chimique), la purification du gaz chaud (diminution des particules solides et surtout conversion des goudrons en CO, H_2 à la température de la réaction) doit être développée en privilégiant la compacité de l'installation et la facilité d'opérations pour la réaction. Pour ce faire, l'addition de filtres catalytiques a été proposés pour compléter la destruction des goudrons en plus de celle déjà réalisée dans le lit fluidisé. Des tests de laboratoire ont montré l'intérêt de cette proposition en conditions réelles de fonctionnement en ajoutant un élément filtrant catalytique à l'intérieur même du lit fluidisé. Le lit fluidisé comprend 3 kg d'olivine (silicate de fer et de magnésium) (dp = 0.48 mm ; $\rho_p = 2500\ kg/m^3$). L'olivine a été choisie car elle possède une très bonne résistance à l'usure mécanique due à la fluidisation en plus de son activité catalytique. La biomasse est constituée de coques d'amandes de diamètre moyen de 1.1 mm. La vitesse d'introduction de cette biomasse est gardée constante (8.43g/min) et celle de vapeur d'eau nécessaire à la gazéification varie de 5.3 g/min à 8 g/min. Le flux d'azote est de 5.7 l/min à 20°C et à pression atmosphérique. Les phases liquides (eau, goudrons) sont condensées à la sortie et analysées et les gaz (H_2, CO, CO_2, CH_4, NH_3 et HS) analysés en ligne.

Pour chaque expérience, le lit (biomasse et olivine) est d'abord fluidisé par l'air, chauffé à la température choisie puis l'azote et la vapeur d'eau sont progressivement introduits. La mesure des condensats et des gaz démarre lorsque l'ensemble du processus de gazéification est à l'état stationnaire. Le contenu en goudrons est déterminé en suivant le protocole « tars » défini par la communauté européenne. Le carbone formé sur l'olivine ou déposé dans le réacteur est quantifié sous forme de CO et CO_2 par oxydation avec une quantité connue d'air.

Quatre types d'expériences ont été réalisés. Elles sont résumées par la figure 1a et 1b.

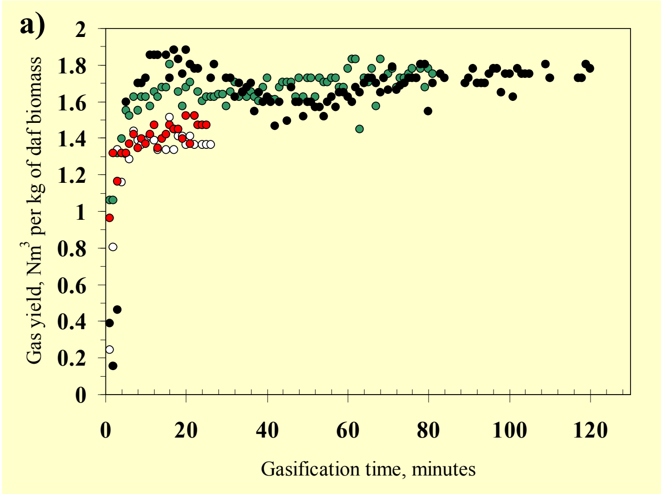

b)

	Tar, g per Nm^3 of dry gas	Char, g per kg of daf biomass
○	1.04	98.11
🔴	1.04	85.71
🟢	0.46	54.18
⚫	0.46	77.90

○ no filter in the gasifier
🔴 non catalytic filter in the gasifier
🟢 catalytic filter in the gasifier not pre-reduced
⚫ catalytic filter in the gasifier pre-reduced

Figure 1 : Tests de gazéification de la biomasse avec ou sans filtre catalytique dans le réacteur de gazéification : rendement en gaz en fonction du temps (a), goudrons recueillis après test (b).

Expérience 1 : pas de filtre dans le réacteur de gazéification
2 : pas de filtre catalytique
3 : filtre catalytique non pré-réduit
4 : filtre catalytique pré-réduit.

Ces premiers tests préliminaires dans des conditions réalistes illustrent le rôle important du filtre catalytique dans le procédé global de destruction à haute température des goudrons et d'élimination des carbones formés dans le processus de gazéification de la biomasse.

L'utilisation de ce type d'appareillage constitue un excellent point de départ pour comprendre les problèmes liés à la gazéification de la biomasse et l'importance du système catalytique sélectionné.

Point 2

Les goudrons et le méthane formés contribuent d'une manière significative au bilan énergétique des gaz produits par la gazéification. Le reformage catalytique des goudrons et du méthane permet de purifier le gaz de synthèse produit et d'augmenter le rendement en hydrogène. De plus, la présence d'un adsorbant de CO_2 permet de diminuer la formation des oxydes de carbone avec comme conséquence la formation d'un gaz riche en H_2. L'objectif du point 2 a été d'étudier la faisabilité du piégeage de CO_2 avec reformage catalytique des goudrons et du méthane. Le toluène, le 1-méthylnaphtalène et le méthane ont été choisis comme hydrocarbures clé. Un catalyseur à base de nickel pour le reformage et la dolomite pour la capture de CO_2 ont été sélectionnés.

Un réacteur spécifique (60 mm ID et 660 mm de hauteur) a été construit spécifiquement, permettant un mélange parfait des réactifs. Les molécules modèles liquides sont introduites sous forme gazeuse via une unité de saturation à température contrôlée. Un des avantages de ce système est que des composés solides à température ambiante tels le naphtalène peuvent être testés, ce qui élargi considérablement les possibilités de choix de molécules modèles des goudrons. Il est aussi possible de modifier facilement la concentration de la molécule modèle.

L'ensemble de la procédure de tests inclut huit étapes principales :

. précalcination de la dolomite : le lit solide (dolomite et catalyseur) est chauffé dans le réacteur jusqu'à 850°C

. réduction du catalyseur : sous 10% H_2/N_2 jusqu'à 850°C

- vaporeformage et captage de CO_2
- calcination de la dolomite après test pour quantifier le CO_2 adsorbé
- combustion du carbone déposé au cours du test pour sa quantification
- analyse du TOC (total organic carbon) de la phase condensée pour quantifier les hydrocarbures liquides éventuellement présents
- analyse en continu de H_2, CO, CO_2, CH_4, quantification
- établissement du bilan carbone global.

Pour le vaporeformage du méthane, le rapport CaO/C a été modifié. La quantité de CaO présent est proportionnelle à la quantité de CO_2 qui peut être théoriquement capturé et C représente le flux entrant de carbone. Ce rapport est un paramètre important industriellement pour évaluer l'activité catalytique et la cinétique de capture de CO_2. Les résultats sont donnés figure 2a, 2b et 2c pour des rapports CaO/C de 5.5, 2.8 et 1.8. Il faut préciser que MgO présent dans la dolomite ne permet pas le captage de CO_2 (équilibre d'adsorption défavorable à la température de la réaction). Son rôle sera essentiellement de diluer CaO en permettant de garder une porosité suffisante et de faciliter la progression de CO_2 vers les sites d'adsorption.

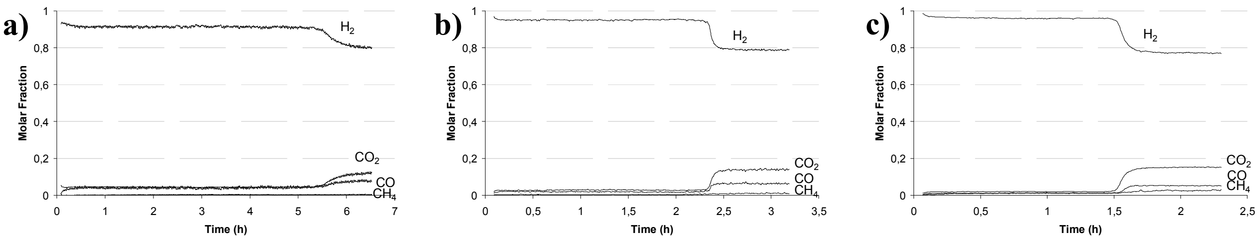

Fig. 2 : Vaporeformage en fonction du temps par variation du rapport CaO/C: a) 5.5, b) 2.8, c) 1.8.

La figure 2 montre les courbes caractéristiques du vaporeformage de CH_4 avec captage de CO_2 : il est clairement établi deux régimes stationnaires avec ou sans adsorption de CO_2 par la dolomite. Les deux régimes sont liés par une zone de rupture correspondant à la diminution de la capacité d'adsorption de la dolomite. Il est aussi établi par ces figures que les phénomènes de transfert de masse et les cinétiques de réaction sont suffisamment rapides pour atteindre un équilibre dans les conditions réactionnelles. Le captage de CO_2 et la conversion de CH_4 ne sont pas affectés par des limitations diffusionnelles.

Des résultats comparables ont été obtenus pour le vaporeformage du toluène et du 1-MN (1-méthylnaphtalène)) (figures 3a et 3b).

Dans la première partie de la courbe, une forte conversion (proche conversion totale) est obtenue comme le montre la forte concentration d'hydrogène dans le gaz à la sortie du réacteur. Les concentrations de CO et CO_2 sont beaucoup plus faibles dans la partie de la courbe qui correspond au captage de CO_2. La mesure du TOC confirme la conversion élevée d%s deux hydrocarbures liquides. Dans la partie où CaO est saturé, la conversion des goudrons modèles chute de 100% à 75-80%. Aucune formation de méthane n'est détectée.

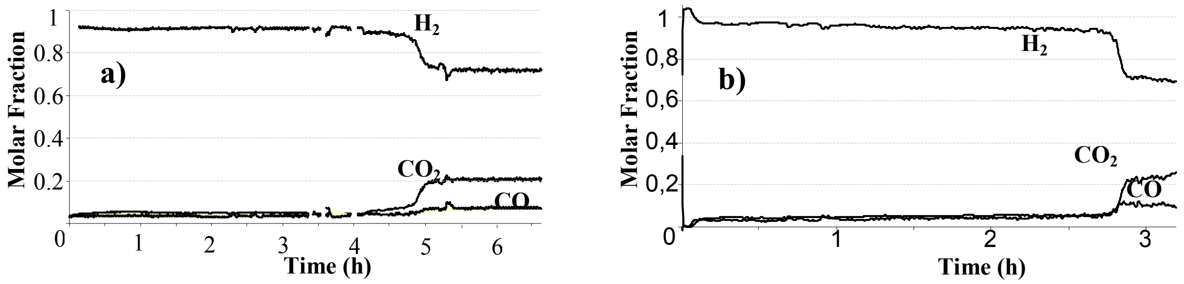

Fig. 3 : Vaporeformage du toluène (a) et du méthyl naphtalène (b) en fonction du temps.

Point 3

Dans ce point 3 nous avons abordé activité catalytique en vaporeformage et en captage de CO_2 de nouveaux catalyseurs obtenus à partir de dolomite imprégnée par un sel de nickel ou de fer, ainsi que les catalyseurs obtenus à partir des deux constituants de la dolomite : M(Ni, Fe)/CaO et M(Ni, Fe)/MgO. L'objectif était d'optimiser la réactivité de la dolomite pour la capture de CO_2 et le vaporeformage d'hydrocarbures.

Nous avons abordé deux voies de préparation (Tableau 1) : une oxydante pour étudier les interactions Fe^{3+} et Ni^{2+} support et une neutre pour évaluer les interactions Fe^{2+}, $Fe^{2,5+}$ support. Pour les deux voies, le sel précurseur du métal est solubilisé dans le solvant d'imprégnation (eau ou éthanol) puis le support est ajouté et agité pour obtenir une suspension.

	Oxidative		**Neutral**
Salt	Nitrate (Fe^{3+})	Nitrate (Ni^{2+})	Acetate (Fe^{2+})
Impregnation solvent	Water	Water	Ethanol
Evaporation temperature (°C)	110	110	80
Thermal treatment atmosphere	Air	Air	Nitrogen

Table 1: voies de préparation

Après évaporation du solvant, le solide est séché, puis broyé (80 <dp<300 μm) et finalement chauffé sous air ou atmosphère inerte à 850 et 1100°C pendant 4h, ceci pour étudier l'influence du traitement thermique sur les phases cristallines obtenues.

Selon le type de métal (Fe, Ni), la nature du support (CaO, MgO, MgO-CaO) l'activité en reformage et en captage de CO_2 a été étudiée, de même que la possibilité d'éventuelles limitations cinétiques pour le captage de CO_2 liées à la présence du métal.

Les techniques de caractérisation des solides ont été: la diffraction des rayons X (XRD), la réduction à température programmée (TPR), la spectroscopie Mössbauer (pour le fer). La TPO (oxydation à température programmée) a permis l'évaluation après test de la quantité de dépôt carboné. XRD et TPR montrent avec Ni/dolomite, la formation de la solution solide NiO/MgO. Avec Ni/dolomite la capacité d'adsorption et la cinétique d'adsorption de CO_2 ont été évaluées et comparées à la dolomite seule. Il est clair que la présence de NiO et la formation de la solution solide NiO-MgO, limitent la réaction de captage de CO_2 même si NiO n'interagit pas directement avec CaO. Cela signifie que NiO en interaction avec MgO, modifie celui-ci et en particulier sa porosité. Ce phénomène s'amplifie si on augmente de 4 à 10% le pourcentage de nickel.

4% Ni/dolomite a été également testé pour la réaction combinée de captage de CO_2 et de vaporeformage du toluène. La limitation cinétique de capture de CO_2 à cause des interactions NiO-MgO est à nouveau mise en évidence (figure 3). La rupture de pente, très nette avec la dolomite seule, est à présent moins évidente et une faible augmentation de la concentration en CO_2, associée à une faible diminution de la production de H_2 est observée jusqu'à saturation complète des sites d'adsorption de CO_2. Ensuite, les concentrations de H_2 et CO_2 restent constantes jusqu'à la fin du test.

Dans ce test, la conversion du toluène est proche de 100% dans la première partie du test et diminue à environ 80% après saturation de la dolomite.

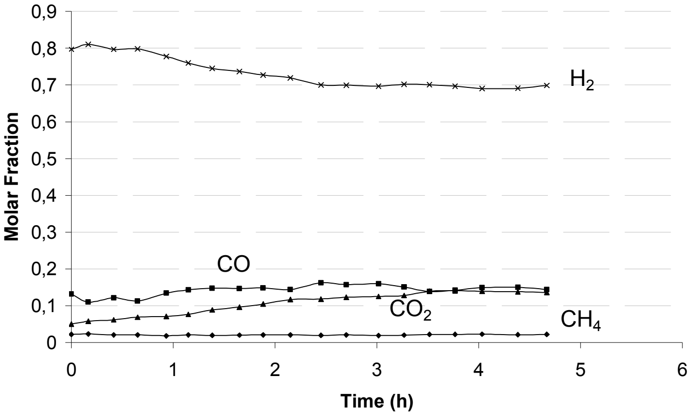

Figure 3 : reforming du toluène et captage de CO_2 avec Ni/dolomite

Pour les catalyseurs Fe/dolomite, les principales phases mises en évidence sont CaO, MgO et $Ca_2Fe_2O_5$. Des oxydes de fer libres ou des composés fer-magnésium oxyde n'ont pas été détectés. Ceci indique que la plus forte interaction se produit entre CaO et Fe^{3+}. Pour la préparation en milieu neutre (Tableau 1), le catalyseur en plus des composés cités contient des ions $Fe^{2,5+}$ sous forme de Fe_3O_4 ou $Fe_{3-x}Mg_xO_4$. Les différentes phases formées ainsi que leur évolution sous atmosphère réductrice (TPR) sont schématisées figure 4 pour les voies oxydantes et neutres.

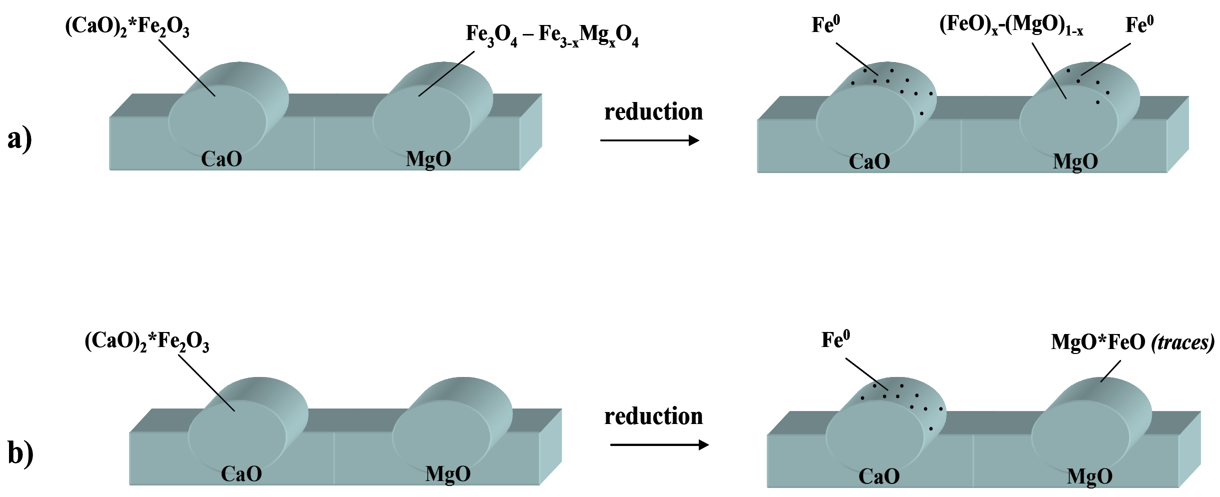

Figure 4 : Modèle des phases obtenues entre fer et dolomite par les voies neutres (a) et oxydantes (b) ainsi que les différentes phases formées après réduction.

Pour ces nouvelles phases, d'éventuelles limitations cinétiques solide-gaz où une modification des propriétés d'adsorption de CO2 ont été étudiées. La capacité d'adsorption de CO_2 décroît avec la quantité de Fe ajouté. Cependant pour 1 et 5% Fe, ni la capacité d'adsorption, ni la cinétique d'adsorption ne sont fortement modifiées.

A 850°C, l'activité de Fe/dolomite, Fe/CaO et Fe/MgO a été testée en vaporeformage du toluène. Aucune augmentation significative de cette conversion n'a été mise en évidence. Cependant, les analyses de TPO après test montrent que la présence de fer limite fortement la quantité de carbone déposé sur la surface. Par exemple le catalyseur 5% Fe/dolomite diminue par un facteur 7 par rapport à la dolomite le carbone formé. Comme la présence de ce carbone est un point critique de la déactivation de la dolomite, la présence de fer sera d'un grand intérêt pour de futurs travaux dans le procédé de gazéification.

Point 4

Le captage de CO_2 est largement étudié pour une application dans les systèmes produisant de l'énergie avec réduction d'émissions de gaz à effet de serre. Un captage possible passe par l'utilisation de solides minéraux naturels tels la dolomite. La régénération par décomposition du carbonate permet de concentrer le CO_2 pour une utilisation ultérieure en chimie. Des tests dynamiques ont été réalisés pour déterminer les vitesses de conversion CaO vers $CaCO_3$ en fonction du temps pour des particules de dimensions variables (0.10 à 1.55 mm). Pour le captage de CO_2 et la régénération de $CaCO_3$, 3 g de dolomite de taille définie sont mélangés avec du sable. Le mélange dolomite-sable est fluidisé avec N_2 et la température portée à 850°C pour convertir tout le $CaCO_3$. La concentration en CO_2 du gaz sortant est analysée en continu. Lorsqu'elle tombe à zéro, la température du lit est ramenée à 650°C en prévision de l'étape de capture de CO_2. CO_2 dilué est alors admis dans le réacteur et adsorbé sur CaO. L'expérience se poursuit jusqu'à ce que les concentrations de CO_2 à l'entrée et à la sortie du réacteur soient identiques. Le flux de CO_2 est alors stoppé, la fluidisation se poursuivant jusqu'à la valeur basse de l'équilibre $CaCO_3 \leftrightarrow CaO + CO_2$.

Un modèle simple décrivant le flux et le processus réactionnel dans le lit fluidisé est résumé figure 5. Les phases gazeuses et solides sont mélangées parfaitement. La vitesse de transfert de CO_2 de la phase gazeuse à la phase solide est proportionnelle à la concentration gazeuse dans le lit Cg et à la fraction de la dolomite n'ayant pas réagi $(Cs\infty - Cs)/Cs\infty$. La valeur finale de $Cs\infty$ est celle expérimentalement obtenue, ce qui est toujours un peu inférieur au niveau de saturation théorique, ce qui confirme que tout le CaO présent n'est pas accessible pour la réaction. Le coefficient global de transfert k prendra en considération les cinétiques réactionnelles et la résistance à la diffusion autour et dans le grain de dolomite. *k* est une constante purement empirique qui a été quantifiée par référence aux résultats expérimentaux avec la possibilité d'être relié quantitativement à une description d'un modèle mécanistique complet.

Les équations bilan de CO_2 sont obtenues à partir de la description de la figure 5.

$$\frac{dC_s}{dt} = k \cdot C_g \cdot \frac{(C_{s\infty} - C_s)}{C_{s\infty}}, \qquad (1)$$

$$\frac{dC_g}{dt} = \frac{q}{V_g} \cdot (C_i - C_g) - k \cdot \frac{V_s}{V_g} \cdot C_g \cdot \frac{(C_{s\infty} - C_s)}{C_{s\infty}} \left(1 - S_{CO_2} C_g\right) \qquad (2)$$

Le seul paramètre inconnu des équations 1 et 2 est le coefficient de transfert global k. En donnant une valeur à k, les équations 1 et 2 sont solubles numériquement pour les concentrations de CO_2 à la fois dans la phase gaz Cg(t) et dans la phase solide Cs(t) du lit fluidisé. Cs(t) doit être proche de la quantité évaluée expérimentalement.

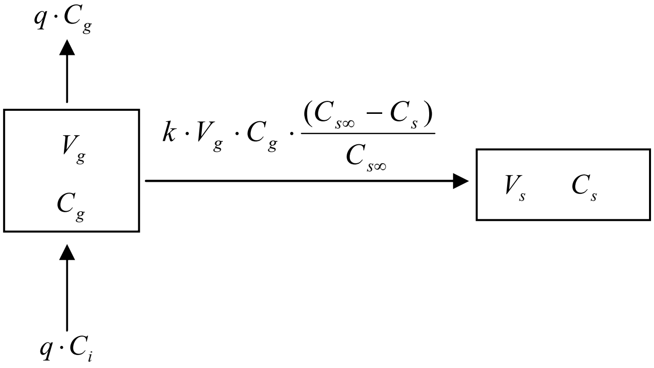

Figure 5 : Modèle descriptif de la capture de CO_2 en lit fluidisé.

Le modèle proposé donne une bonne description de l'évolution du CO_2 entre phase gazeuse et solide. La figure 6 montre comment le paramètre k varie avec le diamètre des particules de dolomite. Une bonne relation linéaire est trouvée dans nos conditions expérimentales. Les vitesses de transfert augmentent progressivement avec la diminution du diamètre des particules.

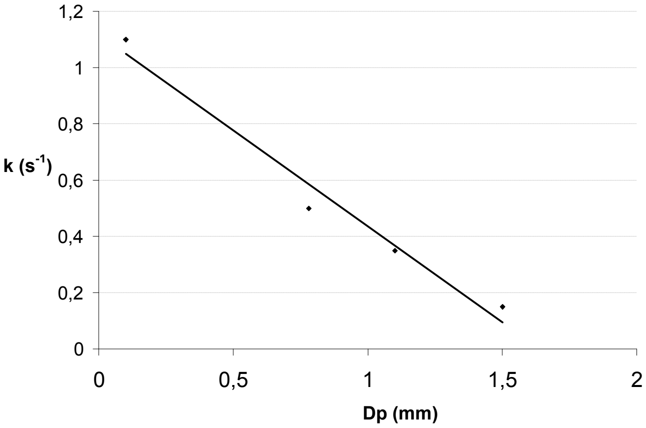

Figure 6 : Evolution du coefficient de transfert k en fonction du diamètre des particules de la dolomite.

Conclusions

Les tests préliminaires de gazéification de la biomasse en lit fluidisé en conditions réalistes nous ont fourni des données pour la compréhension des problèmes complexes associant capture de CO_2 et vaporeformage de goudrons et ont permis de valider cette approche.

Les résultats de vaporeformage de méthane, toluène et 1-MN avec captage de CO_2 indiquent un piégeage important de CO_2 montrant le potentiel de générer l'hydrogène, vecteur d'énergie, en utilisant un adsorbant solide comme piège à CO_2.

De nouveaux catalyseurs M/dolomite (M = Ni, Fe) ont été développés et caractérisés. Avec le nickel, les résultats de Ni/dolomite sont comparables à ceux d'un catalyseur industriel à base de nickel même si certaines limitations dans la réaction gaz-solide de capture de CO_2 ont été mises en évidence et expliquées.

Le Fe/dolomite augmente la résistance au dépôt de carbone par rapport à la dolomite dans le vaporeformage. De plus, ni la capacité de captage de CO_2, ni la cinétique de captage ne sont affectées par la présence de fer sous la forme $Ca_2Fe_2O_5$.

Un travail spécifique sur la cinétique de captage de CO_2 par la dolomite montre une relation directe en vitesse de captage et taille des particules. Ceci est attribué à un phénomène de diffusion interne quantifiable à l'aide du paramètre modèle k qui décroît linéairement lorsque la taille des particules de dolomite augmente.

CHAPTER 1

INTRODUCTION

Abstract: *This chapter is an overview on the gasification process as a suitable route for producing not only heat and electricity, but also a hydrogen energy vector, liquid (diesel, methanol) and gaseous (methane) biofuels, starting from biomass and coal. For the gas upgrading steps involved in BTL (Biomass to Liquid) and SNG (substitute natural gas) synthesis, the produced gas has to be clean (tar free) and with a well defined* H_2/CO *according to the stoichiometry of the process. Pre-combustion* CO_2 *capture has been indicated as an appropriate way to adjust this parameter, e.g. for downstream methanation process (*$H_2:CO = 3:1$*).*

1. Introduction

Gasification of biomass or coal is a thermo-chemical conversion process utilizing air, oxygen, CO_2 and/or steam as gasification agents, that converts carbonaceous materials, such as coal, petroleum residuals or biomass, into a fuel gas rich in hydrogen and carbon monoxide, with a significant content of methane and carbon dioxide. In a gasifier biomass and/or coal goes through drying (100-150°C) and pyrolysis (200-700°C) stages where the volatile compounds and char are formed. These fuels are then converted at 700 - 1600 °C (depending on gasifier technology) to gases (H_2, CO, CO_2, H_2O, CH_4, light hydrocarbons), in addition to organic (tar) and inorganic (H_2S, HCl, NH_3, alkali metals) impurities, and particulate (char, ash). High molecular weight hydrocarbons (tar) are an undesirable and noxious by-product, with concentration ranging from 1 to 100 g/Nm^3 of the producer gas in fluidized bed gasifiers. Tar is a complex mixture of cyclic and polycyclic aromatic hydrocarbons [Abu El-Rub *et al.,* 2004] very harmful for toxicity and cancerous properties. Moreover, corrosive and pollutant characteristics of tar compounds prohibit direct utilization of the gas product stream.

The volatiles can react through secondary reactions with each other and the solids present. The final product distribution largely depends on gas-feedstock properties, contact type and process conditions, as it will be highlighted in this introduction section. The resulting gas mixture is called synthesis gas or syngas and is itself a fuel.

The use of steam, instead of air or CO_2 as gasifying agent, leads to higher H_2 yields due to the additional H_2 produced from the decomposition of H_2O. In addition, compared with partial-oxidation using air, steam or oxygen produce a gas with a higher heating value because dilution with N_2 is avoided.

In the eighties and nineties of the last century CHP (combined heat and power) production based on gasification was investigated intensively and demonstrated at industrial scale. The produced syngas may be burned in order to generate heat and electricity. A schematic process description is shown in Figure 1. A catalyst may be needed depending on the gasifier technology (see Section 2).

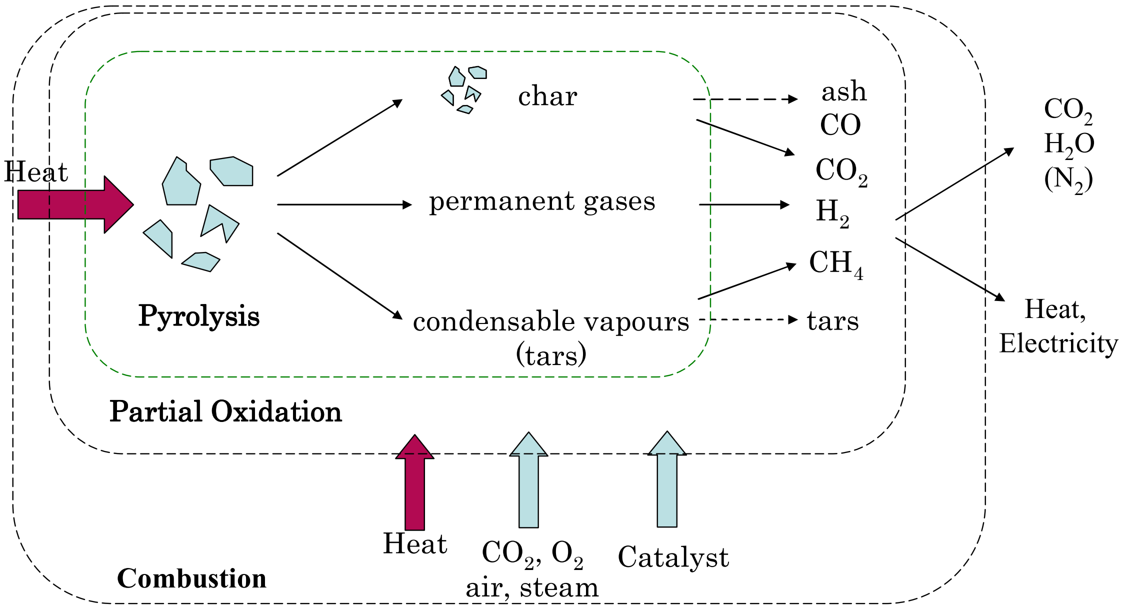

Figure 1: Schematic presentation of gasification as a thermal conversion processes (Handbook of gasification, 2005)

Research and development in gasification are now focused mainly on the production, cleaning, and upgrading of syngas for synthesis processes. Using the Integrated Gasification Combined Cycle (IGCC), cogeneration of electricity, H_2 and chemicals is performed in large scale industrial installations and more applications are planned for the near future (so called "polygeneration" processes). H_2 is currently produced from coal for use as an intermediate for synthesis of chemicals such as methanol, ammonia/urea, Fischer–Tropsch products and substitute natural gas (SNG).

Minchener [Minchener, 2005] reports that, on a worldwide basis, there are some 160 modern, gasification plants in operation and further 35 at the planning stage; from these, 27 plants use coal, 29 use heavy petroleum residues, 22 natural gas and 12 biomass. The best coal based IGCC projects in worldwide applications produce a net power output of 250-310 MW. The primary products that can be produced in such plants include electricity, ammonia, oxy-chemicals, syngas, methanol, and hydrogen, as summarised in Table 1 [USDoE and Gasification Technology Council, 2001]. The majority of these plants are located either in Europe or in the USA.

Many companies have developed IGCC technologies. As an example, there are presently sixty five Chevron Texaco gasification facilities worldwide that produce power, chemicals and H_2 from coal (6 plants), oil derivatives and natural gas. Three of the coal gasification facilities produce ammonia, one produces town gas and electricity, one is an IGCC plant and one is producing methanol and chemicals.

Product	Primary product		Secondary product
	Operating Plant	Planned Plant	
Electricity	35	25	6
Hydrogen	11	1	11
Ammonia	34	3	1
Syngas	14	1	2
Methanol	12	1	11
Oxy-chemicals	22	0	1
Carbon dioxide	7	0	5
Others (FT liquids, fuel gas)	25	4	0
Total	160	35	37

Table 1: Products from fossil fuel gasification plants

Sasol currently operates three major coal to liquid (CTL) complexes in South Africa for the gasification of coal into Fischer– Tropsch (FT) products [Collot, 2006].

The Great Plains Synfuels plant (Dakota Gasification) located in North Dakota (USA) has been producing substitute natural gas (SNG) from lignite using the same technology since 1984 [Collot A.G., 2006].

There are presently also five gasification plants using the Shell gasification technology. Only one of them, which was started up in 1994 in the Netherlands, is fed with coal for the production of electricity. All the remaining gasification plants are fed with petroleum wastes to produce chemicals and/or H_2 [Collot A.G., 2006]. Eight additional coal gasification plants using the Shell Coal Gasification Process (SCGP) for the production of chemicals are planned to be built in China and one in the USA. The plants will all produce syngas for ammonia/urea, Fischer–Tropsch liquids or H_2 as a feedstock for diversified chemical plants, replacing naphtha reformers, oil gasifiers or outdated coal gasifiers.

2. Gasifier technologies

Reactor design is very crucial for gasification in terms of efficiency, heating value of the product gas and also for tar formation. Modification of the gasifier design can be very effective in producing clean gas. Some interesting work on dual fluidized bed reactor conditions are given in [Xu *et al.,* 2006], [Hamel *et al.,* 2005]; pressurised operation conditions on coal gasification processes coupled with CO_2 capture have been reported by Lin and co-workers [Lin *et al.,* 2001, 2002] in the so called HyPr-RING process. A new interesting approach in biomass gasification processes is the use of a catalytic filter candle [Rapagnà *et al.,* 2009], [Ma *et al.,* 2005], [Zhao *et al.,* 2000] inserted in the freeboard of the gasifier reactor. This kind of technology is described in Chapter 2, where biomass gasification tests in a pilot plant will be investigated.

On the whole, gasification technologies can be classified into three categories according to reactor configurations (geometry and flow conditions). In this Ph.D. thesis, the attention will be focused on fluidized bed gasifiers.

2.1. Entrained flow gasifiers

This kind of reactors allows pulverised coal particles and gases to flow co-currently at high speed and temperature, to ensure high carbon conversion. Coal can either be fed dry (commonly using nitrogen as a transport gas) or wet (carried in a water slurry) into the gasifier. These are the most commonly used gasifiers for coal gasification in large plants. They usually operate at high temperatures, of 1200–1600 °C, and pressures, in the range of 2–8 MPa. Raw gas exiting the gasifier usually requires significant cooling (by quenching with water or using a recycled cleaned and cooled syngas) before being cleaned. Entrained flow gasifiers are the most versatile type of gasifiers as they can accept both solid and liquid fuels and operate at high temperature (above ash slagging temperatures) to ensure high carbon conversion and a syngas free of tars. However, such high temperatures have an impact on burners and refractory life and require the use of expensive materials of construction as well as the use of sophisticated high temperature heat exchangers to cool the syngas below the ash softening temperature in order to avoid fouling and control corrosion problems. The required investment costs are consequently high and justified only in case of large applications (hundreds of MW power).

2.2. Fluidized bed gasifiers

2.2.1 Fluidization principles

Fluidization is a process whereby a bed of solid particles is transformed into something closely resembling a liquid. This is achieved by pumping a fluid, either a gas or a liquid, upwards through the bed at a rate that is sufficient to exert a force on the particles that exactly counteracts their weight; in this way, instead of a rigid structure, the bed acquires fluid-like properties, with the particles able to move freely with respect to one another. The lower limit of fluidization is the minimum fluidization velocity (*umf*), when the upward force that the fluid imparts to particles just balances the solid weight and the particles are supported entirely by the force of interaction with the fluid stream (if the fluid velocity is too small the bed stays fixed and operates as a packed bed). The upper limit of fluidization is the terminal velocity, where the magnitude of the interaction force on an isolated particle becomes greater than that due to gravity, giving rise to a net force that causes the solids to accelerate upwards and to be elutriated from the bed container.

The forces acting on each particle in the bed are therefore the result of a fluid-particle interaction f_I and gravity f_g. Under conditions of equilibrium, we have:

$$f_I + f_g = 0$$

where f_I takes into account the Archimedean buoyancy force, due to the pressure gradient in the fluid itself, and the total drag force, which is a consequence of energy dissipation at the particle surface and is proportional to the mean velocity of the fluid relative to that of the particle. For values of Reynolds number conditions higher than 0.1, the drag force f_d becomes a non-linear function of the relative fluid-particle velocity, for which empirical relations are required (Gibilaro, 2001).

In fluidization conditions the bed may “expand” to an essentially homogeneous condition in which the particles are separated from one another more or less uniformly, with relatively little particle motion, the extent of the separation increasing progressively with increasing fluid velocity (homogeneous fluidization). Another possibility is that all the fluid in excess of that required to just bring the particles to the minimum fluidization point forms rising bubbles, which cause considerable particle mixing and give the bed the appearance of a boiling liquid (bubbling fluidization). The kind of fluidization that take place depends from solid and fluid properties; in classifying particles into four groups, Geldart has used the following criteria for gas fluidized beds (Groups A-D):

A. Group A: Whether or not, as the gas flow rate is increased, the fluidized bed will expand significantly before bubbling takes place. This property may be quantified by the ratio *umb/umf*, where *umb* is the minimum velocity at which bubbling occurs. This assessment can only be qualitative as the value of umb is very critically dependent on the conditions under which it is measured.

B. Group B: Whether the rising velocity of the majority of the bubbles, is greater or less than the interstitial gas velocity. The bed bubbles as soon as fluidization begins. Most of the systems relevant for fluidized bed gasifiers are included in this group.
C. Group C: Whether the adhesive forces between particles are so great that the bed tends to channel rather than to fluidize. Channelling depends on a number of factors, including the degree to which the bed has consolidated and the condition of the surface of the particles at the time.
D. Group D: solids are coarse and dense. Largest bubbles rise at velocities less than interstitial gas velocity.

2.2.2 Fluidized bed gasifiers characterisation

In fluidized bed gasifiers coal or biomass particles are suspended in the gas flow; they are mixed with the inert particles in the bed inventory and particles undergoing gasification. This technology can only operate with solid crushed fuels (coal: 0.5–5 mm). The bed is formed of sand/coke/char/sorbent or ash. Residence time of the feed in the gasifier is typically in the order of 10–100 s but can also be much longer. High levels of back-mixing ensure a uniform temperature distribution in the gasifier. Fluidized bed gasifiers usually operate at temperatures well below the ash fusion temperatures of the fuels (900–1050 °C) to avoid ash melting and particle sintering. A consequence of the low operating temperatures is the incomplete carbon conversion in a single stage and it is therefore common for the residual char to be either removed and burnt in a separate combustion unit or recirculated into the gasifier. One of the main advantages of this type of gasifiers is that they can operate at variable loads which gives them a high turndown flexibility. Sulphur which is found in the gas stream as H_2S and COS can be partly retained in the bed (up to 90%) by sorbents such as limestone. This leads to a considerable reduction of the H_2S concentration in downstream equipment and hence a decrease in material corrosion.

The advantages of fluidized beds include:

- possibility to add a catalyst to enhance yield of permanent gases;
- liquid like behavior, easy to control and automate;
- rapid mixing, uniform temperature and concentrations;
- resistance to rapid temperature changes, hence the bed responds slowly to changes in operating conditions and avoids temperature runaway with exothermic reactions;
- applicability to large or small to medium scale operations;

- heat and mass transfer rates are high, requiring smaller exchange surfaces.
- the ash does not melt, which makes its removal relatively simple.

There are two types of fluidized bed gasifiers: bubbling (BFB) and circulating (CFB). They ensure good mixing and excellent heat and mass transfer. The overall simplicity of the bubbling fluidized bed design and a number of other features made its application more attractive for coal gasification than circulating fluidized beds. In biomass industries it finds use in small to medium (<25 MWth) capacities [Basu, 2006]. Circulating fluidized bed gasifiers have advantages over BFBs, such as higher carbon conversion efficiency, lower tar production and smaller size [Basu, 2006]. As a result, they are emerging as the major choice for small (a few MWth) to large (100 MWth or more) biomass gasification projects. Table 2 shows a comparison between BFBs and CFBs, together with updraft and downdraft moving bed gasifiers, described below.

	Fixed beds		Fluidized beds	
	Updraft	Downdraft	Bubbling	Circulating
Sensitivity to:				
Fuel specification	Moderate	Specific	Flexible	Flexible
Fuel size	Very good	Good	Fair	Fair
Moisture content	Very good	Fair	Good	Good
Reaction temperature (°C)	1000	1000	850	850
Gas exit temperature (°C)	250	800	800	850
Tar in gas	Very high	Very low	Moderate	Low
Dust in gas	Good	Moderate	Very high	Very high
Scale-up potential	Good	Poor	Good	Very good
Carbon conversion	Very good	Very good	Fair	Very good
Thermal efficiency	Excellent	Very good	Good	Very good
Low heating value	Poor	Poor	Poor	Fair

Table 2: Comparison of basic characteristics of bubbling and circulating fluidized bed, and updraft and downdraft fixed bed gasifiers [Basu, 2006]

2.3. Moving bed gasifiers

In moving bed, also called fixed bed, gasifiers, the gasification medium flows through, and thus comes into contact with a fixed bed of solid fuel particles. Depending upon the flow direction of the gasifying medium through the bed of fuel, moving bed gasifiers can be distinguished in two main types:

1. Updraft (medium flow upwards);
2. Downdraft (medium flow downward).

A comparison of their performance is reported in Table 2 (data resumed from Basu [Basu, 2006]). Figure 2 shows a schematic of a updraft fixed bed gasifier. It is assumed that the only reaction in the lower zone is carbon combustion to produce carbon dioxide and the heat necessary for the endothermic gasification reaction occurring above. In this zone, char burns to ash, which is drained as shown in Figure 2. Combustion gases and steam go up to the next zone, which provides char to the lower combustion zone. All rate-controlling steam–carbon and hydrogen–carbon reactions occur in this zone. In the highest zone, the producer gas comes into contact with fresh biomass fed from the top: it furnishes heat to the solid for dehumidification and pyrolysis. The low temperature of exiting gases (250°C) ensures a high efficiency of this technology; on the other hand, the gas exiting from the reactor is reach in condensable organic vapours (tar).

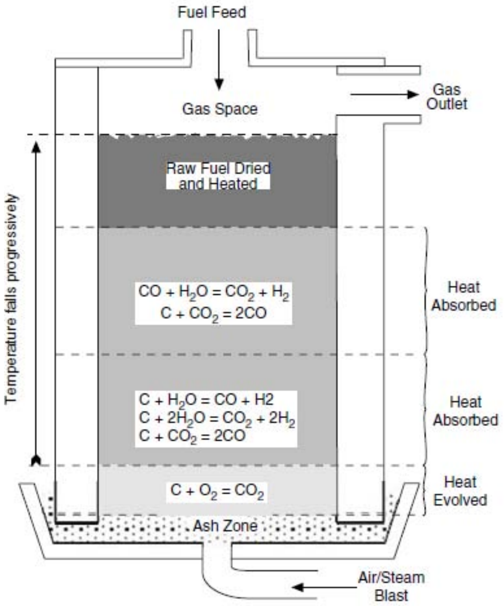

Figure 2: Updraft gasifier [Basu, 2006]

Downdraft gasifiers are very common, especially for biomass gasification. They are typically used for small capacities (1.5 MWth) and occupy more than 75% of the biomass gasification market (Maniatis, 2002). In the downdraft fixed bed gasifier, the gasification agent gas flows in co-current mode with the fuel (downwards). Sometimes heat needs to be added to the upper part of the bed, either by combusting small amounts of the fuel or from external heat sources. The produced gas leaves the gasifier at high temperature, and most of this heat is often transferred to the gasification agent added in the top of the bed, resulting in an energy efficiency level similar to the counter-current type [Basu, 2006]. Since all tars must pass through a hot bed of char in this configuration, tar levels are much lower than the counter-current type.

3. Gasification plants: principles

Different chemical reactions take place in a gasification process, and they are globally endothermic, so that the provision of heat is needed for steady state operation.

Two main different technologies are present in the market, and currently developed in the research field, for biomass and coal gasification. The single bed autothermal gasification, a well known commercial coal gasification plant, and the dual bed allothermal gasification, that is a relatively new approach mainly addressed to biomass gasification.

3.1. Single bed autothermal gasification plant

Figure 3 shows a schematic view of a single bed fluidized bed gasifier. Common gasifying agents used in industrial gasifiers include a mixture of steam and air or oxygen, with the amount of oxygen being generally one-fifth to one-third the amount theoretically required for complete combustion. The necessary heat for gasification is produced by partial combustion of the biomass in the same reaction chamber. However, in this case the producer gas is diluted by nitrogen and the resulting calorific value is low. To avoid this inconvenience, an air fractionation unit is needed at the inlet of a gasifier, as shown in Figure 3. As a result, a mixture of steam and oxygen is proposed to obtain a nitrogen free producer gas which is normally applied in large scale coal gasification. A brief overview on oxygen separation processes is given in the following section.

Figure 3 shows that the gas has to be clean (i.e., sulphur removal) before to enter in the gas turbine for electricity generation. A steam turbine may be also connected with the gas turbine in order to recover the heat of flue gas coming from the combustion chamber.

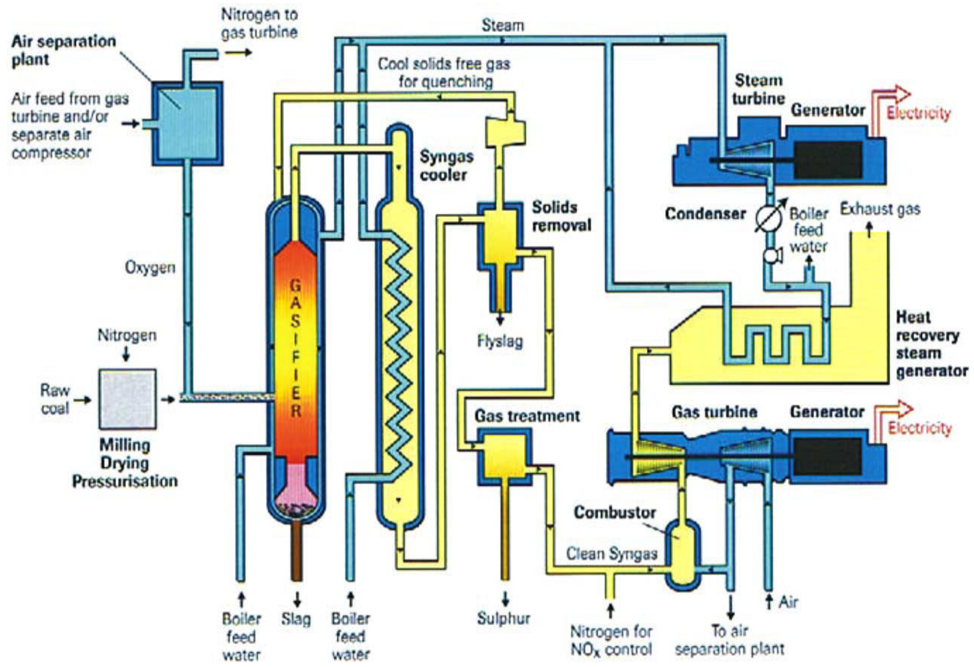

Figure 3: Scheme of IGCC showing key system components [Minchener, 2005]

3.1.1. Oxygen separation techniques

The various separation technologies that produce commercially useful oxygen from air are based on differences in boiling points (cryogenic distillation) or on differences in molecular weights, molecular size and other properties (non-cryogenic separation processes). Non-cryogenic plants are less energy efficient than cryogenic plants (for comparable product purity) but may cost less to build and they are most suitable when high purity product is not required by end-use applications, and at small to medium scale. Non-cryogenic processes employ membranes or sorbents to remove the unwanted components of air. They produce oxygen which is typically 90 to 95% pure.

All cryogenic processes include these steps:

- Filtering and compressing air;
- Removing contaminants, including water vapour and carbon dioxide (which would freeze in the process);
- Cooling the air to very low temperature through heat exchange and refrigeration processes;
- Distilling the partially-condensed air (at about -185°C) to produce desired products.

Oxygen gas typically emerges from the air separation process at close to ambient air temperature and at relatively low pressure.

Non-cryogenic processes belong to one of two major technology categories: adsorption-based processes (Pressure Swing Adsorption or PSA, Vacuum Swing Adsorption or VSA, Vacuum-Pressure Swing Adsorption or VPSA) and membrane diffusion-separation systems that use differences in adsorption of gases on specially-fabricated materials to make the desired separations.

3.2. Dual bed allothermal gasification plant

To avoid an air separation unit especially for small and medium scale biomass gasification, a different approach has been established. This process is based on allothermal gasification, which means that the heat is supplied indirectly via a heat exchanger or a circulating heat carrier. The heat needed for the highly endothermic gasification with pure steam may be provided by:

- transfer of char generated in the gasifier to a combustor;
- combustion of the char generated in the gasifier;
- the use of a circulating solid to transfer the hot solid from the combustor to the gasifier.

Figure 4 shows the principle of the dual fluidized bed steam gasification process. The biomass or coal enters a bubbling fluidized bed gasifier where drying, thermal gasification, and partially heterogeneous char gasification take place at bed temperatures of about 800 – 850 °C. Residual biomass char leaves the gasifier together with the bed material, and is carried towards the combustion reactor.

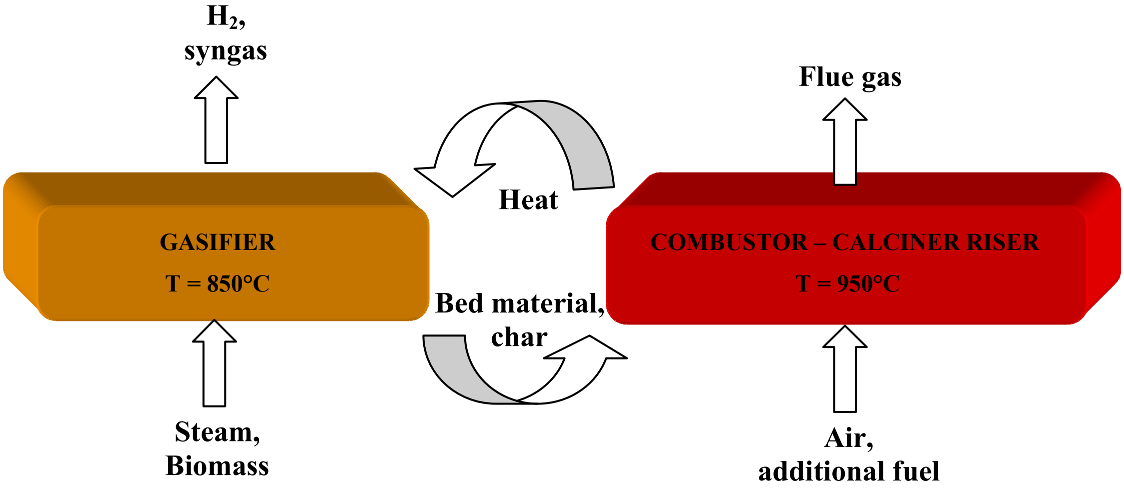

Figure 4: Principle of dual fluidized bed gasifier

The combustion reactor is used for heating up the bed material and is designed as a riser. Air or oxygen may be used as fluidization agent in the riser. After particle separation from the flue gas in a cyclone, the hot bed material flows back to the gasifier via a loop seal. The temperature difference between the combustion and the gasification reactor is determined by the energy needed for gasification as well as the bed material circulation rate. The system is inherently auto-stabilizing since a decrease of the gasification temperature leads to higher amounts of residual char which results in more fuel for the combustion reactor. This, in turn, transports more energy into the gasification zone and thereby stabilizes the temperature. In practical operation, the gasification temperature can be influenced by addition of a secondary fuel (e.g. recycled producer gas) into the combustion reactor. The pressure in both, gasification and combustion reactors, is close to atmospheric conditions. The process yields two separate gas streams, a high quality producer gas and a conventional flue gas, at high temperatures. The producer gas is generally characterized by a relatively low content of condensable higher hydrocarbons (4-8 g/m^3 of so called tars, heavier than toluene), low N_2 (<1 vol% on dry basis), and a significant H_2 content of 36-42 vol% (dry basis) [Pfeifer *et al.*, 2009a,b].

A description of dual fluidized bed gasifiers operated today in Europe (TU Wien and Guessing in Austria, and ECN in The Netherlands), Japan (IHI Co., EBARA, AIST-Tsukuba), and China (Dalian, Hangzhou, and Beijing) is given by Corella [Corella *et al.,* 2007]. No DFB-based gasifiers for biomass are known to be operating in the United States and Canada. Nevertheless, some similar DFB-based concepts or approaches are being developed in coal gasification.

These authors point out two major drawbacks of the DFB biomass gasifiers:

- the low conversion of water (below 10%). Although unconverted or unused H_2O could be recycled, this would require condensation of the steam in the produced gasification gas and further evaporation of H_2O and reheating to the gasifier temperature (850 °C). In all these steps, some energy is wasted or lost, and, therefore, the thermal efficiency of the overall gasification process cannot be high;
- The gasifier in the DFB system operates at temperatures of >800 °C. Because the gasification with pure steam is highly endothermic, it is not easy to reach those temperatures in the gasifier. For this reason, all DFB-based gasification plants require an external supply of energy that has to be considered for economical evaluation of the overall process.

At the ECN in The Netherlands [van der Drift *et al.,* 2005], a DFB-based biomass gasifier (called “Milena”) has been set up. Gasification occurs in a riser and the combustion of char occurs in an external combustor that surrounds the gasifier.

4. Product gas utilization and upgrading: CO_2 capture and tar abatement for poly-generation strategies

Figure 5 shows a general process flow sheet illustrating producer gas or syngas utilization. As mentioned previously, the simplest case is the combustion of the gaseous fuel for industrial heat or for co-firing, as nearly no producer gas cleaning or upgrading is necessary. Most applications try to produce combined heat and power where tar and particle cleaning has to be foreseen. The production of synthetic products requires a specific gas composition (e.g. hydrogen to carbon monoxide ratio) where an extensive gas cleaning and gas upgrading is necessary. From syngas, several interesting synthetic substances can be produced. Currently, the most interesting products are biofuels as they are listed in Table 3 [Hofbauer, 2009]. FT-diesel and methanol are liquid products whereas DME (dimethyl ether) and SNG (substitute natural gas) are gaseous. The reaction conditions are shown in Table 4 [Hofbauer, 2009]. It can be seen that all four reactions need catalysts which are normally extremely sensible to poisoning e.g. by sulphur components. Furthermore, the temperatures are in the range of 200 to 400 °C and a pressurized operation is desirable or necessary.

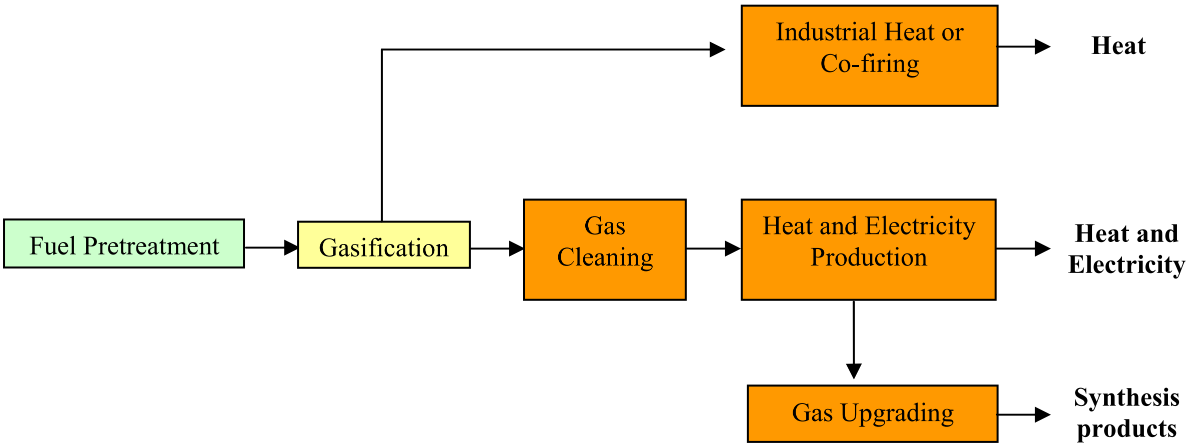

Figure 5: Producer gas alternative utilization paths

Synthesis	H_2/CO Ratio	Synthesis Reactions
F-T	2	$CO+2H_2 \rightarrow -CH_2- +H_2O$
Methanol	2	$CO+2H_2 \leftrightarrow CH_3OH$
DME	2.5	$CO+CO_2+5H_2 \leftrightarrow CH_3OCH_3+2H_2O$
Methanation	3	$CO+3H_2 \leftrightarrow CH_4+H_2O$

Table 3: Synthesis reactions

Synthesis	Catalysts	Pressure bar	Temperature (°C)
F-T	$Fe/Co/ZrO_2/SiO_2$	20 – 40	220 – 300
Methanol	Zn/Cr/Cu/Al	50 – 300	220 – 380
DME	$Cu/Zn/Al_2O_3$	15 – 100	220 – 300
Methanation	Ni/Mg	1 – 10	200 – 400

Table 4: Range of suitable conditions for synthesis reactions

There are a lot of requirements on the syngas main composition and the quality concerning impurities. Table 4 contains some of these requirements [Hofbauer, 2009]. First of all, inert gases which are not involved in the reactions should be avoided. Air as gasification agent leads to about 50% of nitrogen in the syngas which is not a reaction agent for any of the synthesis reactions shown above. Therefore, steam or oxygen/steam mixtures are the preferable gasification agents. As already mentioned the different reactions need different stoichiometric H_2 to CO ratios (Table 3). In practice the required ratio differs from these stoichiometric values slightly, however a certain H_2 to CO ratio is necessary in any case for optimal operation, and its value is normally higher than that would be obtained from gasification without any adjustment. Low tar contents and also low methane contents (exception for methanation) are beneficial. The most serious requirements are concerning poisoning due to sulphur or other undesired traces in the syngas. For example, sulphur has to be removed down to 50 ppb(v) to reach long term operation with sufficiently high yields of the desired products [Hofbauer, 2009]. Finally, those gasification systems which allow pressurized gasification are well suited for syngas production as almost all synthesis reactions are operated under pressure (Table 5).

An interesting development coupled with biomass gasification and that may empower polygeneration strategies is the so-called CO_2 capture process, that is reported in details in the further section. Particular attention will be focused on the pre-combustion and *in situ* CO_2 capture processes, where the Ph.D. work is addressed.

Requirement	Measure
Low content of inert gases (i.e. nitrogen)	Gasification agent steam/oxygen
Optimal H_2/CO ratio	Steam gasification
	Shift reaction downstream
	CO_2 capture option
Low tar content	High temperature gasification
	Tar removal downstream
Mostly, low methane content	High temperature gasification
	Methane removal downstream
Low content of catalysts poisons (i.e. sulphur)	Removal downstream or capture in the gasifier
Mostly, medium or high pressure necessary	Downstream compression

Table 5: Requirements for syngas [Hofbauer, 2009]

4.1. CO_2 capture techniques

Coal and biomass gasification coupled with CO_2 capture may offer a further environmental advantage in addressing concerns over the atmospheric build-up of greenhouse gases. Moreover, when the process is coupled with synthesis of chemicals, a new way for adjusting the right stoichiometric H_2/CO ratio, in favour of polygeneration applications, is proposed.

In general terms, according to the type of installation, CO_2 capture may take place at three different stages, termed post-combustion, pre-combustion, or oxyfuel combustion decarbonisation (see Figure 6). Each of these techniques is at a different stage of maturity and offers its own advantages and drawbacks (cost, energy consumption, etc.).

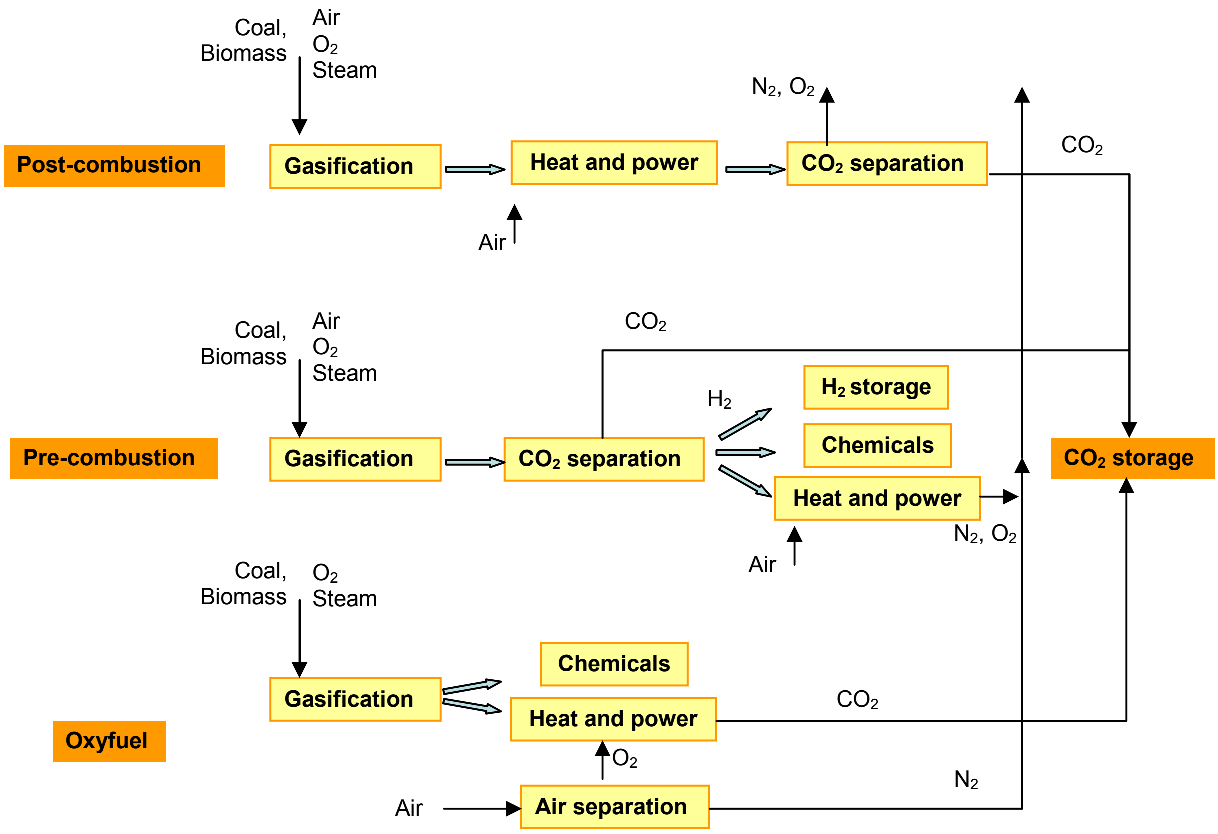

Figure 6: Principles of CO_2 capture techniques

4.1.1. Post-combustion

Post-combustion decarbonisation is the most mature, but also the most costly of the three techniques, and is appropriate for existing installations because modifications in existing plants are required only downstream of the power generation section. It involves separating the CO_2 contained in combustion flue gases, usually by means of a liquid solvent such as mono ethanol amine (MEA) [IPCC-CCS report, 2005], [Rao *et al.*, 2002]. Metal oxides (MO), including CaO, have also been considered as likely sorbent materials for the removal of CO_2 from flue gas in the form of solid metal carbonates (MCO_3) [Gupta *et al.*, 2002], [Iyer *et al.*, 2004].

4.1.2. Pre-combustion

Pre-combustion capture processes refer to the removal of CO_2 from a synthesis gas composed of CO and H_2, i.e., this process requires a preliminary fuel-processing step (e.g. gasification) to convert the fuel to a synthesis gas, followed by a secondary water–gas shift reaction to produce a stream rich in CO_2 and H_2. A concentrated stream of CO_2 can then be produced by separating CO_2 from the product gas stream. In the case of Steam Methane

Reforming for H_2 production, these preliminary reaction steps typically occur in separate reaction vessels [Balasubramanian *et al.*, 1999]. Likely separation techniques include:

- absorption with organic solvents such as mono ethanol amine;
- membrane separation [Adris *et al.*, 1991, 1994], [Chen *et al.*, 2003], [Dogan *et al.*, 2003];
- adsorption, using adsorbent materials such as molecular sieves, activated carbons, zeolites or hydrotalcite-like compounds [Yong et *al.*, 2001, 2002];
- separation of CO_2 from gas mixtures via condensation at cryogenic temperatures [Feng *et al.*, 2007]; [IPCC-CCS report, 2005], [Rao *et al.*, 2002].

Two interesting techniques that may be discussed from a point of view of pre-combustion CO_2 separation, the "in situ CO_2 capture" and the "chemical looping combustion", are covered in 4.1.3. and 4.1.4. paragraphs.

4.1.3. In situ CO_2 capture

In situ CO_2 capture involves the same general steps described above for pre-combustion CO_2 capture. However, the gasification, shift and CO_2 capture steps occur in a single, integrated process by means of a solid sorbent material (a metal oxide) located directly in the gasifier or in the reformer. Integrating these reaction steps involves selecting suitable reaction conditions under which all of the processes can be carried out. The general capture mechanism is represented, according to the reaction:

$$MO_{(s)} + CO_2 \rightarrow MCO_{3(s)} \qquad \textit{(exothermic)} \qquad (1)$$

Metal oxides for in situ CO_2 capture must satisfy several criteria: (i) they must exhibit high reactivity within a temperature range from 550 to 750 °C; (ii) their decomposition temperatures (often referred to as calcination temperature) should be greater than the temperature range for gasification, but not too high (e.g.>1000 °C) to avoid imposing severe energy penalties during the sorbent regeneration step. From an economic point of view, metal oxides that are abundant in naturally occurring rocks represent the cheapest option [Abanades *et al.*, 2004a,b]: limestone ($CaCO_3$) and dolomite ($(Ca,Mg)CO_3$) are therefore considered very attracting materials for this purpose.

The advantages of combining steam reforming with in situ capture of CO_2 can be understood from the influence of CO_2 removal on the thermodynamic equilibria governing the reforming processes [Johnsen *et al.*, 2006]. In methane reforming reaction coupled with CO_2 capture, the hydrogen concentration is predicted to reach a maximum of 98% (dry and nitrogen free basis) at 600 °C for a CaO/CH_4 ratio of 2, whereas the equilibrium concentration of conventional steam reforming is only 74% at that temperature. Sorption enhancement enables lower reaction temperatures, which may reduce catalyst coking and sintering, while enabling use of less expensive materials for the reactor vessel. In addition, heat release by the exothermic carbonation reaction supplies most of the heat required by the endothermic reforming reactions. However, energy is required to regenerate the sorbent to its oxide form by the energy-intensive calcination reaction (that produces a regenerated sorbent), which represents a challenge in terms of heat transfer and reactor construction. The high temperature required for $CaCO_3$ regeneration could also cause sintering of solids, affecting the long-term performance of sorbent. Previous works [Abanades *et al.,* 2003], [Silaban *et al.,* 1995,1996] have reported that the absorption capacity for Ca-based sorbents decays as a function of the number of calcination–carbonation cycles. Silaban [Silaban *et al.,* 1996] found that dolomite ($CaCO_3 \cdot MgCO_3$) was superior to limestone as a sorbent in this respect, with better multi-cycle performance. Its advantages were attributed to differences between the structural properties of calcined dolomite and calcined limestone. Initial calcination produces complete decomposition of dolomite, but carbonation conditions are at such temperature that only CaO is converted to the carbonate form. The excess pore volume created by $MgCO_3$ decomposition is believed to be responsible for the more favourable cycling performance. Some efforts in research to improve the behaviour of calcium based sorbents with respect to cycling deactivation and attrition resistance are reported in the literature [Lu *et al.,* 2006], [Feng *et al.,* 2006], [Marquard-Moellenstedt *et al.,* 2008], [Hughes *et al.,* 2004], [Li *et al.,* 2006b], [Wu *et al.,* 2007,2008], [Satrio *et al.,* 2005,2007], [Sun *et al.,* 2007,2008], [Florin *et al.*, 2008] [Martavaltzi *et al.*, 2008a,b], [Lu *et al.,* 2008] [Harrison, 2008] [Manovic *et al.*, 2009], [Reddy *et al.,* 2004]. More details and bibliographic references on absorption capacity, sorbent regeneration and behaviour trough cycles, is provided in Chapter 6, where the kinetic of CO_2 capture by means of dolomite in multi-cycling condition is investigated.

Experimental investigations for enhancement of steam reforming by in situ removal of CO_2 have mainly been conducted in small or pilot scale fixed and fluidized bed reactors, with the bed containing varying proportions of reforming catalyst and Ca-based sorbent [Lopez *et al.,* 2001], [Johnsen *et al.,* 2006], [Li *et al.,* 2006a],[Balasubramanian *et al.*, 1999] [Yi *et al.,* 2005] [Satrio *et al.*, 2005,2006].

Recently, new developments have been reported to run a gasification process including CO_2 capture, utilising the demonstration plant of Guessing, Austria [Marquard-Moellenstedt *et* *al.,* 2008]. It has been proposed to add a CO_2 sorbent (a natural mineral substance, such as limestone or dolomite) to the FICFB (Fast Internally Circulating fluidized Bed [Marquard-Moellenstedt *et al.,* 2004]) reactor bed inventory. The sorbent circulates between the gasifier - CO_2 capture bubbling bed, and the combustor – calciner riser, in order to run the whole process continuously. In the reactor chamber devoted to biomass gasification and CO_2 capture, the endothermic gasification and the exothermic solid carbonation processes combine well together and their coupling reduces the amount of the solid circulation rate required to sustain thermally the devolatilization and gasification reactions. On the other hand, the riser provides the calcined solid sorbent and the thermal loading, by combustion of residual char (and/or additional fuel). When this is performed utilizing pure oxygen, a CO_2 stream is easily obtained (by steam condensation), available for storage and sequestration. Figure 7 shows a schematic outlook of the process.

The thermodynamic constraints of the reaction between CO_2 and CaO impose, at ambient pressure, a temperature level for gasification somewhat lower (650-700°C) than the usual one (800-850°C), as it is clear from the equilibrium equation [Labiano *et al.,* 2002], [Barin, 1989] (Equation 1) and Figure 8:

$$P_{CO_2\,eq}(atm) = 4.137 \times 10^7 \times \exp\left(-\frac{20474}{T(°K)} \right) \tag{1}$$

where P_{CO2eq} *(atm)* is the equilibrium CO_2 pressure expressed in atmospheres, and *T(K)* the system temperature expressed in K.

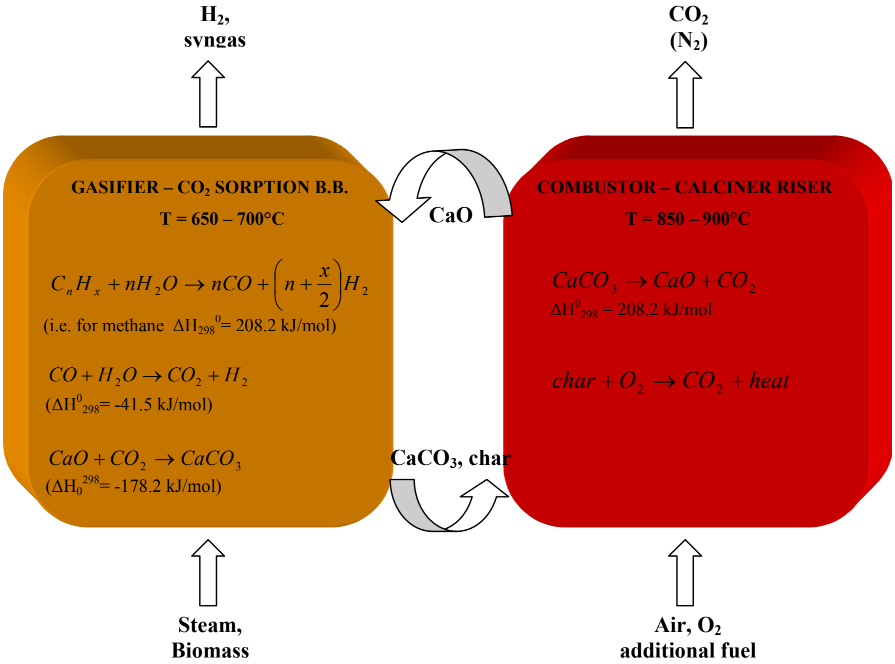

Figure 7: Coupling of two fluidized bed (FB) reactors for the continuous production of a H_2-rich gas from a biomass gasification process

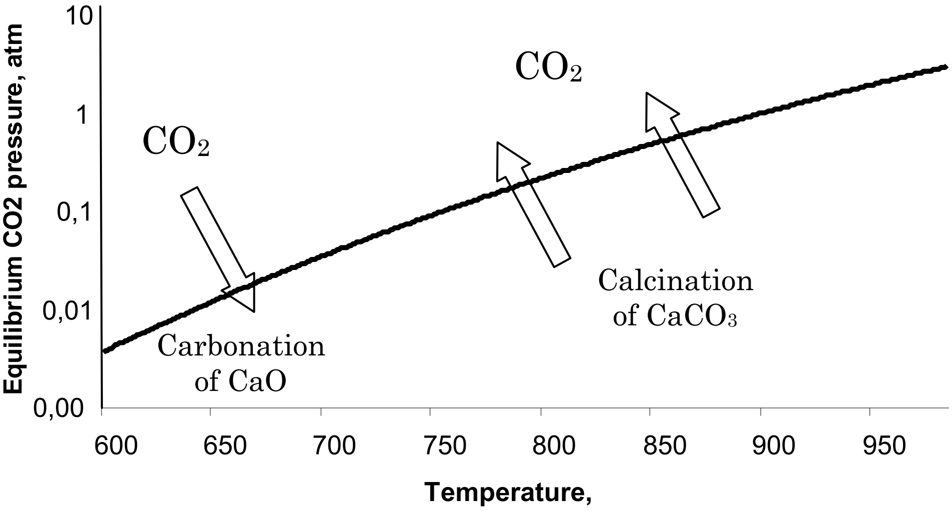

Figure 8: Equilibrium curve for CO_2 capture: arrows refer to ambient pressure systems

	Product gas composition, %vol dry basis	
	8MW Guessing conventional	8 MW Guessing AER
H_2	37.2	50.6
CH_4	11.1	12.9
CO_2	22.3	12.5
CO	23.1	16.5
HC	4.5	5.8

Table 6: Composition of product gas for the gasification process with and without CO_2 capture in the 8 MW_{th} power plant at Guessing

While circa 37% H_2 is obtained during standard operation at Guessing, up to 50% H_2 was measured in AER mode (Table 6). There is still potential for further increasing the H_2 yield, as shown by results from AER gasification in the pilot plant at the University of Vienna. Using the same pre-treated CO_2 sorbent bed material, 65% H_2 was reached. While the H_2 content increases, the CO_2 content decreases: from circa 23% CO_2 under standard conditions to less than 13% CO_2 under AER conditions. The H_2/CO ratio also is significantly modified, from 1.5 to 3, while methane content is quite unaffected by the different processes, meaning that the effect of thermodynamic improvement due to CO_2 capture shifting reforming reactions, and decrease in temperature balance each other out (the yield of methane is favoured by low temperature gasification). This means that the AER should be favourable also as a pre-treatment for a downstream methanation process (see Table 3).

Acharya [Acharya *et al.*, 2009] shows that the use of calcium oxide not only helps to reduce the concentration of carbon dioxide to nearly zero but also increases the hydrogen concentration and helps to maintain the gasifier temperature constant (at 580°C), thus avoiding the need of additional heat required for the endothermic gasification reaction to take place (see also enthalpy values in Figure 7).

4.1.4. Chemical Looping Combustion

An additional interesting process for CO_2 separation is the chemical looping combustion technology, initially proposed by Ritcher [Ritcher *et al.,* 1983].

The flameless combustion, as realised by the chemical looping combustion (CLC) process, is a new emerging technology, with a potential to reduce the cost for CO_2 capture [IPCC-CCS report, 2005]. CLC has the advantage that CO_2 is inherently separated, thus there is no energy loss in the separation and no costs associated with gas separation equipment and operation. In CLC, oxygen is transferred from the combustion air to the gaseous fuel by means of an intermediate solid, oxygen carrier, as in the case of a metal oxide available at different oxidation levels. The system consists of two interconnected reactors, the fuel and the air reactor, and the oxygen carrier cycling between both reactors (see Figure 9). Lyngfelt [Lyngfelt *et al.*, 2001] proposed a circulating system composed of two connected fluidized beds, a high velocity riser acting as the air reactor, and a low-velocity bubbling fluidized bed acting as the fuel reactor. The gaseous fuel (natural gas or syngas) is introduced in the fuel reactor, where it is oxidised by the oxygen carrier to produce CO_2 and H_2O. In this reactor, the metal oxide is reduced by the following general reaction, for a hydrocarbon fuel (Equation 2):

$$(2n+m)Me_xO_y + C_nH_{2m} \rightarrow (2n+m)Me_xO_{y-1} + nCO_2 + mH_2O \tag{2}$$

or for syngas (Equation 3):

$$(2n+m)Me_xO_y + nCO + mH_2 \rightarrow (n+m)Me_xO_{y-1} + nCO_2 + mH_2O \tag{3}$$

Me_xO_y denotes a metal oxide and Me_xO_{y-1} its reduced form. The solid particles of oxygen carrier are transferred to the air reactor where they are regenerated to the original oxidation level by taking up oxygen from air (Eq.4):

$$Me_xO_{y-1} + \frac{1}{2}O_2 \rightarrow Me_xO_y \tag{4}$$

The oxidized carrier is now recirculated to the fuel reactor for a new cycle. The fuel and the combustion air are never mixed, and the gases from the fuel reactor, CO_2 and H_2O, leave the system as a separate stream, completely segregated from the exit of the air reactor. H_2O can easily be removed by condensation and pure CO_2 is obtained. The oxidation of the oxygen-carrier is exothermic, while the reaction in the fuel reactor could be either endothermic or exothermic, depending on the oxygen-carrier and the fuel.

As a example, if methane is used as fuel and NiO as oxygen carrier, reactions (5–6) will occur in the reactors, respectively:

Air reactor: $4Ni + 2O_2 \rightarrow 4NiO \qquad \Delta H_{1200°C} = -938.2 kJ/mol$ (5)

Fuel reactor: $CH_4 + 4NiO \rightarrow CO_2 + 2H_2O + 4Ni \qquad \Delta H_{1200°C} = 136.5 kJ/mol$ (6)

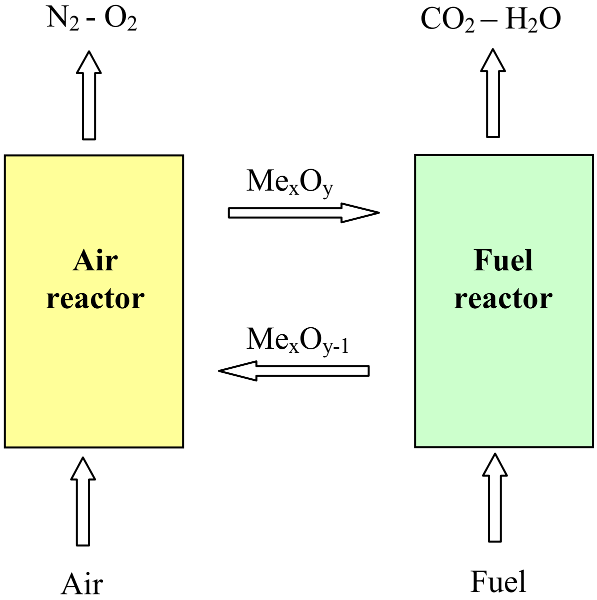

Figure 9: Principle of chemical-looping combustion (CLC)

The total amount of chemical energy released in the whole reactor system is the same as for combustion of the fuel. As a matter of fact, the sum of reactions (5–6) is the complete combustion of CH_4 with oxygen (Eq. 7):

Total reaction: $CH_4 + 2O_2 \rightarrow CO_2 + 2H_2O \qquad \Delta H_{1200°C} = -802.7 kJ/mol$ (7)

Considering that in this process a separate flow of CO_2 is obtained, the advantages with respect to traditional combustion are clear. Different metal oxide systems have been proposed for use as oxygen carriers in CLC: Mn_3O_4/MnO, Fe_2O_3/Fe_3O_4, NiO/Ni, CuO/Cu and CoO/Co [Kronberger *et al.,* 2005], [Jemdal *et al.,* 2006], [Adanez *et al.,* 2005], [de Diego *et al.,* 2004], [Gayàn *et al.,* 2008], [Abad *et al.,* 2007]. The metal oxide is combined with an inert porous support, such as Al_2O_3, ZrO_2, TiO_2 or SiO_2, which may also act as a binder to increase the mechanical strength and improve the resistance to attrition. The oxygen carrier must show high reduction and oxidation reaction rates, otherwise the amount of oxygen-carrier needed in the reactors would be too large. Moreover, the oxygen transfer capacity needs to be sufficient to avoid that circulation of particles between the reactors is too large. An overview of the process, which has been performed on different oxygen-carriers can be found in Adanez [Adanez *et al.,* 2004].

4.1.5. Oxyfuel combustion

Oxyfuel combustion decarbonization is still in the pilot phase. Once again, the efforts of this technology are addressed to avoid a nitrogen diluted flow, that implies high volume of gases and facilities, and lower heating values of product gases.

This technique yields a combustion gas highly concentrated in CO_2 (between 80% and 90% by volume) and could constitute a suitable retrofit technology for existing installations. The process uses high-purity oxygen instead of air for combustion. Oxy-fuel combustion has significant advantages over traditional air-fired plants:

- the mass and volume of the flue gas (and therefore the size of the flue gas treatment equipment) are reduced by approximately 75%;
- because the flue gas volume is reduced, less heat is lost in the flue gas;
- the flue gas is primarily CO_2, suitable for sequestration;
- because nitrogen from air is not allowed in, nitrogen oxides production is greatly reduced.

Therefore, this technology is suitable for near-zero emissions power plants, but nowadays this is not demonstrated in industrial applications. However, because of the energy and economic costs of producing oxygen, an oxy-fuel power plant is significantly less efficient than a traditional air-fired plant. A comprehensive review on oxyfuel combustion technology may be found in Buhre [Buhre *et al.,* 2005].

4.2. Tar depletion in biomass gasification processes

As mentioned in the introduction, tars are problematic in integrated biomass gasification systems for a number of reasons:

- they can condense in exit pipes and on particulate filters leading to blockage of process equipment and clogged filters;
- they can clog fuel lines and injectors in internal combustion engines;
- they may prevent direct utilisation of product gas in a variety of downstream processes, as feedstock for fuel cells or polygeneration plants.

If the end use of the gas requires cooling to near ambient temperature it is possible to use a number of physical removal methods, including wet scrubbing (utilizing water or organic solvents) and filtration, to remove tars. However, a disadvantage of wet scrubbing for product gas conditioning is the formation and accumulation of wastewater. This technique does not eliminate tars but merely transfers the problem from the gas phase to the condensed phase. Also, when tar is removed from the product gas stream, its fuel value is lost and the overall efficiency of the integrated gasification process is reduced.

An attractive hot gas conditioning method for tar destruction is catalytic steam reforming. A number of reviews have been written on biomass gasification hot gas clean-up [Abu El-Rub *et al.*, 2004], [Dayton, 2002], [Sutton *et al.*, 2001], [Devi *et al.,* 2003], [Li *et al.,* 2009], [Torres *et al.,* 2007].

All methods available can be categorized in two types depending on the location where tar is removed; either in the gasifier itself (known as primary method) or outside the gasifier (known as secondary method).

4.2.1. Secondary methods

Secondary methods are conventionally used as treatments to the hot product gas from the gasifier. The concept of secondary methods is given in Figure 10a. These methods can be chemical or physical treatments as follows:

- tar cracking downstream the gasifier either thermally or catalytically [Nordgreen *at al.* 2006];
- mechanical methods such as use of cyclone, ceramic filter, rotating particle separator, electrostatic filter and scrubber.

Downstream gas cleaning methods are reported to be very effective in tar reduction, but in some cases they are not economically viable [Devi *et al.,* 2003].

4.2.2. Primary methods

Primary methods (Figure 10b) can be defined as all measures taken in the gasification step itself to prevent or convert tar formed in the gasifier. For an optimized performance of the gasifier, the main factors are the design and the operation of the gasifier. The operating conditions play a very important role during biomass gasification in all respects, such as carbon conversion, product gas composition, tar formation and tar reduction. The most important influencing parameters include temperature, pressure, heat-up rate of fuel particles, catalysts and additives, equivalence ratio, residence time. The selection of these parameters also depends on the type of gasifier used (entrained flow; moving bed; fluidized bed, bubbling or circulating).

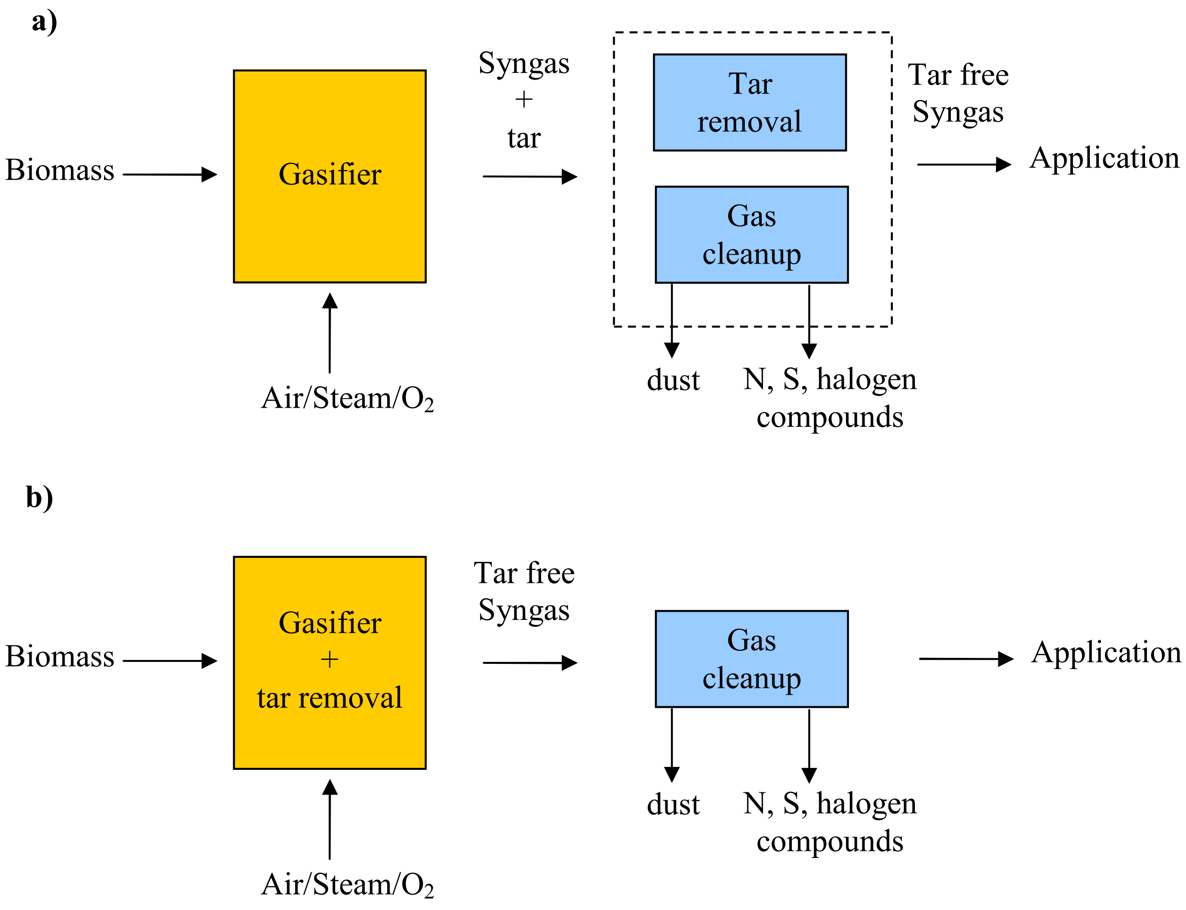

Figure 10: Tar reduction principles by secondary (a) and primary methods (b)) [Devi et al., 2003]

4.2.2.1. Temperature

The level of temperature in the gasifier has two different effects: at low temperatures, between 600 and 720 °C, the pyrolysis of biomass/coal may be relatively fast, but reforming reactions of tar are deprived. High and homogeneous bed temperatures (850-900 °C) in the gasifier are needed to obtain high rates for the endothermic gasification of char and a clean produced gas, in conventional gasification processes.

More than 40% reduction in tar yield was reported when the temperature was raised from 700°C to 900°C [Yu *et al.*, 1997]. Temperature not only affects the amount of tar formed, but also the composition of tar [Kinoshita *et al.,* 1994], [Brage *et al.,* 2000], [Li *et al.,* 2009]. On the other hand, there are several other factors that limit the operating temperature: for instance, the risk of sintering, agglomeration and melting of ashes (together with inert bed inventory) increases by increasing temperature [Li *et al.,* 2009].

4.2.2.2. Additives

The research in new catalytic additives is a crucial step on the development of the applicability of biomass gasification concepts, with the aim of solving the problem of tar elimination for producing a clean gas. Corella [Corella *et al.,* 2006] reports that the presence of some inorganic species (ISs) in the gasifier is an important operation variable on the quality of product gas, acting as catalysts in reactions involving tars, char and oxidant agents. The ISs species may be present in the steam gasification of coal/biomass in two very distinct ways:

- as constituents of the matrix of the coal/biomass and, therefore, of the char and ash generated in the gasification process
- as additives to the gasifier, mixed with the reacting fuel. These additives may be located in the gasifier at the beginning of the gasification or may be continuously fed to the gasifier mixed with the fuel, to replace the amount of additive being continuously lost in the FB gasifier by erosion and elutriation or carryover.

Those authors found that CaO may be the only additive recommended for biomass gasification processes. However, coke-forming reactions deactivate CaO, and/or other ISs, present in the gasifier bed.

Calcined limestone (CaO) and magnesite (MgO) were studied by Delgado [Delgado *et al.*, 1996,1997] and proved to be active for tar elimination in biomass gasification; however, they were not as active as calcined dolomites. Moreover, Orio and co-workers [Orio *et al.,* 1997] mentioned that in-bed use of dolomite results in a similar tar content as using it in a downstream catalytic reactor. Calcined dolomites (CaO-MgO) have the following positive characteristics:

- they have been proven to have a clear activity for in-bed tar elimination [Orio *et al.,* 1997], [Olivarez *at al.,* 1997], [Rapagnà *et al.,* 1998];

- calcined dolomites have also demonstrated to have an anti-agglomeration character [Corella *et al.,* 2004];

Nevertheless, calcined dolomites are soft and erode quickly in a fluidized bed, which generates a high content of fines in the producer gas.

Other workers [Ohtsuka *et al.*, 1987,1997], [Asami *et al.,* 1996] have found how iron-based species (Fe_2O_3, Fe_3O_4, etc.) affect the rate of the overall steam gasification of coal and/or biomass. Other bibliographic references related to iron catalysts are provided in Chapter 4, in relation to investigations on new iron based catalysts.

Dayton recognizes three groups of catalyst materials in biomass gasification systems – alkali metals, non-metallic oxides, and supported metallic oxides. The most widely studied non-metallic catalysts for biomass gasifier are once again dolomites. However, due to a moderate activity, Dayton recommends the effective use of dolomite in a guard bed prior to catalyst reactors containing additional metallic reforming catalysts. High steam concentrations in the product gas, short space times, and high temperatures help to improve the lifetime of the calcined dolomite because the kinetics of steam gasification of carbon are fast enough to remove coke as it is formed on the catalyst surface.

An alternative to dolomite is offered by naturally occurring particles of olivine, which is a mineral made of magnesium and iron oxides, and silica. Olivine is advantageous in terms of its attrition resistance much stronger than that of dolomite. Rapagnà [Rapagnà *et al.*, 2000] investigated the catalytic activity of olivine and observed that it has a good performance in terms of tar reduction and the activity is comparable to calcined dolomite.

A wide variety of Ni-based steam reforming catalysts are commercially available because of their application in the petrochemical industry for naphtha reforming and methane reforming to make syngas. Nickel-based catalysts have also proven to be very effective for hot conditioning of biomass gasification product gases [Rapagnà *et al.,* 1998]. They have high activity for tar destruction, methane in the gasification product gas is reformed, and they have some water-gas shift activity to adjust the H_2:CO ratio of the product gas [Dayton, 2002]. However, the use of nickel catalysts in fluidized bed gasification reactors was discouraged because of the rapid deactivation of these catalysts in the dusty environment of the gasifiers. Coke formation on the catalyst surface, that may be substantial when tar levels in product gases are high, i.e. using primary methods, is a main cause of nickel based catalysts deactivation. Coke can be removed by regenerating the catalyst, however, repeated high temperature processing of nickel catalysts can lead to sintering, phase transformations, and volatilization of the nickel (see reviews cited in Section 4.2). Sulphur, chlorine, and alkali metals that may be present in gasification product gases also act as catalyst poisons [Hepola *et al.,* 1997a,b], [Dou *et al.,* 2002].

Consequently, these metallic catalysts are typically used in secondary fixed bed catalyst reactors. In many cases, they may be used in conjunction with calcined dolomite catalysts in guard beds for the highly active nickel catalysts. However, even if placed in a secondary reactor, nickel catalysts require a hot filter to retain particulates, due to its toxicity properties.

5. Objectives of this work

In previous sections, biomass gasification concepts, technologies, applications and limitations have been explored. The aim of this section is to clarify the role of this Ph. D. work on such a scenery.

The aim of both experimental and theoretical investigations of this work is to improve the applicability of biomass gasification for clean energy production. An important goal of this study is the contact ground between the chemistry approach (preparation and characterization techniques of materials, their use in micro-scale reactors) and chemical engineering methods (mathematical models and larger experimental apparatuses).

The attention is focused on enhancing tar abatement in biomass gasification, with or without the use of a sorbent for capturing CO_2. The process is investigated at real conditions (a pilot plant gasifier) (Chapter 2), using bench scale (fluidized bed, Chapters 3, 6) and small scale (micro-reactor, Chapter 5) rigs. The former is used to highlight the complexity of biomass gasification process at real conditions. On the other hand, the reduced scale facilities, operating on simulated conditions, enhance the comprehension of single steps involved in this complexity: tar steam reforming, CO_2 capture, and a combination of both.

A particular attention has been focused on solid phases involved in heterogeneous catalysis of reforming reactions, and their role on improving gas clean-up. In the pilot plant gasifier (Chapter 2), the effect of the addition of nickel additives in the gasifier, by means of a catalytic filter candle, is investigated as a primary method to perform an efficient tar abatement process. Otherwise, new materials with catalytic properties have been tested (Chapter 5), using model compounds as key descriptive agents for real tar mixtures, in the micro-reactor rig as a testing ground in order to designate the best performances valuable for large scale applications.

The CO_2 capture process has been investigated as a means to improve the global efficiency of reforming reactions, in addition to beneficial effects related to:

- the use of cheap and abundant materials with some moderate catalytic activity on tar abatement (calcium based sorbents);
- the exothermicity of CO_2 capture using calcium based sorbents that supply an additional heat source to the process;
- the production of a pure CO_2 stream available for sequestration.

As a result, this work fits also in the CO_2 separation technologies field and in particular in the pre-combustion separation concept that (as explained in this chapter) influences the H_2/CO ratio and therefore contributes to enlarge the product gas utilization options by means of upgrading steps. The experimental tests in this Ph. D. work may be referred to both in-bed CO_2 capture (i.e., the "Guessing model") and CO_2 capture in a separate vessel, downstream to the gasifier. In fact, it is a synthesis gas that comes into contact with the solid phase sorbent and/or catalyst in most of the experiments shown in further chapters.

Plain CO_2 capture tests and/or the coupled process of steam reforming and CO_2 capture have been therefore investigated using both the bench scale fluidized bed and the micro-reactor rigs. The latter has been used for testing once again new materials with CO_2 capture properties, while the former with conventional solid phases (raw dolomite and/or a commercial nickel catalyst).

New materials have been conceived (Chapter 4) in order to optimize the granular, mineral solid material for a simultaneous hydrocarbon reforming and CO_2 capture process, by improving the catalytic activity of calcium based sorbents for reforming reactions in order it to perform the double function of CO_2 sorbent as well as reforming catalyst. For this purpose, nickel and iron metals have been deposited (by impregnation method) on a sorbent surface, and their catalytic activity and CO_2 capture properties have been investigated, with the aim to reach the final choice of the best performing, combined catalyst-and-sorbent.

Last but not least, some plain CO_2 capture tests have been carried out in the fluidized bed reactor rig, using a dolomite sorbent. In this final step, it is not in-depth examined the topic of material resistance to multi-cycle operation, rather a rigorous model is proposed for extracting kinetic data from heterogeneous systems by application of chemical reaction engineering methodologies.

6. Conclusions

An overview on biomass gasification has been carried out in this Introduction chapter. Gasification plants, gasifier technologies, product gas upgrading and utilization have been highlighted as key concepts in order to understand the state of the art. Particular attention has been focused on CO_2 capture and tar abatement strategies, in order to improve the quality of the product gas. Starting from these basic considerations, the objectives of this work have been envisaged in order to improve the applicability of the biomass gasification processes.

Bibliography

Abanades J.C., Alvarez D., (2003), Conversion limits in the reaction of CO_2 with lime, Energy & Fuels 17, 308-315.

Abanades J.C., Anthony J.E., Lu D.Y., Salvador C., Alvarez D., (2004a), Capture of CO_2 from combustion gases in a fluidized bed of CaO, Environmental and Energy Engineering 50, 1614-1622.

Abanades J.C., Rubin E.S., Anthony E.J., (2004b), Sorbent cost and performance in CO_2 capture systems, Industrial and Engineering Chemistry Research 43, 3462-3466.

Abad A., Adánez J., García-Labiano F., de Diego L.F., Gayán P., Celaya J., (2007), Mapping of the range of operational conditions for Cu-, Fe-, and Ni-based oxygen carriers in chemical-looping combustion, Chemical Engineering Science 62, 533-549.

Abu El-Rub Z., Bramer A.E., Brem G., (2004), Review of catalysts for tar elimination in biomass gasification, Industrial and Engineering Chemistry Research 43, 6911-6919.

Acharya B., Dutta A., Basu P., (2009), Chemical-Looping Gasification of Biomass for Hydrogen-Enriched Gas Production with In-Process Carbon Dioxide Capture, Energy Fuels 23, 5077-5083.

Adanez J., de Diego L.F., Garcia-Labiano F., Gayan P., Abad A., Palacios J.M., (2004), Selection of Oxygen Carriers for Chemical-Looping Combustion, Energy Fuel 18, 371-377.

Adanez J., Garcia-Labiano F., de Diego L.F., Gayan P., Abad A., Celaya J., (2005), Development of oxygen carrier for chemical-looping combustion. In: Thomas D, editor. The CO2 Capture and Storage Project (CCP) for Carbon Dioxide Storage in Deep Geologic Formations For Climate Change Mitigation. Capture and Separation of Carbon Dioxide From Combustion Sources, vol. I. London: Elsevier Science; 2005, 587-604.

Adris A.M., Elnashaie,S.S.E.H., Hughes R., (1991), A fluidized bed membrane reactor for the steam reforming of methane, Canadian Journal of Chemical Engineering 69, 1061-1070.

Adris A.M., Lim C.J., Grace J.R., (1994), The fluidized bed membrane reactor system: a pilot scale experimental study, Chemical Engineering Science 49, 5833-5843.

Asami K., Sears P., Furimsky E., Ohtsuka Y., (1996), Gasification of brown coal and char with carbon dioxide in the presence of finely dispersed iron catalysts, Fuel Process. Technol. 47, 139-151.

Balasubramanian B., Lopez A., Kaytakoglu S., Harrison, D.P., (1999), Hydrogen From Methane in a Single-Step Process. Chem. Eng. Sci. 54, 3543.

Barin I., Thermochemical data of pure substances, Weinheim VCH 1989.

Basu, P., (2006), Combustion and gasification in fluidized beds, Taylor & Francis Group, LLC.

Brage C, Yu Q, Chen G, Sjostrom K., (2000) Tar evaluation profiles obtained from gasification of biomass and coal. Biomass and Bioenergy 18, 87-91.

Buhre B.J.P., Elliott L.K., Sheng C.D., Gupta R.P., Wall T.F., (2005), Oxy-fuel combustion technology for coal-fired power generation, Progress in Energy and Combustion Science 31, 283-307.

Chen Z., Yan Y., Elnashaie S.S.E.H., (2003), Novel circulating fast fluidized bed membrane reformer for efficient production of hydrogen from steam reforming of methane, Chemical Engineering Science 58, 4335-4349.

Collot A.G., (2006), Matching gasification technologies to coal properties, Int. J. of Coal Geology 65, 191- 212.

Corella J., Toledo J.M., Padilla R., (2004), Olivine or dolomite as in-bed additive in biomass gasification with air in a fluidized bed: Which is better?, Energy Fuels 18, 713-720.

Corella J., Toledo J.M., Molina G., (2006), Steam Gasification of Coal at Low-Medium (600-800 °C) Temperature with Simultaneous CO_2 Capture in fluidized Bed at Atmospheric Pressure: The Effect of Inorganic Species. 1. Literature Review and Comments, Ind. Eng. Chem. Res. *45,* 6137-6146

Corella J., Toledo J.M., Molina G., (2007), A Review on Dual fluidized-Bed Biomass Gasifiers, Ind. Eng. Chem. Res. 46, 6831-6839.

Dayton D., (2002), A review of the literature on catalytic biomass tar destruction; NREL/TP-510-32815.

De Diego L. F.,Garcia-Labiano F., Adanez J., Gayan P., Abad A., Corbella B.M., Palacio J.M., (2004), Development of Cu-based oxygen carriers for chemical-looping combustion, Fuel 83, 1749–1757.

Delgado J., Aznar M.P., Corella J., (1996), Calcined Dolomite, Magnesite, and Calcite for Cleaning Hot Gas from a fluidized Bed Biomass Gasifier with Steam: Life and Usefulness, Ind. Eng. Chem. Res. 35, 3637-3643.

Delgado, J.; Aznar, M.P.; Corella, J., (1997), Biomass Gasification with Steam in fluidized Bed: Effectiveness of CaO, MgO and CaO-MgO for Hot Raw Gas Cleaning. Ind. Eng. Chem. Res. 36, 1535- 1543.

Devi L., Ptasinski K. J., Janssen F.J.J.G., (2003), A review of the primary measures for tar elimination in biomass gasification processes, Biomass and Bioenergy 24, 125-140.

Dogan M., Posarac D., Grace J.R., Adris,A.M., Lim C.J., (2003), Modeling of autothermal steam methane reforming in a fluidized bed membrane reactor, International Journal of Chemical Reactor Engineering 1 A2, 1-14.

Dou B., Zhang M., Gao J., Shen W., Sha X., (2002), High-temperature removal of NH_3, organic sulfur, HCl, and tar component from coal-derived gas, Ind. Eng. Chem. Res. 41, 4195–4200.

Feng B., Liu W., Li X., An H., (2006), Overcoming the Problem of Loss-in-Capacity of Calcium Oxide in CO2 Capture, Energy Fuels 20, 2417-2420.

Feng B., An H., Tan E., (2007), Screening of CO_2 adsorbing materials for zero emission power generation systems, Energy and Fuels 21, 426-434.

Florin N.H., Harris A.T., (2008), Enhanced hydrogen production from biomass with in situ carbon dioxide capture using calcium oxide sorbents, Chemical Engineering Science 63, 287-316.

Gayàn P., de Diego L.F., Garcıa-Labiano F., Adanez J., Abad A., Dueso C., (2008), Effect of support on reactivity and selectivity of Ni-based oxygen carriers for chemical-looping combustion, Fuel 87, 2641–2650.

Gibilaro, (2001), Fluidization-dynamics, Butterworth Heinemann publication.

Gupta H., Fan L. S., (2002), Carbonation-calcination cycle using high reactivity calcium oxide for carbon dioxide separation from flue gas, Industrial and Engineering Chemical Research 41, 4035-4042.

Hamel S., Hasselbach H., Weil S., Krumm W., (2005), Autothermal two-stage gasification of low-density waste-derived fuels, Energy 32, 95-107.

Harrison D.P., (2008), Sorption-Enhanced Hydrogen Production: A Review, Ind. Eng. Chem. Res. 47, 6486-6501.

Hepola J., Simell P, (1997a), Sulphur poisoning of nickel-based hot gas cleaning catalysts in synthetic gasification gas I. Effect of different process parameters, Appl. Catal. B 14, 287–303.

Hepola J., Simell P., (1997b), Sulphur poisoning of nickel-based hot gas cleaning catalysts in synthetic gasification gas II. Chemisorption of hydrogen sulphide, Appl. Catal. B 14, 305–321.

Hofbauer H., (2009), Gas Production for Polygeneration Plants, Proceedings of 1st International Conference on Polygeneration Strategies, Vienna, 1-4 September 2009, Vienna.

Hughes R.W., Lu D., Anthony L.J., Wu Y., (2004), Improved long-term conversion of limestone-derived sorbents for in situ capture of CO_2 in a fluidized bed combustor, Ind. Eng. Chem. Res. 43, 5529-5539.

Intergovernmental Panel on Climate Change Special Report. Carbon Dioxide Capture and Storage, Technical Summary, 2005. Available online _http://www.ipcc.ch/

Iyer M.V., Gupta H., Sakadjian B.B., Fan L.-S., (2004), Multicycle study on the simultaneous carbonation and sulfation of high-reactivity CaO, Industrial and Engineering Chemistry Research 43, 3939-3947.

Jerndal E., Mattisson T., Lyngfelt A., (2006), Thermal analysis of chemical looping combustion, Chem. Eng. Res. Des. 84, 795-806.

Johnsen K., Ryu H.J., Grace J.R., Limb C.J., (2006), Sorption-enhanced steam reforming of methane in a fluidized bed reactor with dolomite as CO_2-acceptor, Chemical Engineering Science 61, 1195-1202.

Kinoshita C.M., Wang Y., Zhou J., (1994), Tar formation under different biomass gasification conditions, Journal of Analytical and Applied Pyrolysis 29, 169-81.

Kronberger B., Loffler G., Hofbauer H., (2005) Simulation of Mass and Energy Balances of a Chemical-Looping Combustion System, Clean Air: Int J En Clean Environ 6, 1-14.

Labiano G.F., Abad A., de Diego L.F., Gayan P., Adanez J., (2002), Calcination of calcium-based sorbents at pressure in a broad range of CO2 concentrations, Chem. Eng. Sci. 57, 2381-2393.

Li C., Suzuki K., (2009), Tar property, analysis, reforming mechanism and model for biomass gasification-An overview, Renewable and Sustainable Energy Reviews 13, 594-604.

Li Z., Cai N., Yang J., (2006a), Continuous Production of Hydrogen from Sorption-Enhanced Steam Methane Reforming in Two Parallel Fixed-Bed Reactors Operated in a Cyclic Manner, Ind. Eng. Chem. Res. 45, 8788-8793.

Li Z., Cai N., Huang Y., (2006b), Effect of preparation temperature on cyclic CO_2 capture and multiple carbonation-calcination cycles for a new Ca-based CO_2 sorbent, Ind. Eng. Chem. Res. 45, 1911-1917.

Lin S.-Y., Suzuki Y., Hatano H., Harada M., (2001), Hydrogen production from hydrocarbon by integration of water-carbon reaction and carbon dioxide removal, Energy Fuels 15, 339.

Lin S.-Y., Suzuki Y., Hatano H., Harada M., (2002), Developing an innovative method, HyPr-RING, to produce hydrogen from hydrocarbons, Energy Convers. Manage 43, 1283.

Lopez O. A., Harrison D.P., (2001), Hydrogen production using sorption-enhanced reaction, Ind. Eng. Chem. Res. 40, 5102-5109.

Lu D.Y., Hughes R.W., Anthony E.J., (2008), Ca-based sorbent looping combustion for CO2 capture in pilot-scale dual fluidized beds, Fuel Processing Technology 89, 1386-1395.

Lu H., Reddy E.P., Smirniotis P.G., (2006), Calcium Oxide Based Sorbents for Capture of Carbon Dioxide at High Temperatures, Ind. Eng. Chem. Res. 45, 3944-3949.

Lyngfelt A., Leckner B., Mattisson T., (2001), A fluidized-bed combustor process with inherent CO_2 separation; application of chemical looping combustion, Chem. Eng. Sci. 56, 3101-13.

Ma L., Verelst H., Baron G.V., (2005), Integrated high temperature gas cleaning: Tar removal in biomass gasification with a catalytic filter, Catalysis Today 105, 729–734.

Manovic V., Anthony E.J., Loncarevic D., (2009), CO_2 looping cycles with CaO-based sorbent pre-treated in CO_2 at high temperature, Chemical Engineering Science 64, 3236-3245.

Marquard-Möllenstedt T., Sichler P., Specht M., Michel M., Berger R., Hein K.R.G., Höftberger E., Rauch R., Hofbauer H., (2004) Proceedings of 2nd World Conference on Biomass for Energy, Industry and Climate Protection, Rome, Italy, 10-14 May 2004.

Marquard-Moellenstedt T., Specht M., Zuberbuehler U., Koppatz S., Pfeifer C., Rauch R., Soukup G., Hofbauer H., Koch M., (2008), Transfer of the absorption enhanced reforming (AER)-process from the pilot scale to an 8 mwth gasification plant in Guessing, Austria, Proceedings of the 14th European Conference on Biomass for Energy Industry and Climate Protection, Valencia, Spain, 02-06 June 2008.

Martavaltzi C.S., Lemonidou A.A., (2008a), Development of new CaO based sorbent materials for CO_2 removal at high temperature, Microporous and Mesoporous Materials 110, 119-127.

Martavaltzi C.S., Lemonidou A.A., (2008b), Parametric Study of the $CaO/Ca_{12}Al_{14}O_{33}$ Synthesis with Respect to High CO2 Sorption Capacity and Stability on Multicycle Operation, Ind. Eng. Chem. Res. 47, 9537-9543.

Minchener A. J., (2005), Coal gasification for advanced power generation, Fuel 84, 2222-2235.

Nordgreen T., Liliedahl T., Sjostrom K., (2006), Metallic iron as a tar breakdown catalyst related to atmospheric, fluidized bed gasification of biomass, Fuel 85, 689-694.

Ohtsuka Y., Tamai Y., Tomita A., (1987), Iron-catalyzed gasification of brown coal at low temperatures, Energy Fuels 1, 32-36.

Ohtsuka Y., Asami K., (1997), Highly active catalysts from inexpensive raw materials for coal gasification, Catal. Today 39, 111-125.

Olivares A., Aznar M.P., Caballero M.A., Gil J., Frances E., Corella J., (1997), Biomass gasification: Produced gas upgrading by in-bed use of dolomite. Ind. Eng. Chem. Res. 36, 5220-5226.

Orio A., Corella J., Narvaez I., (1997), Performance of different dolomites on hot raw gas cleaning from biomass gasification with air, Ind. Eng. Chem. Res. 36, 3800-3808.

Pfeifer C., Puchner B., Hofbauer H., (2009a), Comparison of dual fluidized bed steam gasification of biomass with and without selective transport of CO_2, Chemical Engineering Science 64, 5073-5083.

Pfeifer C., (2009b), Experiences and results derived from the dual fluidized bed gasifier at Vienna University of Technology, Proceedings of 1th International Conference on Polygeneration Strategies, Vienna, 1-4 September 2009, Vienna.

Rao, A.B., Rubin, E.S., (2002), A technical, economic and environmental assessment of amine-based CO_2 capture technology for power plant greenhouse gas control, Environmental Science and Technology 36, 4467-4475.

Rapagnà S., Jand N., Foscolo P.U., (1998), Catalytic gasification of biomass to produce hydrogen rich gas, Int. J. Hydrogen Energy 23, 551-557.

Rapagnà S., Jand N., Kiennemann A., Foscolo P.U., (2000), Steam-gasification of biomass in a fluidized-bed of olivine particles, Biomass and Bioenergy 19, 187-197.

Rapagnà S., Gallucci K., Di Marcello M., Foscolo P.U., Nacken M., Heidenreich S., In situ catalytic ceramic candle filtration for tar reforming and particulate abatement in a fluidized-bed biomass gasifier, Energy Fuels 23, 3804–3809.

Reddy E.P., Smirniotis P.G., (2004), High-Temperature Sorbents for CO_2 Made of Alkali Metals Doped on CaO Supports, J. Phys. Chem. B 108, 7794-7800.

Satrio J.A., Shanks B.H., Wheelock T.D., (2005), Development of a Novel Combined Catalyst and Sorbent for Hydrocarbon Reforming, Ind. Eng. Chem. Res. 44, 3901-3911.

Satrio J.A., Shanks B.H., Wheelock T.D., (2007), A combined catalyst and sorbent for enhancing hydrogen production from coal or biomass, Energy Fuels 21, 322-326.

Silaban, A., Harrison, D.P., (1995), High temperature capture of carbon dioxide: characteristics of the reversible reaction between CaO(s) and CO_2(g), Chemical Engineering Communication 137, 177-190.

Silaban, A., Narcida, M., Harrison, D.P., (1996), Characteristics of the reversible reaction between $CO_{2(g)}$ and calcined dolomite, Chemical Engineering Communications 146, 149-162.

Sun P., Grace J.R., Lim C.J., Anthony E.J., (2007), Removal of CO_2 by calcium-based sorbents in the presence of SO2, Energy Fuels 21, 163-170.

Sun P., Grace J.R., Lim C.J., Anthony E.J., (2008), Investigation of Attempts to Improve Cyclic CO_2 Capture by Sorbent Hydration and Modification, Ind. Eng. Chem. Res. 47, 2024-2032.

Sutton D., Kelleher B., Ross J.R.H., (2001), Review of literature on catalysts for biomass gasification, Fuel Processing Technology 72, 155-173.

Torres W., Pansare S.S., Goodwin J.G. Jr., (2007), Hot Gas Removal of Tars, Ammonia, and Hydrogen Sulfide from Biomass Gasification Gas, Catalysis Reviews 49, 407 - 456.

Turn S., Kinoshita C., Zhang Z., Ishimura D., Zhou J., (1988), An experimental investigation of hydrogen production from biomass gasification, Int. J. of Hydrogen Energy 23, 641-648.

USDoE and Gasification Technology Council, World Gasification Database 2001.

van der Drift, A., van der Meijden, C. M., Boerrigter, H., (2005), MILENA gasification technology for high efficient SNG production from biomass. Proceedings of the 14th European Conference on Biomass for Energy Industry and Climate Protection, Paris, France, 17-21 October 2005.

Wu S.F., Beum T.H., Yang J.I., Kim J.N., (2007), Properties of Ca-Base CO_2 Sorbent Using Ca(OH)2 as Precursor, Ind. Eng. Chem. Res. 46, 7896-7899.

Wu S.F., Li Q.H., Kim J.N., Yi K.B., (2008), Properties of a Nano CaO/Al_2O_3 CO_2 Sorbent, Ind. Eng. Chem. Res. 47, 180-184.

Xu G., Murakami T., Suda T., Matsuzawa Y., Tani H., (2006), Ind. Eng. Chem. Res. 45, 2281-2286.

Yi K.B., Harrison D.P., (2005), Low Pressure Sorption Enhanced Hydrogen Production, Ind. Eng. Chem. Res. 44, 1665.

Yong, Z., Mata, V., Rodrigues, A.E., (2001), Adsorption of carbon dioxide onto hydrotalcite-like compounds (HTLcs) at high temperatures, Industrial and Engineering Chemistry Research 40, 204-209.

Yong Z., Mata V., Rodrigues A.E., (2002), Adsorption of carbon dioxide at high temperature - a review, Separation and Purification Technology 26, 195-205.

Yu Q., Brage C., Chen G., Sjostrom K., (1997), Temperature impact on the formation of tar from biomass pyrolysis in a free-fall reactor. Journal of Analytical and Applied Pyrolysis 40-41, 481-489.

Zhao H., Draelants D.J., Baron G.V., (2000), Preparation and characterisation of nickel-modified ceramic filters, Catalysis Today 56, 229–237.

CHAPTER 2

LABORATORY TESTS OF A BIOMASS GASIFICATION PROCESS

Abstract: *Laboratory tests of a biomass gasification process have been investigated at real process conditions by means of a catalytically activated filter element inserted in the freeboard of a pilot plant fluidized bed steam gasifier, where olivine is located. This work allows to understand the complex problems associated with biomass gasification with respect to process conditions and in-bed additives, in terms of product gas (amount and composition), tar and char content (amount) in the product gas.*

1. Introduction

In this Chapter, some experimental tests of biomass gasification at real process conditions are reported. The purpose of this work is to place emphasis on quantification and understanding of complexity of a biomass gasification process at real conditions, how introduced in the objectives of the thesis. The obtained data represent the starting point from which further investigation in smaller scale and in simulated conditions will depart. A crucial step on enhancing the applicability of biomass gasification processes and to render it suitable for renewable hydrogen production, is the efficiency on tar removing from the product gas. The effect of the addition of a nickel additive in the gasifier, impregnated in a standard hot gas filter element, is investigated as a primary method to perform an efficient tar abatement process.

Filter elements have been prepared by Pall Filtersystems GmbH, by impregnation of silicon carbide-based filter elements, in order to provide filter elements for catalytic tar removal from biomass-derived syngas. Some works of Pall research group on this field (preparation, characterization and catalytic tests of filter candle elements) have been published recently [Nacken *et al.,* 2007a, 2007b, 2009]. In the Dutch city of Buggenum, one of the world's largest coal gasification plant for electricity generation (a 253 MWe IGCC power plant), a key part of the gas cleaning equipment of the plant is a Pall ceramic hot gas filter system [Heidenreich *et al.,* 2004].

2. Experimental

A schematic model of the laboratory gasification plant is reported in Figure 1a. It is composed of a fluidized bed gasifier with an internal diameter of 0.11 m, externally heated by means of a 6 kW electric furnace. A cylindrical (non catalytic or catalytic) filter candle (0.4 m long and 0.06 m outside diameter) may be inserted in the freeboard (Figure 1b). The biomass is introduced from the top of the bed by means of a continuous feeder unit. A cyclone and a ceramic filter are connected to the gasifier outlet to remove elutriated solid particles, such as ash (when the filter candle in the reactor freeboard is absent). Three condensers in series are used to separate condensable components. Online gas analyzers (IR and TCD), for the volume composition detection of CO, CO_2, CH_4, H_2 and NH_3 are fed at cold gas rates of 1.5 L min^{-1} and output to a PC where the experimental data are stored as functions of time. Temperatures were measured in various plant locations by means of 5 thermocouples; the pressure drop though the candle and the fluidized bed, as well as the pressure into the gasifier were monitored by means of water manometers. Steam was generated from liquid water fed by means of a peristaltic pump to a cylindrical, stainless steel evaporator placed in a 2.4 kW electric furnace. The water flow rate was controlled by a peristaltic pump.

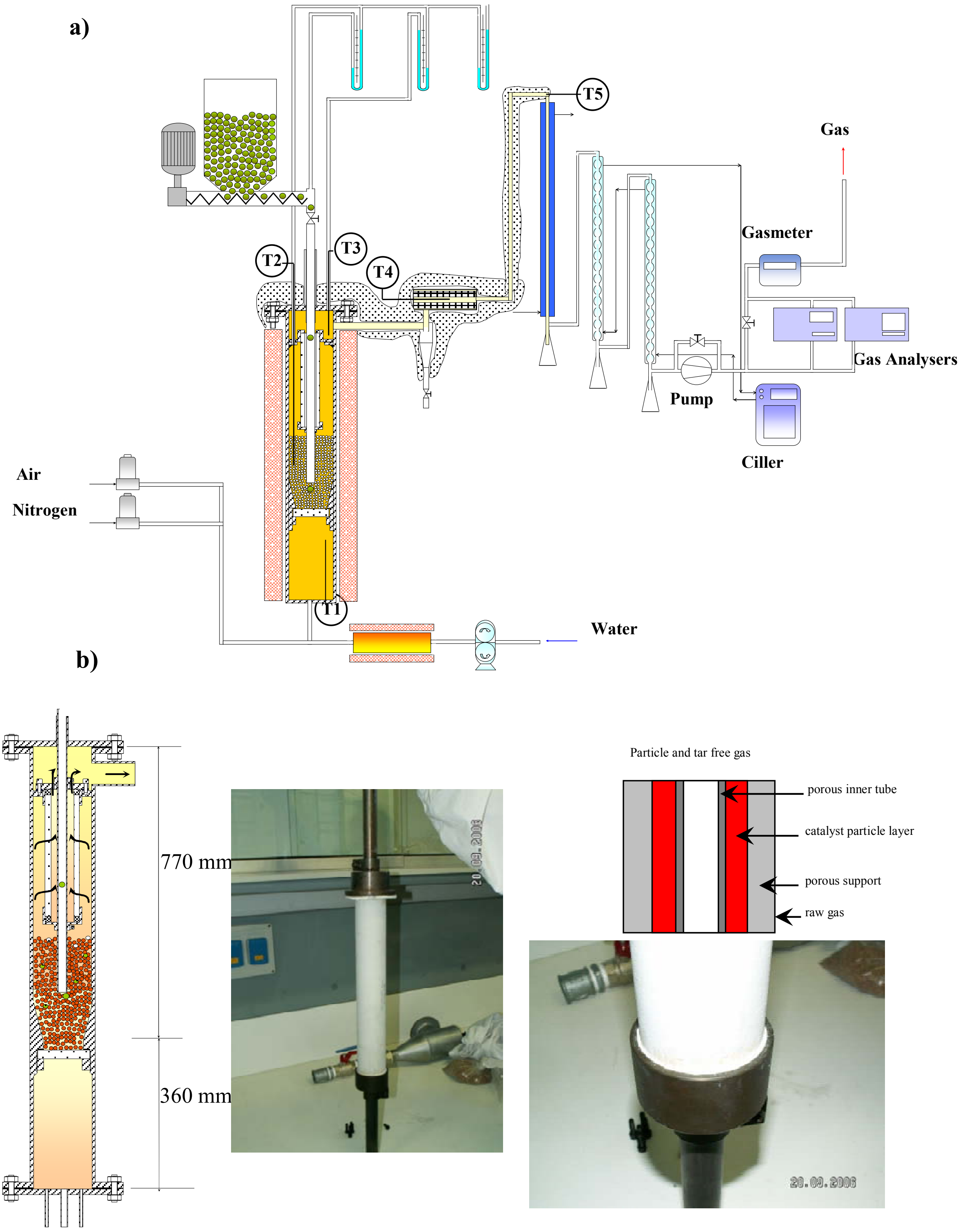

Figure 1: Schematic model of the laboratory gasification plant (a), and some particular of catalytic ceramic filter (b).

The fluidized bed consisted of 3 kg of 0.48 mm olivine particles of density 2500 kg/m^3; olivine is well known in literature having good resistance to mechanical erosion in the fluidized bed and is catalytically active with regard to the chemical conversion of char (see references in Chapter 1).

For each experimental trial, the bed was first fluidized with air and heated to the chosen operating temperature (700-900 °C); the fluidising gas was then switched to a nitrogen-steam mixture. The gasification process was then initiated by feeding continuously the biomass particles; almond shells with average particle diameter of 1.1 mm are utilized, and fuel gas production and condensate yield are measured. The tar content was determined by means of TOC analysis of the condensate. The carbon quantity detected has been converted in grams of tar by assuming naphthalene as tar key component. At the end of the gasification runs the amount of char accumulated in the gasifier was determined by measuring the amount of CO and CO_2 produced by feeding a known air flow rate to the reactor to burnt-off it.

Before starting the gasification test, during the reactor heat-up phase, a gas stream containing about 3.5% by volume of H_2 in N_2 has been used, to reduce the catalyst for test T3 (see Section 4). Proximate and elemental composition of biomass used in gasification tests are reported in Table 1.

	as received	**dry**	**dry-ash-free (daf)**
Moisture (wt%)	7.9	-	-
Ash (wt%)	1.3	1.4	-
Volatile matter (wt%)	72.5	78.7	79.8
Elemental composition (wt%)			
C	47.0	51.0	51.7
H	5.5	6.0	6.1
O	37.6	40.8	41.4
N	0.69	0.75	0.76
LHV (kJ/kg)	18350		
Cellulose (wt%)	29		
Hemicellulose (wt%)	28		
Lignin (wt%)	35		
Density (kg/m^3)	1200		

Table 1: Biomass chemical composition and physical properties

3. Data analysis

In this section detailed calculations techniques that have been used in biomass gasification tests are described.

3.1. Inlet flow rates and compositions

The measured inlet quantities are the *g/min* of biomass, *g/min* of water, and *L/h* (at ambient temperature) of nitrogen. From these data, the following parameters have been calculated (Eqs. 1-7, see also the legend at the end of this Chapter):

biomass :

$$\left(\frac{g}{\min}\right)_{daf} = \left(\frac{g}{\min}\right)_{ar} \cdot \left[1-\left(y_{moisture}+y_{ash}\right)\right] \tag{1}$$

water:

$$\left(\frac{g}{\min}\right)_{w} = \left(\frac{g}{\min}\right)_{pump} + \left[\left(\frac{g}{\min}\right)_{ar} \cdot \left(y_{moisture}\right)\right] \tag{2}$$

(steam)/(biomass dry) (S/B)

$$\frac{\left(\frac{g}{\min}\right)_{w}}{\left(\frac{g}{\min}\right)_{ar} \cdot \left(1-y_{moisture}\right)} \tag{3}$$

Carbon:

$$\left(\frac{g}{\min}\right)_{C} = \left(\frac{g}{\min}\right)_{daf} \cdot yC \tag{4}$$

Oxygen:

$$\left(\frac{g}{\min}\right)_{O} = \left(\frac{g}{\min}\right)_{daf} \cdot yO \tag{5}$$

Hydrogen:

$$\left(\frac{g}{\min}\right)_{H} = \left(\frac{g}{\min}\right)_{daf} \cdot yH \tag{6}$$

Nitrogen (in the biomass):

$$\left(\frac{g}{\min}\right)_{N} = \left(\frac{g}{\min}\right)_{daf} \cdot yN \tag{7}$$

3.2. Conversion calculations

The readily available experimental data in the reactor and at the reactor exit are:

- process temperature;
- total volumetric flow exiting from the reactor;
- % volume of H_2, CO, CO_2, CH_4 at the reactor exit;
- g of condensed phase collected;

From these data, the following parameters have been calculated (Eqs. 8-18):

H_2

$$\left(\frac{mol}{\min}\right)_{H2} = y_{H2} \cdot \left(\frac{mol}{\min}\right)_{gas\ dnf} \tag{8}$$

CO

$$\left(\frac{mol}{\min}\right)_{CO} = y_{CO} \cdot \left(\frac{mol}{\min}\right)_{gas\ dnf} \tag{9}$$

CO_2

$$\left(\frac{mol}{\min}\right)_{CO2} = y_{CO2} \cdot \left(\frac{mol}{\min}\right)_{gas\ dnf} \tag{10}$$

CH_4

$$\left(\frac{mol}{\min}\right)_{CH4} = y_{CH4} \cdot \left(\frac{mol}{\min}\right)_{gas\ dnf} \tag{11}$$

steam

$$\frac{\left(\frac{g}{\min}\right)_{w} \cdot \left(1 - X_{water}\right)}{m.w._{H2O}} \tag{12}$$

water conversion *(X_{water})*

$$\frac{\left(\frac{g}{\min}\right)_{w} \cdot t_{test} - \left(g_{(water+naph)} - g_{(naph)}\right)}{\left(\frac{g}{\min}\right)_{w} \cdot t_{test}} \tag{13}$$

gas yield, Nm^3/kg daf

$$\frac{\left(\frac{NL}{\min}\right)_{gas\ dnf}}{\left(\frac{g}{\min}\right)_{daf}} \tag{14}$$

tar content, g/Nm^3 dnf

$$\frac{g_{(naph)}}{\left(\frac{NL}{\min}\right)_{gas\ dnf} \cdot t_{test}} \cdot 10^{-3} \tag{15}$$

residual char, g/kg daf

$$\frac{g_{char}}{\left(\frac{g}{\min}\right)_{daf} \cdot t_{test}} \cdot 10^{-3} \tag{16}$$

Carbon conversion, %

$$\frac{\left[\left(\frac{mol}{\min}\right)_{CO} + \left(\frac{mol}{\min}\right)_{CO2} + \left(\frac{mol}{\min}\right)_{CH4}\right] \cdot m.w._{C}}{\left(\frac{g}{\min}\right)_{C}} \cdot 100 \tag{17}$$

WGSR experimental ratio

$$\frac{\left(\frac{mol}{\min}\right)_{H2} \cdot \left(\frac{mol}{\min}\right)_{CO2}}{\left(\frac{mol}{\min}\right)_{CO} \cdot \left(\frac{mol}{\min}\right)_{steam}} \tag{18}$$

As already mentioned, tar concentration, $(g/L)_C$ in the condensed phase, has been detected by a Total Organic Carbon analyser (Dr. Lange kit) and has been referred to naphthalene (Eq. 19):

naphthalene in the condensed phase (grams)

$$L_{condensed} \cdot \left(\frac{g}{L} \right)_C \cdot \frac{m.w._{(naph)}}{10 \cdot m.w._{(C)}} \tag{19}$$

4. Results of gasification tests

Four different experimental trials have been performed:

Test 1- no filter candle in the gasifier;

Test 2- filter candle in the gasifier;

Test 3- catalytic filter candle in the gasifier, not pre-reduced;

Test 4- catalytic filter candle in the gasifier, pre-reduced.

Tests without the catalytic candle have lasted about half hour, whereas that with the catalytic filter candle has been prolonged to record the effect of the progressive behaviour of nickel.

	T1	T2	T3
reactor configuration	no filter candle in the gasifier	filter candle in the gasifier	catalytic filter candle in the gasifier, not pre-reduced
Biomass in (g/min) ar	8.53	8.48	8.48
Steam in (g/min)	8.37	8.37	8.37
Nitrogen in (ambient L/min)	5.7	5.6	5.7
reactor outlet temperature (°C)	785	720	710
gasifier bed temperature (°C)	843	840	849
steam/biomass dry	1.15	1.16	1.16
water conversion %	14.98	22.25	33.26
gas yield, Nm^3 dry/kg daf	1.39	1.39	1.72
tar content, g/Nm^3 dry	1.10	1.10	0.48
char residue, g/kg daf	98.11	85.71	54.18
carbon conversion %	75.02	77.65	88.17
H_2 (vol% dry gas, N_2 free)	43.50	44.00	50.50
CO (vol% dry gas, N_2free)	24.50	26.00	25.00
CO_2 (vol% dry gas, N_2free)	20.00	20.00	19.00
CH_4 (vol% dry gas, N_2free)	8.00	8.00	5.50
$[H_2][CO_2]/[CO][H_2O]$	0.38	0.39	0.64

Table 2: Experimental results for biomass gasification tests T1-T3

reactor configuration	catalytic filter candle in the gasifier, pre-reduced					
Periods (min)	I (12-22)	II (22-42)	III (42-60)	IV (60-80)	V (80-100)	VI (100-120)
Biomass in (g/min) ar	8.48	8.48	8.48	8.48	8.48	8.48
Steam in (g/min)	6.00	6.00	6.00	8.67	8.67	8.67
Nitrogen in (ambient L/min)	5.7	5.7	5.7	5.7	5.7	5.7
reactor outlet temperature (°C)	706	701	704	714	717	715
gasifier bed temperature (°C)	868	873	885	895	890	885
steam/biomass dry	0.77	0.77	0.77	1.11	1.11	1.11
water conversion %	45.40	40.79	43.10	36.20	32.60	29.40
gas yield, Nm^3 dry/kg daf	1.85	1.67	1.61	1.72	1.76	1.76
tar content, g/Nm^3 dry	0.29	0.43	0.51	0.57	0.57	0.55
char residue, g/kg daf	77.92	77.92	77.92	77.92	77.92	77.92
carbon conversion %	85.1	83.0	84.4	87.1	88.4	87.8
H_2 (vol% dry gas, N_2 free)	55.55	52.12	49.37	51.1	51.5	51.8
CO (vol% dry gas, N_2 free)	26.82	26.97	27.23	23.7	23.1	22.5
CO_2 (vol% dry gas, N_2 free)	15.68	16.65	17.37	19.5	19.8	20.1
CH_4 (vol% dry gas, N_2 free)	1.94	4.26	6.03	5.7	5.6	5.6
$[H_2][CO_2]/[CO][H_2O]$	1.03	0.88	0.87	0.78	0.77	0.77

Table 3: experimental results for biomass gasification test T4

The experimental results are summarised in Table 2 for Tests 1-3, and Table 3 for Test T4, where the overall duration of test has been divided in 6 periods. In Table 3 the residual char is attributed proportionally to each test according to the corresponding time interval. Moreover, Test 4 (catalytic filter candle in the gasifier, pre-reduced) has been carried out increasing the steam fed to the reactor for periods IV, V and VI, where results become similar to those obtained in Test 3 (catalytic filter candle in the gasifier, not pre-reduced).

It is clear that a significant improvement of all relevant performance indicators result from the use of the catalytic filter candle (see Figure 2 for (Nm^3 gas yield)/(kg biomass daf) parameter). These data are in agreement with previous works on application of metal doped catalytic filter elements ([Zhao *et al.,* 2000], [Ma *et al.,* 2005, 2008], [Engelen *et al.,* 2003], [Toledo *et al.,* 2006]). The ratio $[H_2][CO_2]/[CO][H_2O]$ is considerably higher in presence of nickel in the gasifier, highlighting the role of this metal in catalysing not only tar reforming reactions, but also water-gas shift reaction (see also Chapter 5). In particular for tests T1-T3, an opposite relation is observed between product gas and residual char, as expected by mole balance of the system; also water conversion is inversely proportional to char yield, whereas increase by increasing carbon conversion. A slightly higher amount of solid carbon is obtained in the T4 test, where the mean value is calculated on the basis of three periods (equal to half the entire test) with a lower steam/biomass ratio, evidencing that this parameter has a positive effect on char gasification and consequently on dry gas yield, other conditions being equal. On the other hand, increasing the steam/biomass ratio increases the tar content in the product gas, probably as a result of partial nickel oxidation, or increased face filtration velocity (reduced contact time).

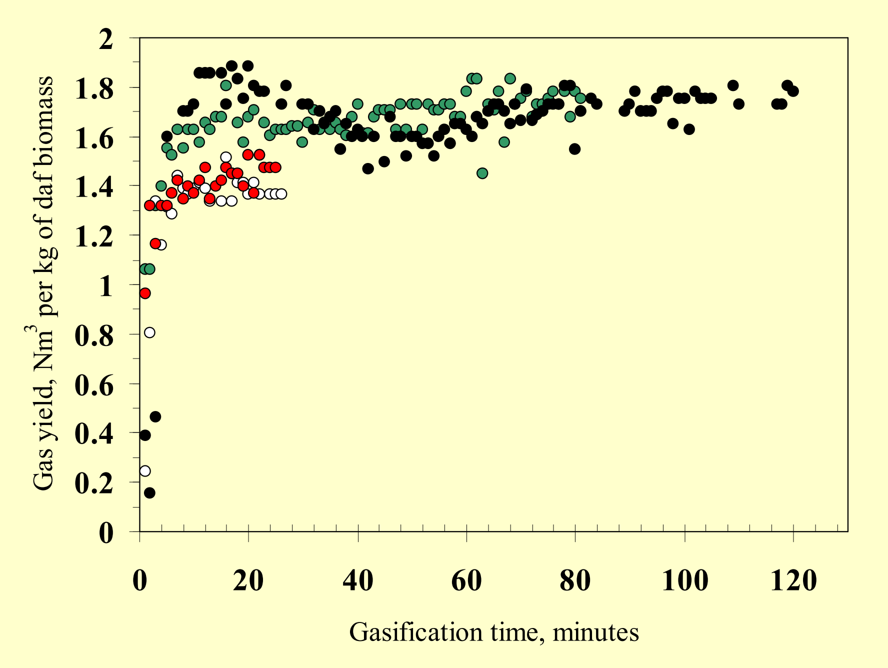

○ no filter candle in the gasifier
🔴 filter candle in the gasifier
🟢 catalytic filter candle in the gasifier, not pre-reduced
● catalytic filter candle in the gasifier, pre-reduced

Figure 2: (Nm^3 gas yield)/(kg biomass daf) produced for tests T1-T4: the enhancing effect of nickel as additive for tar abatement

The exiting concentrations of H_2, CO, CO_2 and CH_4 for T3 and T4 tests (catalytic candle with and without pre-reduction, respectively) are shown in Figure 3. Both experiments show very similar results after one hour on test: as a matter of fact, during the first hour on test, the catalytic filter candle not previously reduced is activated in the reactive flow atmosphere. The partial deactivation observed for the pre-reduced filter candle could be probably due to hydrogen sulphide, which is present in the producer gas. H_2S does not cause irreversible deactivation of the catalytic filter element, although it certainly reduces its activity [Ma *et al.,* 2005].

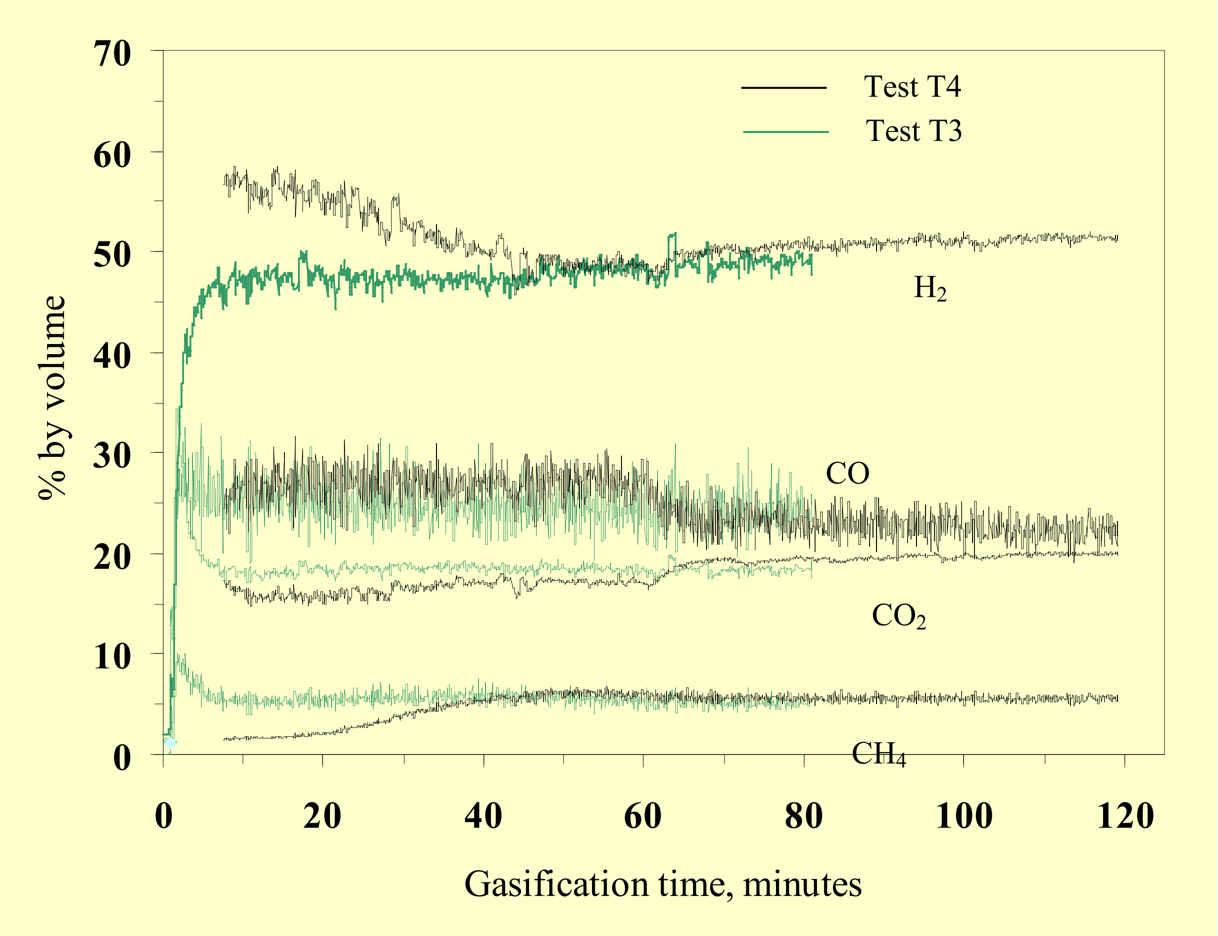

Figure 3: % composition of H_2, CO, CO_2 and CH_4 for T3 and T4 tests (catalytic candle with and without pre-reduction, respectively)

5. Conclusions

The biomass gasification tests reviewed in this Chapter have been performed with the aim to offer a practical support for further investigations on the role of catalytic materials to enhance the quality of fuel gas obtained at real process conditions. Different performance indicators have been proposed and calculation methods have been shown in details in order to characterise this complex process. Nickel, impregnated in a hot filter candle inserted in the gasifier freeboard, has been found to successfully perform tar abatement, even if H_2S has been recognised as a deactivation agent for this catalyst.

Notation

daf:	dry and ash free (referred to biomass);
dnf:	dry and nitrogen free (referred to product gas)
ar:	as received;
y:	weight (referred to biomass) and molar (referred to gases) fraction;
$\left(\frac{mol}{\min}\right)_{gas\ dnf}$:	product gas (H_2+CO+CO_2+CH_4) dry and nitrogen free
$\left(\frac{g}{\min}\right)_{pump}$:	water fed by peristaltic pump
$\left(\frac{g}{\min}\right)_{w}$:	total water fed (peristaltic pump + % moisture in biomass)
$m.w._C$	molecular weight of carbon
$m.w._{H2O}$	molecular weight of water
t_{test}:	time (minutes) referred to test period
$g_{(water+naph)}$:	collected grams of condensed phase (referred to water + naphthalene)
$g_{(naph)}$:	grams of naphthalene in the condensed phase
$m.w._{(naph)}$:	molecular weight of naphthalene (128 Da.)
$m.w._{(C)}$:	molecular weight of carbon contained in naphthalene (120 Da.)
$L_{condensed}$:	liters of condensed phase collected at the end of each test (or period)

Bibliography

Engelen K., Zhang Y., Draelants D.J., Baron G.V., (2003), A novel catalytic filter for tar removal from biomass gasification gas: Improvement of the catalytic activity in presence of H2S, Chem. Eng. Sci. 58, 665–670.

Heidenreich S., Wolters C., (2004), Hot gas filter contributes to IGCC power plant’s reliable operation, Filtration and Separation 41, 22-24.

Nacken M., Ma L., Engelen K., Heidenreich S., Baron G.V., (2007a), Development of a Tar Reforming Catalyst for Integration in a Ceramic Filter Element and Use in Hot Gas Cleaning, Ind. Eng. Chem. Res. 46, 1945–1951.

Nacken M., Heidenreich S., Hackel M., Schaub G., (2007b), Catalytic activation of ceramic filter elements for combined particle separation, NOx removal and VOC total oxidation Appl. Catal. B: Environ. 70, 370–376.

Nacken M., Mab L., Heidenreich S., Baron G.V., (2009), Performance of a catalytically activated ceramic hot gas filter for catalytic tar removal from biomass gasification gas, Applied Catalysis B: Environmental 88, 292–298.

Ma L., Verelst H., Baron G.V., (2005), Integrated high temperature gas cleaning: Tar removal in biomass gasification with a catalytic filter, Catalysis Today 105, 729-734.

Ma L., Baron G.V., (2008), Mixed zirconia–alumina supports for Ni/MgO based catalytic filters for biomass fuel gas cleaning, Powder Technology 180, 21–29.

Toledo J. M., Corella J., Molina G., (2006), Catalytic hot gas cleaning with monoliths in biomass gasification in fluidized beds. 4. Performance of an advanced, second-generation, two-layers-based monolithic reactor. Ind. Eng. Chem. Res. 45, 1389–1396.

Zhao H., Draelants D.J., Baron G.V., (2000), Performance of a Nickel-Activated Candle Filter for Naphthalene Cracking in Synthetic Biomass Gasification Gas,_Ind. Eng. Chem. Res. 39, 3195–3201.

CHAPTER 3

HYDROCARBON STEAM REFORMING AND CO_2 CAPTURE IN A FLUIDIZED BED

Abstract: *This chapter proposes the study of catalytic steam reforming of model compounds of a biomass gasification process, with simultaneous CO_2 capture by means of calcined dolomite; CH_4, toluene and 1-methyl naphthalene (1-Mn) have been chosen as biomass gasification key primary products. A commercial nickel catalyst has been used as a catalyst for steam reforming, and dolomite as a sorbent for CO_2 capture. A bench-scale fluidized bed reactor has been utilized for the experimental tests. In this way, using conventional additives for the process, the potential of using dolomite to enhance tar and methane reforming reactions is investigated.*

1. Introduction

The previous chapter had showed the feasibility of a biomass gasification process carried out in a conventional way (temperature: 800°C, bed material: olivine, catalytic active phase: nickel), where the produced gas contains about 50% vol. of H_2. The aim of this chapter is to show experimentally the potential of using a dolomite sorbent to enhance tar and methane steam reforming reactions, and therefore the hydrogen content on the product gas, with the purpose of simulate the tar and methane abatement step of a biomass gasification process. Calcined dolomite has been used as in-bed CO_2 sorbent, and nickel has been adopted as catalyst for reforming reactions. These materials have been extensively described in the Introduction Chapter, and Table 1 summarizes the main advantages and inconveniences related to their utilization.

	Advantages	**Disadvantages**
Dolomite	• cheap and abundant	• soft (loss by attrition, high fines content in the product gas)
	• moderate activity in tar elimination	• deactivation by coke
Nickel catalysts	• cheap and easily available	• toxic: problems on contamination of both, char withdrawn from the bed and gasification product gas.
	• very active in tar reforming	• deactivation by coke

Table 1: Main advantages and inconveniences using nickel catalysts and dolomite.

On development of such a laboratory small-medium scale research, the selection of the appropriated model tar compound is clearly the key step: a preliminary bibliographic study of real tar composition has been realized with this purpose. Steam reforming of model tarry compounds as toluene [Swierczynski *et al.*, 2007 and 2008], [Jess *et al.*, 1996], [Taralas *et al.*, 2003], phenol [Abu El-Rub *et al.*, 2008], [Polychronopoulou *et al.*, 2004 and 2006], naphthalene [Abu El-Rub *et al.*, 2008], [Devi *et al.*, 2005], [Jess *et al.*, 1996], 1-methyl naphthalene [Dou *et al.*, 2003], and benzene [Simmel *et al.*, 1997] (this is not considered a tar compound, but represents a stable aromatic structure noticeable in the rich in aromatics product gas of a gasification process) have been studied in the literature, but further investigations are necessary for a successful application of biomass-derived producer gas [Li *et al.*, 2008].

Monocyclic aromatic hydrocarbons are considered the most representative tar compounds, reaching 46% of overall biomass tar [Abu El-Rub *et al.*, 2004]. Two rings aromatic hydrocarbons represent about 28% of biomass tar [Abu El-Rub *et al.*, 2004]. So, the reactivity of about 75% of biomass tar can be studied by choosing the appropriate model tar compounds: in this work, toluene and 1-methyl naphthalene (1-Mn). For some applications, the quality of the syngas may be enhanced also by low methane content as required for product gas utilization and upgrading techniques (see Table 5 in Chapter 1 [Hofbauer, 2009]). Experimental tests of CH_4 steam reforming using calcium based in-bed CO_2 sorbent have been reported in published works [Johnsen *et al.*, 2006], [Zhen-shan Li *et al.*, 2006], [Satrio *et al.*, 2007]; in this work, the absorption behavior of dolomite has been investigated by performing up to twelve consecutive cycles of *in situ* CO_2 capture during methane reforming tests (at constant conditions through cycles). The variation of the CaO-to-C ratio, varying the entering methane flow (but keeping constant the total entering flow and the mass of in-bed dolomite and nickel catalyst) has been also investigated.

The results of methane, toluene and 1-methyl naphthalene steam reforming and water gas shift tests are therefore reported in this Chapter. The experiments have been carried out in a bench scale rig, with a fluidized bed inventory allowing for simultaneous hydrocarbons reforming and CO_2 sorption by means of a commercial nickel catalyst mixed with calcined dolomite. It is worth mentioning here that dolomite is known to have a catalytic activity in tar reforming [Delgado *et al.*, 1996 and 1997] [Corella *et al.*, 2004], [Orio *et al.*, 1997], and at the same time is a very attracting material to absorb CO_2 from syngas [Harrison, 2008] [Marquard-Möllenstedt *et al.*, 2004 and 2008] in its calcined form.

2. Experimental

2.1. Materials

The bed material used in this work allows both capturing CO_2 and performing the catalytic steam reforming of hydrocarbon model compounds. A commercial nickel catalyst (Johnson Matthey Plc) mixed with dolomite kindly provided by Pilkington (see Table 2 for elemental analysis and specific surface area of dolomite) have been used for this purpose. The use of a catalyst is essential because dolomite only has been found to be not active in catalysing methane and toluene reforming reactions in the temperature range of the process (630-650°C).

2.2. Reactivity tests: Bench-scale fluidized-bed experimental tests

The experiments for catalytic steam reforming of tar components and CO_2 capture were carried out using a bench scale fluidized bed rig (Figure 1).

	Fe	CaO	MgO
Elemental analysis (weight % of fresh dolomite)	0.01	30.39	20.56
Specific surface area of fresh dolomite	0.1 m^2/g		
Specific surface area of calcined dolomite*	15.2 m^2/g		
*at 850°C for 4h in fluidized bed			

Table 2: Elemental analysis of fresh dolomite and specific surface area of fresh and calcined dolomite.

A properly designed laboratory-scale quartz reactor (60 mm ID and 660 mm high), labelled (3) in Figure 1, has been utilised, encased in an electrically heated cylindrical furnace (2). The gas distributor plate, made of sintered quartz glass with sufficient pressure drop to assure an even gas flow, supports the bed material (4). An annular jacket where the reactants are mixed together and heated up to the reaction temperature surrounds the reactor wall. The entire apparatus has been conceived to carry out both gas and vapour reforming reactions, leading to a comprehensive understanding of methane and tar compounds steam reforming reactions that would take place in a CO_2 sorbent assisted biomass gasification process.

The whole test procedure includes 6 main steps:

1. pre-calcination of dolomite: the bed material (dolomite and catalyst) in the reactor is heated up to 850°C, with a heating rate of 10°C/min, under a total flow rate of 70NL/h of nitrogen;
2. catalyst reduction: the bed material is heated up to 850°C, with a heating rate of 10°C/min, in 10% H_2 in N_2 gaseous flow, with total flow rate of 66 NL/h;
3. steam reforming and water-gas shift: different tests have been carried out in this work (see Table 3 for experimental conditions). Tests T1-T3 refers to multicycle operations (see Section 2.6. for experimental details); tests T4-T6 to the variation of CaO-to-C ratio (see Section 2.7.); test T7 and T8 to toluene and 1-Mn reforming reactions (Section 2.3.); tests T9 and T10 to water-gas shift reaction (Section 2.5.);

4. calcination of dolomite after test: allows to quantify the CO_2 adsorbed at the end of steam reforming test. It has been carried out by using the same experimental conditions than those described in step 1;
5. combustion (and quantification) of carbon deposited during the test: at about 830°C, in a flow of 60 NL/h of nitrogen and 15 NL/h of air (4% O_2);
6. analysis of total organic carbon in the condensed phase: to detect liquid hydrocarbons eventually present in the reactor outlet stream.

The outlet gas stream, after rapid cooling and steam and vapours condensation and separation, is fed to the analytical section, where H_2, CO, CO_2 and CH_4 are measured on-line by an ABB gas analyser (acquisition time: 10 seconds, labelled 10 in Figure 1). In each test N_2 has been always added to the reactant gases at a fixed and known molar flow rate, so that to allow for the desired fluidization conditions and to provide a reference flow to evaluate the absolute yield of the reaction products.

Natural dolomite and commercial nickel catalyst have been crushed and sieved separately to obtain fractions with average diameter of 200 μm and 300 μm, respectively. The minimum fluidization velocity of dolomite and catalyst particle samples has been measured experimentally at ambient conditions according to a standardised method (bed pressure drop vs. superficial velocity profile): for the dolomite sample, with a density of 1490 kg/m^3, the measured minimum fluidization velocity in air is 3.2 cm/s, while for the catalyst sample the corresponding value is 3.9 cm/s. On the basis of these measurements it is expected that the bed remains well mixed during the experimental tests.

2.3. Tar steam reforming

On the left hand side of the schematic diagram in Figure 1, the tar model compound feeding system (labelled (1) in Figure 1) is shown: a nitrogen flow passes through a saturation unit (a heated flask), where the model tar compound (toluene or 1-Mn) is located. Figure 2 shows a detailed design of tar feeding system. A thermal fluid circulates between a thermostat and an annular jacket that surrounds completely a saturation unit (a flask where the model tar compound is located), to avoid cold points where hydrocarbons may condense before the gas outlet. A nitrogen flow is forced to bubble through the organic liquid in the heated flask and enters the reactor after saturation by passing through a short heated tube. An additional advantage of using this hydrocarbons feeding system is that solid (at ambient temperature) model tar compounds, as phenol or 2-methyl naphthalene, may be used, making possible to check the reactivity behaviour of a broad range of model tar compounds.

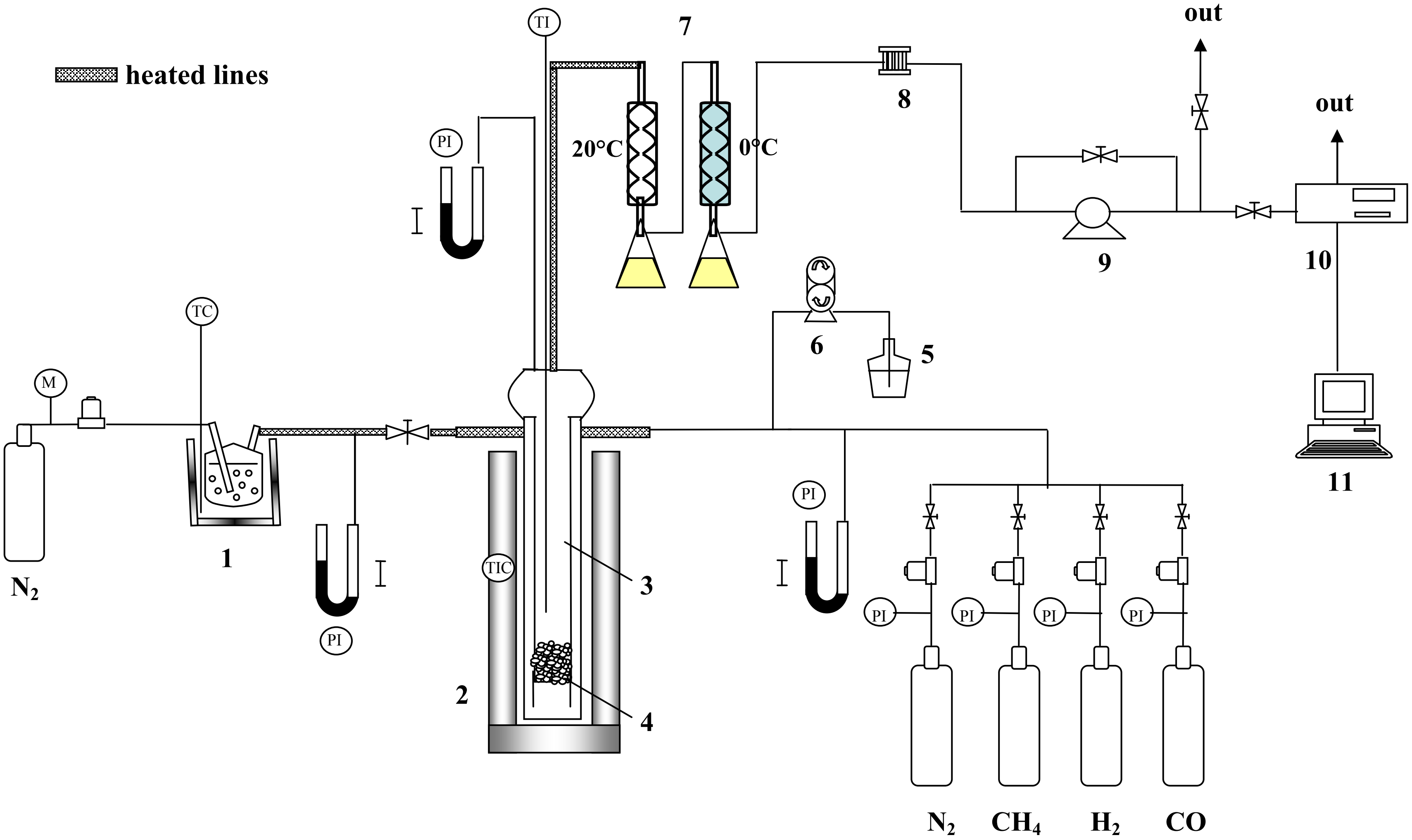

Figure 1: Schematic diagram of the experimental apparatus (fluidized bed reactor): 1, model tar compound saturator; 2, furnace; 3, quartz reactor; 4, catalyst bed; 5, water flask; 6, peristaltic pump; 7 water and tar condenser; 8, particle filter; 9, pump; 10, analysis system; 11, acquisition system; TI, temperature indicator; PI, pressure indicator; TIC, temperature indicator controller.

Test number	**T1**	**T2**	**T3**	**T4**	**T5**	**T6**	**T7**	**T8**	**T9**	**T10**
Test	**CH_4 S.R. (cycle 1)**	**CH_4 S.R. (cycle 6)**	**CH_4 S.R. (cycle 12)**	**CH_4 S.R. CaO-to-C: 5.5**	**CH_4 S.R. CaO-to-C: 2.8**	**CH_4 S.R. CaO-to-C: 1.8**	**Toluene S.R.**	**1-Mn S.R.**	**WGSR-1**	**WGSR-2**
Primary N_2 (NL/h)	40	40	40	65	40	15	30.7	30.7	70	70
Secondary N_2 (NL/h)	-	-	-	-	-	-	28.5	28.5	-	-
CH_4 (NL/h)	10	10	10	5	10	15	-	-	-	-
CO (NL/h)	-	-	-	-	-	-	-	-	10	10
1-Mn (NL/h vapour)	-	-	-	-	-	-	-	0.45	-	-
Toluene (NL/h of vapour)	-	-	-	-	-	-	0.67	-	-	-
H_2O (NL/h of steam)	40	40	40	20	40	60	14.7	15	30	30
Reaction temperature (°C)	630	630	630	650	650	650	645	645	630	630
Fresh dolomite mass (g)	90	90	90	120	120	120	125	80	92	98.2
Nickel catalyst mass (g)	48	48	48	30	30	30	30	20	49.4	-
Contact time (s)	6.8	6.8	6.8	7.4	7.4	7.4	6.1	3.9	5.5	3.7

Table 3: Experimental conditions for steam reforming and water-gas shift reactions. S.R.: Steam Reforming

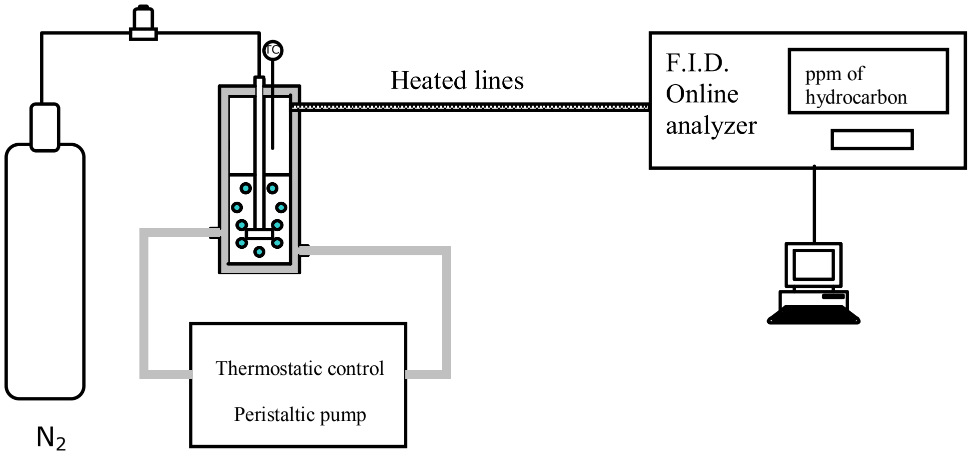

Figure 2: Continuous tar feeding system for fluidized bed reactor rig

With such a system, the exiting tar concentration depends only from the temperature level in the saturation flask, which may be carefully monitored with a thermocouple placed in the vapour zone. The concentration may be predicted by Antoine law, depending from saturation vapour pressure of different hydrocarbons, and has been verified before each test by a MultiFID 14 analyser (Figure 2), to confirm the saturation level of the N_2 flow entering the reactor.

The tar-saturated nitrogen stream is then fed to the reactor via a heated line (40 cm length). With such a system, by varying the temperature level of the saturation unit, mixtures of 1-Mn or toluene with N_2 are obtainable in a broad range of partial pressures.

Theoretical toluene or 1-Mn concentration in the reactor feeding stream are expressed by Antoine Law (Equation (1) and (2), Figure 3). The Antoine equation is a vapour pressure equation and describes the relation between vapour pressure and temperature for pure components, starting from the empirical equation:

$$\ln P = A - \frac{B}{C + T}$$

where P is the vapour pressure, T is temperature and A, B and C are component-specific constants (found in CHEMCAD database in this work).

$$for\ Toluene:\ \ln P_{(atm)} = 9.63 - \frac{3242.4}{-47.181 + T} \tag{1}$$

$$for\ 1 - MN:\ \ln P_{(atm)} = 9.64 - \frac{4265}{-75.47 + T} \tag{2}$$

In agreement with the equilibrium data, the temperature level in the saturation flask has been adjusted to 16°C for toluene, to obtain a partial pressure corresponding to about 22000 ppm

(90 g of toluene/Nm^3), and 118°C for 1-Mn, which would assure a concentration of 14500 ppm (90 g of 1-Mn/Nm^3). The exact toluene and 1-Mn concentration in the reactor feeding stream has been monitored by a MultiFID 14 analyser, before each test, to confirm the saturation level of the N_2 flow entering the reactor.

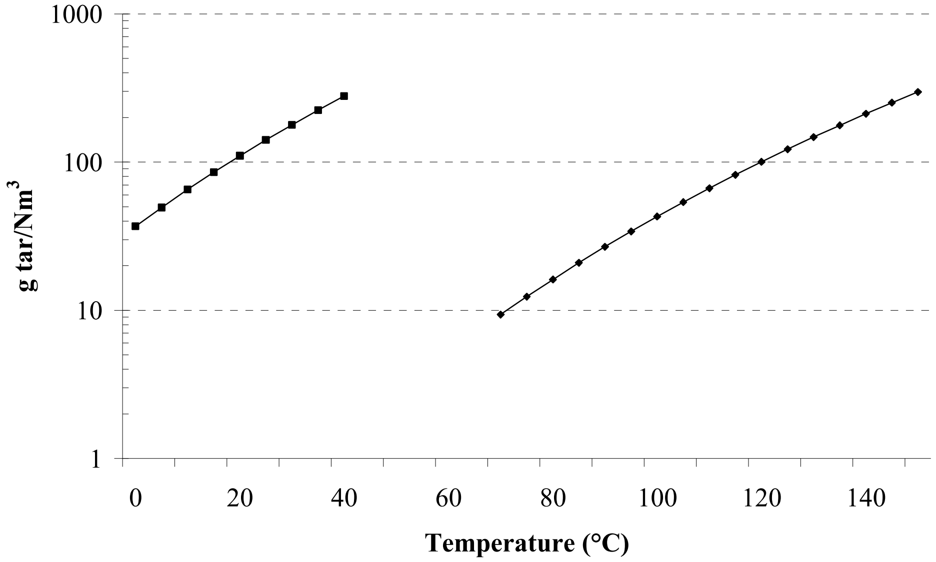

Figure 3: Logarithmic plot of g tar/Nm^3 gas as a function of the saturation temperature, according to the Antoine Law, at ambient pressure, for 1-Mn (♦) and toluene (■)

Table 3 shows the overall experimental conditions for toluene and 1-Mn steam reforming tests. The steam feeding flow rate corresponds to about 1.5 times the stoichiometric value required for total conversion of the model tar compounds. The contact time is given by the ratio between the volume occupied by solids in the reactor, measured in fixed bed conditions before test, and the overall volumetric flow rate entering the reactor, evaluated at normal conditions.

2.4. F.I.D. measurements

The response of the F.I.D. online analyzer is expressed in ppm of equivalent propane, that may be converted in *g tar/Nm^3* as follows (for the nomenclature, see “Notation” at the end of the paragraph):

$$\frac{g_{tar}}{Nm^3} = ppm_{eq.prop.} \cdot \frac{3}{n_{C(tar)}} \cdot m.w._{(tar)} \cdot \frac{10^{-3}}{V_m} \tag{3}$$

Tests with different nitrogen flows have been carried out for checking the stability of model tar compound concentration exiting from the saturation unit, with different nitrogen residence time in the saturator. In Figure 4a and b, tests with a flow rate of 120 NL/h, and 30 NL/h are shown, respectively, for toluene, and are in good mutual agreement, also with respect to the concentration of toluene predicted by Antoine law (90g/Nm^3). The milder flow of 30 NL/h will be used in the test, to avoid excessive pressure drops during the steam reforming tests.

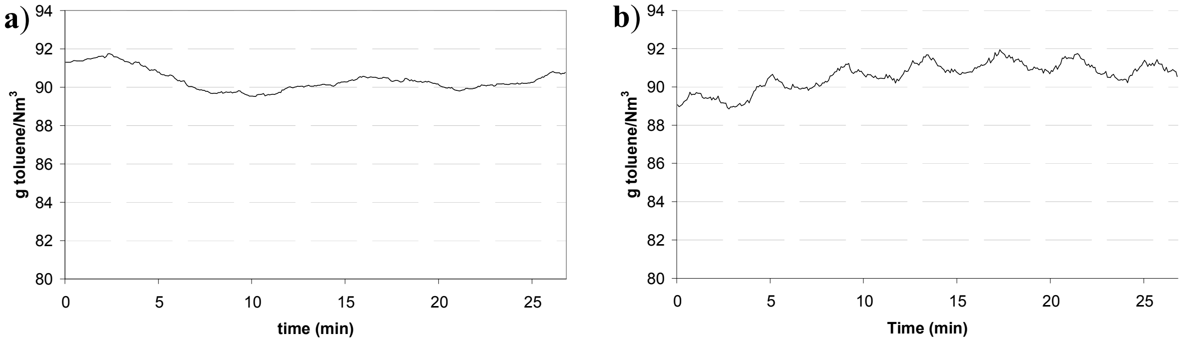

Figure 4: toluene (g/Nm^3) exiting from saturation unit measured by F.I.D., 120NL/h N_2 (a) and 30 NL/h N_2 (b)

The same tests have been successfully carried out also using 1-Mn as model tar compound (Figure 5); this is a key result due to the lower vapour pressure of this hydrocarbon that renders feeding at constant composition more difficult.

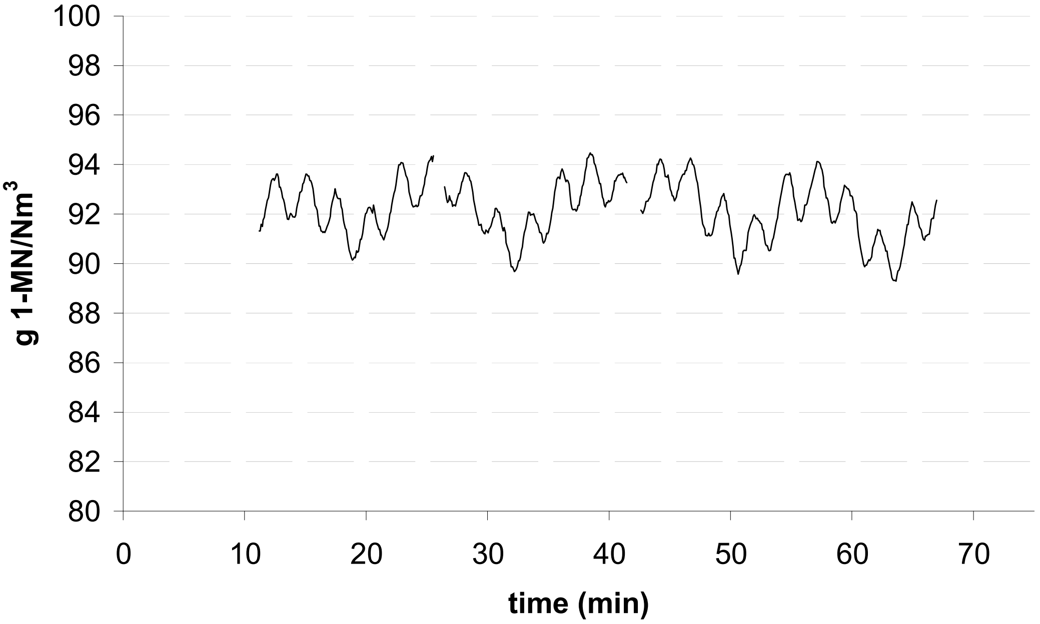

Figure 5: 1-Mn (g/Nm^3) exiting from saturation unit measured by F.I.D., 30 NL/h N_2

2.5. Methane steam reforming and water-gas shift reactions

In the right side of Figure 1, a gas cylinders station is connected to the reactor, together with a water inlet flow controlled by means of a dosing pump with variable speed (labelled 5 and 6 in Figure 1); water is then vaporised and mixed with the gas stream inside the reactor jacket. The flow rate of the gaseous compounds is measured by mass flow meters. In this way, methane steam reforming and water-gas shift reaction tests have been carried out by using the conditions shown in Table 3 (T1-T6, T9, T10).

2.6. Multi-cycle experimental conditions

When alternate calcination and carbonation tests are performed in series, to check the sorbent behavior under multi-cycle operating conditions, the main steps of the experimental procedure are:

- initial pre-calcination of dolomite and reduction of catalyst, as described in section 2.2 (point 1 and 2);
- steam reforming test and calcination of dolomite after test (point 3 and 4), performed iteratively. Catalyst reduction is not repeated between cycles.

Experimental conditions for these investigations are shown in Table 3, where 1st, 6th and 12th cycle are considered as representative tests (T1, T2 and T3).

2.7. Experimental conditions for different CaO-to-C ratio

The experimental conditions adopted are summarised in Table 3 (T4-T6). The total inlet gas flow (90NL/h), the CH_4:H_2O ratio (1:4), the bed inventory (60g of calcined dolomite, 30g of commercial nickel catalyst) and the temperature (650°C) have been kept constant in each test, but the methane inlet flow has been increased from 5 NL/h (for a CaO-to-C ratio of 5.5 h) to 15 NL/h (CaO-to-C ratio of 1.8 h). The same dolomite-and-nickel bed has been used in each test, dolomite being regenerated by calcination between tests (steps 4 and 5 in Section 2.2), and nickel catalyst being reactivated by a reduction period (step 2 in Section 2.2) before the new test.

3. Results and discussion

3.1. Step 1: pre-calcination of dolomite

Detailed analyses of calcination curves of dolomite, steps 1 and 4, have been extensively studied in the laboratory of L'Aquila [Mancini, 2006], [Giancaterino, 2006]. The total moles of CO_2 desorbed from dolomite may be calculated as follows (method 1):

$$mol_{CO2} = \frac{\int_0^{t_f} y_{CO2} \cdot q_{tot} dt}{V_m} \tag{4}$$

and q_{tot} may be easily obtained from the following relations:

$$q_{CO2} = y_{CO2} \cdot q_{tot} \tag{5}$$

$$q_{tot} = \frac{q_{N2}}{(1 - y_{H2})} \tag{6}$$

A different method for the quantification of the CO_2 desorbed in the calcination step, is the direct measure of the weight loss derived from calcination (method 2). The data obtained with both methods are mutually consistent and are summarized in Table 4 for some representative test.

Typical curves of CO_2 desorption as a function of time and temperature profiles (Step 1 of the experimental procedure), are given in Figure 6a and b for dolomite used in steam reforming tests number T7 and T8, respectively. The surface areas are different because of different amounts of dolomite are used (see Table 3).

Test number	CO_2 moles contained in the fresh dolomite	measured CO_2 desorbed (moles) (method 1)	measured CO_2 desorbed (moles) (method 2)
T1	1.01	1.05	0.98
T7	1.39	1.45	1.37
T8	0.90	0.92	0.90

Table 4: CO_2 moles desorbed after pre-calcination of raw dolomite (Step 1)

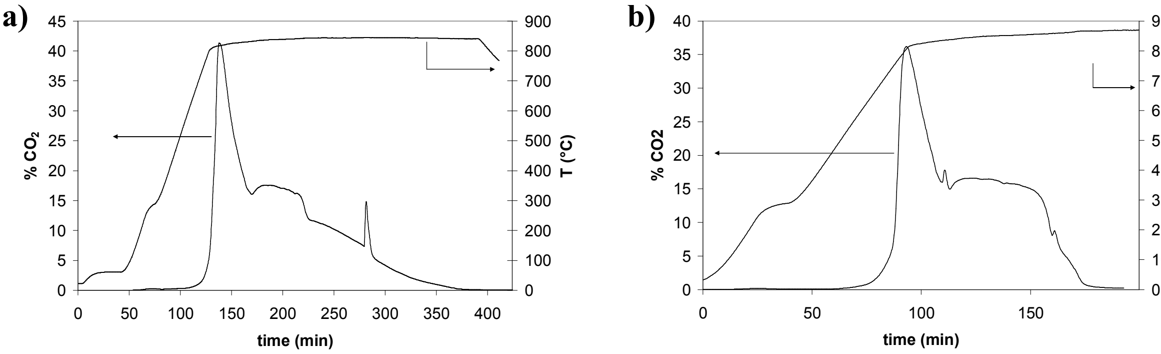

Figure 6: CO_2 desorption and temperature profiles as functions of time, in the pre-calcination of dolomite used in steam reforming tests T7 (a) and T8 (b)

3.2. Step 2: catalyst reduction

The commercial nature of the catalyst ensure a good and reproducible reduction behaviour. For completeness, two catalyst pre-reduction curves (for T3 and T8 tests) are shown in Figure 7a and b. From the area enclosed between the outlet H_2 concentration and H_2 baseline (the entering hydrogen concentration) it is possible to calculate the moles of hydrogen consumed (and therefore the moles of nickel reduced).

$$mol_{H2} = \frac{\dfrac{y_{H2(bas.)} q_{N2}}{1 - y_{H2(bas.)}} \cdot t_f - \displaystyle\int_0^{t_f} \left(\frac{y_{H2} q_{N2}}{1 - y_{H2}} \right) dt}{V_m} \tag{7}$$

where $y_{H2(bas.)}$ represents the constant molar fraction of hydrogen fed (about 0.1 in the total flow). This relation points out the amount of active nickel catalyst present in the bed, as shown in Table 5 for some typical tests. The surface areas are different because of different amounts of nickel are used (see Table 3).

Test number	**%w. of nickel reduced in the catalyst mass**
T4	20
T5	21
T7	28
T8	15

Table 5: Calculated %w. of nickel reduced in the commercial catalyst used for some representative reforming test

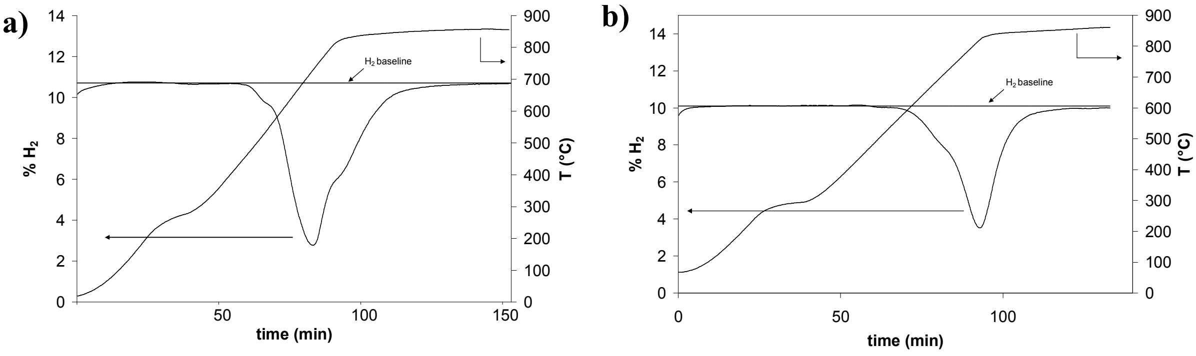

Figure 7: H_2 consumption and temperature as a function of time, for reduction of catalysts used in reforming tests T3 (a) and T8 (b)

3.3. Step 3: hydrocarbons steam reforming and CO_2 capture

In the presence of nickel catalyst and calcined dolomite, the main reactions that take place in the product gas generated by coal or biomass steam gasification are:

Steam reforming of methane:	$CH_4 + H_2O \rightarrow CO + 3H_2$	$\Delta H^0_{298} = 208.2\ kJ/mol$	(8)
Steam reforming of hydrocarbons:	$C_xH_y + xH_2O \rightarrow xCO + \left(x + \frac{y}{2}\right)H_2$	for toluene: $\Delta H^0_{298} = 869\ kJ/mol$ for 1-Mn $\Delta H^0_{298} = 1238.3\ kJ/mol$	(9)
Water-gas shift:	$CO + H_2O \leftrightarrow CO_2 + H_2$	$\Delta H^0_{298} = -41.5\ kJ/mol$	(10)
CO_2 capture:	$CaO + CO_2 \rightarrow CaCO_3$	$\Delta H^0_{298} = -178.2\ kJ/mol$	(11)

Some hydrocarbon dry reforming and cracking are also possible; coke deposited on the solid surface can eventually react with steam or carbon dioxide.

Endothermic and exothermic reactions are therefore combined together. Following the enthalpy values of reaction system (8)-(11), the global reaction enthalpy term in the energy balance will depend on the gas composition. On the other hand, the equilibrium conditions for CO_2 capture at ambient pressure (CO_2 partial pressure as a function of temperature, evidenced in Chapter 1, Section 4.1.3.) impose to operate over a limited temperature range: the fluidized bed reactor, as introduced in Chapter 1, is the only technology that ensure good solid and gas phase mixing, allowing temperature homogeneity and therefore a careful control of the effective temperature level across the whole reaction volume.

Some representative tests have been performed to study the reactions taking place in the gas phase separately, in presence of catalyst and calcined dolomite. Once the dolomite sorption capacity is exhausted, a further calcination is performed to regenerate the CO_2 sorbent.

Typical results obtained as a function of time are shown in Figures 8, 10 (a, b, c) 11, 12, 13 (a, b) for methane, toluene, 1-methyl naphthalene steam reforming and water-gas shift, respectively. It is observed that two different steady state conditions are clearly established at the reactor outlet, with or without CO_2 sorption by dolomite, separated by a rather narrow breakthrough zone, corresponding to the exhaustion of the CO_2 absorption capacity of dolomite.

3.3.1. CH_4 steam reforming calculations

The main reactions taking place into the system are (8), (10) and (11).

In the pre-breakthrough steady state, the carbon mole balance may be written as:

$$F_{CH4(in)} - F_{CH4(out)} = F_{CO(out)} + F_{CO2(out)} + F_{CO2(captured)} \tag{12}$$

where F represent the molar flow of each gaseous specie. The conversion between % composition and molar flows of components of the product gas (H_2, CO, CO_2 and CH_4) may be easily obtained from the relation:

$$q_{tot} = q_{N2} + q_{tot} \cdot \left(y_{H2} + y_{CO2} + y_{CO} + y_{CH_4}\right) \tag{13}$$

where:

$$q_{tot} = \frac{q_{N2}}{1-\left(y_{H2} + y_{CO2} + y_{CO} + y_{CH_4}\right)} \tag{14}$$

The term $F_{CO2(captured)}$ may be therefore found from relation (12), and is verified experimentally through the measure of the number of CO_2 moles desorbed from dolomite in the following calcination (step 4), obtained with method 1 described in Section 3.1.

The same term $F_{CO2(captured)}$ is zero in the post-breakthrough time, where the carbon balance may be directly obtained from relation (12).

The conversion of methane may be easily calculated, the ABB analyser allowing to identify the methane exiting from the reactor:

$$X_{CH4} = \frac{F_{CH4(in)} - F_{CH4(out)}}{F_{CH4(in)}} \tag{15}$$

Table 6 summarize the comprehensive mole balance for T5 as a representative test on methane reforming.

	Test number: T4	
	pre-breakthrough	**post-breakthrough**
F_{H2} *(Nmol/h)*	1.804	1.701
F_{CO} *(Nmol/h)*	0.066	0.135
F_{CO2} *(Nmol/h)*	0.103	0.298
F_{CH4} *(Nmol/h)*	0.008	0.020
X_{CH4} *(Nmol/h)*	0.983	0.955
$F_{CO2(captured)}$ *(Nmol/h)*	0.274	-
moles of CO_2 captured (method 1)	0.611	-

Table 6: Comprehensive carbon balance for T5 experiment.

3.3.1.1. Multi-cycle operation

The experimental data for T1 (Figure 8) show clearly two distinct equilibrium zones, as described above, with and without CO_2 capture reaction (Eq. 11). The enhanced hydrogen yield is well evident from the experimental data: in the pre-breakthrough time, CO_2, CO and CH_4 concentrations are almost brought to zero, and H_2 content in the product gas is very high (97.5%, on dry and nitrogen-free basis); then the H_2 concentration decreases to a value of 76.7% (dry and nitrogen-free basis), whereas the CH_4, CO_2, CO concentrations increase. Therefore, as expected, the saturation of dolomite causes an exhaustion of thermodynamic driving force for methane steam reforming and water-gas shift reactions.

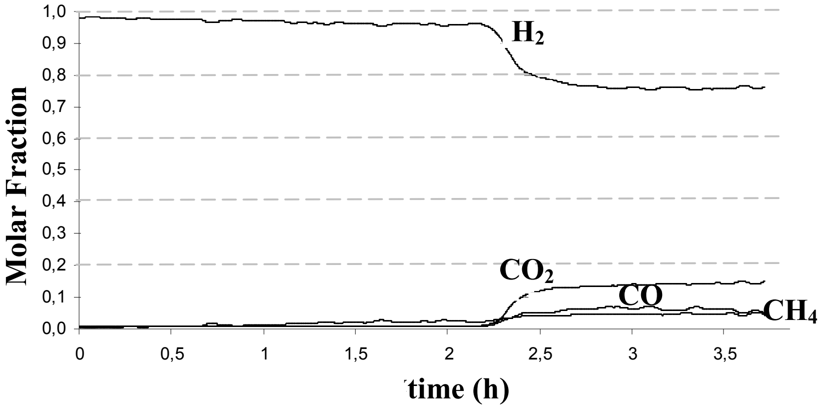

Figure 8: Methane steam reforming and CO_2 capture test: experimental concentrations (dry and nitrogen-free basis) as a function of time

The influence of the CO_2 capture step on enhancing CH_4 conversion and CO_2 partial pressure during the capture phase is close to thermodynamic equilibrium predictions (Chapter 1-Equation 1 and Figure 9 below). This has also been observed for toluene and 1-Mn steam reforming.

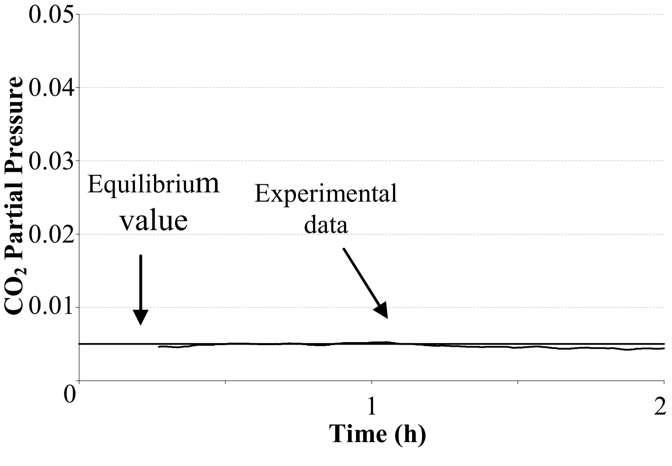

Figure 9: CO_2 partial pressure in the reactor compared with theoretical value at 630°C for CH_4 steam reforming

Re-calcination of dolomite allows to obtain a regenerated sorbent and to run a multi-cycle steam reforming and CO_2 capture test. This step is essential for evaluating the possibility of making the whole process continuous and amenable to industrial exploitation. Twelve calcination-steam reforming and CO_2 capture cycles have been carried out in the fluidized bed rig, for methane reforming. It is observed (Table 7) that concentration of H_2, CO, CO_2 and CH_4, during pre- and post-breakthrough, are quite constant throughout the cycles, evidencing that equilibrium is reached for each cycle, as reported in a previous work [Johnsen *et al.,* 2006]. Moreover, the observed breakthrough time, that is the time required for saturation of dolomite, is close to that corresponding to the theoretical value in the 1st cycle (T1), while is reduced to 80% of its initial value in the 12th cycle (T3), evidencing a progressive (although rather limited) loss of sorption capacity during cycles, a phenomenon quite well known in the literature and often related to structural modifications of the sorbent particles [Gallucci *et al.,* 2008].

	1st cycle (T1)		
	pre-breakthrough	**post-breakthrough**	**breakthrough time (h)**
H_2	97.5	76.7	2.3
CO	0.7	4.6	
CO_2	0.9	13.9	
CH_4	0.9	4.8	
	6th cycle (T2)		
	pre-breakthrough	**post-breakthrough**	**breakthrough time (h)**
H_2	95.2	76.0	2.2
CO	1.5	6.5	
CO_2	0.6	10.7	
CH_4	2.7	6.8	
	12th cycle (T3)		
	pre-breakthrough	**post-breakthrough**	**breakthrough time (h)**
H_2	98	79.0	1.9
CO	0.6	3.7	
CO_2	0.6	11.6	
CH_4	0.8	5.7	

Table 7: Experimental gas concentrations (dry and nitrogen-free basis) obtained in multi-cycle CH_4 steam reforming tests, for the 1st, 6th and 12th cycle.

3.3.1.2. Methane steam reforming varying the CaO-to-C ratio

In this paragraph the variation of CaO-to-C ratio, where CaO represents the moles of in bed active sites of dolomite for CO_2 capture and C is the entering molar flow of carbon (as methane) is reported. This ratio is an important parameter from an industrial point of view, to evaluate catalytic activity and CO_2 capture kinetic. The experimental conditions assumed are summarised in Table 3, whereas results are shown in Figures 10a, b and c.

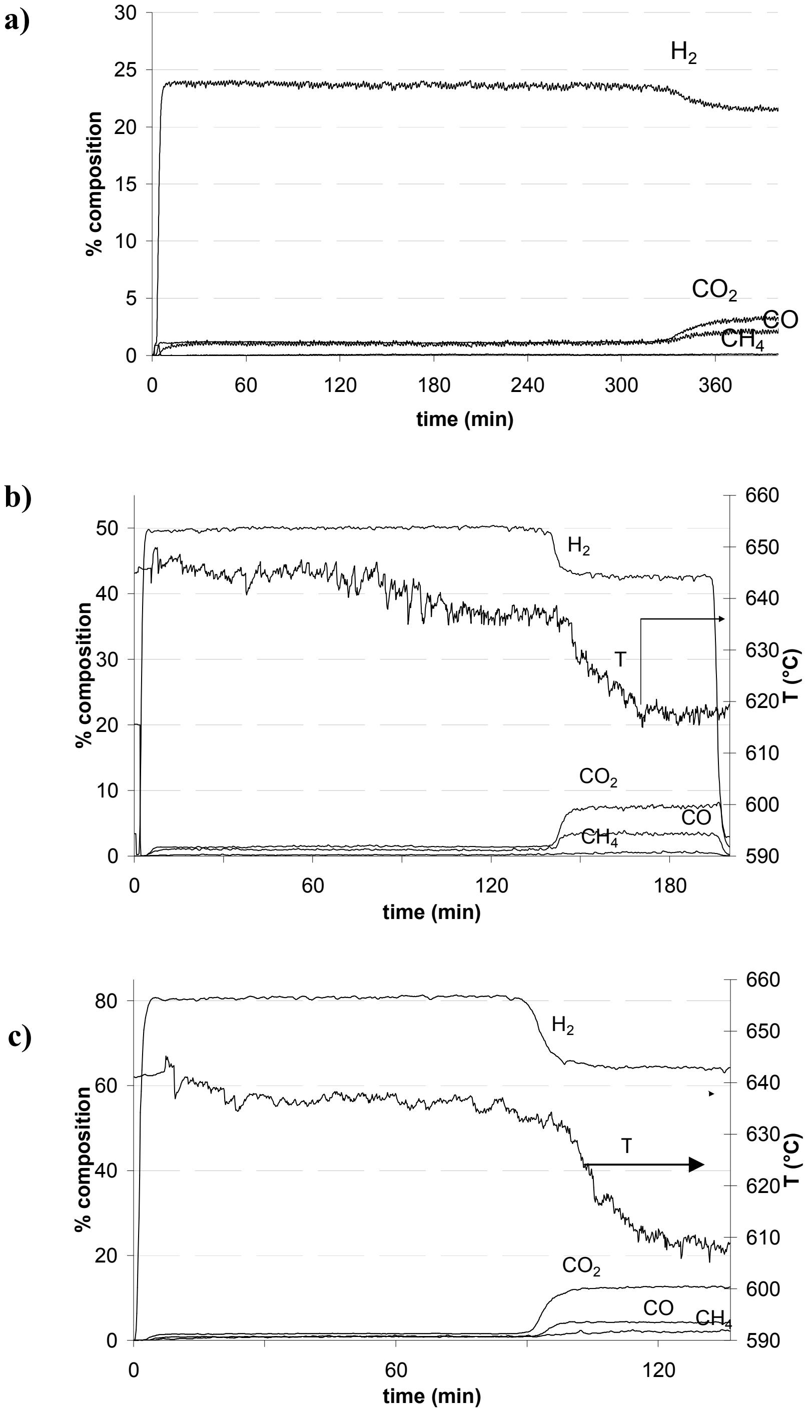

Figure 10: CH_4 steam reforming tests varying the CaO-to-C ratio: a) 5.5; b) 2.8; c) 1.8. Experimental gas concentrations and temperature profile as functions of time

The temperatures in the bed are continuously controlled. They vary somewhat with time-on-stream, as indicated in Figure 10. It can be seen in Figure 10 how, even with external ovens, it was difficult to keep the temperature rigorously constant in the bed, and this evidence increases with the methane fed for the test. The main reason is that the exothermal reaction (11) progressively decreases and stops after saturation of dolomite. At the same time, the highly endothermic methane steam reforming reaction continues. The data are in agreement with the trend evidenced in this experimental series, where the temperature drop (before and after the breakthrough time) increases by increasing the CH_4 feeding rate (from a to c). For Figure 10a, there are not significant temperature variations, and this parameter has been not reported.

The mean output of hydrogen on dry, nitrogen free base, as well as CH_4 conversion, is shown in Table 8.

	pre-breakthrough		**post-breakthrough**	
test number	**% X_{CH4}**	**y_{H2} (dry and nitrogen free)**	**% X_{CH4}**	**y_{H2} (dry and nitrogen free)**
T4	99.1	0.95	98.2	0.80
T5	99	0.95	98	0.79
T6	98.5	0.96	95.5	0.77

Table 8: mean output of hydrogen on dry, nitrogen free base, and CH_4 conversion obtained with tests T4, T5 and T6.

It is evident that the breakthrough time decreases by decreasing the CaO-to-C ratio, although both mass transfer and reaction kinetics are fast enough to approach equilibrium within the given range of operating conditions: the CO_2 capture and CH_4 conversion either before or after the capacity of the sorbent was exhausted, are quite unaffected by kinetic limitations in the range of operation conditions adopted.

3.3.2. Tar steam reforming

For toluene and 1-Mn, is not possible to check online the unconverted tar fraction. Therefore, it will be calculated from a carbon balance:

$$x \cdot \left(F_{CxHy(in)} - F_{CxHy(out)}\right) = \left(F_{CO} + F_{CO2} + F_{CH4}\right)_{out} + F_{CO2(captured)} \qquad (16)$$

The conversion of model tar compound may therefore be written as follows:

$$X = \frac{\left(F_{CO} + F_{CO2} + F_{CH4}\right)_{out} + F_{CO2(captured)}}{x \cdot (F_{CxHy})_{in}} \tag{17}$$

where $F_{CO2(captured)}$ is zero in the post-breakthrough time. In this case, the term $F_{(CxHy)out}$ of Equation (16) is unknown. Therefore, the only way to calculate $F_{CO2(captured)}$ is the quantification of CO_2 moles adsorbed during the whole test, in the following calcination (step 5). Dividing this amount by the breakthrough time, a mean $F_{CO2(captured)}$ value may be extracted, and therefore the $F_{(CxHy)out}$ (and conversion X) become available.

The hydrogen balance may be also useful for calculating conversion. In the pre-breakthrough time, being the CO concentration very low for both T7 and T8 (less than 1% vol.), the maximum of hydrocarbon conversion may be expresses as:

$$X_{CxHy} = \frac{F_{H2(out)}}{(\frac{y}{2} + 2x) \cdot F_{CxHy(in)}} \tag{18}$$

where water-gas shift reaction is considered complete, due to the conversion improvement promoted by CO_2 capture. In the post-breakthrough time, the maximum of hydrocarbon conversion that may be obtained is limited by the thermodynamic constraint of water-gas shift reaction. In this case, the system may be simply modelled with two reactors in series, the former assuming a total conversion for reaction (9), and the latter taking into account the thermodynamic equilibrium for reaction (10). The steam entering to the first reactor reproduces the (steam):(model tar compound) ratio adopted in the tests.

I reactor:

$$\left[C_xH_y + 3xH_2O\right]_{in} \rightarrow \left[xCO + \left(\frac{y}{2} + x\right)H_2 + 2xH_2O\right]_{out} \tag{19}$$

$$F_{CO(out)} = F_{CxHy} \cdot x \tag{20}$$

$$F_{H2(out)} = F_{CxHy} \cdot \left(\frac{y}{2} + x\right) \tag{21}$$

$$F_{H2O(out)} = F_{CxHy} \cdot 2x \tag{22}$$

$$F_{CO2(out)} = 0 \tag{23}$$

II reactor:

$$\left[xCO + \left(\frac{y}{2} + x\right)H_2 + 2xH_2O\right]_{in} \rightarrow \left[(x - \xi)CO + \left(\frac{y}{2} + x + \xi\right)H_2 + (2x - \xi)H_2O + \xi CO_2\right]_{out} \tag{24}$$

$$F_{CO(out)} = F_{CxHy} \cdot (x - \xi) \tag{25}$$

$$F_{H2(out)} = F_{CxHy} \cdot \left(\frac{y}{2} + x + \xi \right) \tag{26}$$

$$F_{H2O(out)} = (2x - \xi) \cdot F_{CxHy} \tag{27}$$

$$F_{CO2(out)} = F_{CxHy} \cdot \xi \tag{28}$$

From this balance it is possible to calculate the enhancement degree ξ of water-gas shift reaction at equilibrium (the value calculated for thermodynamic constant of water gas shift reaction at 650°C, $K_{eq(650°C)}$, is 1.93):

$$K_{eq(650°C)} = \frac{\left(\frac{y}{2} + x + \xi \right) \cdot (\xi)}{(x - \xi) \cdot (2x - \xi)} = 1.93 \tag{29}$$

and consequently the maximum conversion reachable for the system at hand, when the experimental $F_{H2(out)}$ value is known:

$$X_{CxHy} = \frac{F_{H2(out)}}{F_{CxHy} \cdot \left(\frac{y}{2} + x + \xi \right)} \tag{30}$$

3.3.2.1. Toluene steam reforming

Results similar to those for CH_4 steam reforming have been obtained for toluene steam reforming (Figure 11). In this case, the main reactions are the following:

$$C_7H_8 + 7H_2O \rightarrow 7CO + 11H_2 \tag{31}$$

$$CO + H_2O \leftrightarrow CO_2 + H_2 \tag{10}$$

$$CaO_{(s)} + CO_{2(g)} \rightarrow CaCO_{3(s)} \tag{11}$$

In the pre-breakthrough time period, from Equation (18) a high toluene conversion (0.98) is evaluated from the H_2 content in the gas exiting the reactor (16.5% vol., 92% on dry, nitrogen-free basis). This value corresponds to a nearly total conversion of the toluene feed. The CO and CO_2 concentrations are much lower during the CO_2 absorption phase than the corresponding values after saturation of dolomite.

After saturation of dolomite, from Equation (29) it is extracted a value for ξ of 3.96. This value means that 58% of carbon contained in toluene (7 carbon atoms) becomes CO_2; the toluene conversion decreases to about 0.9. The concentrations detected in the total flow are: 12.5% H_2 (72% on dry, nitrogen-free basis), 1.3% of CO (7.3% on dry, nitrogen-free basis), 3.6% of CO_2 (20.7% on dry, nitrogen-free basis). No methane formation is detected.

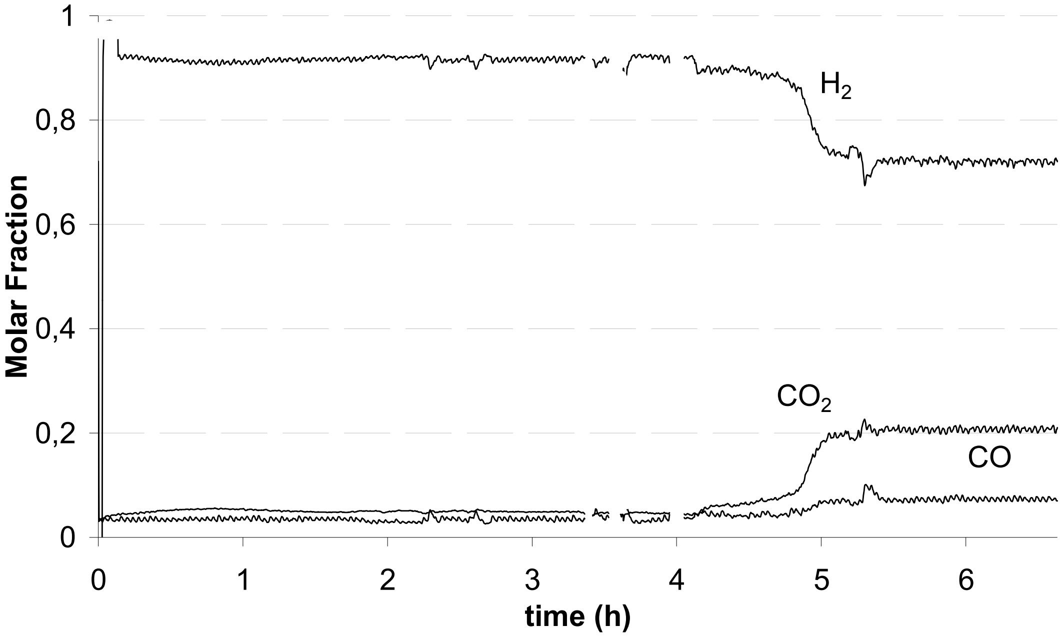

Figure 11: Toluene steam reforming and CO_2 capture test: experimental gas concentrations (dry and nitrogen-free basis) as functions of time

3.3.2.2. 1-Mn steam reforming

The key reactions that occur in 1-Mn steam reforming are:

$$C_{11}H_{10} + 11H_2O \rightarrow 11CO + 16H_2 \tag{32}$$

$$CO + H_2O \leftrightarrow CO_2 + H_2 \tag{10}$$

$$CaO_{(s)} + CO_{2(g)} \rightarrow CaCO_{3(s)} \tag{11}$$

Two rings compounds have been indicated as the most suitable for use as model tar compounds exhibiting a lower reaction rate with respect to steam reforming [Coll *et al.,* 2001]. However, absorption enhanced reforming evidences once again an excellent efficiency (Figure 12), with a high conversion of 1-Mn. Hydrogen produced during the CO_2 absorption phase corresponds to an average volumetric concentration of 19.5% in the total flow (92% on dry, nitrogen-free basis), that means a nearly total conversion of 1-Mn (0.95 from Equation (18)). However, it is observed a progressive slight decrease as a function of time of the H_2 concentration at the exit of the reactor, and a corresponding steady increase of CO and CO_2 before the breakthrough conditions are reached (Figure 12). In comparison with the previous reforming test with toluene, the required carbon absorption rate per unit mass of dolomite is now substantially increased, and this may help to explain the observed behaviour in terms of kinetic considerations. Dolomite carbonation degree increases progressively with time, making more difficult a further absorption of CO_2, for a number of reasons: among these, reduction of internal particle pore volume, and increase of the thickness of the product layer ($CaCO_3$) built up around each CaO grain.

After saturation of dolomite, the H_2 yield decreases abruptly, while a simultaneous increase in CO and CO_2 concentrations at the reactor outlet is observed: a 1-Mn conversion of about 0.9 is evaluated from Eq. (30), with $\xi = 6.33$ from Eq. (29). This value is obviously higher than for toluene steam reforming due to the higher carbon number of 1-Mn (11 carbon atoms), but the percentage of carbon contained in the parent hydrocarbon that becomes CO_2 results once again about 58%. The measured H_2, CO, and CO_2 content in this second equilibrium zone, decrease to 16% (70% on dry, nitrogen-free basis), 2.05% (10%) and 4.65% (20%).

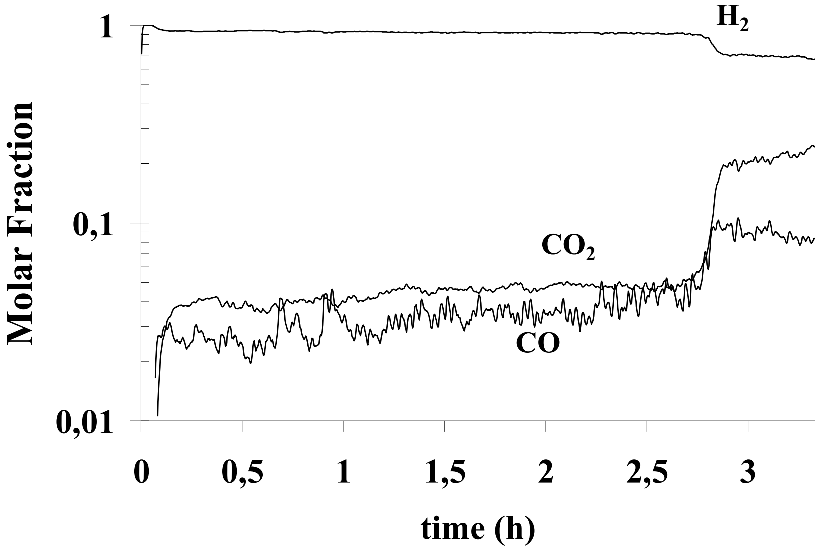

Figure 12: : Logarithmic plot of 1-Mn steam reforming and CO_2 capture test: experimental gas concentrations (dry and nitrogen-free basis) as functions of time

3.3.3. Water-gas shift reaction

Water-gas shift has been studied experimentally with and without Ni-catalyst, however always in presence of dolomite, and at the same temperature level as that of methane-steam reforming tests. Figure 13a shows that it is possible to obtain high reaction conversion and hydrogen content using a reactor bed of dolomite alone, and the addition of a pre-reduced Ni-catalyst in the bed makes the hydrogen concentration to increase slightly (Figure 13b). On the other hand, when the sorption capacity of dolomite is exhausted (post-breakthrough), the water-gas shift reaction is considerably enhanced by the presence of catalyst (CO, CO_2

and H_2 concentrations are close to equilibrium conditions – Figure 13b), in comparison to test without Ni-catalyst (Figure 13a). In both cases H_2/CO_2 ratio is equal to 1 after dolomite saturation, in accordance with the stoichiometry of reaction (6).

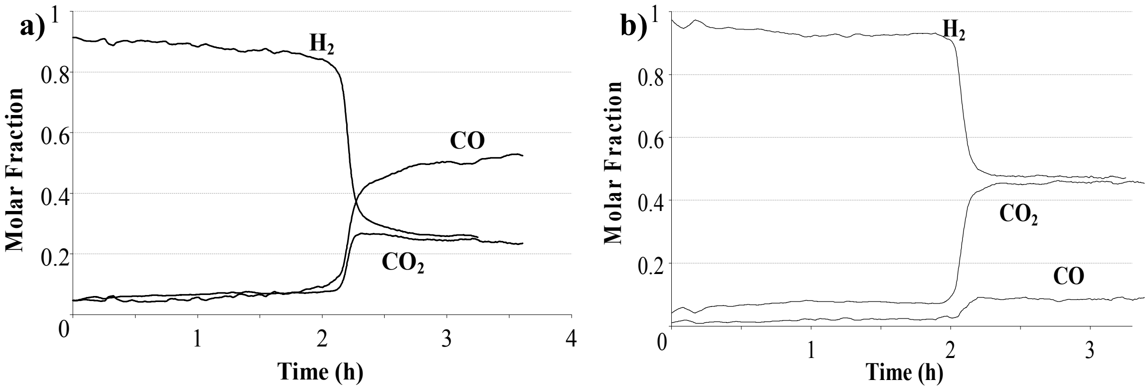

Figure 13: Water-gas shift reaction using a) dolomite and b) dolomite and Nickel catalyst as bed inventory: experimental gas concentrations (dry and nitrogen-free basis) as functions of time

3.4. Steps 4 and 5

At the end of the reforming step, carbon is trapped in the reactor bed either as $CaCO_3$, and in the form of coke deposited on the solid surface as a result of secondary cracking processes. To allow an estimate of such quantities, calcination in nitrogen atmosphere, and combustion with air are performed sequentially.

During the former calcination step, as indicated in Figure 14 for toluene steam reforming test, $CaCO_3$ decomposition produces CO_2 (labelled as CO_{2calc}) that is partially converted in CO (CO_{calc}) by coke dry reforming:

$$C + CO_{2(calc)} \rightarrow 2CO_{(calc)} \tag{33}$$

In the subsequent combustion, the remaining coke is converted into CO_2 (labelled as CO_{2comb}) and CO (CO_{comb}) (Figure 15).

As a result, the $CaCO_3$ moles formed in the toluene reforming step can be estimated as follows:

$$mol(CaCO_3) = \frac{1}{2} mol(CO)_{calc} + mol(CO_2)_{calc} \tag{34}$$

while carbon deposited on dolomite and catalyst surface is given by:

$$mol(C) = \frac{1}{2} mol(CO)_{calc} + mol(CO)_{comb} + mol(CO_2)_{comb} \tag{35}$$

Equation 35 allows to estimate that about 1.4 g of coke are produced during the test, that is 8.7% of toluene feed is cracked.

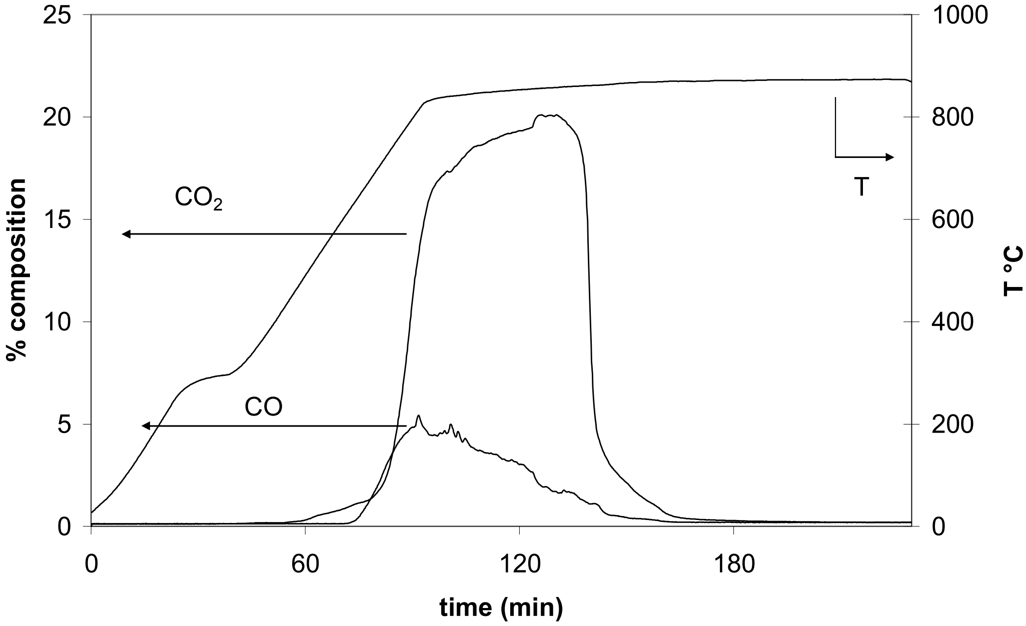

Figure 14: CO and CO_2 produced during re-calcination of dolomite after toluene steam reforming: experimental gas concentrations as functions of time

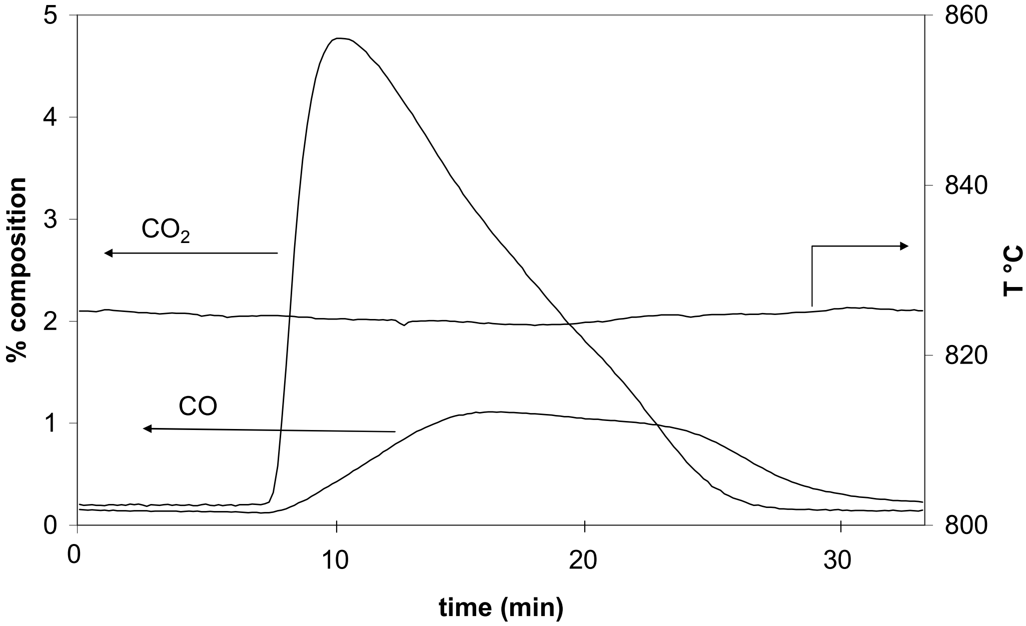

Figure 15: CO and CO_2 produced during combustion after toluene steam reforming: experimental gas concentrations as functions of time

On the other hand, CO_2 moles absorbed on dolomite, as results from Equation (34), are equal to 0.7, in good agreement with CaO moles initially present in the reactor, confirming an absorption efficiency near to 100%.

Sequential calcination and combustion steps have been carried out in the same manner for 1-Mn steam reforming test. The former results very close to the theoretical absorption capacity of dolomite loaded in the reactor, altogether 0.43 moles of CO_2. The latter is found to be much less than carbon deposited in the toluene reforming test (corresponding to about 0.5% of 1-Mn feed), showing a superior thermal stability or an enhanced resistance to catalytic cracking of 1-Mn at the process temperature.

The calculation of CO_2 moles desorbed allows to evaluate the carbon balance for T7 and T8 (toluene and 1-Mn reforming tests), including the values of CO_2 moles in Equation (17). The information obtained from this check is in good agreement with that obtained from the hydrogen balance, resulting in conversion values of about 0.95 for pre-breakthrough time in both T8 and T9.

For methane steam reforming tests (T1-T6) the carbon detected during steps 4 and 5 is negligible. This evidence may be due to a higher thermal stability of methane, but also to a lower CH_4:H_2O ratio (1:4 in CH_4 steam reforming vs. 1:3 in tar steam reforming tests).

3.5. Step 6

The analysis of total organic carbon in the condensed phase is carried out off-line (as the last step of the experimental procedure), in order to detect liquid hydrocarbons (unconverted tars) eventually present in the reactor outlet stream. This step has been therefore carried out only for toluene and 1-Mn steam reforming reactions (T7 and T8).

Total Organic Carbon (TOC) analysis in the condensed phase collected at the reactor outlet, indicates once again a very low carbon concentration level, about 0,9 g/L C in 20g of water for T8, and 1g/L in 40g of condensed phase for T9 (1-Mn test). These values are very low considering that the model tar compound entering flow rate is 2.7 g/h.

4. Conclusions

The results obtained for methane reforming and simultaneous CO_2 capture confirm those reported in the literature [Johnsen *et al.,* 2006] and indicate a promising sorption performance of dolomite in cyclic operation, while those related to water-gas shift, toluene and 1-Mn reforming allow to extend to a biomass syngas the experimental evidence on simultaneous CO_2 capture and heavy hydrocarbons (tar) reforming, showing the potential of generating a hydrogen energy vector by using a particulate solid acting as CO_2 sorbent.

Mixtures of a commercial nickel catalyst and calcined dolomite perform very well in catalytic steam reforming of methane, toluene and 1-Mn carried out in a fluidized bed reactor, with conversion reaching nearly 100% during the pre-breakthrough time period.

The feasibility of simultaneous CO_2 capture and reforming reactions has been therefore demonstrated in this work, together with the evidence of the improved tar and methane conversion and a higher quality of the produced gas when dolomite is used as in-bed sorbent.

Notation

$\frac{g_{tar}}{Nm^3}$: grams of model tar compound/Nm^3 gas.

$ppm_{eq.prop.}$: ppm of equivalent propane.

$n_{C(tar)}$: carbon atoms number in the model tar compound.

$m.w._{(tar)}$: molecular weight of model tar compound.

V_m: molar volume at normal conditions (T = 273.15 K, P = 1 bar).

y: molar fraction (referred to CO, CO_2, H_2, CH_4, N_2, steam).

q: volumetric flow (referred to CO, CO_2, H_2, CH_4, N_2, steam) at normal conditions.

q_{tot} : total volumetric flow exiting from the reactor at normal conditions.

$y_{H2bas.}$: H_2 baseline (the entering H_2 concentration).

t_f : final time.

F_{in} : molar flow entering to the reactor (referred to C_xH_y, CH_4).

F_{out} : molar flow exiting from the reactor (referred to C_xH_y, CO, CO_2, H_2, CH_4, N_2, steam).

ξ : enhancement degree.

Bibliography

Abu El-Rub Z., Bramer E.A., Brem G., (2004), Review of catalysts for tar elimination in biomass gasification processes, Ind Eng Chem Res 43, 6911-6919.

Abu El-Rub Z., Bramer E.A., Brem G., (2008), Experimental comparison of biomass chars with other catalysts for tar reduction, Fuel 87, 2243–2252.

Coll R., Salvadó J., Farriol X., Montané D., (2001), Steam reforming model compounds of biomass gasification tars: conversion at different operating conditions and tendency towards coke formation, Fuel Processing Technology 74, 19-31.

Corella J., Toledo J.M., Padilla R., (2004), Olivine or dolomite as in-bed additive in biomass gasification with air in a fluidized bed: Which is better?, Energy Fuels 18, 713-720.

Delgado J., Aznar M.P., Corella J., (1996), Calcined Dolomite, Magnesite, and Calcite for Cleaning Hot Gas from a fluidized Bed Biomass Gasifier with Steam: Life and Usefulness, Ind. Eng. Chem. Res. 35, 3637-3643.

Delgado, J.; Aznar, M.P.; Corella, J., (1997), Biomass Gasification with Steam in fluidized Bed: Effectiveness of CaO, MgO and CaO-MgO for Hot Raw Gas Cleaning. Ind. Eng. Chem. Res. 36, 1535- 1543.

Devi L., Ptasinski K.J., Janssen F.J.J.C., (2005), Pretreated olivine as tar removal catalyst for biomass gasifiers: investigation using naphthalene as model biomass tar, Fuel Process Technol 86, 707-730.

Dou B., Gao J., Sha X., Baek S.W., (2003), Catalytic cracking of tar component from high-temperature fuel gas, Appl Therm Eng 23, 2229-2239.

Gallucci K., Stendardo S., Foscolo P.U., (2008), CO_2 capture by means of dolomite in hydrogen production from syn gas, International Journal of Hydrogen Energy 33, 3049-3055.

Giancaterino L., (2006), University of L'Aquila, Chemical reactors Laboratory, Master Thesis.

Harrison D.P., (2008), Sorption-Enhanced Hydrogen Production: A Review, Ind. Eng. Chem. Res. 47, 6486-6501.

Hofbauer H., (2009), Gas Production for Polygeneration Plants, Proceedings of 1st International Conference on Polygeneration Strategies, Vienna, 1-4 September 2009, Vienna.

Jess A., (1996), Mechanisms and kinetics of thermal reactions of aromatic hydrocarbons from pyrolysis of solid fuels Fuel 75, 1441-1448.

Johnsen K., Ryu H.J., Grace J.R., Limb C.J., (2006), Sorption-enhanced steam reforming of methane in a fluidized bed reactor with dolomite as CO_2-acceptor, Chemical Engineering Science 61, 1195-1202.

Li C., Suzuki K., (2009), Tar property, analysis, reforming mechanism and model for biomass gasification—An overview, Renew Sustain Energy Rev 13, 594-604.

Mancini G., (2006), University of L'Aquila, Chemical reactors Laboratory, Master Thesis.

Marquard-Möllenstedt T., Sichler P., Specht M., Michel M., Berger R., Hein K.R.G., Höftberger E., Rauch R., Hofbauer H., (2004) Proceedings of 2nd World Conference on Biomass for Energy, Industry and Climate Protection, Rome, Italy, 10-14 May 2004.

Marquard-Moellenstedt T., Specht M., Zuberbuehler U., Koppatz S., Pfeifer C., Rauch R., Soukup G., Hofbauer H., Koch M., (2008), Transfer of the absorption enhanced reforming (AER)-process from the pilot scale to an 8 mwth gasification plant in Guessing, Austria, Proceedings of the 14th European Conference on Biomass for Energy Industry and Climate Protection, Valencia, Spain, 02-06 June 2008.

Orio A., Corella J., Narvaez I., (1997), Performance of different dolomites on hot raw gas cleaning from biomass gasification with air, Ind. Eng. Chem. Res. 36, 3800-3808.

Polychronopoulou K., Fierro J.L.G., Efstathiou A.M., (2004), The phenol steam reforming reaction over MgO-based supported Rh catalysts, Journal of Catalysis 228, 417–432.

Polychronopoulou K., Bakandritsos A., Tzitzios V., Fierro J.L.G., Efstathiou A.M., (2006), Absorption-enhanced reforming of phenol by steam over supported Fe catalysts, Journal of Catalysis 241, 132–148.

Satrio J.A., Shanks B.H., Wheelock T.D., (2007), A Combined Catalyst and Sorbent for Enhancing Hydrogen Production from Coal or Biomass, Energy Fuels 21, 322–326.

Swierczynski D., Courson C., Kiennemann A., (2008), Study of steam reforming of toluene used as model compound of tar produced by biomass gasification, Chem Eng Process 47, 508-513.

Swierczynski D., Libs S., Courson C., Kiennemann A., (2007), Steam reforming of tar from a biomass gasification process over Ni/olivine catalyst using toluene as a model compound, Appl Catal B 74, 211-222.

Taralas G., Kontominas M.G., Katatsios X., (2003), Modeling the thermal destruction of toluene (C_7H_8) as tar-related species for fuel gas cleanup, Energy Fuel 17, 329-337.

Zhen-shan Li, Ning-sheng Cai, Jing-biao Yang, (2006), Continuous Production of Hydrogen from Sorption-Enhanced Steam Methane Reforming in Two Parallel Fixed-Bed Reactors Operated in a Cyclic Manner, Ind. Eng. Chem. Res. 45, 8788–8793.

CHAPTER 4

IRON AND NICKEL SUPPORTED ON CALCINED DOLOMITE, CaO AND MgO : A STUDY ON CHARACTERIZATION

Abstract: *This chapter shows a study of new calcined dolomite, CaO and MgO based combined catalysts and sorbents, M/dolomite, M/CaO and M/MgO (M=Ni, Fe), with the aim to optimise the granular, mineral solid material for a biomass gasification process including* CO_2 *capture, by improving catalytic activity of alkaline earth oxides CaO, MgO and calcined dolomite (a CaO-MgO solid solution). This experimental work has been addressed to catalysts preparation and characterisation, using the typical investigation techniques of catalysis (TPR, TPO, X-ray diffraction, Mossbauer spectroscopy).*

1. Introduction

In the previous chapter, the potential of using dolomite sorbent to enhance tar and methane reforming reaction, and therefore hydrogen yield in the product gas, has been investigated. However, conventional materials (raw dolomite and a commercial nickel catalyst) have been used for this purpose. The search for new combined catalytic materials and CO_2 capture materials is the aim of Chaps. 4 and 5, as a worthwhile research activity that is focused on realistic features of potential materials for commercial exploitation: these should consist of cheap materials so as to minimize manufacturing and final disposal costs. The development of catalysts with such characteristics is the aim of the research presented in this and in the following chapter.

Purification of tarry fuel gas is a crucial step in the development of biomass or coal gasification processes for the production of a H_2 rich gas that may be exploitable to fuel gas turbines and engines, solid oxide and molten carbonate fuel cells, or upgraded for synthesis processes. A promising method is the use of catalysts capable to convert tars in syngas, performing the double function of cleaning the product gas from high molecular weight hydrocarbons, and recovering their energy content.

The research in new materials with catalytic properties is an important stage on the development of the applicability of biomass gasification concepts, with the aim of overcoming problems of in-situ tar elimination for producing a clean gas suitable for feeding fuel cells. Catalytic reforming/cracking of tar is generally carried out at 650-900°C using different materials [Torres *et al.,* 2007], [Sutton *et al.,* 2001], [Abu El Rub *et al.,* 2004]. Among these, olivine and dolomite are considered the most interesting, because they are not expensive and relatively abundant natural minerals [Corella *et al.,* 2004]. Olivine is less active in gasification [Corella *et al.,* 2004], [Rapagnà *et al.,* 2000] but shows the optimal hardness required for the fluidized bed reactor used in the process. Dolomite seems to be more active in tar reforming, and is well known for CO_2 capture properties [Harrison, 2008]. This characteristic, in particular, makes possible the gasification process at lower temperature (650-700 °C, the so called Adsorption Enhanced Reforming, AER process [Marquard-Möllenstedt *et al.,* 2004]) than the conventional 850-900°C, without a real increase in tar content downstream to the gasifier [Marquard-Möllenstedt *et al.,* 2008]. However, dolomite and olivine are not sufficiently active for tar conversion. In order to improve the catalytic activity of these raw materials, the effect of catalytic additives needs to be investigated.

Nickel based catalysts are very active in tar abatement [Swierczynski *et al.,* 2007]. However there are different reasons that limit their use: nickel suffers from deactivation by carbon deposition, and due to its toxicity, it needs a hot gas filter candle to retain nickel particles in the gasifier [Rapagnà *et al.,* 2009].

It has been demonstrated [Swierczynski *et al.,* 2006], [Mondal *et al.,* 2005], [Simmell *et al.,* 1992], [Azhar Uddin *et al.,* 2008], [Polychronopoulou *et al.,* 2006], [Nordgreen *et al.,* 2006a,b], [Tamhankar *et al.,* 1985], [Murata *et al.,* 2003], [Matsuoka *et al.,* 2006], [Wang *et al.,* 2005], [Kiennemann *et al.,* 2009], [Asari *et al.*, 1996], [Ohtsuka *et al.,* 1987] that iron, in different oxidation states, is potentially active in the biomass gasification process, i.e. tar and methane cracking/ reforming, coke reforming and water-gas shift reaction.

Other transition metal-based catalysts, such as Pt, Ru, or Rh, show a good catalytic activity, but the use in a large scale plant of such materials is limited by very high manufacturing costs.

The aim of this work is to investigate synthesis methods, characterization and catalytic tests at different temperatures (650-850°C) of new cheap catalysts for gasification reactions, using toluene and 1-methyl naphthalene as model tar compounds, in a fixed bed microreactor. Their use is proposed as application in both primary and secondary methods for tar abatement (see Chapter 1). Nickel and iron have been added to dolomite, CaO and MgO substrates, in order to improve their catalytic activity. The choice of the support is a crucial step, because deactivation of iron and nickel particles caused by sintering of the surface [Bleeker *et al.,* 2007], [Bartholomew, 2001] and coke formation [Bartholomew, 2001] is well known in literature. Calcined dolomite (Ca,Mg)O, as well as related materials CaO and MgO, may perform as suitable substrates but the MgO-(Fe,Ni) and CaO-(Fe,Ni) interactions have to be deeply investigated. The general formula referred to these catalysts is M/substrate, where M=(Fe, Ni) and substrate=(CaO, MgO, dolomite). These topics will be discussed in details in this Chapter, that is organized in two main sections:

1. a study on characterization of the iron-calcined dolomite (Fe/dol), iron-lime (Fe/CaO) and iron-magnesia (Fe/MgO);
2. a study on characterization of the nickel-calcined dolomite (Ni/dol) and nickel-lime (Ni/CaO);

Nickel and iron metals, impregnated on dolomite, CaO and MgO will be therefore characterized in order to clarify the interactions between cheap, largely used additives in biomass gasification processes.

2. Iron supported on calcined dolomite, CaO and MgO: characterization

2.1 Iron in biomass gasification: a bibliographic survey

Iron, even if less active than other metal-based catalysts described above, offers several advantages: it is an inexpensive, abundant and not toxic material, meaning that it may be employed with higher amounts. In the literature iron has been studied with the aim of clarify the role of this metal in tar and methane cracking as well as reforming catalyst.

Simmel and co-workers [Simmel *et al.*, 1992] have studied catalytic activity of ankerite, a natural mineral containing iron $(Ca, Mg, Fe)(CO_3)_2$, in comparison with other synthetic iron and nickel based catalysts and natural calcined rocks such as limestone and dolomite. They found that the presence of iron might improve the activity of carbonate rocks on decomposition of condensable tarry constituents of fuel gas.

Tamhankar and co-workers [Tamhankar *et al.*, 1985], studying catalytic cracking of benzene on iron oxide-silica substrate, found that this material is very active in particular when iron is present as metallic form. An important issue of this work is that metallic iron catalyses the opening of the benzene ring toward primary coke; in presence of H_2, coke may react with hydrogen producing methane and avoiding catalyst deactivation.

Nordgreen and co-workers [Nordgreen *et al.*, 2006a,b] investigate iron catalytic activity in tar cracking of a biomass gasification process. They found that, at 900°C, small sintered balls of hematite pre-reduced to metallic iron, perform very well in tar abatement downstream to a gasifier. This result is significantly improved when increasing the oxidizing power of the gasification atmosphere up to an Equivalence Ratio (the ratio between the experimental and stoichiometric fuel-to-oxidizer values) of 0.2. However, iron oxides FeO, Fe_3O_4 and Fe_2O_3 do not show any catalytic activity.

Murata and co-workers [Murata *et al.*, 2003] investigate CH_4 decomposition over a $Fe/MgO/Al_2O_3$ catalyst. They found that Fe_3C carbide species are formed by carbon deposition on the catalyst surface, but catalyst deactivation is avoided by $MgFe_2O_4$ phase when an oxidant agent as well as O_2 or CO_2 is also present in the product gas.

Kiennemann and co-workers [Kiennemann *et al.*, 2009] found the efficiency of iron /olivine catalysts for model tar reforming in gasification conditions and assign it to specific interaction between the iron outside of the olivine structure and the iron oxide of the structure.

Polychronopoulou and co-workers [Polychronopoulou *et al.*, 2006] have studied steam reforming of phenol using various supported iron catalysts. They show that iron activity strongly depends from the kind of substrate used: for instance, a 5% Fe/MgO/γ-alumina does not perform in phenol steam reforming, because a Mg_x-Fe_{1-x}-Al_2O_3 spinel inactive phase is formed. The best choice was a CeO-MgO support, containing 5% of iron: the catalytic activity of the iron based catalyst in the 600-700°C temperature window results comparable with a commercial nickel based catalyst. This study at an unusual low temperature shows the feasibility of the *AER* (Absorption Enhanced Reforming) process using an iron catalyst, by mechanical mixing of CeO-MgO-Fe and calcite in a microreactor.

Azhar Uddin and co-workers [Azhar Uddin *et al.*, 2008] have studied catalytic gasification of wood biomass using Fe_2O_3/Al_2O_3 catalysts in a microreactor at 600-850°C. They bring to light the iron contribute, in the form of Fe_3O_4 phase, in tar cracking and water gas shift reaction. In the reaction mechanism hypothesized by authors, the carbon deposited on the iron surface is susceptible to be removed by steam oxidation, producing H_2 and CO.

Matsuoka and co-workers [Matsuoka *et al.*, 2006], working on steam reforming of woody biomass in a fluidized bed at 500 - 700°C using a Fe/γ-alumina catalyst, found that a redox reaction system takes place on the iron oxide surface:

$$Fe_3O_4 + CO \rightarrow 3FeO + CO_2 \tag{1}$$

$$3FeO + H_2O \rightarrow Fe_3O_4 + H_2 \tag{2}$$

CO produced during steam reforming was consumed to reduce Fe_3O_4 (Eq.1), and the FeO resulting from this reaction might react with steam to form H_2 (Eq.2). The WGSR promoted by iron as redox catalyst, rather than reforming of the coke, seems to be the predominant pathway for H_2 production. Moreover, it has been hypothesized that iron may improve catalytic activity of dolomite when it is present as impurity in this substrate [Orio *et al.*, 1997], but there are not in-depth investigations about chemical interactions and active phases of these materials. From the given literature, it seems that the oxidation state of the iron element is not very clear: some authors indicate that metallic iron is the active phase, other that Fe_3O_4 has an effect on tar cracking and WGSR (water-gas shift reaction). This point needs to be highlighted.

2.2 Catalyst preparation

The catalytic systems used in this work consist of pre-calcined dolomite (Ca,Mg)O, lime (CaO) and magnesia (MgO) impregnated by 1-5-10-20% of iron by weight. An exhaustive characterization study has been carried out for the 20% by weight of iron with different substrates and is reported in the Section 2.5, being therefore used as reference for all others iron catalysts.

Because of the iron number oxidation variability, a key step in the preparation and characterization of the iron-based catalysts is the comprehension of the redox reactions involving iron species in different preparation conditions (iron salt, solvent for impregnation, atmosphere of calcination). Therefore, in this work two preparation pathways have been developed (Table 1): an oxidative one, focused on the evaluation of the Fe (3+)–substrate interaction, and a neutral one to evaluate the Fe (2+, 2.5+)–substrate interaction. The prepared samples are listed in Table 2 and associated with their nomenclature.

	Oxidative	**Neutral**
Iron salt	Nitrate (Fe^{3+})	Acetate (Fe^{2+})
Impregnation solvent	Water	Ethanol
Evaporation temperature (°C)	110	80
Thermal treatment atmosphere	Air	Nitrogen

Table 1: Preparation pathways

For both preparation methods, the iron salt is solubilized in the impregnation solvent, then the substrate is added and stirred to obtain a suspension. The solvent is evaporated at the appropriated temperature and the solid is recovered, dried (120°C, 5h) and crashed ($80<d_p<300$ μm). The material is then thermally treated under the appropriate atmosphere at 850°C and 1100°C for 4 h, with a heating rate of 3°C/min, in order to investigate also the influence of thermal treatment on the crystalline phases obtained.

Preparation pathways	**Substrate**	**Nomenclature**
Oxidative	CaO	OxiCa
	MgO	OxiMg
	Calcined dolomite	OxiDolo
Neutral	CaO	NeuCa
	MgO	NeuMg
	Calcined dolomite	NeuDolo

Table 2: Samples and nomenclature

The starting materials consist of a natural dolomite ((Ca,Mg)CO_3) (see Chapter 3 for elemental composition), a natural limestone ($CaCO_3$) coming from L'Aquila rocks, a magnesium nitrate ($Mg(NO_3)_2$) salt used as substrate, an iron (3+) nitrate and an iron (2+) acetate salt (Acros Organics) used as metal precursors. In all cases, the substrate used is pre-calcined at 900°C for 4h with a 3°C/min heating rate, producing (Ca,Mg)O, CaO and MgO.

2.3. Catalyst characterization

The calcined dolomite formula (Ca,Mg)O, suggest that iron may interact with both magnesium and calcium oxides. Therefore, starting from iron acetate or iron nitrate salts and following the neutral and oxidative pathways, a separated analysis of iron (2+, 2.5+, 3+)-calcium oxide and iron (2+, 2.5+, 3+)-magnesium oxide is useful also to clarify the nature of the iron-dolomite interaction.

The Fe/substrate catalysts have been characterized by X-Ray diffraction (XRD), Temperature Programmed Reduction (TPR) and Mössbauer analysis (see Appendix for more details concerning these techniques).

2.4. Thermodynamic Study

Because of the variability of the iron oxidation number (0, 2+, 2.5+ or 3+), iron may interact with the product gas of a biomass gasification process (H_2, CO, CO_2 and H_2O), as schematized below. A preliminary thermodynamic study of iron species with respect to the oxidizing power of the product gas may be useful in the comprehension of the potential active iron phases in catalytic tar abatement.

Oxidizing agent	$\mathbf{Fe^0 \rightarrow Fe^2}$	$\mathbf{Fe^2 \rightarrow Fe^{2.5}}$	$\mathbf{Fe^{2.5} \rightarrow Fe^3}$
H_2O	$Fe^0 + H_2O \leftrightarrow FeO + H_2$	$3FeO + H_2O \leftrightarrow Fe_3O_4 + H_2$	$2Fe_3O_4 + H_2O \leftrightarrow 3Fe_2O_3 + H_2$
CO_2	$Fe^0 + CO_2 \leftrightarrow FeO + CO$	$3FeO + CO_2 \leftrightarrow Fe_3O_4 + H_2$	$2Fe_3O_4 + CO_2 \leftrightarrow 3Fe_2O_3 + CO$

A thermodynamic evaluation of iron oxidation state with respect to these gaseous components has been carried out on the basis of thermodynamic data of reactants and products (Table 3) [Perry's, sixth edition].

Thermodynamic equilibrium curves can be plotted in a graph of partial pressures ratio P_{red}/P_{ox} as a function of temperature (Figure 1) (P_{red}: partial pressure of the reducing agents H_2 or CO; P_{ox}: partial pressure of oxidizing agents CO_2 and H_2O). To evaluate the driving force, Gibbs' energy for the reactions has been obtained starting from ΔH_0^{298} and ΔS_0^{298} indicated in Table 4 and integrating C_p terms up to the corresponding reaction temperature.

Compound	Heat of formation ΔH at 298°K, kcal/mole	Free energy of formation ΔG at 298°K, kcal/mole	Heat capacity C_p (cal/deg mol) at constant pressure, T=K
Fe (s)	0	0	4.13 + 6.38e-3T (273<T<1041) 6.12 + 0.00336T (1041<T<1179)
FeO (s)	-64620	-59380	12.62 + 1.492e-3T − 76200/T^2
Fe_3O_4 (s)	-266900	-242300	41.17 + 0.01882T - 979500/T^2
Fe_2O_3 (s)	-198500	-179100	24.72 + 0.01604 - 423400/T^2
H_2O	-57797,9	-54635,1	8.22 + 1.5e-4T + 1.34e-6T^2
H_2	0	0	6.62 + 8.17e-4T
CO	-26416	-32808	6.6 + 0.00120T
CO_2	-94052	-94260	10.34 + 0.00274T – 195500/T^2

Table 3: Thermodynamic data of reactants and products in the redox system of Fe and product gas

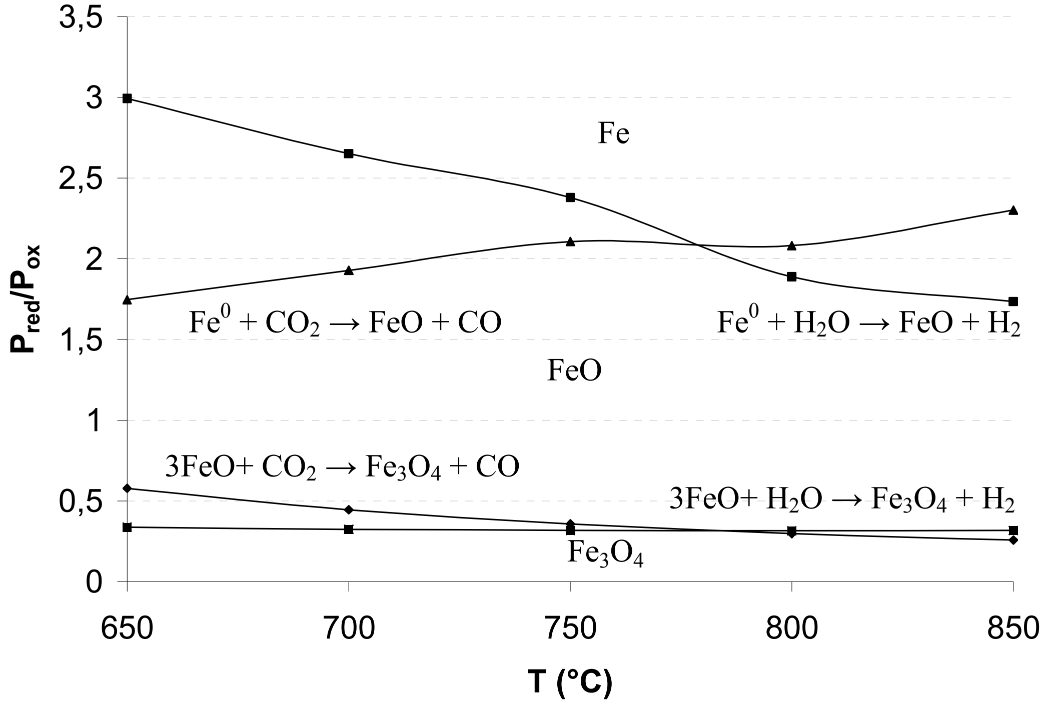

Figure 1: Thermodynamic equilibrium at different temperatures for iron species with respect to main gaseous phases involved in a gasification process

From Figure 1, it is clearly established that FeO is the thermodynamically favourite iron specie in gasification conditions ($P_{red}/P_{ox} \approx 1$, T = 650-850°C). Only when $P_{red}/P_{ox} < 0.5$ or >1.5 – 2, depending on temperature, thermodynamic data allow the formation of Fe_3O_4 and metallic iron, respectively. For instance, Ohtsuka and co-workers [Ohtsuka *et al.,* 1987], have found (by Mössbauer analysis) after 30 minutes of gasification test the following distribution of iron species: 15% metallic iron, 20% Fe_3O_4, 65% FeO. Instead, the transition $Fe_3O_4 \rightarrow Fe_2O_3$ is inhibited when steam or CO_2 are used as oxidant agents. This is a first important information to determine the possibility to discriminate between the oxidation states of iron in the reaction atmosphere of a biomass gasification process, and these data will be considered in Chapter 5, where characterization after catalytic tests will be investigated.

2.5. Phases characterization: 20%Fe/Substrate

2.5.1. Fe/MgO - oxidative and neutral pathway

Many authors have carried out interesting works on the characterization of interaction between magnesium oxide and iron (3+) [Bond *et al.,* 1997], [Stobbe *et al.,* 1991a,b]. Magnesium oxide has been shown to stabilize the supported iron particles and to retard sintering, and may also be favorable in maintaining the mechanical strength and growth of carbon in ethyl benzene dehydrogenation in presence of steam (see references in [Stobb *et al.*, 1991a]). X-ray diffraction (Figure 2) allows to compare the synthesized OxiMg with the raw materials incorporated in this structure, i.e. MgO and Fe_2O_3. In this way, it is well evident that, following the oxidative pathway, a $MgFe_2O_4$ (magnesioferrite) phase is obtained, detectable as well defined peaks but also as shoulder in the right side of some MgO peaks, as evidenced in the zoom zone of Fig. 2, for the sample calcined at 1100°C. Free Fe_2O_3 oxides are not detected.

The Fe-MgO interaction has been also focused in the investigation on reduced species between iron and MgO, following the neutral pathway discussed in Section 2.2. The XRD (X-ray diffraction) analysis in Figure 3 shows a comparison between the NeuMg calcined at 1100°C and the raw materials incorporated in this structure, i.e. MgO and FeO. A strong shift of the MgO peaks toward FeO is observed in the NeuMg diffractogram, (see zoom zone in the figure); this experimental observation evidences that most of the iron is integrated in the MgO substrate as FeO-MgO solid solution .The average composition of the solid solution has been determined from Vegard law as $Fe_{0.1}MgO_{0.9}$.

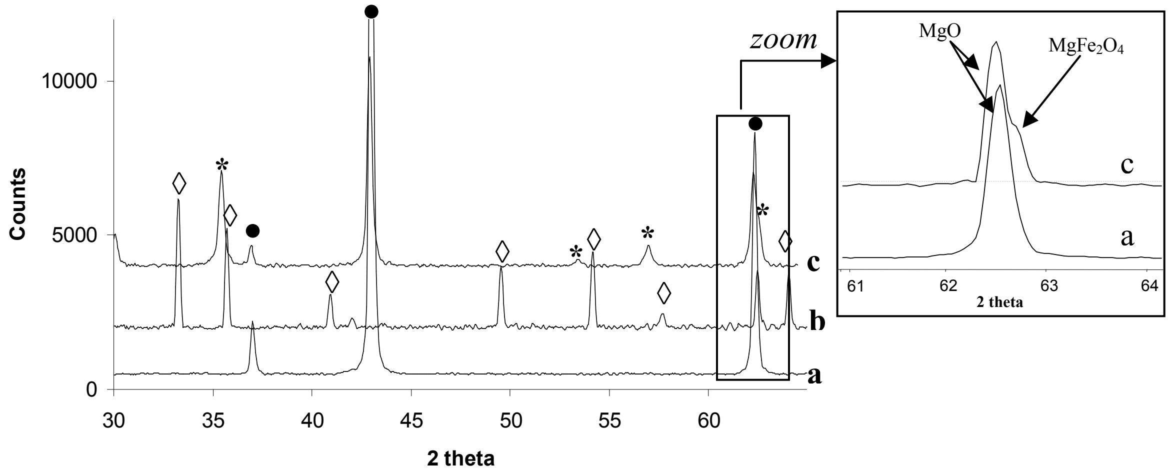

Figure 2: X-RD spectra of MgO (a), Fe_2O_3 (b) and OxiMg calcined at 1100°C (c); the peaks of MgO (●), Fe_2O_3 (◊) and $MgFe_2O_4$ (*)

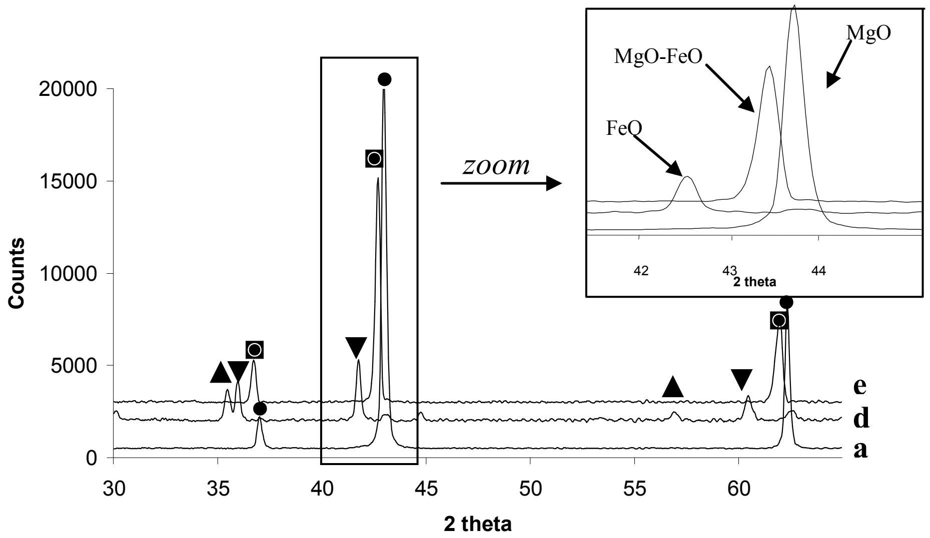

Figure 3: X-RD spectra of MgO (a), Fe_3O_4-FeO (d), and NeuMg calcined at 1100°C (e); the peaks of MgO (●), FeO (▼), Fe_3O_4 (▲) and MgO-FeO (◙)

In order to support X-ray diffraction data, Mössbauer analysis has been carried out for the synthesized samples OxiMg (Fig. 4a) and NeuMg (Fig. 4b), calcined at 1100°C (see Table 4). The OxiMg sample contains only iron in the valence state Fe (3+), and this iron is in the magnetically ordered form, that is in good agreement with spinel $MgFe_2O_4$ detected by X-ray diffraction analysis.

For the NeuMg sample, the paramagnetic doublet is observed: this parameter shows that all iron is in the valence state of Fe (2+) in the structure, once again in accordance with the FeO-MgO solid solution detected by X-ray diffraction.

The samples calcined at 850°C show the same general behavior, the same phases appearing in the X-ray diffraction analysis. However, in this case the analysis shows a general broader peak shape, evidencing that crystalline phases are less defined. Moreover, for the NeuMg sample, a small peak in the Fe_3O_4 zone is also detected (see Fig. 8). It has been reported [Stobb *et al.*, 1991a] that Mg (2+) ions may replace Fe (2+) in the Fe_3O_4 lattice; consequently this phase may be attributed to free iron oxides (Fe_3O_4), to a $Fe_{3-x}Mg_xO_4$ interaction, or to a combination of both (Fe_3O_4-$Fe_{3-x}Mg_xO_4$). This last suggestion will be highlighted by TPR analysis, Section 2.6.1 and Fig. 11, where two separate reduction peaks are associated with Fe (2.5+) species.

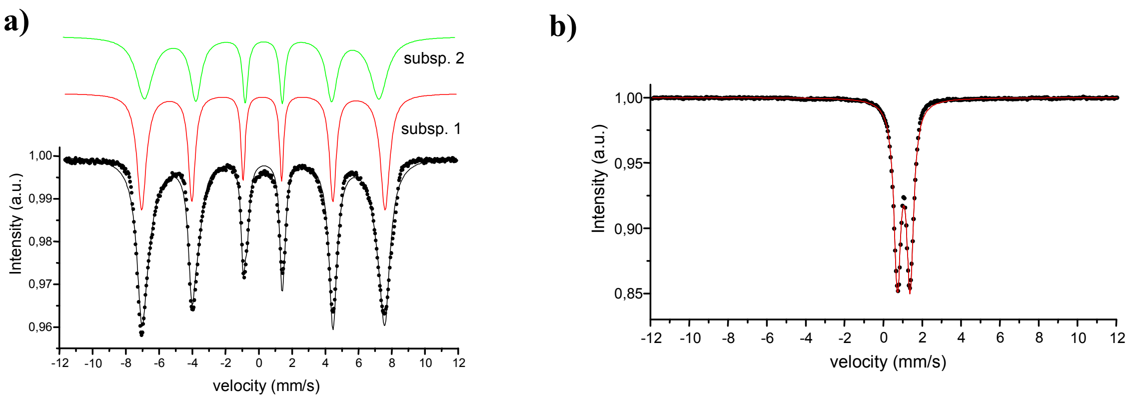

Figure 4: ^{57}Fe Mössbauer spectra room temperature of OxiMg (a) and NeuMg (b) calcined at 1100°C.

	OxiMg (1100°C)		NeuMg (1100°C)
	Subsp. 1	Subsp. 2	Subsp. 1
Isomer shift $\boldsymbol{\delta}$	0,24 mm/s	0,33 mm/s	1,05 mm/s
Quadrupole splitting $\boldsymbol{\Delta E_Q}$	0,06 mm/s	-0,12 mm/s	0,65 mm/s
Hyperfine field $\boldsymbol{B_{HF}}$	45,5 T	43,8 T	
Full line width at half height	2,7 T	6,1 T mm/s	0,43 mm/s
Relative area (%)	45	55	100

Table 4: Mössbauer parameters of components present in the Fe/MgO system, obtained by the oxidative and neutral preparation pathway, respectively

2.5.2. Fe/CaO - oxidative and neutral pathway

The interaction between Fe_2O_3 and CaO has been investigated by X-ray diffraction. Figure 5 shows, for NeuCa calcined at 850°C and OxiCa calcined at 1100°C, that iron is present only as $Ca_2Fe_2O_5$ phase (calcium ferrite, a brownmillerite structure). Iron in the (2+, 2.5+)

oxidation state, as well as free Fe_2O_3 iron oxides, are not detected, using both preparation conditions described in Table 1. This evidence may be due to the possibility of brownmillerite structure to stabilize the oxygen defects [Hirabayashi *et al.,* 2006] and to allow a high oxygen mobility.

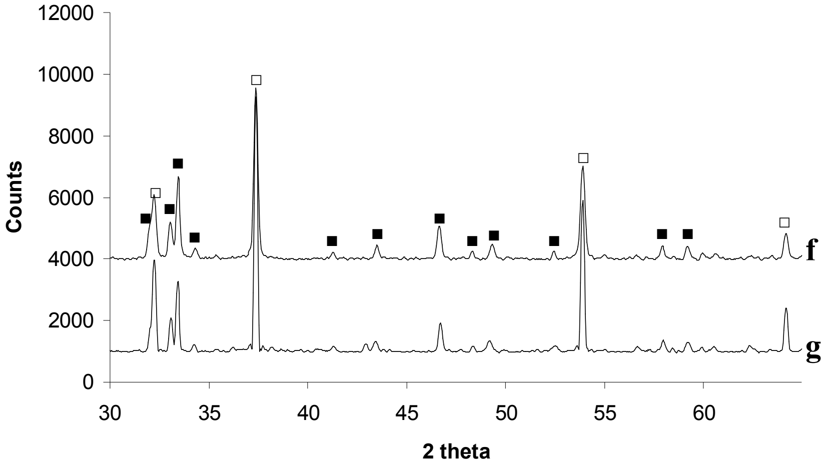

Figure 5: X-RD spectra of OxiCa calcined at 1100°C (f) and NeuCa calcined at 850°C (g); the peaks of CaO (□) and $Ca_2Fe_2O_5$ *(■)*

Mössbauer analysis, carried out for the samples OxiCa calcined at 1100°C, and the NeuCa calcined at 850°C, confirms this evidence, as summarized in Figure 6 a,b and Table 5.

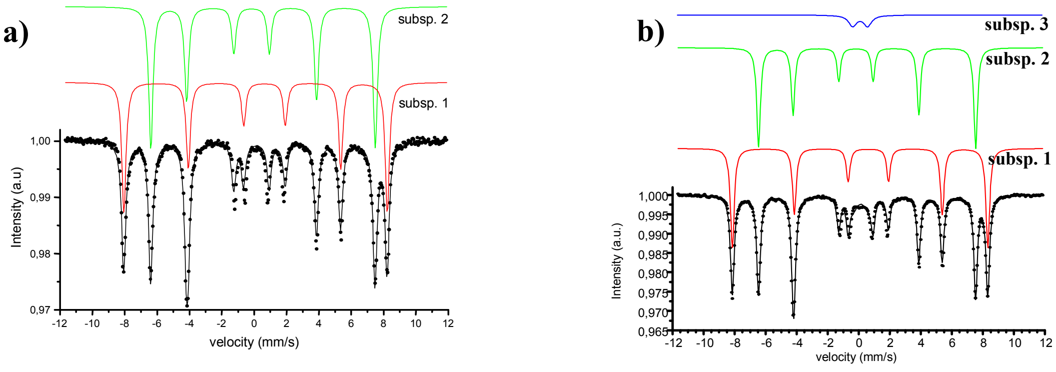

Figure 6: ^{57}*Fe Mössbauer spectra at room temperature of OxiCa calcined at 1100°C (a) and NeuCa calcined at 850°C (b)*

For both catalysts, two sextets correspond to brownmillerite-type $Ca_2Fe_2O_5$. Subspectrum 1 corresponds to the octahedral site Fe^{3+} while subspectrum 2 to the tetrahedral site Fe^{3+}. For the sample NeuCa, calcined at 850°C, the subspectrum 3 (5% of iron) corresponds to trivalent iron in paramagnetic phase; the larger width of the line may represent some phases without good crystallinity.

	NeuCa			OxiCa	
	Subsp. 1	Subsp. 2	Subsp. 3	Subsp. 1	Subsp. 2
Isomer shift **δ**	0,35 mm/s	0,18 mm/s	0,13 mm/s	0,35 mm/s	0,18 mm/s
Quadrupole splitting **ΔE_Q**	0,53 mm/s	0,72 mm/s	0,99 mm/s	-0,55 mm/s	0,71 mm/s
Hyperfine field **B_{HF}**	51,2 T	43,5 T	N/A	50,6 T	43,1 T
Full line width at half height	0,29 mm/s	0,28 mm/s	0,60 mm/s	0,31 mm/s	0,31 mm/s
Relative area (%)	48	47	5	48	52

Table 5: Mössbauer parameters of components present in Fe/CaO system; OxiCa sample calcined at 1100°C, and NeuCa calcined at 850°C

2.5.3. Fe/dolomite - oxidative and neutral pathway

From the study carried out on Fe/MgO and Fe/CaO, it is expected that Fe/dolomite interactions take place as $Ca_2Fe_2O_5$ and $MgFe_2O_4$ phases in the oxidative pathway, and as $Ca_2Fe_2O_5$, FeO-MgO and Fe_3O_4-$Fe_{3-x}Mg_xO_4$ in the so-called neutral pathway. Therefore, this study will proceed comparing these three phases for the respective preparation methods. Since there have not been detected significant variations between the two temperatures of calcination for the Oxi- and Neu- catalysts, only the samples calcined at 850°C will be investigated in this section.

X-ray diffraction of the OxiDolo (Fig.7, diffractogram h) is compared to X-ray diffraction of $Ca_2Fe_2O_5$ (Fig.7, i) and $MgFe_2O_4$ (Fig.7, j). It is evident that $MgFe_2O_4$ phase is not detected but that iron interacts strongly with CaO as $Ca_2Fe_2O_5$. As no other MgO-iron oxide is evidenced, it appears that all Fe (3+) reacted with CaO.

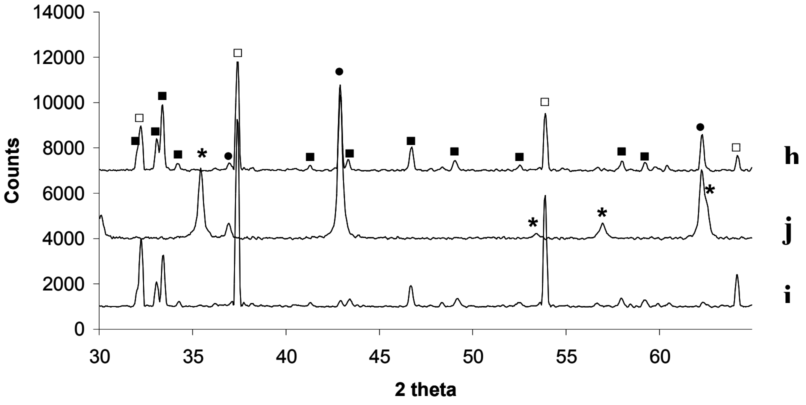

Figure 7: X-RD spectra of OxiDolo (h), OxiCa (i) and OxiMg (j) calcined at 850°C; the peaks of CaO (□), MgO(●), $Ca_2Fe_2O_5$ (■) and $MgFe_2O_4$ (*)

For the neutral pathway (Figure 8), X-ray diffraction shows once again a strong presence of $Ca_2Fe_2O_5$, but a peak in the Fe_3O_4 zone is also clearly detected, that is perfectly superposed with the peak of NeuMg sample calcined at 850°C. This means that the same Fe_3O_4-$Fe_{3-x}Mg_xO_4$ mixed phase has been detected. Superposition of TPR analyses between NeuMg and NeuDolo calcined at 850°C (see Section 2.6.3, Fig. 13), also supports this evidence. The FeO-MgO solid solution is not detected by shift in the MgO peaks, as it was evidenced in the NeuMg sample.

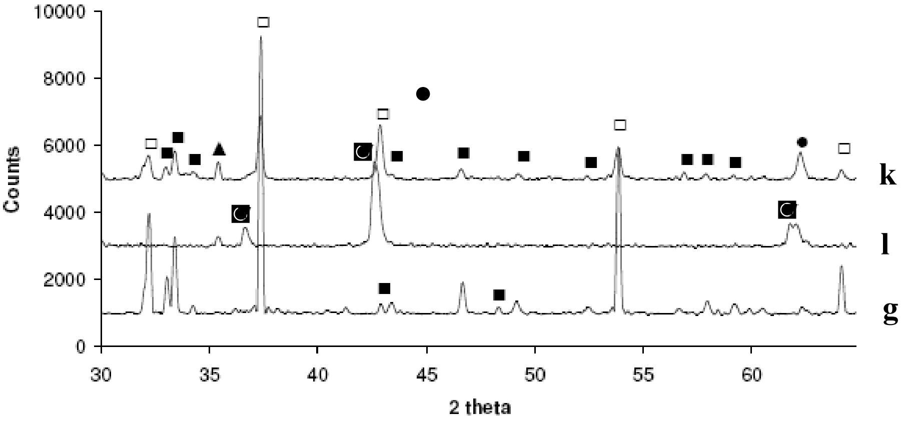

Figure 8: X-RD spectra of NeuDolo (k), NeuCa (g) and NeuMg (l) calcined at 850°C; the peaks of CaO (□), MgO (●), $Ca_2Fe_2O_5$ (■), Fe_3O_4-$MgFe_3O_5$ (▲) and MgO-FeO (◙)

In order to better interpret the XRD results, a Mössbauer analysis has been carried out for both OxiDolo and NeuDolo (Figure 9 a,b and Table 6) calcined at 850°C; the former contains 88% of iron as brownmillerite-type $Ca_2Fe_2O_5$, and the remaining 12% results in a Fe (3+) valence state representing paramagnetic phase of iron. The latter contains 43% of iron in the $Ca_2Fe_2O_5$ phase (subspectrum 1 and 3), 25% of iron in the spinel phase (subspectrum 2 and 4), and 32% of the iron representing sample in the paramagnetic phase in the mixed valence state Fe(2+) – Fe(3+). The spinel phase could be attributed to Fe_3O_4-$Fe_{3-x}Mg_xO_4$ as evidenced by X-ray diffraction; the subspectrum 2 represents iron (3+) in the tetrahedral coordination, while subspectrum 4 represents iron (2+ - 3+) in the octahedral coordination.

Resuming the interactions of Fe/CaO, Fe/MgO and Fe/dolomite catalysts, we can argue that:

- Fe/CaO favors strongly Fe (3+) species in a well detectable interaction with the substrate, a $Ca_2Fe_2O_5$ brownmillerite structure, whatever the starting degree of iron oxidation and the nature of the solvent;

- Fe/MgO interaction has been found to takes place with both Fe (2+) and Fe (3+) species, as FeO-MgO solid solution and $MgFe_2O_4$, but also a small amount of Fe_3O_4-$Fe_{3-x}Mg_xO_4$ has been detected;

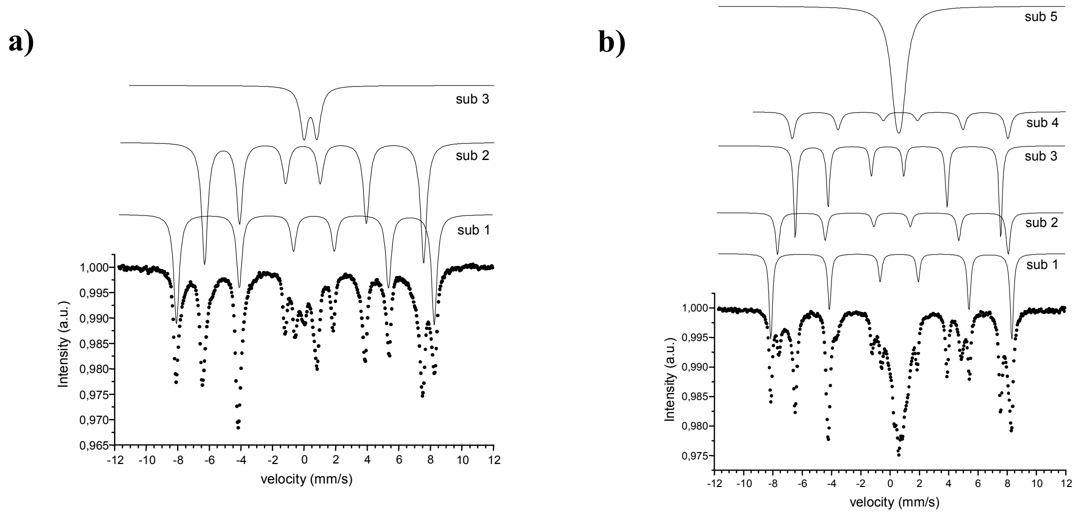

Figure 9: ^{57}Fe Mössbauer spectra measured at room temperature of OxiDolo (a) and NeuDolo (b) calcined at 850°C.

	Oxidolo (850°C)		
	Subsp. 1	Subsp. 2	Subsp. 3
Isomer shift ***δ***	0,35 mm/s	0,18 mm/s	0,30 mm/s
Quadrupole splitting $\boldsymbol{\Delta E_Q}$	-0,54 mm/s	0,71 mm/s	0,82 mm/s
Hyperfine field $\boldsymbol{B_{HF}}$	50,7 T	43,5 T	N/A
Full line width at half height	0,40 mm/s	0,49 mm/s	0,56 mm/s
Relative area (%)	39	49	12

	Neudolo (850°C)				
	Subsp. 1	Subsp. 2	Subsp. 3	Subsp. 4	Subsp. 5
Isomer shift ***δ***	0,35 mm/s	0,27 mm/s	0,18 mm/s	0,64 mm/s	0,59 mm/s
Quadrupole splitting $\boldsymbol{\Delta E_Q}$	-0,54 mm/s	0,05 mm/s	0,71 mm/s	-0,03 mm/s	0,39 mm/s
Hyperfine field $\boldsymbol{B_{HF}}$	51,1 T	48,9 T	43,6 T	45,8 T	N/A
Full line width at half height	0,26 mm/s	0,32 mm/s	0,26 mm/s	0,46 mm/s	0,90 mm/s
Relative area (%)	21	13	22	12	32

Table 6: ^{57}Fe Mössbauer parameters of components present in Fe/dolomite system; Oxidolo sample calcined at 850°C, and Neudolo sample calcined at 850°C

- Fe/dolomite interaction, in particular with the OxiDolo sample, has been found to be very dependent from Fe/CaO interaction ($Ca_2Fe_2O_5$). The NeuDolo catalyst may contains iron as (2.5+) specie, that has been pointed out as Fe_3O_4-$Fe_{3-x}Mg_xO_4$.

In the reductive reaction atmosphere, these phases could change due to the tendency towards the thermodynamic constraints of iron redox reactions discussed in Section 2.4; Fe (2+) is identified as the favorite specie in gasification conditions. This aspect will be investigated in Chapter 5, where a catalyst characterization after test will be examined. Before that, the reduction pathway of these kinds of iron catalysts has been investigated with TPR (Temperature Programmed Reduction) analysis. The identification of reduction intermediates of iron on the CaO, MgO, and dolomite surface, and the evaluation of their stability as a function of temperature, is of great interest because they may represent the active forms in the catalytic steam reforming and water-gas shift reactions, allowing to understand the possible evolution of iron oxidation state when it is in contact with the reductive gasifier atmosphere.

2.6. Reduction behaviour of iron

The first step in the understanding of an iron supported catalyst reduction pathway is the evaluation of free iron oxides reduction. In this respect, hematite reduction is known from literature [Messi *et al.,* 2001] to take place in different ways, including direct reduction to Fe(0) and successive reductions and disproportions involving Fe_3O_4, FeO and Fe (0) [Stobbe *et al.,* 1991b].

TPR of small particles of hematite and magnetite have been carried out as blank tests. Hematite shows a first reduction peak at 440°C, that may corresponds to $Fe_2O_3 \rightarrow Fe_3O_4$ transition. Fe_3O_4 reduction peak appears at 590°C. A final peak, the reduction of FeO to Fe, is detected at approximately 800°C.

A very different and more complex situation may occur as far as supported iron phases are concerned, because of the development of oxide-support interactions.

2.6.1. Fe/MgO reduction

The TPR of OxiMg and NeuMg are shown in Figures 10 and 11, respectively. TPR peaks of OxiMg (as well as NeuMg) are slightly shifted toward higher temperatures with respect to free iron oxide, as evidenced in particular in the transition zone FeO→Fe (0), where the solid solution MgO-FeO reduction takes place. This interaction is known to preserve iron (2+) species [Stobbe *et al.,* 1991b] (the transition FeO→Fe (0) may be not completed) even in a strongly reductive atmosphere. The sample calcined at 850°C shows a first peak at 480°C that is absent with the sample calcined at 1100°C, evidencing a more reducible (less associated to the support) iron oxide. This datum agrees with XRD analysis that showed a broader peaks shape (less defined crystalline structures) for the lower calcination temperature. The sample calcined at 1100 °C evidences a reduction pathway almost unresolved, where the absence of free Fe_2O_3 is confirmed by the starting temperature of the reduction, 500°C instead of 400°C. More precisely, three reduction peaks are noticeable, which fit well with the OxiMg sample calcined at 850°C: the first peak, appearing at 600°C, may be ascribed to the $MgFe_2O_4 \rightarrow Fe_3O_4\text{-}Fe_{3-x}Mg_xO_4$ transition, the second reduction zone, between 650-800°C, to the $Fe_3O_4\text{-}Fe_{3-x}Mg_xO_4 \rightarrow MgO\text{-}FeO$, while the third (900°C) corresponds well to the above mentioned FeO reduction zone.

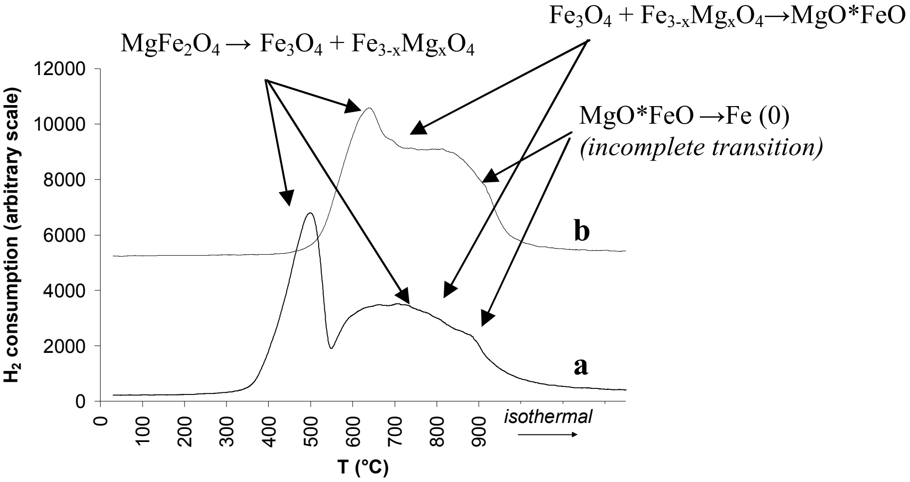

Figure 10: TPR analysis for OxiMg calcined at 850 (a) and 1100°C (b)

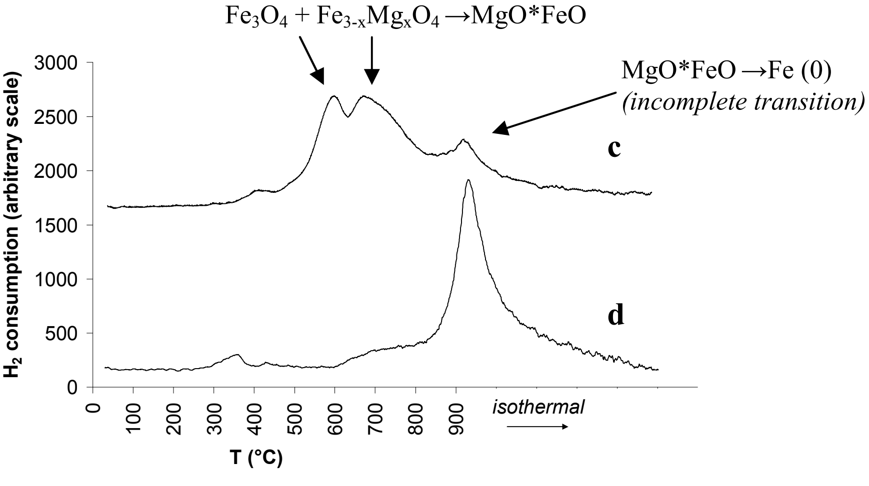

Figure 11: TPR analysis for NeuMg calcined at 850 (c) and 1100°C (d)

In the NeuMg sample calcined at 1100°C (Fig.11), the only phase present, the FeO-MgO solid solution, is reduced at very high temperature (900°C), and it is clear from the low intensity of this peak that the transition FeO→Fe(0) is not completed, the FeO-MgO interaction allowing to stabilise Fe (2+) species. For the sample calcined at 850°C, once again the weak interaction predicted by X-ray diffraction and the evidence of some Fe (2.5+) specie are confirmed, two reduction peaks at 600 and 750°C evidencing the reduction pathway of small amount of Fe_3O_4-$Fe_{3-x}Mg_xO_4$ phases. In particular, the former peak fits well with the reduction temperature of free Fe_3O_4, and the second one may be associated with a Fe (2.5+) more intimately mixed with the substrate, in the $Fe_{3-x}Mg_xO_4$ phase, as indicated in Figure 11.

2.6.2. Fe/CaO reduction

TPR analysis of calcium ferrite $Ca_2Fe_2O_5$ detected by XRD for the Fe/CaO - oxidative and neutral preparation pathways (Fig. 12), evidences a single broad reduction peak, near 880°C; this high reduction temperature reveals the stability of this phase. In this case iron seems to be forced toward the unique transition Fe (3+)→Fe (0), evidencing once again that Fe (2+) is not a stable phase in the Fe-CaO interaction, as highlighted in the NeuCa sample analysis.

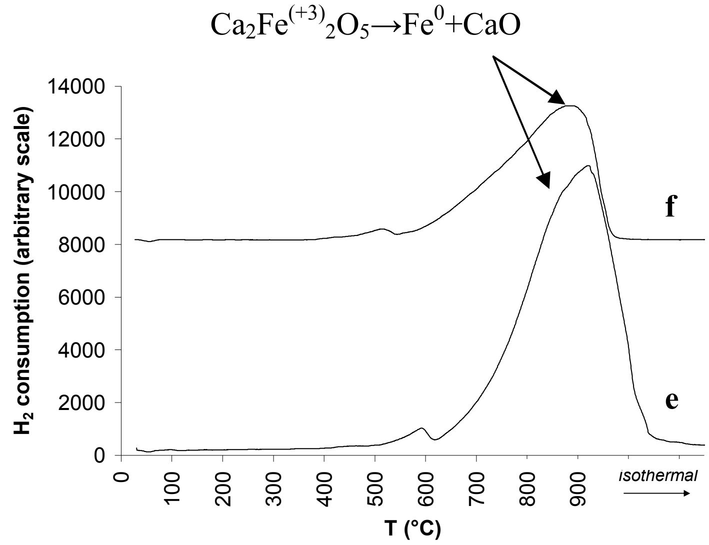

Figure 12: TPR analysis for OxiCa calcined at 1100°C(e) and NeuCa calcined at 1100°C(f)

2.6.3. Fe/dolomite reduction

As done previously for XRD analysis, a first qualitative characterization of the reduction behaviour of the Fe/dolomite catalysts (calcined at 850 and 1100°C) may be obtained from a superposition with their components. In particular, the OxiDolo sample evidences a good superposition with the OxiCa sample, confirming XRD and Mössbauer analyses.

Also TPR of NeuDolo calcined at 850°C, is consistent with previous analyses (Section 2.5.3). A plain method to resolve TPR of this sample (Fig. 13), evidencing the presence of four main peaks, is the superposition with the sample NeuMg calcined at 850°C. The first, the second and the fourth peak may be associated to the Fe-Mg reduction pathway, being associated to $Fe_3O_4 – Fe_{3-x}Mg_xO_4 \rightarrow FeO$ (600-750°C) → Fe (0) (900°C) reduction pathway. In this way, the third peak appearing at 880°C may be easily related to the $Ca_2Fe_2O_5 \rightarrow Fe$ (0) + CaO reduction.

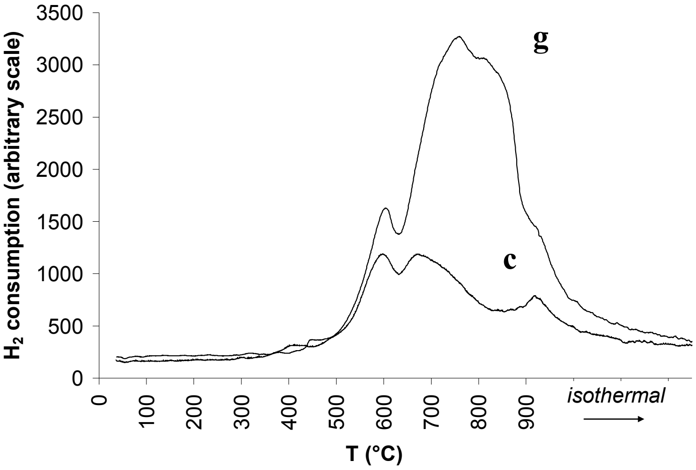

Figure 13: TPR analysis for Neudolo (g) compared with NeuMg (c) calcined at 850°C

2.7. Catalyst characterization after reduction

In order to complete characterisation of Fe-CaO, Fe-MgO and Fe-dolomite catalysts, these materials have been analysed after TPR by X-ray diffraction and Mössbauer analysis.

2.7.1 Fe/MgO after TPR

After TPR, the magnesioferrite peaks of OxiMg detected by X-ray diffraction in Section 2.5.1 are disappeared. However, instead of this phase, metallic iron is well detectable (not indicated here) and a shoulder appears now in the left side of the MgO peaks, as evidenced in the zoom of Fig. 14a: this is the FeO-MgO solid solution zone, demonstrating that part of iron in the magnesioferrite reduction pathway from Fe (3+) to Fe (0) is preserved to Fe (2+) due to the stability of FeO-MgO interaction.

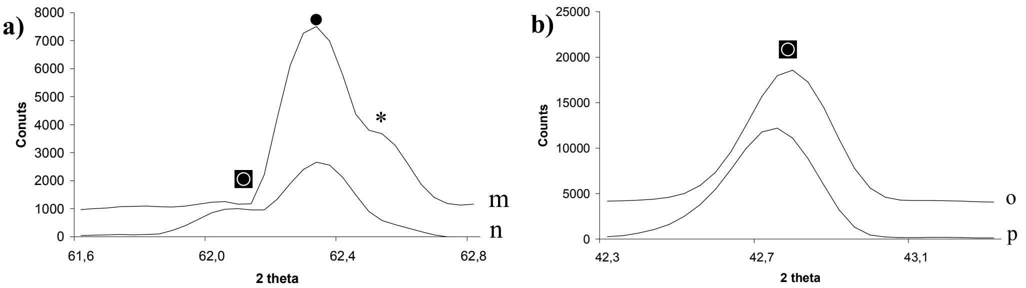

Figure 14: Diffractogram zoom zones of a) OxiMg and b) NeuMg samples before (m, p) and after (n, o) TPR, the peaks of MgO (●), $MgFe_2O_4$ (*) and MgO-FeO (◙) solid solution

This behaviour is even more evident when the NeuMg sample is analysed by X-ray diffraction. Figure 14b shows, in a zoom zone of the diffractogram, that the shifted peak of MgO-FeO solid solution is yet well evident, confirming the low reduction peak of FeO-MgO into Fe(0) detected by TPR.

Mössbauer analysis for OxiMg and NeuMg has been carried out in order to quantify the relative amounts of iron species after TPR. The former sample contains 21% of Fe (2+), and the greatest amount (75%) is in the form of alfa-Fe (metallic iron); but there is also some residue of Fe (3+), about 4%. In the latter sample (NeuMg) the amount of metallic iron is much smaller: the sample contains 18% of α-Fe (metallic iron) and 82 % of Fe (2+).

2.7.2. Fe/CaO after TPR

For both OxiCa and NeuCa, the $Ca_2Fe_2O_5$ phase is not detectable after TPR by X-ray diffraction analysis, neither iron in (2+) form. This means that, even if the reduction of $Ca_2Fe_2O_5$ takes place at high temperature, the transition Fe (3+) → Fe (0) is quite complete.

2.7.3. Fe/dolomite after TPR

X-ray diffraction analysis for both OxiDolo and NeuDolo shows similar results, because iron is extracted from the dolomite particle in the metallic form, $Ca_2Fe_2O_5$ (for OxiDolo and NeuDolo) and Fe_3O_4 – $Fe_{3-x}Mg_xO_4$ (for NeuDolo only) peaks do not appear in the diffractogram. Mössbauer analysis of these samples evidences that, together with metallic iron as the predominant phase, 6% of iron is preserved as Fe (2+) for the OxiDolo, and a 20% for the NeuDolo. This result is in agreement with previous considerations: a preferential Fe (3+) →Fe (0) reduction for the iron-calcium oxide interaction, as is the case of OxiDolo catalyst, and a more complex pathway for the iron-magnesium oxide system, detected only in the NeuDolo sample. In this latter case, with a transition through Fe (2.5+) specie that is partially extracted from the structure as Fe_3O_4-$Fe_{3-x}Mg_xO_4$ phase, iron (3+) is reduced to FeO and easily captured by magnesium oxide matrix in the stabilized FeO-MgO solid solution, avoiding a complete reduction to the metallic form.

A schematic model of the phases obtained in the OxiDolo and NeuDolo catalysts and their reduction behaviour is shown in Fig. 15.

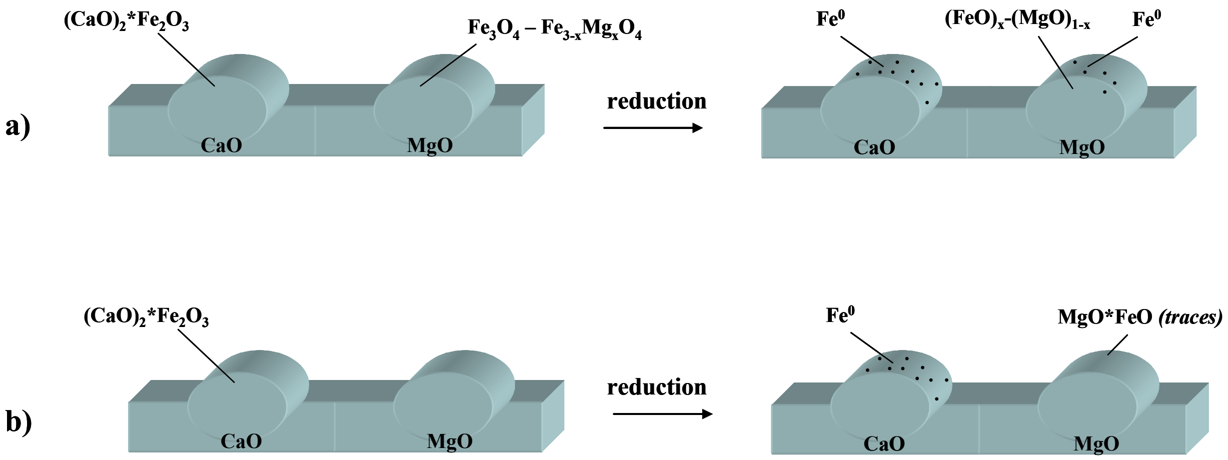

Figure 15: A schematic model of the phases obtained in the NeuDolo (a) and OxiDolo (b)catalysts, and their reduction behaviour

2.8. Different iron quantities in the Fe/Substrate materials

Different quantities of iron, from 1 to 20%, have been added on CaO, MgO and (Ca,Mg)O following the oxidative pathway described in Section 2.2, and samples were calcined at 850°C. From characterization results it is clear that different percentages of iron do not have any influence in the detected phases for every synthesized catalyst. For the Fe/CaO catalysts series, iron is always detected as $Ca_2Fe_2O_5$, dicalcium ferrite phase, together with CaO; for Fe/MgO, a $MgFe_2O_4$ (magnesioferrite) phase is produced. Free iron oxides have not been detected. The principal phases evidenced for Fe/dol are CaO, MgO and $Ca_2Fe_2O_5$; free iron oxides or iron-magnesium oxide interactions have not been evidenced, confirming a strong interaction between iron (III) and calcium oxide. This evidence is in good agreement with previous works on ankerite [Milodowski *et al.,* 1989], a natural mineral substance with formula $Ca(Fe^{II}_{(1-x)}Mg_x)(CO_3)_2$. When this material is calcined up to 900°C, in a pure CO_2 atmosphere, the iron(II) is rapidly oxidized to iron(III) and leads to the formation of the $Ca_2Fe_2O_5$ phase.

3. Nickel supported on calcined dolomite and CaO: characterization

3.1. Catalysts preparation

The catalytic systems used for nickel based catalysts consist of the same pre-calcined dolomite (Ca,Mg)O and lime (CaO) described in Section 2.2, impregnated by 4 and 10% of nickel by weight. The same impregnation method described in Section 2.2 (oxidative pathway) has been used for nickel supported catalysts; nickel nitrate ($Ni(NO_3)_2$) salt (Acros Organics) has been adopted as precursor salt. After impregnation, the samples are calcined at 900 and 1100°C in air, 3°C/min for 4h.

3.2. Catalysts characterization

3.2.1. Ni/dolomite interaction

The characterization of Ni/dolomite catalyst, prepared according to the methodology explained in Appendix, highlights the interactions between NiO and CaO-MgO dolomite substrate.

When calcined dolomite and Ni/dolomite samples are compared, the X-ray diffraction analysis (Figure 16 for 4%Ni/dolomite) shows that there are not new phases in the Ni/dolomite catalyst with respect to the raw calcined dolomite.

This means that a solid solution between calcined dolomite and NiO is produced, and in particular, due to the slight difference on atomic radius between Mg and Ni (about 10%) we can infer that a solid solution MgO-NiO is obtained. This interaction is known from previous works [Swierczynski *et al.*, 2006, 2007] to have beneficial effects on increasing carbon deposition resistance.

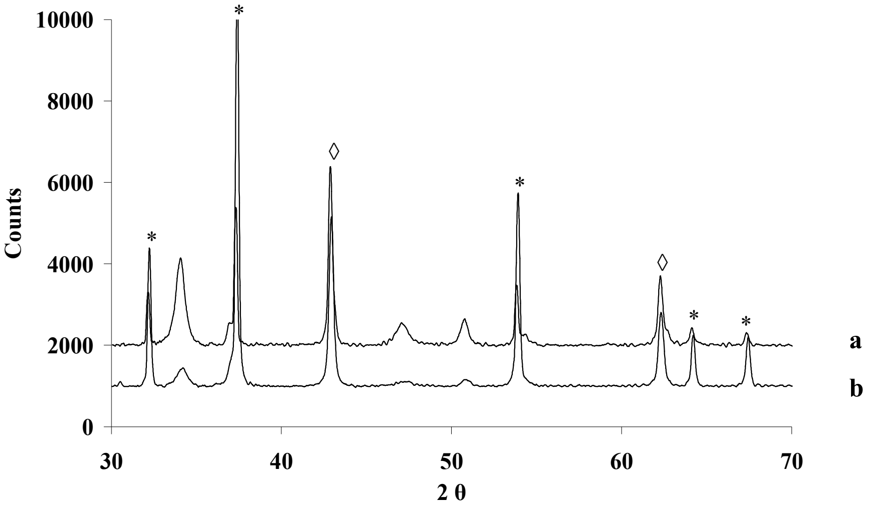

*Figure 16: X-Ray diffraction for the 4% Ni/dolomite catalyst (a) compared with calcined dolomite (b) (◊ = CaO; * = MgO)*

TPR analysis of the samples calcined at 900 and 1100°C shows a key difference in the behavior of this NiO-MgO solid solution with respect to calcination temperature. For both catalysts, a high reduction temperature (900°C) has been observed, that may be identified as the reduction zone of NiO in the NiO-MgO solid solution. In fact, NiO in the crystal lattice of MgO is strongly bounded with the substrate and therefore less available for the reduction. However, the sample calcined at 900°C shows a reducibility of about 25% calculated by the calibration method; on the other hand, the sample calcined at 1100°C evidences only a very small peak (about 4%) near 900°C for NiO reduction. This information is very important considering that reduction is the key step to activate a nickel based catalyst. As a matter of fact, the sample calcined at 1100°C did not exhibit any catalytic activity, and only data related to the Ni/dolomite sample calcined at 900°C are shown here. A similar tendency has been previously found with Ni/olivine samples calcined at 1100 and at 1400°C, respectively, for methane and toluene reforming [Courson *et al.,* 2002], [Swierczynski *et al.,* 2006].

3.2.2. Ni/CaO interaction

This work has been focused on Ni/CaO catalysts, because of a main reasons: nickel interacting with CaO should be completely reduced in the metallic form at reaction conditions, that is more nickel active sites should become available for catalysing reforming reactions.

These outlooks have been investigated in this work, in order to discriminate the better support for nickel between CaO and (Ca,Mg)O. Being the interaction between nickel and dolomite as NiO-MgO solid solution, a plain catalyst NiO-MgO has not been considered of interest.

X-ray diffraction of 4% and 10% Ni/CaO shows clearly the presence of both, well distinguished CaO and NiO phases. Therefore, TPR of these samples have been carried out in order to understand the reducibility of nickel on the surface of CaO. Figure 17 shows TPR for the 10% Ni/CaO sample: it is clear that in this case nickel is free on the surface of the substrate, the reduction peak beginning to appear at 400°C. A near total metal reduction (about 95%) has been calculated by the calibration method, for both 10%Ni/CaO and 4%Ni/CaO.

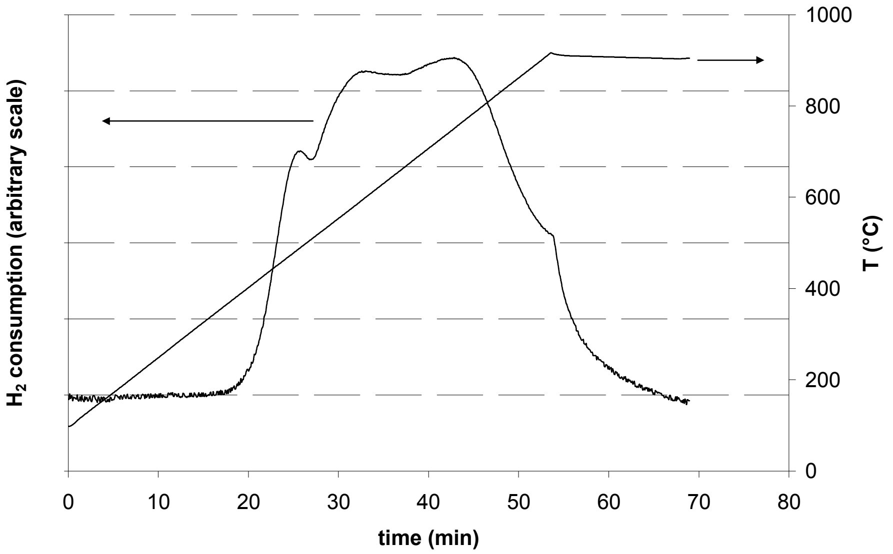

Figure 17: Temperature Programmed Reduction of 10% Ni/CaO

4. Conclusions

The interactions highlighted in this chapter between nickel and iron metals and CaO, MgO and (Ca,Mg)O substrates are summarized in Table 7. It may be emphasized that:

- M (2+) (Fe, Ni) interacts merely with MgO; when no MgO is present in the substrate, M (2+) may be oxidised by oxygen supplied from the substrate itself (i.e., for iron), or is free on the substrate surface (i.e., for nickel);
- M (3+) (i.e., Fe) may interact with both CaO (as $Ca_2Fe_2O_5$) and MgO (as $MgFe_2O_4$) substrates. In presence of dolomite, the M (3+)-CaO interaction is prevailing;
- The reduction of M (2+) (Fe, Ni) is strongly limited by the interaction MO-MgO. For both Fe and Ni, no more than 20-25% of metal is formed after TPR; when no MgO is present in the substrate, M (2+) may be easily and fully reduced to metallic specie (i.e., for nickel);
- The reduction of M (3+) (i.e., Fe) proceeds in different ways depending on the interactions with the substrate. It has been reported that iron seems to be forced to the unique transition, at very high temperature, Fe (3+)→Fe (0) for the M (3+)/CaO interaction, whereas it is capable of a higher mobility in the M (3+)/MgO system, with the transitions Fe (3+)→Fe (2.5+)→Fe (2+)→Fe (0) allowed.

Substrate Metal	MgO	CaO	(Ca,Mg)O
Iron (III)	Magnesioferrite $MgFe_2O_4$	Brownmillerite-like $Ca_2Fe_2O_5$	Brownmillerite-like $Ca_2Fe_2O_5$
Iron (II)	(Fe,Mg)O solid solution	Brownmillerite-like $Ca_2Fe_2O_5$	Brownmillerite-like $Ca_2Fe_2O_5$ + Fe_3O_4-$Fe_{3-x}Mg_xO_4$
Nickel (II)	-	NiO, CaO	(Ni,Mg)O solid solution

Table 7: M/substrates interactions

Bibliography

Abu El-Rub Z., Bramer A.E., Brem G., (2004), Review of catalysts for tar elimination in biomass gasification, Industrial and Engineering Chemistry Research 43, 6911-6919.

Asami K., Sears P., Furimsky E., Ohtsuka Y., (1996), Gasification of brown coal and char with carbon dioxide in the presence of finely dispersed iron catalysts. Fuel Process. Technol. 47, 139-151.

Azhar Uddin Md., Tsuda H., Wu S., Sasaoka E., (2008), Catalytic decomposition of biomass tars with iron oxide catalysts, Fuel 87, 451-459.

Bartholomew C.H., (2001), Mechanisms of catalyst deactivation, Applied Catalysis A: General 212, 17–60.

Bleeker M.F., Kersten S.R.A., Veringa H.J., (2007), Pure hydrogen from pyrolysis oil using the steam-iron process , Catalysis Today 127, 278–290.

Bond G., Molloy K.C., Stone F. S., (1997), Reduction of MgO-supported iron oxide: formation and characterization of Fe/MgO catalysts, Solid State Ionics 101-103, 697-705.

Corella J., Toledo J.M., Padilla R., (2004), Olivine or dolomite as in-bed additive in biomass gasification with air in a fluidized bed: Which is better?, Energy Fuels 18, 713-720.

Courson C., Udron L., Swierczynski D., Petit C., Kiennemann A., (2002), Hydrogen production from biomass gasification on nickel catalysts: Tests for dry reforming of methane, Catalysis Today 76, 75-86

Harrison D.P., (2008), Sorption-Enhanced Hydrogen Production: A Review, Ind. Eng. Chem. Res. 47, 6486-6501.

Hirabayashi D., Yoshikawa T., Mochizuki K., Suzuki K., Sakaib Y., (2006), Formation of brownmillerite type calcium ferrite ($Ca_2Fe_2O_5$) and catalytic properties in propylene combustion, Catalysis Letters 110, 155-160.

Kiennemann A., Courson C., Virginie M., Catalyseurs pour le reformage de goudrons utilisables dans la vapogazéification de la biomasse, Demande Brevet Français, mai 2009.

Marquard-Moellenstedt T., Specht M., Zuberbuehler U., Koppatz S., Pfeifer C., Rauch R., Soukup G., Hofbauer H., Koch M., (2008), Transfer of the absorption enhanced reforming (AER)-process from the pilot scale to an 8 mwth gasification plant in Guessing, Austria, Proceedings of the 14th European Conference on Biomass for Energy Industry and Climate Protection, Valencia, Spain, 02-06 June 2008.

Marquard-Möllenstedt T., Sichler P., Specht M., Michel M., Berger R., Hein K.R.G., Höftberger E., Rauch R., Hofbauer H., (2004) Proceedings of 2nd World Conference on Biomass for Energy, Industry and Climate Protection, Rome, Italy, 10-14 May 2004.

Matsuoka K., Shimbori T., Kuramoto K., Hatano H., Suzuki Y., (2006), Steam Reforming of Woody Biomass in a Fluidized Bed of Iron Oxide-Impregnated Porous Alumina, Energy & Fuels 20, 2727-2731.

Messi C., Carniti P., Gervasini A., (2008), Kinetics of reduction of supported nanoparticles of iron oxide, Journal of Thermal Analysis and Calorimetry 91, 93–100.

Milodowsky A.E., Morgan D.J., (1989), Thermal analysis studies of the dolomite-ferroan dolomite-ankerite series. II. Decomposition mechanism in flowing CO_2 atmosphere, Thermochimica Acta 152, 279-297.

Mondal K., Piotrowski K., Dasgupta D., Hippo E., Wiltowski T., (2005), Hydrogen from Coal in a Single Step, Ind. Eng. Chem. Res. 44, 5508-5517.

Murata K., Inaba M., Saito M., Takahara I., Mimura N., (2003), Methane decomposition over iron-based catalysts in the presence of O_2 and CO_2, Journal of Japan Petroleum Institute 46, 196-202.

Nordgreen T., Liliedahl T., Sjostrom K., (2006a), Metallic iron as a tar breakdown catalyst related to atmospheric, fluidized bed gasification of biomass, Fuel 85, 689-694.

Nordgreen T., Liliedahl T., Sjostrom K., (2006b), Elemental Iron as a Tar Breakdown Catalyst in Conjunction with Atmospheric Fluidized Bed, Energy & Fuels 20, 890-895.

Ohtsuka Y., Tamai Y., Tomita A., (1987), Iron-catalyzed gasification of brown coal at low temperatures, Energy Fuels 1, 32-36.

Orio A., Corella J., Narvaez I., (1997), Performance of different dolomites on hot raw gas cleaning from biomass gasification with air, Ind. Eng. Chem. Res. 36, 3800-3808.

Perry's Chemical Engineers' handbook, sixth edition.

Polychronopoulou K., Bakandritsos A., Tzitzios V., Fierro J.L.G., Efstathiou A.M., (2006), Absorption-enhanced reforming of phenol by steam over supported Fe catalysts, Journal of Catalysis, 241, 132-148.

Rapagnà S., Jand N., Kiennemann A., Foscolo P.U., (2000), Steam-gasification of biomass in a fluidized-bed of olivine particles, Biomass and Bioenergy 19, 187-197.

Rapagnà S., Gallucci K., Di Marcello M., Foscolo P.U., Nacken M., Heidenreich S., (2009), In situ catalytic ceramic candle filtration for tar reforming and particulate abatement in a fluidized-bed biomass gasifier, Energy Fuels 23, 3804–3809.

Simmell P.A., Leppalahti J.K., Bredenberg J. B-son, (1992), Catalytic purification of tarry fuel gas with carbonate rocks and ferrous materials, Fuel 71, 211-218.

Stobbe E.D., van Buren R., (1991a), Iron oxide dehydrogenation catalysts supported on magnesium oxide. Part 1.- Preparation and characterization, J. Chem. Soc. Faraday Trans. 87, 1623-1629.

Stobbe E.D., van Buren R., (1991b), Iron oxide dehydrogenation catalysts supported on magnesium oxide. Part 2.- Reduction behaviour, J. Chem. Soc. Faraday Trans. 87, 1631 – 1637.

Sutton D., Kelleher B., Ross J.R.H., (2001), Review of literature on catalysts for biomass gasification, Fuel Processing Technology 72, 155-173.

Swierczynski D., Courson C., Bedel L., Kiennemann A., Guille J., (2006), Characterization of Ni Fe/MgO/Olivine Catalyst for Fluidized Bed Steam Gasification of Biomass, Chem. Mater. 18, 4025-4032.

Swierczynski D., Courson C., Kiennemann A., (2007), Study of steam reforming of toluene used as model compound of tar produced by biomass gasification, Chemical Engineering and Processing: Process Intensification 47, 508-513.

Tamhankar S.S., Tsuchiya K., Riggs J.B., (1985), Catalytic cracking of benzene on iron oxide-silica: catalyst activity and reaction mechanism, Applied Catalysis 16, 103-121.

Torres W., Pansare S.S., Goodwin J.G. Jr., (2007), Hot Gas Removal of Tars, Ammonia, and Hydrogen Sulfide from Biomass Gasification Gas, Catalysis Reviews 49, 407 - 456.

Wang T., Chang J., Lu P., Novel Catalyst for Cracking of Biomass Tar, (2005), Energy & Fuels 19, 22-27.

CHAPTER 5

IRON AND NICKEL SUPPORTED ON CALCINED DOLOMITE, CaO AND MgO : A STUDY ON REACTIVITY

Abstract: *In this chapter, the catalytic activity on tar reforming of new iron and nickel based catalysts supported on alkaline earth oxides CaO, MgO and on calcined dolomite has been investigated, using toluene and 1-methyl naphthalene as model tar compounds, at different temperatures (650-850°C). The* CO_2 *absorption kinetic and absorption capacity of the new Fe/dolomite and Ni/dolomite have been also investigated under milder temperature conditions (650°C), where the sorption process is thermodynamically favoured. As a result, it has been found that iron and nickel may be optimised in the substrate particles in order to improve catalytic activity and/or carbon deposition resistance during catalytic tests, and at the same time minimising critical limitations on* CO_2 *capture capacity and kinetics.*

1. Introduction

In this Chapter the reactivity of nickel and iron based catalysts supported on CaO, MgO and (Ca,Mg)O (calcined dolomite) will be investigated in a fixed bed microreactor, using toluene and 1-methyl naphthalene as model tar compound.

Due to the CO_2 absorption properties of calcium oxide-containing substrates, the CO_2 absorption kinetic and absorption capacity of metal doped CaO and (Ca,Mg)O have been also investigated, in order to check the CO_2 sorption function, coupled with that of gasification catalyst. This work is therefore aimed also to optimize the metal content in the substrate-sorbent in order to find a good compromise between catalytic activity and CO_2 capture properties of different M/substrates.

2. Reactivity tests

2.1. Experimental apparatus

The experiments for testing new materials for catalytic steam reforming of toluene (TSR), 1-methyl naphthalene (1-MnSR) and CO_2 capture, were carried out in a fixed bed microreactor rig under atmospheric pressure. A quartz reactor (8 mm I.D.) (labelled (1) in Figure 1) was charged with a variable amount (400-800 mg) of catalyst ($80 < d_p < 300\mu$m), inserted between two plugs of quartz wool, and then placed in the middle of an electric furnace (labelled (2) in Figure 1). The instantaneous catalyst bed temperature was monitored by a thermocouple located near to the catalyst bed. The flow rate of the gaseous compounds is measured by mass flow meters (5), and the feeding system consists of two main lines (named 1 and 2 in Figure 1). Nitrogen has been always added to the reactant gases at a fixed and known molar flow rate, so that to provide a reference flow to evaluate the absolute yield of the reaction products, allowing to normalize the area of gas-chromatographic peaks. The outlet gas, passing through a condensation unit (3) has been analyzed by two gas-chromatographs equipped with TCD. The former indicating the amount of H_2, N_2, CH_4, CO separated on a molecular sieve 5Å, and the latter quantifying Ar, CH_4 and CO_2 separated on a column Hayesep Q. The GC calibration has been done by employing a gas cylinder containing a reference mixture for CH_4 (19.58%), H_2 (22%), CO (18.83%), CO_2 (19.8%) and N_2 (19.81%).

2.1.1. Steam reforming tests

Line 1, feeding directly the reactor, has been used to preserve the catalyst bed in a neutral (argon) atmosphere during heat-treatments (the temperature is raised until 850°C at a rate of

10°C/min, and then the reforming test starts) or purge of the gas-chromatographs downstream of the reactor, when necessary.

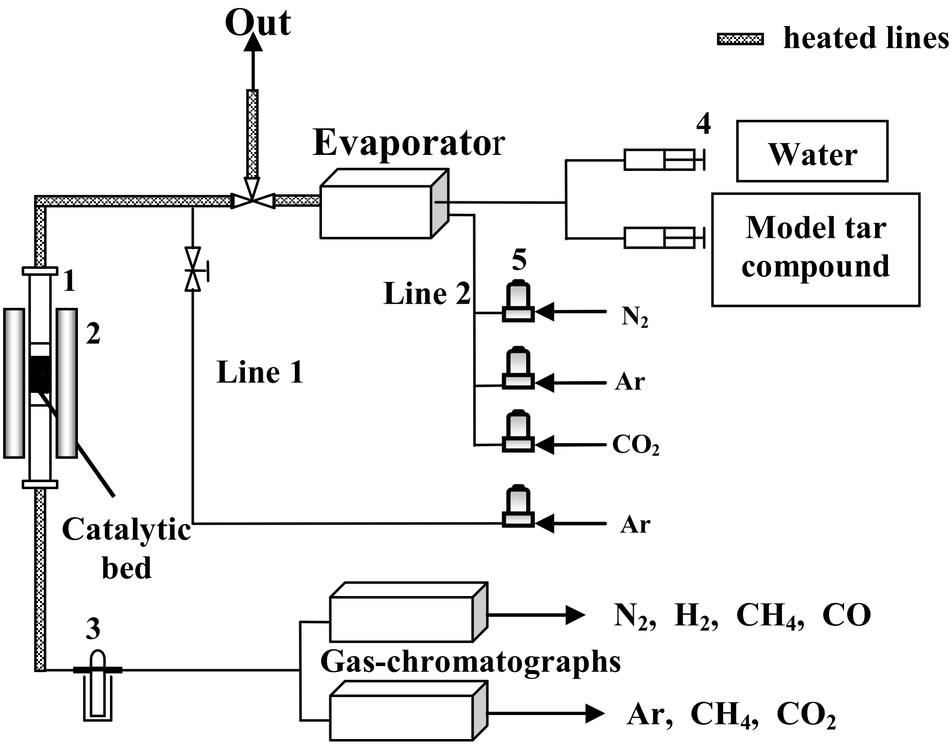

Figure 1: *Schematic diagram of the experimental apparatus (fixed bed microreactor): 1, quartz microreactor; 2, furnace; 3, condenser; 4, motorised syringes for feeding liquids; 5, mass flows controllers*

Line 2 (Ar and N_2 mixture), acts as a carrier gas for steam and tar model compounds during catalytic tests, passing through an evaporation chamber where water and model tar compounds are introduced as liquids by motorised syringes (labelled 4 in Figure 1). The temperature of the evaporation chamber, as well as the temperature of all feeding tubes, is kept above the dew point of toluene and 1-methyl naphthalene (250°C), to prevent condensation. Pre-reduction of iron has not been carried out before each test, because metallic iron may be easily reoxidated by steam or CO_2 in reaction conditions, as evidenced by the thermodynamic analysis discussed in Chapter 4. With nickel based catalysts, tests have been also carried out without a preliminary reduction, being this metal directly activated (reduced) in the reactant gas flow.

Toluene steam reforming reactions have been performed for all catalytic systems (raw substrates CaO, MgO and dolomite, 1-5-10-20% Fe/(Ca,Mg)O and Fe/CaO, 5-20% Fe/MgO, 4-10% Ni/(Ca,Mg)O and Ni/CaO), whereas 1-Methyl naphthalene reforming tests have been carried out for the nickel based catalyst series, 4-10% Ni/(Ca,Mg)O and Ni/CaO. The adopted experimental conditions are described in Table 1. The feeding gas mixture composition has been adjusted in order to obtain a tar concentration of 30 g/Nm^3, which corresponds roughly to the higher limit for the gas phase in a biomass gasifier. The (steam)/(model tar compound) ratio for toluene and 1-Mn steam reforming tests is slightly higher (18:1 and 27:1, respectively) than the stoichiometric value for complete conversion into H_2 and CO_2 (14:1 and 22:1, respectively).

2.1.2. CO_2 capture and Absorption Enhanced Reforming tests

The same apparatus has been used to perform plain CO_2 capture and absorption enhanced reforming tests (Figure 1). In both cases, temperature is raised to 850°C, 10°C/min, and the flue gas is monitored to ensure a complete calcination of bed material (even if pre-calcined, CaO and MgO based substrates may absorb some CO_2 from atmosphere). Then, the temperature is adjusted to 650°C, and the test was started (see experimental conditions in Table 2). In the CO_2 capture tests, a CO_2 mass flow meter is connected with Line 2, and the test was running until the end of absorption is reached.

For Absorption Enhanced Reforming tests, the nickel based catalyst is activated at 850°C, in the reaction gas flow, for about 30 minutes. Then the atmosphere is switched to inert flow (from Line 2 to Line 1), the temperature is decreased to 650°C, and finally the Absorption Enhanced Reforming test is started switching again the inlet gas from Line 1 to Line 2.

	T.S.R.	**1-Mn S.R.**
Parameter	**Value**	**Value**
Ar (NL/h)	2.02	2.02
H_2O (NL/h of steam)	0.36	0.36
Toluene (NL/h vapour)	0.02	-
1-Mn (NL/h)	-	0.013
N_2 (NL/h)	0.60	0.60
Reactor temperature (°C)	850	850
Particle size (µm)	80-300	80-300
Bed mass (mg)	400	400

Table 1: Feeding composition and test conditions for Toluene and 1-Mn steam reforming tests

	CO_2 absorption test	**Absorption Enhanced Reforming test**
Parameter	**Value**	**Value**
Ar (NL/h)	2.02	2.02
H_2O (NL/h of steam)	-	0.36
CO_2 (NL/h vapour)	0.14	-
Toluene (NL/h vapour)	-	0.02
N_2 (NL/h)	0.60	0.60
Reactor temperature (°C)	650	650
Particle size (µm)	80-300	80-300
Bed mass (mg)	400	800

Table 2: Experimental conditions for CO_2 capture tests

CO_2 capture tests have been carried out with raw dolomite and CaO, 1-5-20% Fe/(Ca,Mg)O, 4-10% Ni/(Ca,Mg)O. Due to the limited CO_2 absorption properties of the natural limestone used in this work, as will be highlighted in Section 4.1, the doped lime has not been considered of interest in this series of experiments.

Absorption enhanced reforming tests have been carried out with 4%Ni/(Ca,Mg)O. As a matter of fact, iron has been found to be not active in toluene steam reforming at the limited temperature window where CO_2 capture is thermodynamically favoured (650°C in ours tests).

3. Catalytic activity of Fe/(CaO, MgO, dolomite) on toluene steam reforming

3.1. 20%Fe/Substrates: a comparison between Oxi- and Neu- catalysts

The catalytic activity in toluene steam reforming of supports and supported catalysts has been studied at 850°C. The main reactions that take place in the system are:

Steam reforming of toluene $C_7H_8 + 7H_2O \rightarrow 7CO^{(a)} + 11H_2$ (R1)

Water-gas shift $CO^{(b)} + H_2O \leftrightarrow CO_2 + H_2$ (R2)

The overall conversion of toluene may be expressed as a function of carbon-containing components in the gas-phase, X_t (Eq.1).

$$X_t = \frac{\left[CO^{(b)}\right]+\left[CO_2\right]+\left[CH_4\right]}{7\cdot\left[C_7H_8\right]_{in}} \tag{1}$$

where square brackets indicate molar concentration of each gaseous specie. The influence of each separated reaction, in terms of conversion X, may be estimated by the stoichiometric equations (Eq. 2), (Eq. 3):

$$X_{R1} = \frac{\left[CO^{(b)}\right]+\left[CO_2\right]}{7\cdot\left[C_7H_8\right]_{in}} \tag{2}$$

$$X_{R2} = \frac{\left[CO_2\right]}{\left[CO^{(b)}\right]+\left[CO_2\right]} \tag{3}$$

and a hydrogen balance, useful to check the accuracy of X_t, $X_{(R1)}$ and $X_{(R2)}$, may be arranged as (Eq. 4):

$$\left[H_2\right] = 11\cdot\left[C_7H_8\right]_{in}\cdot X_{(R1)} + \left(\left[CO^b\right]+\left[CO_2\right]\right)\cdot X_{(R2)} \tag{4}$$

The "theoretical" hydrogen values obtained applying Eq.(4) are therefore compared with the experimental H_2 concentration obtained in each test, to quantify the % error that affects the test. It needs to be evidenced from now that some methane is always produced during steam reforming of toluene and 1-Mn; this evidence is not surprising because methane is more difficult to be reformed than higher cyclic hydrocarbons.

Results of catalytic tests (see Table 1 for experimental conditions) using different catalytic systems containing 20% of iron are shown in Figure 2a (for CaO, MgO and dolomite supports) and b (for OxiCa, OxiMg, OxiDolo, see Chapter 4) in terms of %Xt (% of toluene conversion) as a function of time. Mean values for outlet concentrations obtained for H_2, CO, CO_2 and CH_4 are shown in Table 3, whereas mean values of X_{R1} and X_{R2}, and the % error on hydrogen balance, are shown in Table 4, Section 2.2, together with others % iron on dolomite.

The reactivity tests with calcined dolomite, lime and magnesia, confirm the reactivity trends obtained by other authors [Delgado *et al.,* 1997], the activity of dolomite being superior to CaO and MgO activities due to some degree of distortion in the array of the Ca or Mg atoms, generating thus more active sites. CaO and MgO are considerably less active than dolomite, and in addition need an activation time in the reactive flow, before reaching a plateau of reactivity. When iron is added to alkaline-earth oxides, i.e. calcined dolomite, magnesia and lime, the improvement on catalytic activity of these materials is mainly related to the metal-support interaction and cooperation, due to the weak evidence (only for NeuMg and NeuDolo) of free iron oxides in such catalytic systems (see Chapter 4).

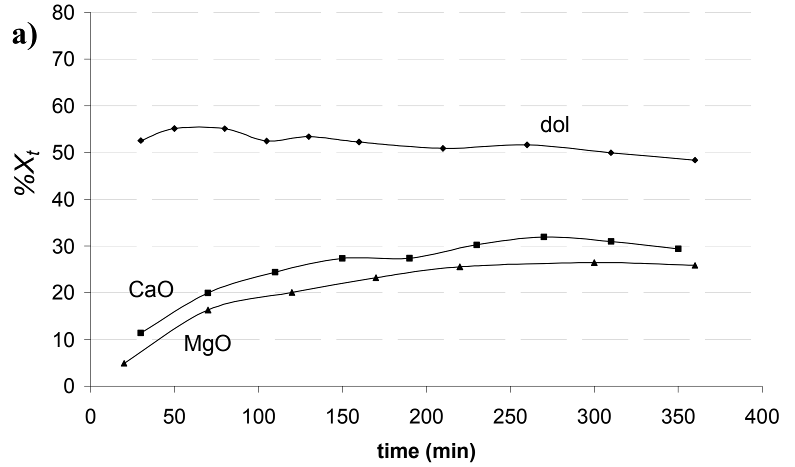

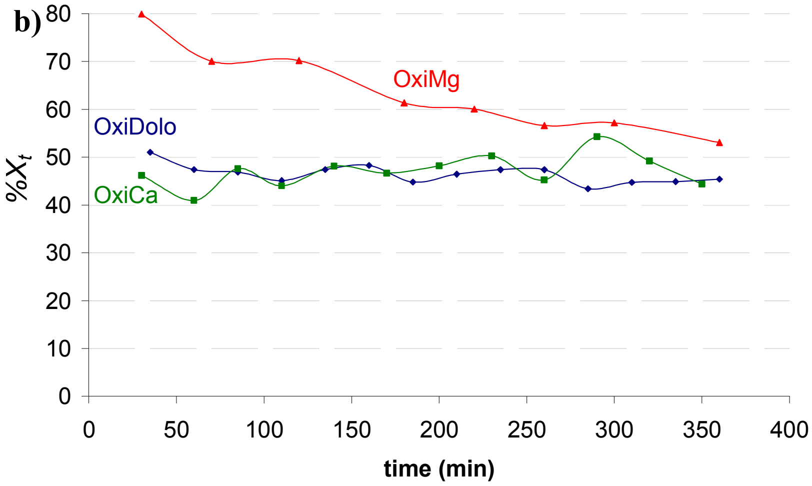

Figure 2: Toluene conversion, as defined in Eq. 1, as function of time for supports (a) and for the 20% iron catalysts prepared in the oxidative pathway (b).

	OxiCa	**OxiMg**	**OxiDolo**	**CaO**	**MgO**	**(Ca,Mg)O**
%H_2	5.42	7.16	5.65	3.04	1.94	6.07
%CO	1.03	1.50	0.81	0.34	0.28	0.98
%CO_2	1.41	1.82	1.68	1.04	0.60	1.79
%CH_4	0.19	0.15	0.19	0.03	0.34	0.08

Table 3: Mean values of % concentration in the outlet gas for toluene steam reforming using 20%Fe/(dolomite, CaO, MgO), oxidative pathway.

OxiCa and OxiDolo show the same reactivity, whereas OxiMg shows a slightly superior toluene conversion, which decreases during the 6 hours on test, from 77% to about 55% of toluene conversion. For the OxiDolo sample, no substantial improvement on toluene conversion is observed with respect to raw dolomite. OxiCa, however, is able to rise the catalytic toluene conversion of raw CaO, from values below 30% up to 45-50% of conversion. This result is very interesting because lime has been indicated as the most recommended additive for steam gasification in a fluidized bed at low-medium (600-800°C) temperature [Corella *et al.,* 2006], being less soft and therefore less susceptible to erosion in a fluidized bed. The disadvantage of being less active than dolomite in tar elimination has been overcame in this study by adding iron to this substrate, which determines an useful improvement in catalytic activity.

The OxiMg system also improves considerably catalytic activity of pure MgO, toluene conversion rising from 25% to about 60% when iron is added to the substrate. This improvement on reactivity is absent in the Fe/dolomite reactivity, meaning that iron, even in a reductive atmosphere, remains mainly bounded with calcium oxide as $Ca_2Fe_2O_5$, as it will shown in the sections dedicated to catalyst characterization after tests (Sections 6.1 and 6.2). Similar trends are obtained for the samples prepared with the neutral pathway (Figure 3): a slight increase (about 10%) in conversion values with respect to Fig. 2b has been recorded. However, due to a low reactivity difference, a slight deactivation observed and a high cost of manufacturing with respect to the oxidative pathway, the Neu- pathway is not interesting to prepare a catalyst suitable for scale up or further investigations. It has been however useful for understanding the Fe/CaO-MgO-dolomite interactions, investigated in Chapter 4.

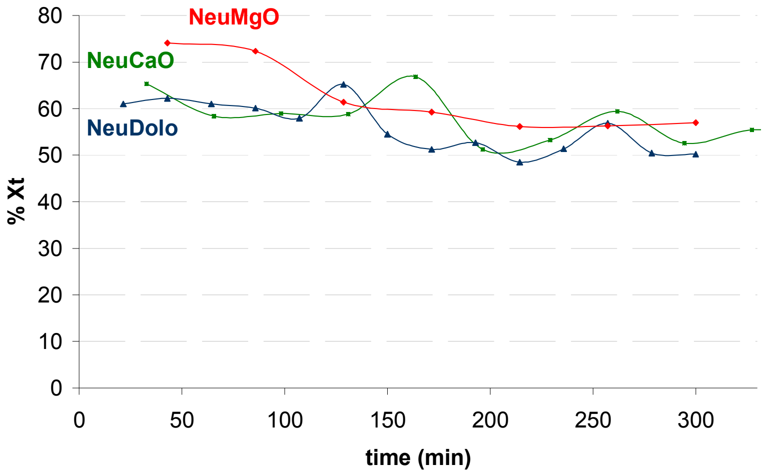

Figure 3: Toluene conversion, as defined in Eq. 1, as a function of time for 20% iron catalysts prepared according to the neutral pathway.

3.2. Fe/(CaO, MgO, dolomite): differences on reactivity varying the iron content

The second step in the investigation of iron based catalysts supported on CaO, MgO and (Ca,Mg)O is to optimize the iron content in each catalytic system that will assure the greatest conversion values in toluene steam reforming. Results of catalytic tests using different percentages of iron in the Fe/dol, Fe/CaO and Fe/MgO systems are shown in Figure 4a, b, and c respectively, in terms of $\%X_t$ (% of toluene conversion, Eq.1) as a function of time. Reactivity tests using 10%Fe/(CaO, dolomite) are similar to those of 20%Fe/(CaO, dolomite), and are not reported in the Figure. Table 4 shows mean calculated values for $X_{(R1)}$, $X_{(R2)}$, and the % error on hydrogen balance that results always below 5%. It is noticeable that, at constant inlet composition, $X_{(R2)}$ is negatively affected by $X_{(R1)}$, because when the catalytic action is strong, more H_2 and less steam are available in the system as a result of reaction (*R1*), and the H_2/H_2O ratio has a clear influence on the water-gas shift reaction. Figure 5 shows a general variation tendency of X_{R2} with respect to X_{R1}. Data have been divided into three groups, each of them with similar X_{R1} values, to render their X_{R2} values comparable. It may be clearly observed that catalysts performing better for water-gas shift reaction are dolomite and Fe/MgO (higher values of X_{R2} with similar X_{R1}) in the groups 1 and 2 respectively. For Group 3, it may be understood that Fe/dolomite shows a better activity with respect to Fe/CaO in improving the water-gas shift reaction rate. This general behaviour may be explained following the catalyst characterization carried out after test (Sections 5.1 and 5.2). Dolomite and iron based catalysts are known in literature to have beneficial effects on accelerating the water-gas shift reaction rate [Xie *et al.,* 2009], however the activity of iron is strongly dependent from its redox behaviour (see Equations 1 and 2 in Chapter 4). This characteristic, that may be called iron "mobility" [Asami *et al.,* 1996] between different oxidation species, is clearly affected by iron-substrate interactions. As it will be highlighted in Sections 5.1 and 5.2, the iron mobility is strongly limited when CaO only is used as substrate, and therefore the lower reactivity on water-gas shift reaction may be explained. For Fe/MgO systems, however, it has been yet reported in Chapter 4 an higher iron mobility, being the transitions Fe (3+)→Fe (2.5+)→Fe (2+)→Fe (0) allowed over a broad temperature range.

For Fe/(Ca,Mg)O, catalyst characterization carried out after test (Sections 5.1 and 5.2) will highlight a superior iron mobility with respect to CaO, because of the MgO role on stabilizing Fe (2+) species.

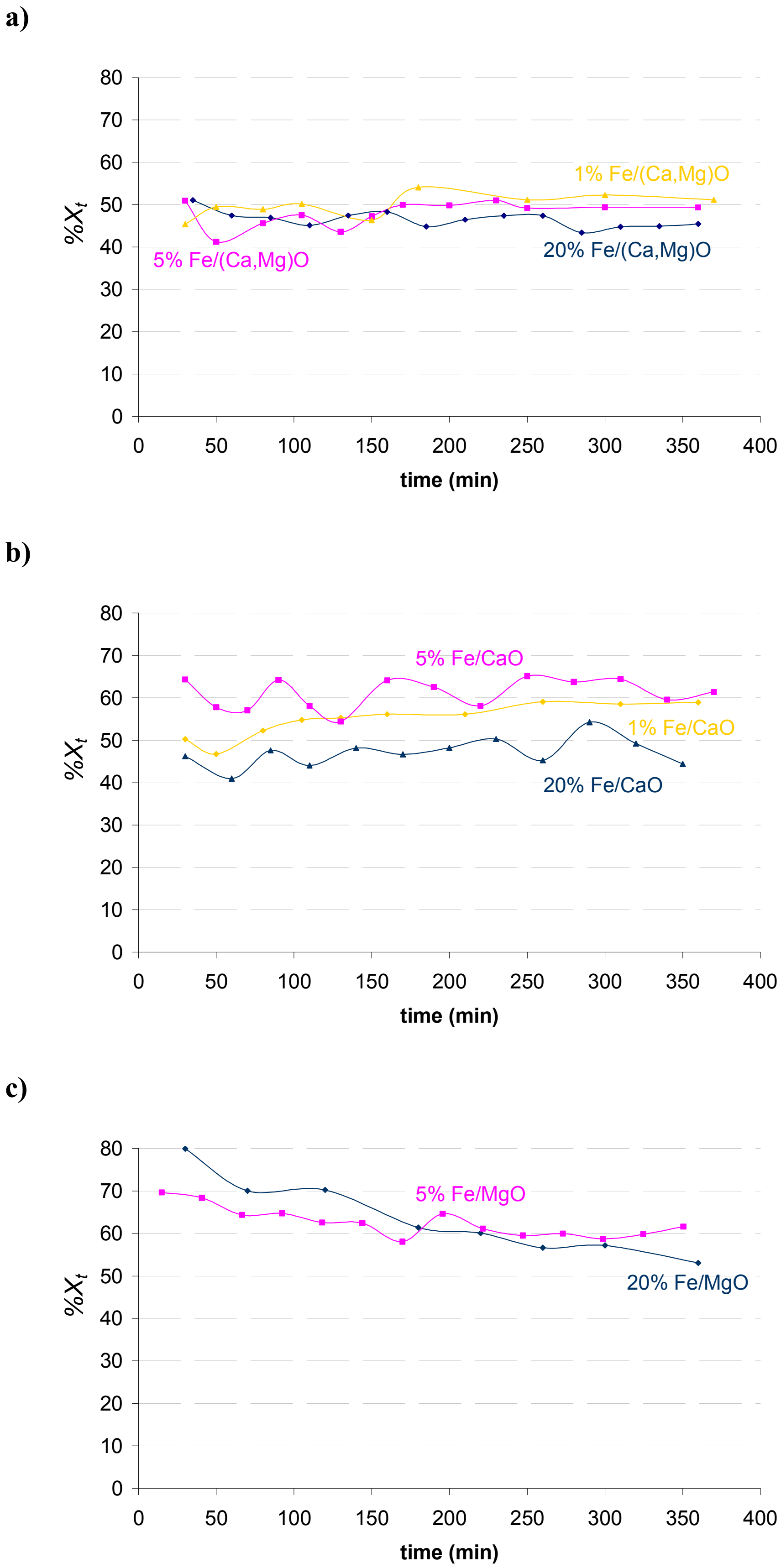

Figure 4:Toluene conversion as a function of time in steam reforming tests using (a) 1%, 5% and 20% Fe/dol, (b) 1%, 5% and 20% Fe/CaO and (c) 5% and 20% Fe/MgO.

Catalyst	%$X_{(R1)}$	%$X_{(R2)}$	% error on H_2 balance
1%Fe/CaO	50.4	60.9	1.6
5%Fe/CaO	56.7	48.5	4.8
20%Fe/CaO	44.1	57.6	4.6
1%Fe/dol	46.7	63.1	1.5
5%Fe/dol	46.2	59.3	3
20%Fe/dol	44.3	65	3.8
5%Fe/MgO	59	56.8	2.8
20%Fe/MgO	60	55.4	1.6
Dol	50.7	64.6	1.1
CaO	25.3	76.1	5
MgO	16.3	73.6	2.5

Table 4: Mean calculated values for X(R1), X(R2) and the % error on hydrogen balance, for toluene steam reforming tests using different catalysts.

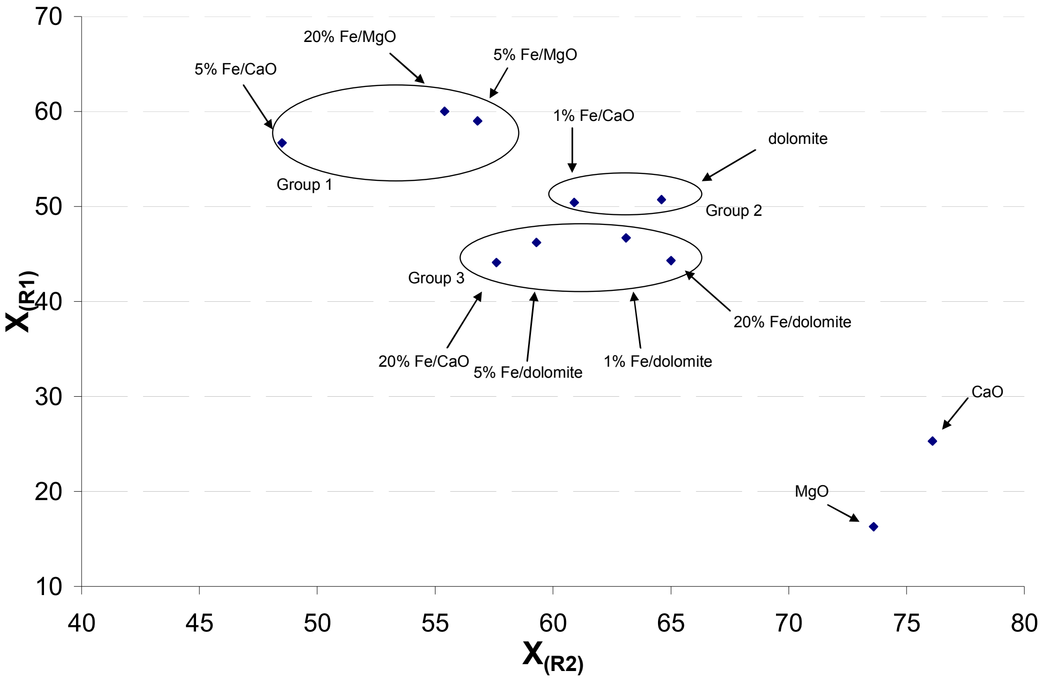

Figure 5: Variation of X_{R2} as a function of X_{R1} for toluene steam reforming tests, using raw substrates and Fe/(CaO, MgO, dolomite) catalysts

Varying the percentage of iron, a substantial improvement on toluene conversion is not observed with respect to raw dolomite for Fe/(Ca,Mg)O systems. However, catalysts containing smaller iron amounts (1%, 5%) are somewhat more active than 10 and 20% Fe/dolomite. Fe/CaO, however, is able to double the catalytic toluene conversion obtained with raw CaO, with the reactivity order 5%Fe>1%Fe>10%Fe≈20%Fe. The Fe/MgO system also shows a great improvement on toluene conversion with respect to the raw substrate; 5% iron shows the greatest improvement of the catalytic activity (conversion rises from 25% to 60%). With respect to 20%Fe/MgO, it is less active at the beginning of test, but leads to a major stability of the catalytic activity during the six hours on test.

4. Catalytic activity of Ni/(CaO, dolomite)

4.1. Toluene steam reforming

Nickel based catalysts Ni/(CaO, (Ca,Mg)O) have been tested in identical conditions as iron based catalysts (Table 1), in order to check differences on reactivity between metals in interaction with the same substrates. Also in this case no catalyst pre-reduction has been carried out before each test. All catalytic systems adopted perform high toluene conversion (X_t and X_{R1}, defined in Eq.1 and 2, are near to 100%); no deactivation is observed during the 6 hours on test (Figure 6a, b, c and d, Table 5).

It is interesting to observe the P_{CO}/P_{CO2} ratio obtained with different nickel contents and catalytic systems (Figure 7). The fraction of CO decreases by increasing the amount of metallic nickel available for the reaction; this amount of nickel depends on both % loaded on the catalyst and interaction with the substrate. The 4%Ni/dolomite is the sample that offers less metallic nickel for the reaction, because this metal is in strong interaction with MgO, allowing for a reduction of only 25% of total nickel loaded on the substrate; this catalyst present the higher value of P_{CO}/P_{CO2}, about 1.65. 4%Ni/CaO and 10%Ni/dolomite catalysts, both offer for the reactions a similar quantity of metallic nickel, being once again the reduction limited to 25% of total nickel loaded for the 10%Ni/dolomite, whereas it is near total for the 4%Ni/CaO catalyst. The calculated values for P_{CO}/P_{CO2} ratio assume in this case the intermediate values of 1.56 (for 10%Ni/dolomite) and 1.55 (for 4%Ni/CaO). Finally, 10%Ni/CaO is the catalyst that produces the highest amount of metallic nickel, and gives back the lowest value for the P_{CO}/P_{CO2} ratio, equal to about 1.46. This tendency evidences the role of metallic nickel to act as a catalyst for water-gas shift reaction.

	4%Ni/dol	10%Ni/dol	4%Ni/CaO	10%Ni/CaO
%H_2	10.16	10.50	9.71	9.99
%CO	2.96	2.89	2.85	2.83
%CO_2	1.79	1.85	1.85	1.93
%CH_4	0.18	0.18	0.24	0.19

Table 5: mean values of % concentrations in the outlet gas for toluene steam reforming using 4-10%Ni/(CaO, dolomite) after 400 min

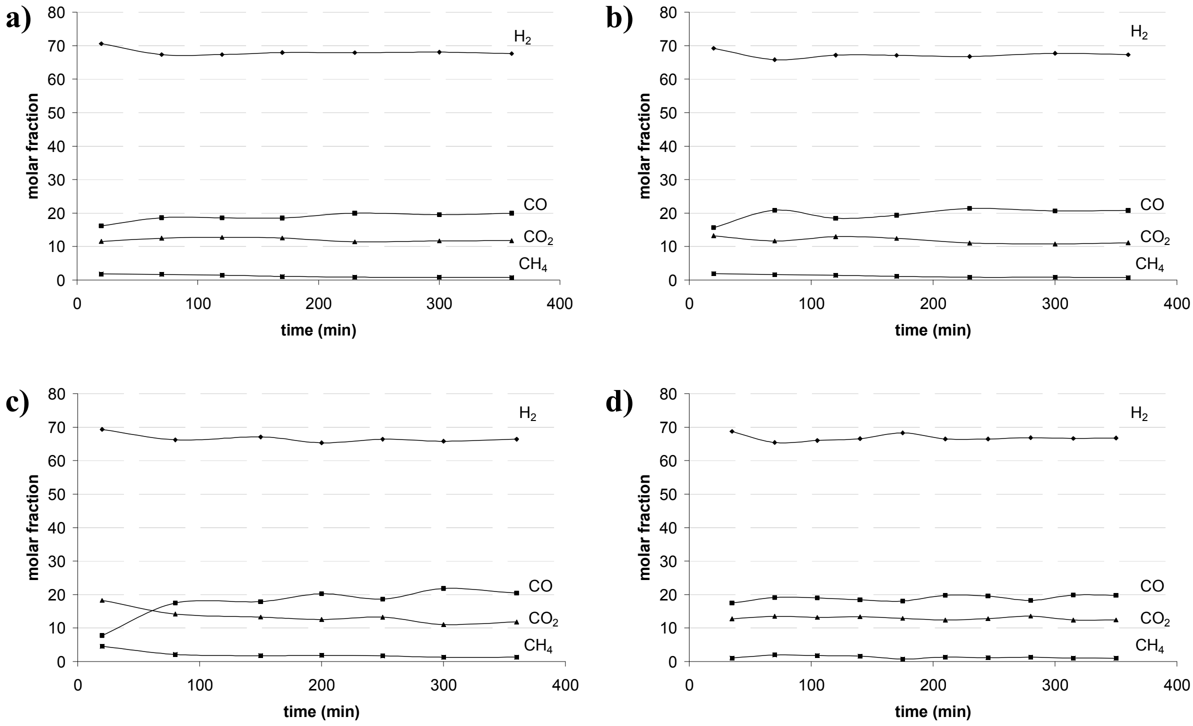

Figure 6: Toluene steam reforming tests: experimental gas concentrations (dry and nitrogen-free basis) as a function of time for a) 4%Ni/dolomite, b) 10%Ni/dolomite, c) 4%Ni/CaO, d) 10%Ni/CaO

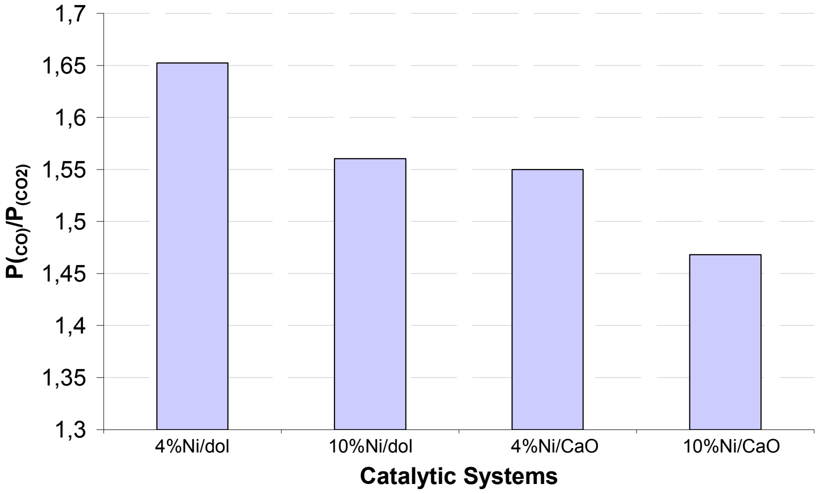

Figure 7: P_{CO}/P_{CO2} ratio produced with different nickel contents and catalytic systems in toluene steam reforming tests after 400 min

4.2. 1-Mn Steam Reforming

The Ni/Substrate series present, varying the amount of nickel in the catalytic systems and the substrate itself, the same catalytic activity with respect to toluene steam reforming. In order to discriminate the best catalyst in terms of conversion (Eq. 1), some tests have been carried out using an additional model tar compound. It has been reported [Coll *et al.,* 2001] that, in general, the more are the aromatic rings in the molecule, the lower is the reaction rate, although naphthalene is an exception. For cyclic and polycyclic aromatic hydrocarbons the order of reactivity with respect to catalytic steam reforming is benzene > toluene >> anthracene >> pyrene > naphthalene. Naphthalene is therefore the most suitable compound for use as a key molecule of biomass gasification tar, being the least reactive. However, naphthalene is solid at ambient temperature, and therefore it may not be introduced to the feeding system using motorized syringes as described in Figure 1. For these reasons, 1-methyl naphthalene (liquid at ambient temperature) has been used as model tar compound in this work. Experimental conditions adopted are summarized in Table 1, whereas results of 1-Mn conversion, calculated according to (R3) and (R4) reaction stoichiometries, and Equation 5, are shown in Figure 8 (for 10%Ni/Substrate) and 9 (4%Ni/Substrate). Finally, Table 6 shows the outlet gas composition for H_2, CO, CO_2 and CH_4.

It is clear that, even if nickel is less reducible in the Ni/dolomite system, the catalytic activity of Ni/dolomite is comparable with that of Ni/CaO catalysts, where the nickel reduction is near complete. Therefore, the NiO-MgO solid solution does not decrease the potential of nickel to catalyse tar reforming reactions, and at the same time ensures a strong metal support interaction, which is absolutely necessary considering that the final use of such a catalysts is the fluidized bed reactor where attrition may be harmful due to nickel losses.

$$C_{11}H_{10} + 11H_2O \rightarrow 11CO + 16H_2 \tag{R3}$$

$$CO + H_2O \leftrightarrow CO_2 + H_2 \tag{R4}$$

$$X_{1-Mn} = \frac{[CO] + [CO_2] + [CH_4]}{11 \cdot [C_{11}H_{10}]_{in}} \tag{5}$$

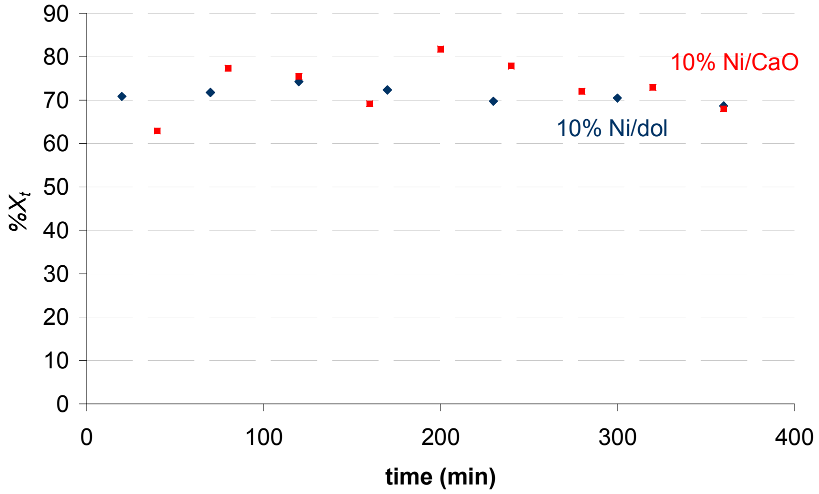

Figure 8: 1-Mn conversion, as defined in Eq. 5, as a function of time for 10% nickel based catalysts

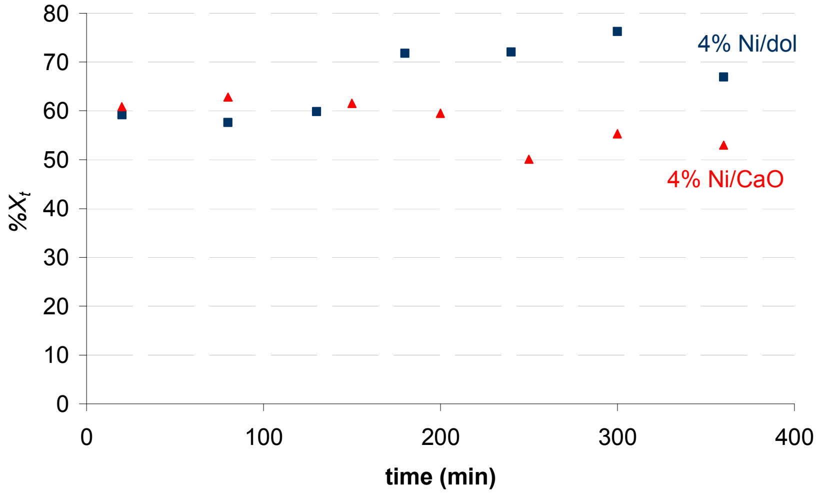

Figure 9: 1-Mn conversion, as defined in Eq. 5, as a function of time for 4% nickel based catalysts

	4% Ni/dol	**10% Ni/dol**	**4% Ni/CaO**	**10% Ni/CaO**
%H_2	6.13	6.02	4.91	6.60
%CO	1.36	1.56	1.09	1.68
%CO_2	1.52	1.47	1.27	1.54
%CH_4	0.33	0.37	0.34	0.31

Table 6: Outlet gas composition, as %H_2, %CO,%CO_2 and %CH_4 for 1-Mn steam reforming tests using nickel based catalysts after 400 min

5. CO_2 absorption tests

5.1. Dolomite and CaO

The equilibrium equation for the reaction between CO_2 and CaO, at ambient pressure, is expressed by Equation (6) [Garcia-Labiano *et al.*, 2002]:

$$P_{CO_2 eq}(atm) = 4.137 \times 10^7 \times \exp\left(-\frac{20474}{T(K)}\right) \tag{6}$$

where $P_{CO2\ eq}(atm)$ is the equilibrium CO_2 pressure expressed in atmospheres, and $T(K)$ the system temperature expressed in K. This equation predicts the value of 0.96% for CO_2 composition exiting from the reactor at ambient pressure, when absorption takes place without kinetic limitations at 650°C.

The experimental conditions adopted are summarized in Table 2. Figure 10 shows CO_2 absorption curves using dolomite and CaO as sorbents, respectively. The knowledge of the CO_2 feeding moles, the bed overall sorption capacity and the corresponding thermodynamic equilibrium concentration at test conditions allows to estimate a breakthrough time (i.e., the time needed for the sorbent saturation) of about 46 minutes for dolomite (marked in Figure 10 with a dotted vertical line), and 85 minutes for CaO.

Figure 10 shows that absorption of CO_2 is in good agreement with theoretical breakthrough time for dolomite; however a strong reduction in CO_2 capture capacity of CaO sorbent is noticeable. The problem with pure CaO particles, in fact, is that reaction on the surface results in a local increase in solid volume (the $CaCO_3$ molar volume being much greater than that of CaO) blocking the particle pores, and impeding access of gaseous CO_2 to the particle interior, thereby reducing significantly its CO_2 capture capacity [Abanades *et al.,* 2003]. On the other hand, MgO in the dolomite does not react with CO_2 at the test operating temperature, thereby providing a continuous free passage for CO_2 diffusion, and renders accessible virtually the entire active particle. It is worth mentioning here that other samples of pure CaO do not show a similar gap between theoretical and experimental values of absorption capacity (see for instance [Marquard-Möllenstedt *et al.,* 2004 and 2008]).

As a result, the conversion of dolomite and CaO, as defined in the Equation 7 of the following paragraph, is calculated to be equal to 0.93 and 0.26, respectively.

In what follows, only M/dolomite sorbents will be considered for CO_2 capture tests.

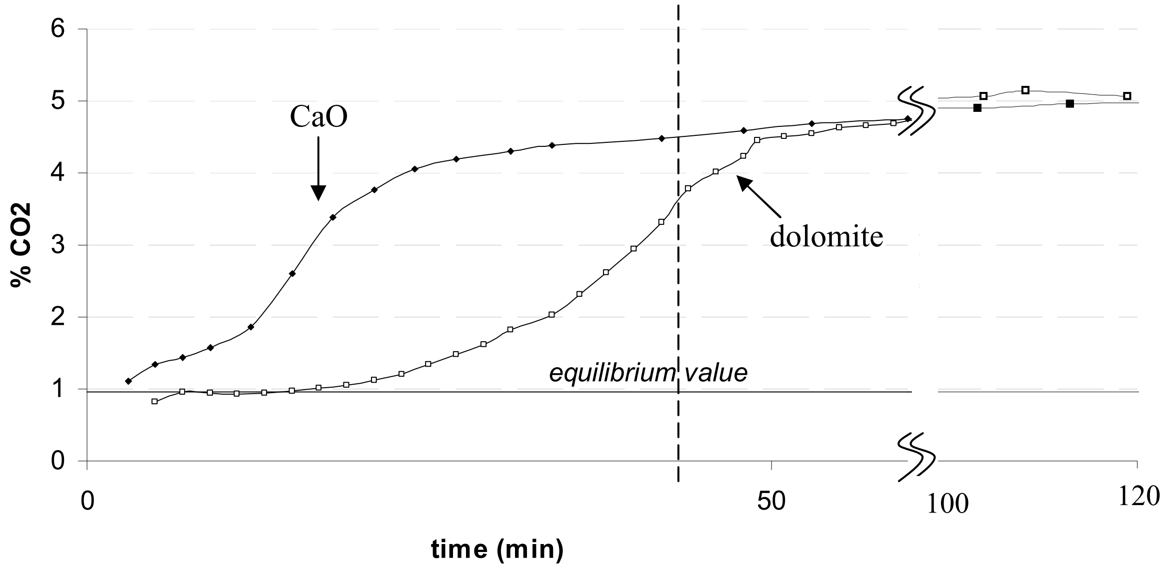

Figure 10: CO_2 volume % composition in the reactor exit stream, as a function of time, for CO_2 capture tests using CaO (♦) and calcined dolomite (□)

5.2. M/dolomite: CO_2 absorption

The addiction of metal oxides on the surface of dolomite will be investigated in Sections 4.2.1 and 4.2.2, in order to check the presence of additional gas-solid kinetic limitations and/or sorption capacity decay. Chapter 4 had showed that iron interacts mainly with CaO, as $Ca_2Fe_2O_5$, and nickel with MgO, as NiO-MgO solid solution. Therefore, a general behaviour of M/dolomite sorbent can be described as schematized in Figure 11, when the metal interacts either with MgO or CaO.

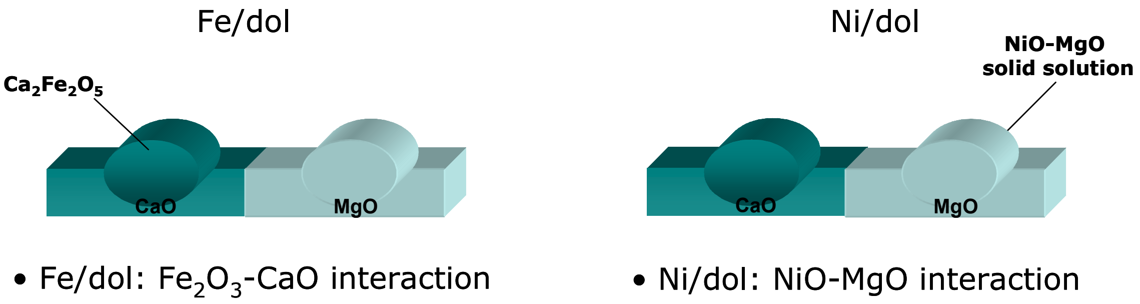

Figure 11: M/dolomite interaction for Fe/dol and Ni/dol

5.2.1. Fe/dolomite: CO_2 absorption

The experimental conditions adopted for CO_2 capture tests are summarized in Table 2. The effect of iron addition on dolomite is shown in Figure 12a and b, the latter showing the conversion of CaO (X_{CaO}) sites as follows (Eq. 7):

$$X_{CaO} = \frac{C_t}{C_{\max}} \tag{7}$$

where C_t represent the CO_2 moles absorbed at any time instant, and C_{max} the theoretical value for 100% CaO conversion. In Figure 12b it is clear that CO_2 absorption capacity decays by increasing the iron amount in the sorbent, meaning that $Ca_2Fe_2O_5$ is not capable to capturing CO_2 and releasing free Fe_2O_3, according to the reaction (Eq. 8):

$$Ca_2Fe_2O_5 + 2CO_2 \rightarrow 2CaCO_3 + Fe_2O_3 \tag{8}$$

This behaviour is verified in Section 5.2, where after test X-ray analyses are discussed. However, the kinetics of CO_2 capture results quite unaffected by iron loading in the substrate.

Similar results have been obtained with Fe/CaO sorbents, but they are clearly less significant, the final CaO conversion reaching just about a fraction of 0.26 of the overall sorption capacity.

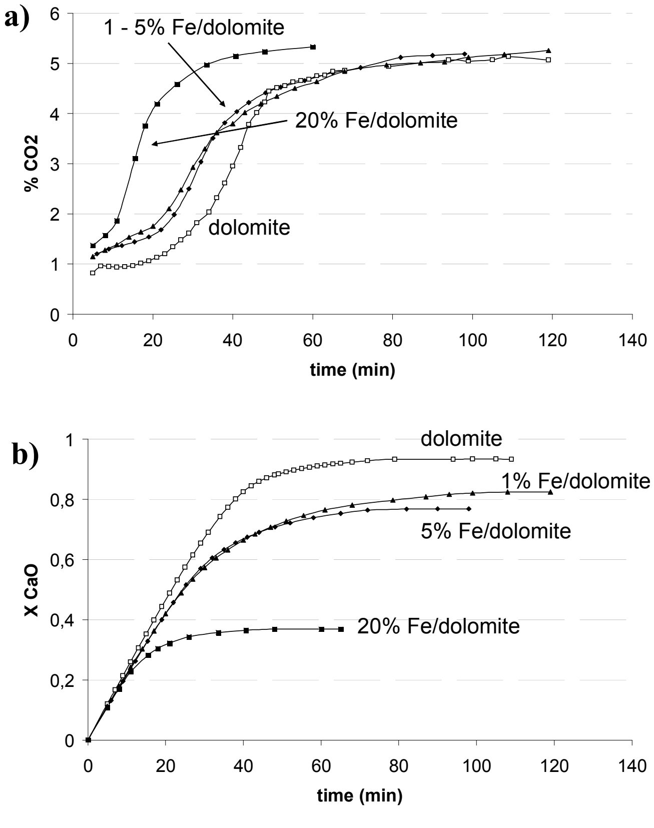

Figure 12: %CO_2 capture (a) and CaO conversion (b) as a function of time, for CO_2 capture tests using calcined dolomite (□), 1% Fe/dol (▲), 5% Fe/dol (♦) and 20% Fe/dol (■).

5.2.2. Ni/dolomite: CO_2 absorption

A preliminary study on reactivity of Ni/dolomite catalysts and sorbents has been carried out in order to check the CO_2 absorption capacity and kinetic modifications, in relation to the amount of metal on the particle surface and/or mass of dolomite. Table 2 shows experimental conditions and Figures 13a and b show the outlet gas concentration (as $\%CO_2$) and conversion of CaO (X_{CaO}), respectively.

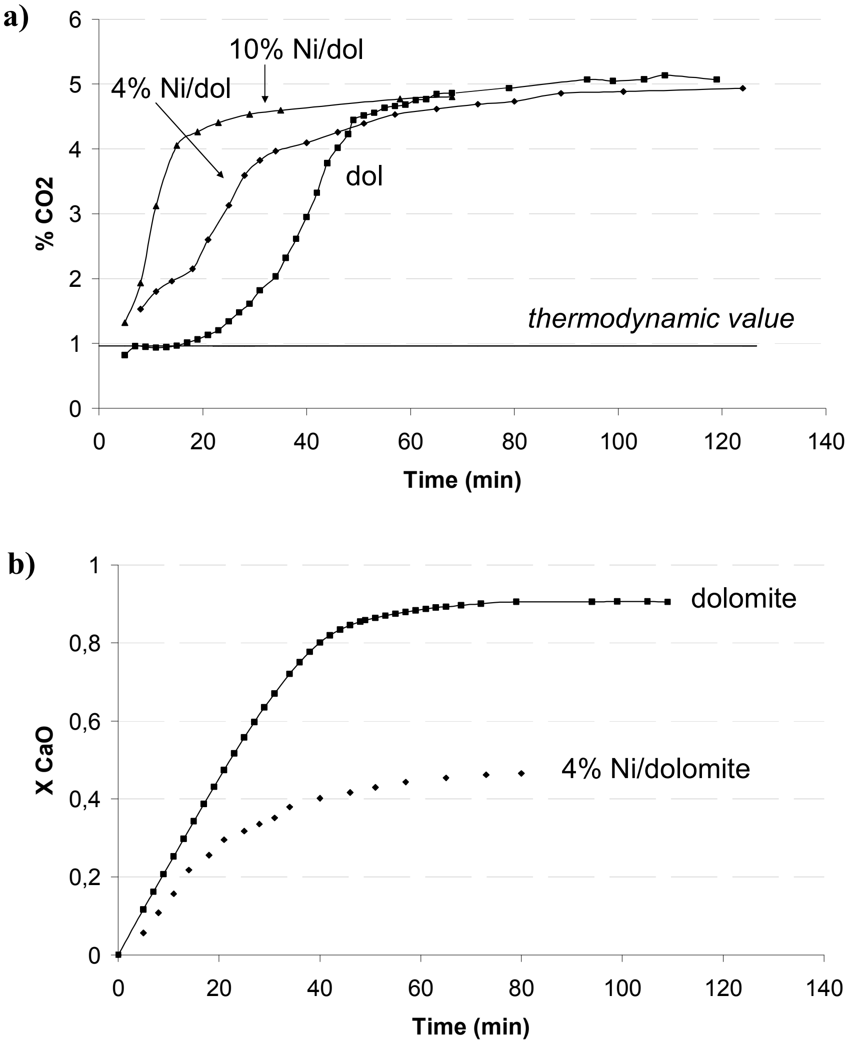

Figure 13: a) outlet gas concentration (as $\%CO_2$) and b) conversion of CaO (X_{CaO}) as a function of time for dolomite and Ni/dolomite.

It is clear that nickel has the effect of limiting gas-solid reaction between CO_2 and active sites for absorption in the bulk particle of dolomite, even if the metal does not interact directly with CaO. This means that nickel oxide, in solid solution with MgO (the nickel reduction to the metallic form is strongly limited by this kind of interaction) causes some change in the inert porous matrix of MgO, leading to a partial pore blockage. This result is confirmed by the evidence that, by increasing the nickel loaded in the substrate from 4% to 10%, the CO_2 absorption process in considerably inhibited (Fig. 13a), and obviously this last combination of metal and sorbent is not of great interest for the combined process of steam reforming and CO_2 capture using a single mineral solid phase.

5.3. Toluene steam reforming and CO_2 capture test: Absorption Enhanced Reforming

As a result of the evaluation of the CO_2 capture behaviour and the activity on tar model compounds reforming of nickel based catalysts and sorbents, the 4%Ni/dolomite is proposed for the combined toluene steam reforming and CO_2 capture test (see Table 2 for experimental conditions). It shows the best performance on CO_2 absorption, and a catalytic activity on toluene steam reforming comparable with other nickel based catalysts. The proposed process, i.e. the feasibility of a one step, combined process of steam reforming, CO_2 capture and water-gas shift using a single mineral solid phase, is schematized in Figure 14.

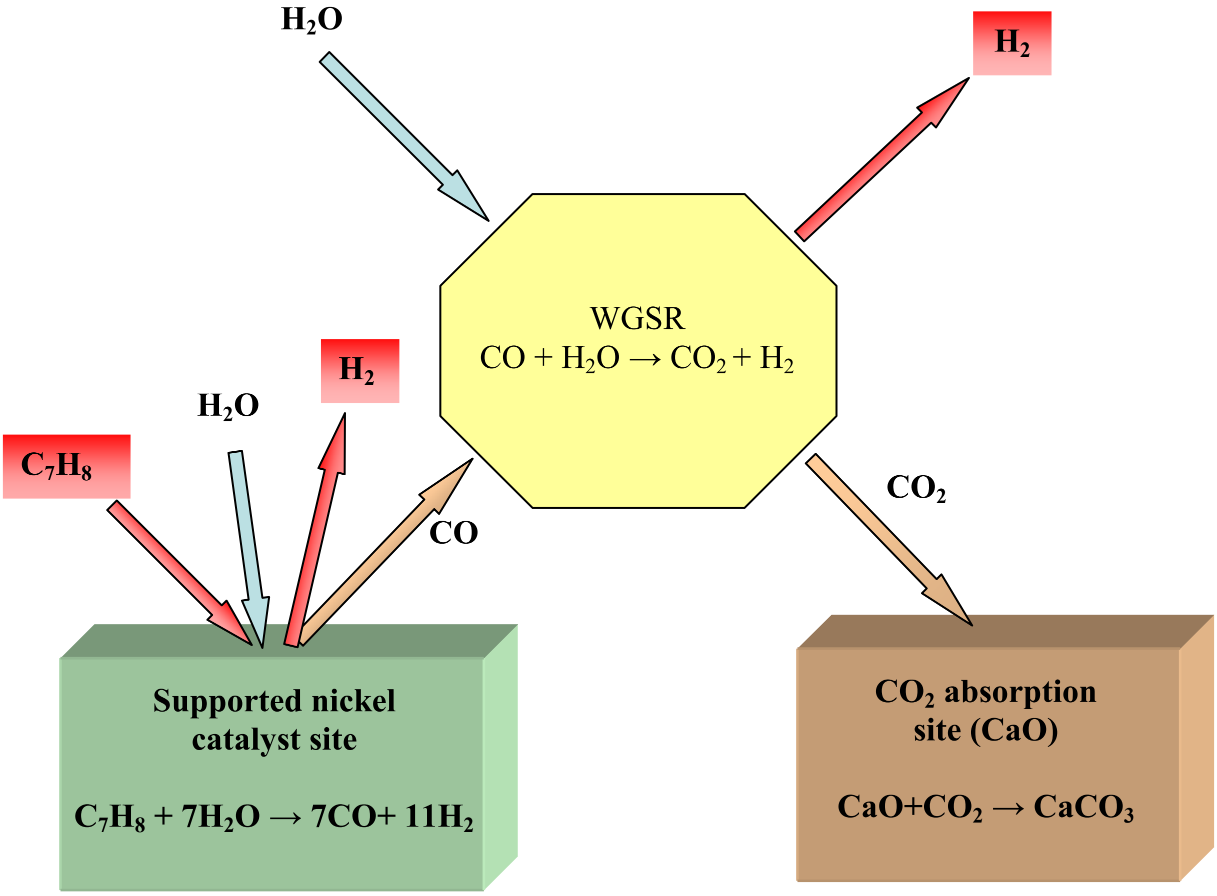

Figure 14: Combined process of steam reforming, CO_2 capture and water-gas shift using a single mineral solid phase

Figure 15 shows the experimental results obtained. The kinetic limitations of CO_2 capture due to NiO-MgO interaction, detected with plain CO_2 capture tests, are again evident in the combined steam reforming and CO_2 capture test of Figure 13. The narrow breakthrough zone that has characterised previous tests using raw dolomite and commercial nickel catalyst (see Chapter 3) is now less evident, and a slight steady increase of CO_2 concentration in the outlet gas, together with a simultaneous decrease in H_2 production is observed during test, until the complete saturation of available sites for CO_2 capture is reached. This state corresponds to about 55% conversion of CaO in the bed; after that, the concentrations of CO_2 and H_2 keep quite constant values until the end of the test.

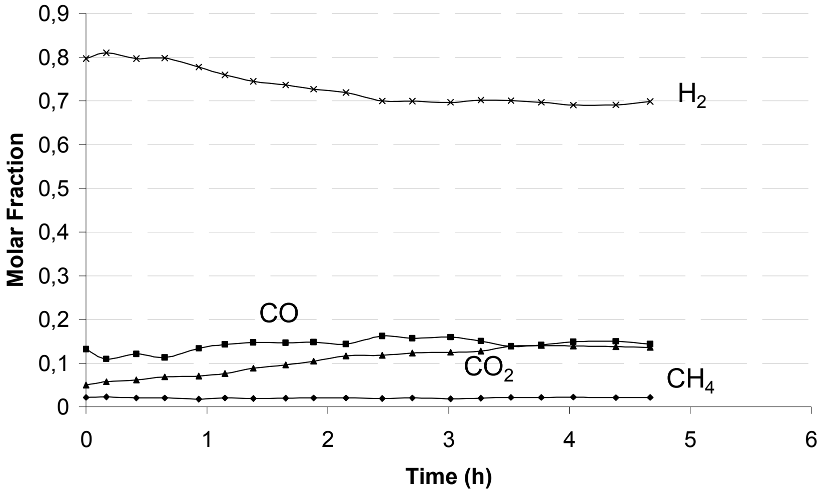

Figure 15: Experimental gas concentrations (dry and nitrogen-free basis) as a function of time (catalyst and sorbent: 4% Ni/dolomite)

The value of saturation is slightly higher than those reported for plain CO_2 capture test; it may be justified considering that part of nickel is extracted from the NiO-MgO solid solution in the bulk of dolomite, due to the partial reduction of nickel in the reactive atmosphere.

The reforming conversion may be obtained following the hydrogen concentration in the gas exiting from the reactor, Eq. 9, because in this case carbon balance estimates are complicated by CO_2 capture mechanism:

$$X_t = \frac{[H_2]_{out}}{18 \cdot [C_7H_8]_{in}} \tag{9}$$

Such a calculation is justified by considering Table 4, that showed a good closure of both hydrogen and carbon balances in the reforming tests. When CO_2 absorption is added to the reforming reactions, carbon balance is not anyone possible; however, considering the correspondence found previously from the simple reforming tests, we could assume that hydrogen balance is a reliable approach to draw significant conclusions. Starting from these considerations, toluene conversion has been found to be near total in the first part of the test, and decays to about 85% after saturation of dolomite.

An additional interesting parameter for Adsorption Enhanced Reforming reactions, as pointed out for nickel based catalysts, is the P_{CO}/P_{CO2} ratio. In this case, such a ratio reduces its value from 2.65, as observed at the beginning of the test when the capture of CO_2 proceeds at the higher rate, to 1.06 at the end of the test, when CO_2 is not absorbed any more. This value is clearly lower than the values observed for nickel based catalysts at 850°C (1.46-1.65, see Figure 7), in agreement with the thermodynamic equilibrium of water-gas shift reaction, which is shifted toward a lower CO (and therefore higher H_2 and CO_2) concentration at 650°C.

The methane content in the product gas has been also monitored during the test. Absorption Enhanced Reforming processes, as recalled in Chapter 1, may shift reforming reactions beyond their conventional thermodynamic limits; however, a temperature decrease toward the window where CO_2 capture is thermodynamically favoured reverses this point of view, because the endothermic reforming reactions are inhibited at lower temperature and therefore the yield of methane is favoured by low temperature gasification. In the tests shown in Figures 6 and 15, a near total conversion of the model tar compound (toluene) has been found in the temperature range of 650-850°C. However, methane content is considerably higher (about two times) in the AER process (650°C) than in the case of conventional reforming reactions at 850°C. It is important to take into account this experimental evidence for the following reasons:

- The AER process may be used as a CO_2 capture pre-combustion technique for downstream methanation process (see Chapter 1), and therefore in-bed methane abatement is not essential for this purpose;
- The enthalpy of combustion for methane, -891 kJ/mol, is considerably higher than that of hydrogen, −286 kJ/mol; this means that an higher concentration of CH_4 in the product gas should be beneficial in terms of heating value of the product gas.

The methane content in the AER process product gas and for conventional steam reforming reactions with the nickel based catalyst series is shown in Figure 16, expressed as (exiting methane concentration)/(entering toluene concentration) ratio.

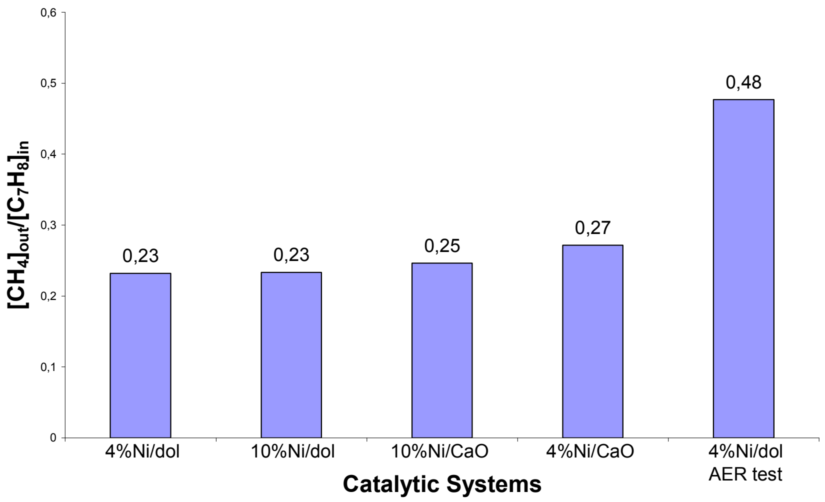

Figure 16: Methane content in the fuel gas obtained from toluene steam reforming with nickel based catalysts: AER (650°C) and conventional processes (850°C)

6. Characterization after tests

6.1. 20%Fe/dolomite oxidative and neutral pathway

The characterization after catalytic tests is useful to check the active phases of iron in toluene steam reforming, with respect to the kind of substrate used in each test.

XRD analysis reveals a FeO-MgO solid solution for OxiMg. This means that, at the reaction conditions, the magnesioferrite phase of OxiMg is susceptible to be reduced by CO and H_2 to wurstite FeO, that is stabilized by MgO. Metallic iron is not detected, meaning that the solid solution represents a very stable form of the iron-substrate interaction. Iron (2+) catalyst is able to catalyse steam reforming reactions even in the form of FeO-MgO solid solution.

A Mössbauer analysis has been carried out for OxiCa and OxiDolo. The former shows that all the iron remains in the $Ca_2Fe_2O_5$ phase. This is not surprising because of the stability of this phase proven by the high reduction temperature of the Fe (3+)→Fe (0) system (Sections 2.6.2 in Chapter 4). However, in the OxiDolo sample, 81% of iron oxide is in the $Ca_2Fe_2O_5$ phase, whereas 19% is detected as Fe (2+), meaning that part of iron may be forced in the Fe (3+) → Fe (2+) reduction predicted by thermodynamic evaluations when $0.5<P_{red}/P_{ox}<1.5$ (Section 2.4 in Chapter 4). Therefore MgO participates as a stabilizing agent for Fe (2+) specie.

From a point of view of reactivity, the behaviour of catalysts may be explained in the light of these characterizations. When iron oxide is added to CaO and MgO substrates, it activates them as Fe (3+) ($Ca_2Fe_2O_5$) and as Fe (2+) (MgO-FeO solid solution), respectively. When it is added to dolomite, it neutralizes the beneficial distortion coming from the Ca or Mg atoms arrangement, and replaces it with the activity of $Ca_2Fe_2O_5$. The progressive transition $Ca_2Fe_2O_5 \rightarrow CaO$ + MgO-FeO should slightly activate the Fe/dolomite system, due to the somewhat higher reactivity of FeO-MgO with respect to $Ca_2Fe_2O_5$ phase, but this is not observed in Figures 2b and 4a. This means that the MgO-FeO sites are not available as active sites in catalysing the reaction system, when $Ca_2Fe_2O_5$ is present. This evidence may be explained considering that:

- at the beginning of the reaction, all iron oxides are found on the particle surface as a $(CaO)_2{*}Fe_2O_3$ precipitate. During the reaction iron is partly captured and solubilized in the MgO lattice, becoming virtually less accessible than the competitive sites of $Ca_2Fe_2O_5$ at the surface, and his contribution to enhance reaction kinetic becomes negligible;
- only 20% of iron is interested to Fe (3+) → Fe (2+) transition, and therefore difference on reactivity should be not important.

For NeuDolo catalyst, Mössbauer analysis reveals $Ca_2Fe_2O_5$ (36%, a value slightly lower than the starting one, 44%), divalent iron in paramagnetic compound (50%), that may be associated to FeO-MgO solid solution, but also some amount of metallic iron (8%), and 6% of trivalent iron in paramagnetic phase. Therefore the iron active phases are in a more reduced form with respect to OxiDolo, but also in this case, the catalytic system is not significantly improved. Iron, interacting with dolomite, is present in $Ca_2Fe_2O_5$ phase as Fe (3+), and in FeO-MgO solid solution as (Fe 2+). Between these two very stable phases, the only iron specie that has been partly extracted from the substrate in the neutral pathway, Fe_3O_4-$Fe_{3-x}Mg_xO_4$, is not observed after catalytic test, because it is easily captured in the FeO-MgO solid solution. The absence of free iron oxides may explain the lack of activation for the Fe/dolomite catalytic system, leading to an activity of (Ca, Mg)O comparable to those of $Ca_2Fe_2O_5$ and FeO-MgO. The presence of metallic iron in such a small amount (8%) is unable to improve catalytic activity. However, for CaO and MgO, this activation is observed and could be interesting for further investigations and scaling-up.

6.2. Additional iron contents on the substrate

Similar results have been obtained using different percentages of iron. Figure 17 and Table 7 show Mössbauer analysis for the 5% Fe/dolomite sample. Two sextets (sub-spectra 1 and 2) correspond to brownmillerite-type $Ca_2Fe_2O_5$ (71% of total iron). Subspectrum 1 corresponds to the octahedral site Fe (3+) while subspectrum 2 to the tetrahedral site Fe (3+).

Subspectrum 3 corresponds to divalent iron in paramagnetic, once again the FeO-MgO solid solution (20% of iron, in accordance with the sample OxiDolo). Subspectrum 4 (9% of iron) corresponds to trivalent iron in paramagnetic compound.

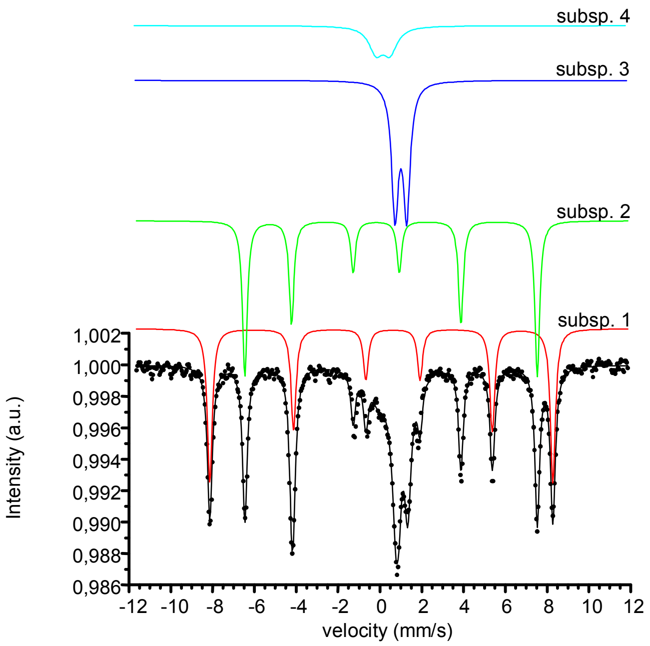

Figure 17 : ^{57}Fe Mössbauer spectra measured at room temperature: 5%Fe/dolomite sample

	Subsp. 1	Subsp. 2	Subsp. 3	Subsp. 4
Isomer shift $\boldsymbol{\delta}$	0,35 mm/s	0,18 mm/s	1,06 mm/s	0,32 mm/s
Quadrupole splitting $\boldsymbol{\Delta E_Q}$	-0,55 mm/s	0,71 mm/s	0,56 mm/s	0,67 mm/s
Hyperfine field $\boldsymbol{B_{HF}}$	51,0 T	43,4 T	N/A	N/A
Full line width at half height	0,29 mm/s	0,27 mm/s	0,40 mm/s	0,77 mm/s
Relative area (%)	37	34	20	9
Interpretation	Fe(3+)	Fe(3+)	Fe(2+)	Fe(3+)

Table 7 : 57Fe Mössbauer parameters of components present in the 5% Fe/dolomite sample

Results of Mössbauer analysis for 5%Fe/CaO and 5%Fe/MgO are shown in Table 8 and 9, respectively. The former shows in this case di-trivalent iron in paramagnetic compound, 12% of Fe(2+,3+), which, due to the very large width of the line, should represent a phase with poor crystallinity. The higher amount of iron is detected as $Ca_2Fe_2O_5$ phase (87% of iron). Once again Fe (2+) is not detected when MgO is absent in the substrate.

For the latter, Subspectrum 1 (23% of iron) corresponds to di-trivalent iron in paramagnetic compound – once again, due to the very large width of the line, it must be a phase with poor crystallinity. Subspectrum 2 corresponds to divalent iron in paramagnetic compound, the FeO-MgO solid solution.

	Subsp. 1	Subsp. 2	Subsp. 3	Subsp. 4
Isomer shift ***δ***	0,35 mm/s	0,18 mm/s	0,42 mm/s	0,67 mm/s
Quadrupole splitting ΔE_Q	-0,54 mm/s	0,72 mm/s	0,77 mm/s	0,86 mm/s
Hyperfine field B_{HF}	51,0 T	43,4 T	N/A	N/A
Full line width at half height	0,31 mm/s	0,30 mm/s	0,11 mm/s	1,37 mm/s
Relative area (%)	45	42	1	12
Interpretation	Fe(3+)	Fe(3+)	Fe(3+)	Fe(2+,3+)

Table 8: ^{57}Fe Mössbauer parameters of components present in the 5%Fe/CaO sample

	Subsp. 1	Subsp. 2
Isomer shift ***δ***	0,54 mm/s	1,03 mm/s
Quadrupole splitting ΔE_Q	0,89 mm/s	0,48 mm/s
Hyperfine field B_{HF}	N/A	N/A
Full line width at half height	0,52 mm/s	0,40 mm/s
Relative area (%)	23	77
Interpretation	Fe(2+,3+)	Fe(2+)

Table 9: 57Fe Mössbauer parameters of components present in the 5%Fe/MgO sample

For CO_2 capture tests using iron based catalysts (1-5-20% Fe/dolomite), X-ray diffraction analysis shows MgO, $CaCO_3$ and $Ca_2Fe_2O_5$ phases after tests, evidencing that calcium iron oxide $Ca_2Fe_2O_5$ cannot absorb CO_2 expelling iron oxides.

6.3. Evaluation of carbon deposited during the tests

Nickel and iron based catalysts behaviour have been characterized following the carbon and hydrogen containing compounds in the product gas of tar reforming reactions. However, another parameter that has to be taken into account is the analysis of carbon deposited during the reforming tests, because this parameter is considered an important catalyst deactivation source in gasification processes, in particular for dolomite and nickel based catalysts.

6.3.1. Temperature Programmed Oxidation of iron based catalysts

TPO analyses after catalytic tests have been carried out for substrates and iron based catalysts series (see Appendix for experimental apparatus and conditions adopted). Figure 18a shows the exiting flow of CO_2 as a function of temperature during temperature programmed oxidation, for CaO, (Ca,Mg)O, 5%Fe/CaO and 5%Fe/(Ca,Mg)O, and Figure 18b shows the same parameters for 5% and 20%Fe/MgO. The Figure evidences that iron strongly limits the carbon deposited on the catalyst surface. For calcium containing catalysts, TPO permits to observe two types of carbon of the same nature for raw substrates and iron based catalysts. The former one oxidized at low temperatures which can be attributed to carbide phase [Swierczynski *et al.*, 2007] and the latter one oxidized at 650-730 °C corresponding to filamentous and graphitic carbon.

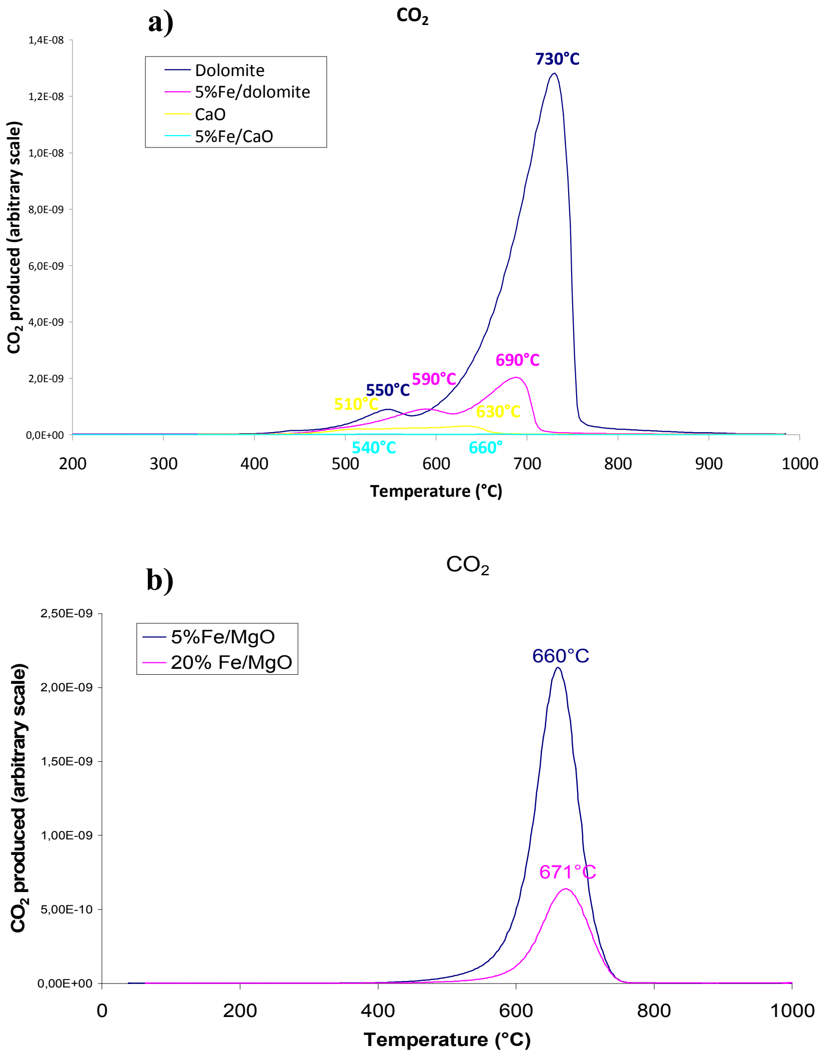

Figure 18: TPO profiles for (Ca,Mg)O, CaO, 5%Fe/(Ca,Mg)O, 5%Fe/CaO (a) and 5%Fe/MgO, 20%Fe/MgO after steam reforming of toluene at 850°C

The relative intensity of CO_2 integration peaks reveals that dolomite is the catalyst containing more carbon; this may explain the slow deactivation observed in Fig.2a during steam reforming tests.

The 5%Fe/dol reduces by 1:7 the value of carbon obtained with raw dolomite. 5%Fe/CaO, that improves toluene catalytic conversion by 20% with respect to dolomite activity, reduces this amount of carbon by 1:360 compared with dolomite itself. For Fe/MgO, the carbon deposition resistance is not improved significantly with respect to dolomite, with a ratio of 1:3 for 5%Fe/MgO, and 1:9 for 20%Fe/MgO. These data may explain deactivation of these catalysts highlighted in Figures 2b and 4c; another explanation for this deactivation may be the evidence of a progressive depletion of Fe (3+) reduced to Fe (2+) in the MgO lattice (Sections 6.1 and 6.2). A lower carbon deposition has been detected also for CaO and MgO, about 1:25 less than for dolomite, but in this case the low toluene conversion obtained with these substrates renders them less interesting for applications as additives in gasification processes.

These data are reported in Figure 19 in terms of the ratio (Eq.10):

$$\frac{g_{(carbon\ deposited)}}{g_{(catalyst)} \cdot g_{(T\ reacted)}} \tag{10}$$

where *g* indicates grams and (*T reacted*) represents the fraction of toluene reacted, calculated by $X_{(R1)}$ values (Table 4, Equation 2).

From the bibliographic survey carried out in Section 2.1 of Chapter 4, it has been reported that carbon deposited on the iron surface is susceptible to be removed by both, steam oxidation [Azhar Uddin *et al.*, 2008] or oxidation by CO_2 (Eq. 11-12):

$$C + H_2O \rightarrow CO + H_2 \tag{11}$$

$$C + CO_2 \rightarrow 2CO \tag{12}$$

or, in presence of H_2, reaction of coke with hydrogen, producing methane [Tamhankar *et al.,* 1985]:

$$C + 2H_2 \rightarrow CH_4 \tag{13}$$

The methane content has been monitored in the product gas of toluene steam reforming reactions, and is shown in Figure 20. The amount of methane doubles with Fe/dolomite catalyst series, and triplicates for Fe/CaO series. However, the hydrogenation of coke (Eq.13) is not sufficient to justify the strong reduction of carbon detected by TPO analysis, meaning that most of carbon is depleted by steam and CO_2 oxidation.

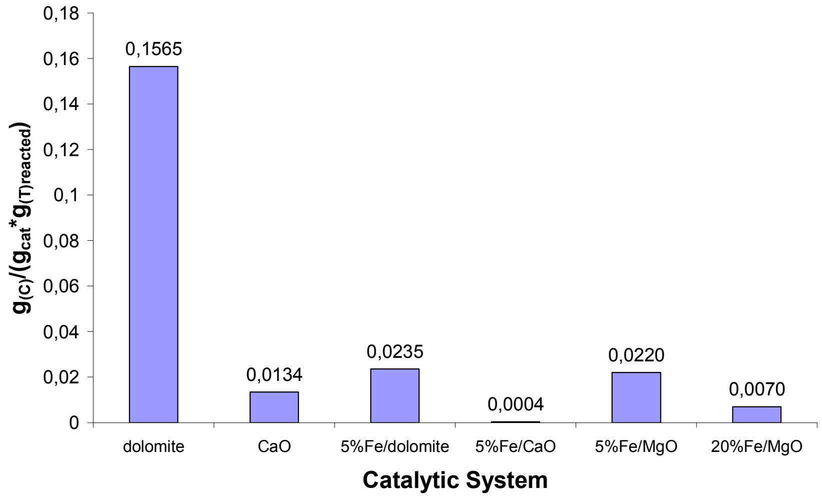

Figure 19: Carbon content for different substrates and iron based catalytic systems

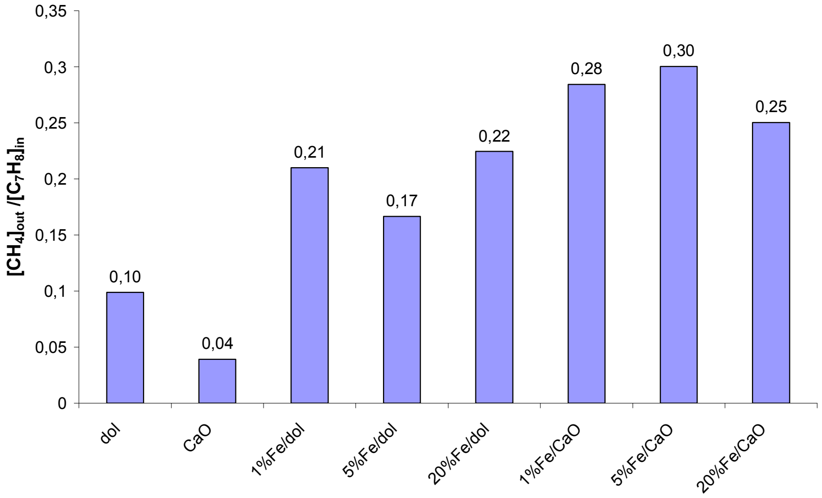

Figure 20: Methane content for toluene steam reforming reactions at 850°C, with different substrates and iron based catalytic systems

In the light of these characterization tests, if carbon deposition represents a critical point for dolomite deactivation, as reported in literature [Corella *et al.,* 2006, 2008], [Kuramoto *et al.*, 2003], the use of iron may be of great interest for further investigations in biomass gasification processes.

6.3.2. Carbon deposition on nickel based catalysts

Carbon deposited has been detected by elemental analysis for toluene and 1-Mn steam reforming test using 4, 10% Ni/CaO and 4, 10% Ni/(Ca,Mg)O catalysts, and is expressed in Table 10 as ratio:

$$\frac{g_{(carbon\ deposited)}}{g_{(catalyst)} \cdot g_{(tar\ reacted)}} \tag{14}$$

where g indicates grams and (*tar reacted*) represents the fraction of tar reacted, calculed by conversion values of steam reforming reaction.

It is clear that nickel not only improve toluene conversion on steam reforming, but also have a positive effect on improving carbon deposition resistance with respect to those detected for raw CaO and dolomite. As a example, the value of carbon deposited on dolomite (see Figure 19), is 70 times higher than 4% Ni/CaO.

	$\frac{g_{(carbon\ deposited)}}{g_{(catalyst)} \cdot g_{(tar\ reacted)}}$	
	TSR	**1-MnSR**
4% Ni/(Ca,Mg)O	0.0027	0.1219
4% Ni/CaO	0.0022	0.1100
10% Ni/(Ca,Mg)O	0.0047	0.0957
10% Ni/CaO	0.0029	0.1489

Table 10: carbon deposited during toluene and 1-Mn steam reforming tests at 850°C on nickel based catalysts

7. Conclusions

New catalysts for tar reforming in biomass gasification processes have been conceived in this work, with the aim to investigate new paths for tar abatement using cheap and abundant materials. Iron has been found to improve catalytic activity of CaO and MgO substrates, in order to render them more active than the activity of dolomite, making these materials more attracting for scale up applications. Also carbon deposition resistance is improved adding iron to these raw substrates.

When CaO is present in the substrate (as lime or calcined dolomite), iron may be preserved as Fe (3+) specie, while it is reduced to Fe (2+) in the Fe/MgO system. This redox behaviour in the product gas atmosphere, is strongly dependent on the kind of substrate adopted and interactions taking place. Even if Fe (3+) is a thermodynamically unfavoured oxidation state when steam and carbon dioxide are the oxidant agents (Chapter 4, Section 2.4), the $Ca_2Fe_2O_5$ structure allows to stabilize this iron specie. This is an important quality for an iron based catalyst because iron reduction, utilizing CO and H_2 as reductive agents, causes a loss of heating value of the product gas.

The Fe (2+) specie predicted by thermodynamic evaluations is detected in the Fe-MgO system, where it is stabilized by FeO-MgO solid solution.

Nickel based catalysts have been found very active; Ni/dolomite shows the same activity on toluene and 1-Mn steam reforming than Ni/CaO although only 25% of nickel is reduced to metallic form during TPR analysis. This means that Ni/dolomite catalyst presents a more intimate bond between metal and substrate, that may be considered as a preferential condition for larger scale fluidized bed applications. Moreover, an improved carbon deposition resistance has been detected with nickel based catalysts series with respect to raw calcined dolomite and CaO.

For each M/substrate, from a point of view of reactivity, it has been found that low metal contents may perform tar abatement with the same (or even higher, i.e. for iron) order of magnitude than higher metal concentrations. This behaviour is favourable from a point of view of CO_2 capture properties, because of the following considerations:

- onset of kinetic limitations due to the metal loaded in the substrate is limited, supposing that lower metal content causes lower kinetic limitations between CO_2 absorption sites and CO_2 itself (i.e. for nickel);
- the absorption capacity decay is limited, if the metal deactivates the CO_2 absorption sites (i.e., for iron).

As a result, the investigations carried out in this work have been successful for the optimization of the metal content in the substrate-sorbent, in order to find a good compromise between catalytic activity and CO_2 capture properties of different M/substrates.

From the point of view of CO_2 capture properties, it has been also demonstrated that, when metal interacts with CaO (as detected for iron), kinetic limitations are less important than in the case of metal-MgO (as reported for nickel) interactions, bringing to light the critical role of MgO on accelerating the rate of CO_2 capture gas-solid reaction.

Bibliography

Abanades J.C., Alvarez D., (2003), Conversion Limits in the Reaction of CO_2 with Lime, Energy & Fuels 17, 308-315.

Asami K., Sears P., Furimsky E., Ohtsuka Y., (1996), Gasification of brown coal and char with carbon dioxide in the presence of finely dispersed iron catalysts. Fuel Process. Technol. 47, 139-151.

Azhar Uddin Md., Tsuda H., Wu S., Sasaoka E., (2008), Catalytic decomposition of biomass tars with iron oxide catalysts, Fuel 87, 451-459.

Coll R., Salvado J., Farriol X., Montane D., (2001), Steam reforming model compounds of biomass gasification tars: conversion at different operating conditions and tendency towards coke formation, Fuel Processing Technology 74, 19-31.

Corella J., Toledo J.M., Molina G., (2006), Steam Gasification of Coal at Low-Medium (600-800 °C) Temperature with Simultaneous CO_2 Capture in Fluidized Bed at Atmospheric Pressure: The Effect of Inorganic Species. 1. Literature Review and Comments, Ind. Eng. Chem. Res. 45, 6137-6146.

Corella J., Toledo J.M., Molina G., (2008), Steam Gasification of Coal at Low-Medium (600-800 °C) Temperature with Simultaneous CO_2 Capture in a Bubbling Fluidized Bed at Atmospheric Pressure. 2. Results and Recommendations for Scaling Up, Ind. Eng. Chem. Res. 47, 1798-1811.

Delgado J., Aznar M.P., Corella J., (1997), Biomass Gasification with Steam in Fluidized Bed: Effectiveness of CaO, MgO, and CaO-MgO for Hot Raw Gas Cleaning, Ind. Eng. Chem. Res. 36, 1535-1543.

Garcia-Labiano F., Abad A., de Diego L.F., Gayan P. and Adanez J., (2002), Calcination of calcium-based sorbents at pressure in a broad range of CO_2 concentrations, Chem. Eng. Sci. 57, 2381-2393.

Kuramoto K., Shibano S., Fujimoto S., Kimura T., Kimura T., Suzuki Y., Hatano H., Shi-Ying L., Harada M., Morishita K., Takarada T., (2003), Deactivation of Ca-Based Sorbents by Coal-Derived Minerals during Multicycle CO_2 Sorption under Elevated Pressure and Temperature, Ind. Eng. Chem. Res. 42, 3566-3570.

Marquard-Möllenstedt T., Sichler P., Specht M., Michel M., Berger R., Hein K.R.G., Höftberger E., Rauch R., Hofbauer H., (2004) Proceedings of 2nd World Conference on Biomass for Energy, Industry and Climate Protection, Rome, Italy, 10-14 May 2004.

Marquard-Moellenstedt T., Specht M., Zuberbuehler U., Koppatz S., Pfeifer C., Rauch R., Soukup G., Hofbauer H., Koch M., (2008), Transfer of the absorption enhanced reforming (AER)-process from the pilot scale to an 8 mwth gasification plant in Guessing, Austria, Proceedings of the 14th European Conference on Biomass for Energy Industry and Climate Protection, Valencia, Spain, 02-06 June 2008.

Swierczynski D., Courson C., Kiennemann A., (2007), Study of steam reforming of toluene used as model compound of tar produced by biomass gasification, Chemical Engineering and Processing: Process Intensification 47, 508-513.

Tamhankar S.S., Tsuchiya K., Riggs J.B., (1985), Catalytic cracking of benzene on iron oxide-silica: catalyst activity and reaction mechanism, Applied Catalysis 16, 103-121.

Xie Y.R., Shen L.H., Xiao J., Xie D.X., Zhu J., (2009), Influences of Additives on Steam Gasification of Biomass. 1. Pyrolysis Procedure, Energy Fuels 23, 5199–5205.

CHAPTER 6

CO_2 CAPTURE BY DOLOMITE PARTICLES IN A GAS FLUIDIZED BED

Abstract: *The capture of CO_2 by particles of calcined dolomite in a gas-fluidized bed was investigated experimentally in a laboratory-scale reactor. Step-response experiments were performed to determine CaO conversion rates in the bed as a function of time and dolomite particle diameter. A simple flow-with-reaction model of the process was proposed; it provided a good description of the transient behaviour in terms of an empirical transfer coefficient, which was found to depend linearly on dolomite particle diameter. The effect of cyclic, sorption followed by regeneration, operation was also studied.*

1. Introduction

After experimental studies on the feasibility of CO_2 capture concepts carried out in previous chapters, a model study is presented in this chapter in order to study the development and application of a short-cut model with lumped parameters for characterizing dolomite CO_2 absorption kinetics. By assuming a linear dependence of sorption kinetics with respect to CO_2 concentration in the gas phase, sorbent volume, and particle saturation (expressed as CaO conversion), the values of the global kinetic constant that better approximates the sorption curves will be available, in particular as a function of the particle diameter.

Carbon dioxide capture is widely studied with a view to its application in energy generation systems as a means of reducing greenhouse gas emissions; solid sorbents, capable of being regenerated, could provide an effective means for carrying out this operation [Harrison, 2008], [Floris *et al.,* 2008]. When CO_2 capture is combined with steam gasification of biomass or coal [Marquard-Möllenstedt *et al.,* 2006], or steam reforming of methane [Johnsen *et al.,* 2006], [Lopez Ortiz *et al.,* 2001] or higher molecular weight hydrocarbons, the quality of the resulting fuel-gas is markedly improved, hydrogen yield being substantially increased and reduced operating temperatures becoming permissible.

Calcined dolomite – consisting essentially of compacted grains of calcium and magnesium carbonates – appears a well-suited sorbent for CO_2 capture. The active ingredient for the purpose is the CaO, which under suitable conditions – temperatures up to about 700°C – reacts to form $CaCO_3$, which in turn may be readily regenerated, for instance by simply raising the temperature. A problem with pure CaO, however, is that its initial reaction with CO_2 on the surface of the particles results in a local increase in volume, the $CaCO_3$ produced there blocking the pores, impeding access of CO_2 to the particle interior and therefore much reducing the CO_2 capture capacity [Abanades *et al.,* 2003], [Bhatia *et al.*, 1983], [Mess *et al.,* 1999], [Hughes *et al.,* 2004]. The MgO in the dolomite, however, does not react with CO_2 at temperatures suitable for its capture by CaO; it thereby provides a continuously free passage for CO_2 diffusion, rendering accessible virtually the entire active particle volume [Silaban *et al.*, 1996].

This chapter reports a study of CO_2 capture by dolomite and the subsequent regeneration of the dolomite carried out in a laboratory-scale fluidized-bed reactor (the same adopted in chapter 3). Dynamic step-response tests were performed to determine CaO conversion rates as a function of time for dolomite particles of various sizes – in the range 0.10 to 1.55 mm. The total amount of dolomite used in these experiments was a small fraction of the overall solid content of the bed; this meant that the temperature profile in the system could be maintained constant regardless of the exothermic nature of the CO_2 absorption process. On-line measurement of CO_2 concentration in the gas outlet stream provided the response curves from which the take-up rate of CO_2 in the dolomite could be calculated as a function of time. Some deactivation of the dolomite was observed which resulted in a reduction in its sorption capacity with progressive cycles – ten of which were carried out for two of the dolomite particle sizes tested.

2. Experimental procedure

The experimental layout is shown in Figure 1 and described in more detail in chapter 3. It consists essentially of a cylindrical tube 6 cm in diameter and 66 cm long fitted into a furnace. The tube is equipped with a distributor and fed for each run with 295 g of 210 μm sand particles of density 2500 kg/m^3 – resulting in a particle bed some 7 cm in height of void-fraction approximately 0.4.

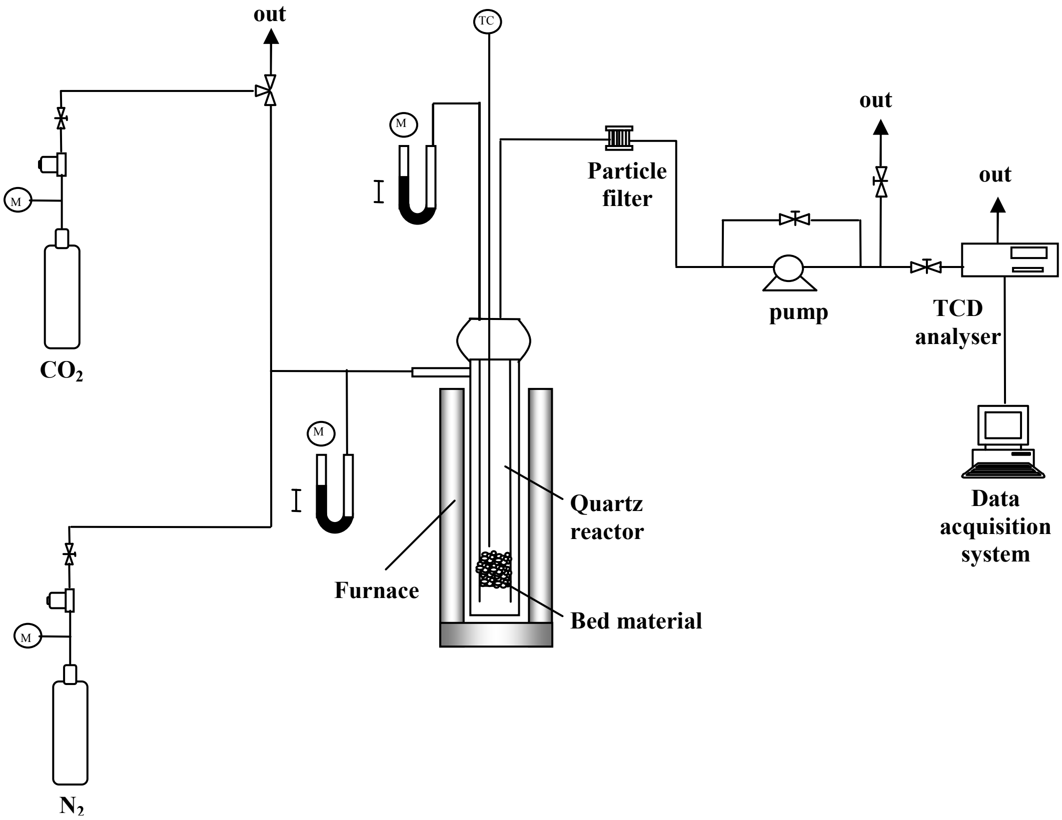

Figure 1: The fluidized bed reactor and related equipment.

For a CO_2 capture and CaO regeneration experiment, 3g of dolomite (1490 kg/m^3, for chemical and physical properties see Table 2 in chapter 3) of a selected size was added to the sand – four different dolomite particle diameters (0.10, 0.78, 1.10 and 1.55 mm) being used for these tests. The bed was then fluidized with 0.0278 NL/s N_2 and the temperature raised to 850°C (at a rate of 10°C/min) to convert any $CaCO_3$ present to CaO. The CO_2 concentration of gas leaving the reactor was monitored continuously on-line by means of a thermal-conductivity-detector-analyser (ABB); when the CO_2 concentration had fallen to zero the bed temperature was reduced to 650°C in preparation for a CO_2 capture run. This was then started by stepping the inlet gas concentration of CO_2 from zero to 0.0050 NL/s, which resulted in an inlet gas concentration of 0.0068 NL/s. Mass flow controllers were used to set and maintain these flow conditions. When the CO_2 outlet concentration had reached the constant level of that of the inlet, the CO_2 feed was stepped down to zero and fluidization with N_2 continued until the outlet CO_2 concentration had fallen to the low equilibrium value for the reversible capture/regeneration reaction at 650°C; the temperature was then raised again to 850°C (10°C/min) to regenerate the bed in preparation for the next CO_2 capture run. Figure 2 describes the time dependence of this complete CO_2 capture/regeneration process. (particle size: 1.5, cycle 1).

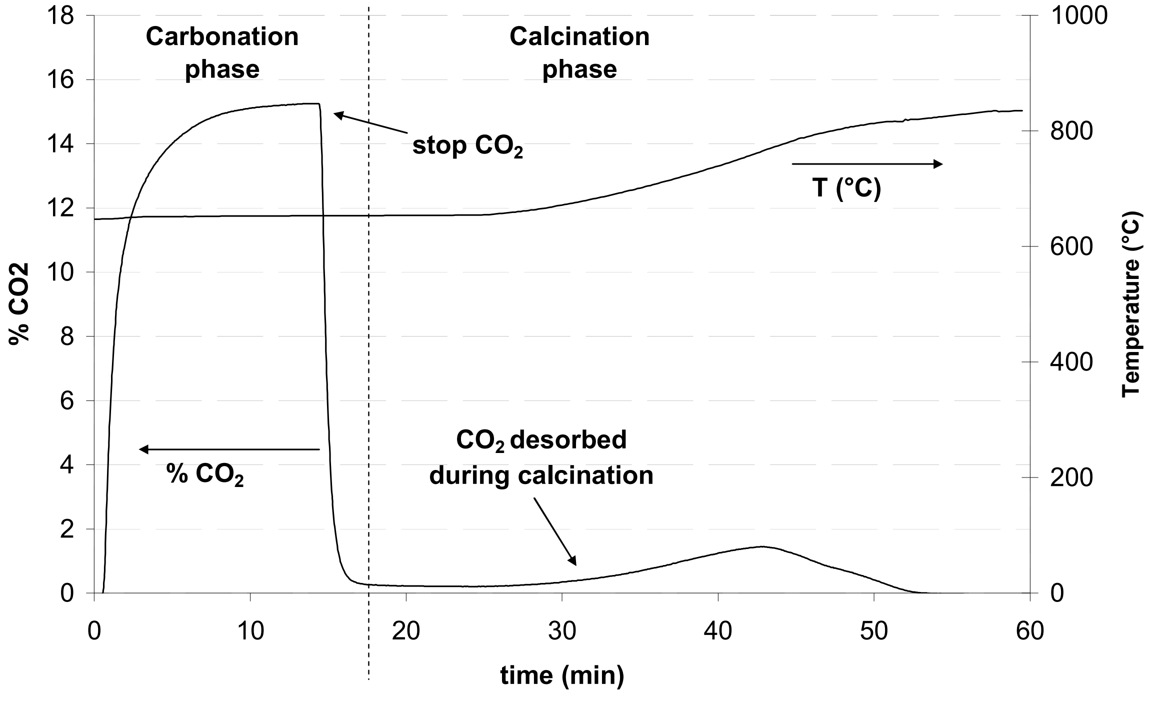

Figure 2: Experimental CO_2 concentration and temperature in function of time, for the whole procedure of carbonation-calcination cycle (particle size: 1.5, cycle 1)

The above procedure was repeated for each of the four dolomite particle diameters, and also for a blank test with no dolomite present. As will be seen, the results of the blank test were to prove essential for the analysis of the transient behaviour recorded for CO_2 capture.

After tests, particles with diameters of 0.78, 1.10 and 1.55 mm have been recovered by sieving smaller inert bed particles, and weighted in order to verify that dolomite has not been lost by attrition.

3. Experimental results

3.1 Blank test

Figure 3 shows the outlet CO_2 concentration response for the blank test (i.e. with no dolomite in the bed).

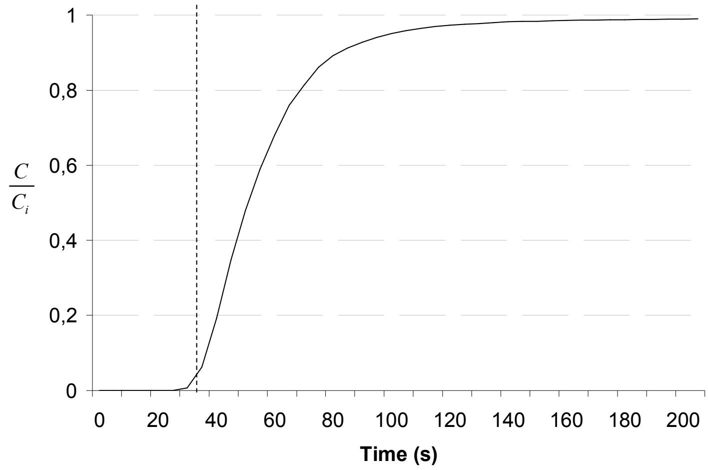

Figure 3: Step response of the fluidized bed in the absence of dolomite: normalised CO_2 outlet concentration as a function of time.

It is clear from Figure 1 and the data presented above that the response curve shown in Figure 3 is dominated by flow-mixing in the ancillary equipment, the volume of gas in the fluidized bed reactor itself amounting to only some 5% of the volume of gas in the system as a whole. The same can be said for the response curves for the dolomite containing beds shown below, Figures 5, 8 and 9. At first sight this would appear to pose severe problems for the task of relating the gas outlet responses to the CO_2 capture characteristics of the fluidized bed itself. The blank test result of Figure 3, however, provides a means of confronting this problem; it enables a simple descriptive model of the gas phase of the entire system to be formulated which can then be used to extract the response of the particle phase of the fluidized bed from the measured gas phase response of the entire system under CO_2 capture conditions.

The first use of the response curve of Figure 3 is to find the holdup in mols of the total gas phase H_G. This is simply the product of the total molar throughput of gas and the area enclosed by the response curve and ordinate 1: which gives H_G = 0.0905 mol and corresponds to a volume of 2.03 NL.

The second use of Figure 3 is to fit a simple flow-mixing model to the overall gas phase response. It would appear from the form of this response that a series combination of a well-mixed volume and a dead-time of 35 s would provide an adequate description of flow-mixing in the system, and this on further examination turns out to be so – the volume of the two gas phase regions becoming immediately available as shown in Figure 4. As is clear from the above discussion, however, the dynamics of the gas phase of the fluidized bed itself is buried deep within this overall model description.

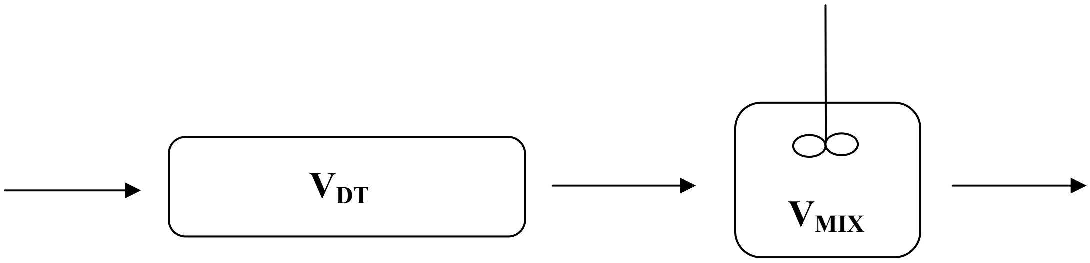

Figure 4: The descriptive first-order-with-dead-time model for gas mixing in the entire system: first-order volume V_{mix} = 0.882 NL, dead-time volume V_{dt} = 1.148 NL.

3.2. CO_2 capture tests

These are performed in exactly the same way as the blank test considered above, the only difference being that the fluidized bed now contains 3 g of dolomite particles of a chosen mean diameter. Figure 5 shows the response curve for the bed fed with 0.78 mm dolomite particles and compares it with that of the blank test, differences being due solely to CO_2 capture in the former case.

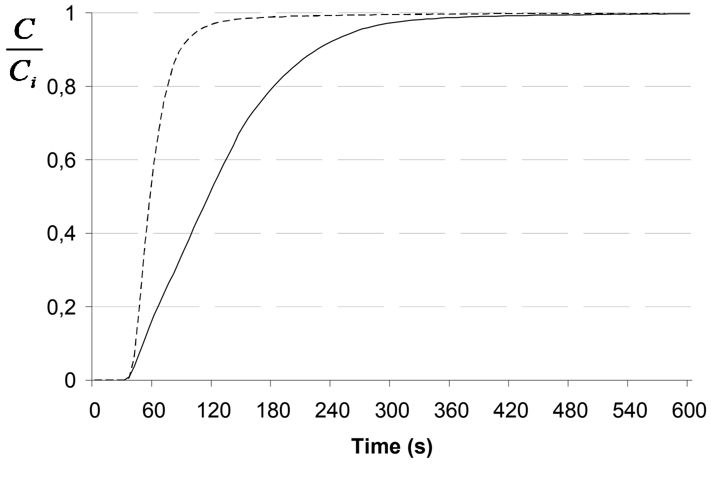

Figure 5: Step response of the fluidized bed in the presence of 0. 78 mm dolomite particles: normalised CO_2 outlet concentration as a function of time. Step response for the blank test, Figure 2, shown as a broken line.

The response curve of Figure 5 may be used to evaluate the total amount of CO_2 present in the whole system as a function of time – i.e. its holdup $H_T(t)$: the moles of CO_2 that have entered the system at time t minus those that have left:

$$H_T(t) \quad = \quad q_{CO_2} \int_0^t \left(1 - \frac{C(t_1)}{C_i}\right) dt_1 , \tag{1}$$

where q_{CO2} is the molar flow rate of CO_2 to the system from time zero – equal to 0.0050/22.414=0.000223 mol/s).

Figure 6 shows how the total CO_2 holdup of the entire system varies with time.

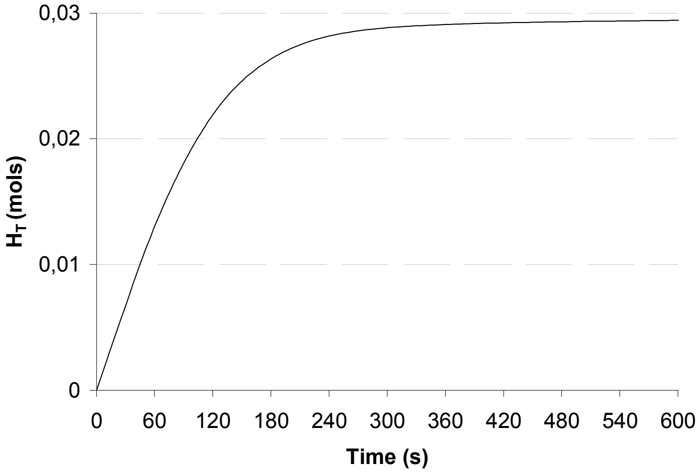

Figure 6: Total holdup of CO_2 for the entire system with 0. 78 mm dolomite particles.

The CO_2 holdup in the solid phase of the fluidized bed $H_S(t)$ – i.e. the CO_2 captured by the dolomite – is simply the total holdup of the entire system $H_T(t)$ (shown in Figure 6 for the 0.78 mm particle system) minus the holdup of the gas phase of the entire system $H_G(t)$:

$$H_S(t) \quad = \quad H_T(t) \quad - \quad H_G(t) . \tag{2}$$

The gas phase model, shown in Figure 4, obtained by means of the blank test, enables $H_G(t)$ to be estimated and hence, from Eqs.(1 and 2), $H_S(t)$ – the captured CO_2 as a function of time.

3.2.1. Evaluation of the holdup of CO_2 in the gas phase of the entire system $H_G(t)$

On the basis of the flow model of Figure 4, nothing leaves the system before the dead-time of approximately 35 seconds, so that the total holdup of CO_2 during this initial period is simply that which has entered, namely $q_{CO2}t$. The dead-time is clearly unaffected by CO_2 capture, being the same for the blank test as for all the others. With the assumption that CO_2

transfer to the dolomite only takes place to a significant extent after this dead-time has elapsed, then the first 35 seconds following the step input of CO_2 serves solely to fill the dead-time region, resulting in a CO_2 holdup there of 0.0078 mol after 35 seconds. Thereafter the CO_2 starts to accumulate in the well mixed region, to transfer to the dolomite and to exit from the system where its concentration – that of the well mixed region – is measured; CO_2 holdup in the well mixed region at any time t is therefore $C(t)V_{MIX}$, where V_{MIX} was found from the blank test to be equal to 0.882 NL, and $C(t)$ mol/NL is the measured CO_2 concentration leaving the system for the CO_2 capture runs – Figures 5, 8 and 9. On this basis, the holdup of CO_2 in the gas phase of the entire system is given by:

$$H_G(t) \quad = \quad 0.000223\,t \qquad\qquad 0 < t < 35 \;.$$

$$H_G(t) \quad = \quad 0.0078 \quad + \quad 0.882\,C(t) \qquad t > 35 \tag{3}$$

This result is shown in Figure 7 together with the key result of this analysis: the holdup of CO_2 in the dolomite $H_S(t)$, obtained from Eqs.(1 and 2).

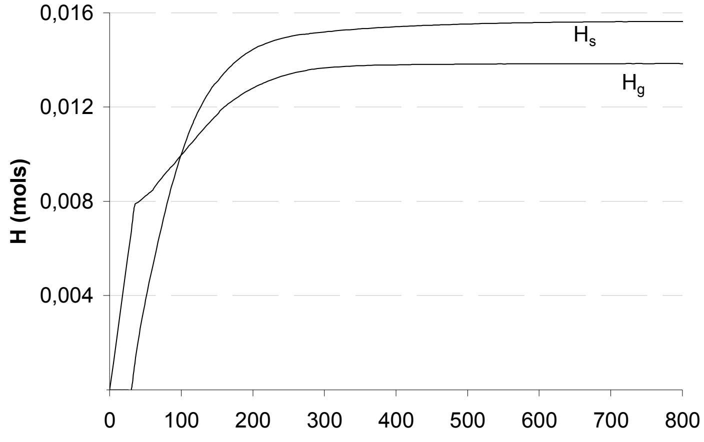

Figure 7: Holdup of CO_2 in the gas phase of the entire system $H_G(t)$ and in the dolomite $H_S(t)$ for CO_2 capture with 0. 78 mm dolomite particles.

3.2.2. Holdup of CO_2 in the dolomite for all CO_2 capture runs

The step response results for all the diameter dolomite particle systems are shown in Figure 8.

On processing the response curves of Figure 8 in the same way as illustrated above for the 0.78 mm dolomite particle system, holdups of CO_2 in the dolomite $H_S(t)$ mol may be evaluated as functions of time and expressed in terms of the concentration of captured CO_2 in the solid phase of the fluidized bed C_s:

$$C_s(t) \quad = \quad H_S(t)/v_s \, , \tag{4}$$

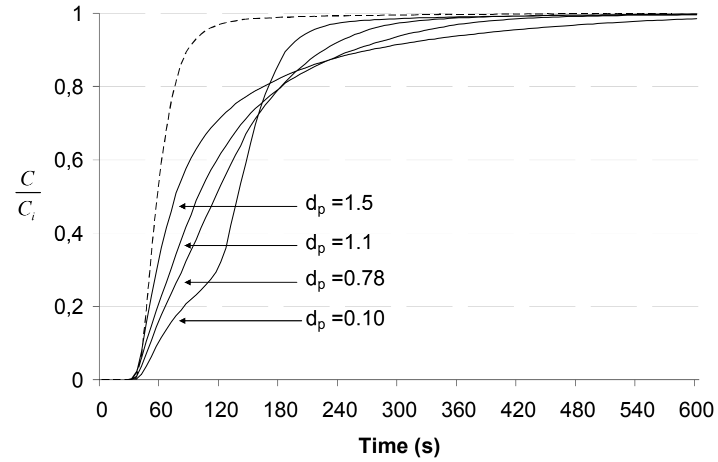

Figure 8: Step response of the fluidized bed for all dolomite particle systems: normalised CO_2 outlet concentration as a function of time. Step response for the blank test, Figure 2, shown as a broken line.

where v_s is the volume of the solid phase of the fluidized bed – equal to 0.12 l for all runs. These results, which fully quantify the CO_2 capture process, are shown in Figure 9. The now superfluous 35 s dead-time has been removed from these responses.

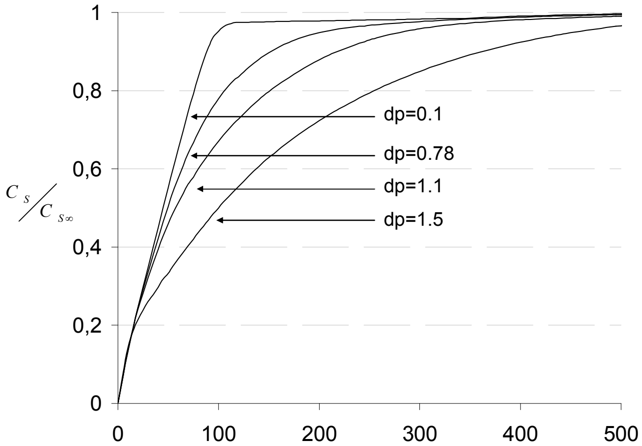

Figure 9: Experimental results for the concentration of captured CO_2 in the solid phase of the fluidized bed as a function of time.

3.3. A descriptive model for CO_2 capture

A simple model description of the flow and reaction process in the fluidized bed is shown in Figure 10.

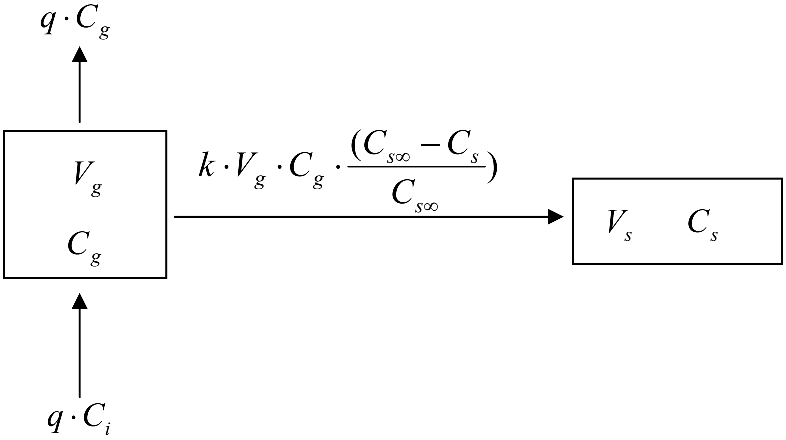

Figure 10: A descriptive model for CO_2 capture in a fluidized bed.

Both gas and solid phases are assumed perfectly mixed. The rate of transfer from the gas to the solid phase of CO_2 clearly depends on to its gas phase concentration in the bed C_g and the fractional unconverted dolomite concentration ($C_{S\infty}$ - C_S) / $C_{S\infty}$: the model assumes this rate to be simply proportional to these two quantities. For convenience, the solid phase concentrations are expressed with respect to the entire solid phase, sand plus dolomite – as was assumed for Eq.(4); the final value $C_{s\infty}$ is the experimentally obtained value, which is always somewhat lower than the theoretical saturation level, indicating that not quite all the CaO present is accessible for reaction. The global transfer coefficient *k* has to take into account the reaction kinetics and diffusional resistances around and within the dolomite grains. It remains for now a purely empirical constant, to be quantified by reference to the experimental results, though having the potential to be related quantitatively to a more complete mechanistic model description.

Mass balance equations for CO_2 follow from the model description of Figure 10:

$$\frac{dC_s}{dt} = k \cdot C_g \cdot \frac{\left(C_{s\infty} - C_s\right)}{C_{s\infty}} , \tag{5}$$

$$\frac{dC_g}{dt} = \frac{q}{V_g} \cdot (C_i - C_g) - k \cdot \frac{V_s}{V_g} \cdot C_g \cdot \frac{\left(C_{s\infty} - C_s\right)}{C_{s\infty}} \left(1 - S_{CO_2} C_g\right) . \tag{6}$$

The final bracketed expression in Eq.(6) takes into account the reduction in total outflow *q* from the system as a result of CO_2 capture. It is included here for the sake of completeness but was found to make little difference to the computed results.

The only unknown parameter appearing in Eqs.(5 and 6) is the global transfer coefficient *k*. Other parameter values relating to experimental test conditions are shown in Table 1.

parameter	*value*
q	0.0328 NL/s
V_g	0.08 l
V_s	0.12 l
C_i	0.0068 mol/NL
S_{CO_2}	22.414 NL/mol

Table 1: Parameter values relating to the experimental tests

By adopting the parameter values given in Table 1 and assigning a value to k, Eqs.(5 and 6) may be solved numerically for the CO_2 concentrations in both the gas phase $C_g(t)$ and the solid phase $C_s(t)$ of the fluidized bed. It is only the solid phase concentration $C_s(t)$ that is useful here as this is the same quantity as that evaluated from the experimental runs and displayed in Figure 9.

Numerical solutions of Eqs.(5 and 6) were obtained iterating values of k to approximate the results obtained experimentally and shown in Figure 9. Figure 11 shows the result of these comparisons: it will be seen that the model is well able to reproduce the experimental profiles.

Figure 12 shows how the fitted k values vary with dolomite particle diameter; a good linear relationship is found for the conditions examined (d_p<1.5 mm), transfer rates increasing progressively with decreasing particle diameter:

$$k = 1.0461 - 0.6133 d_p \tag{7}$$

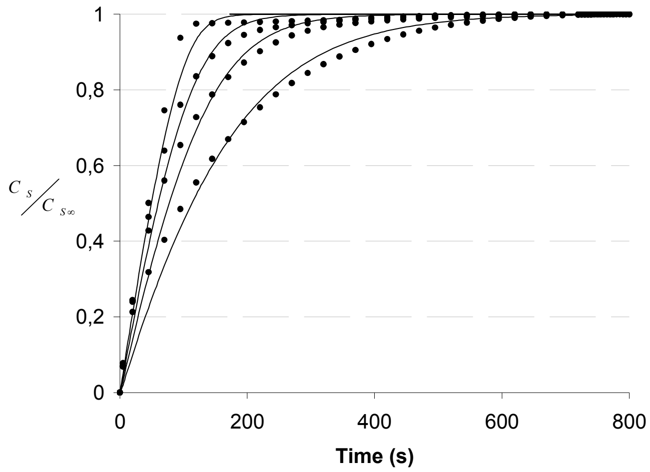

Figure 11: Captured CO_2 concentration in the solid phase of the fluidized bed: comparison of the experimentally determined results of Figure 8 (points) with solutions of the model equations using fitted values of k (continuous curves).

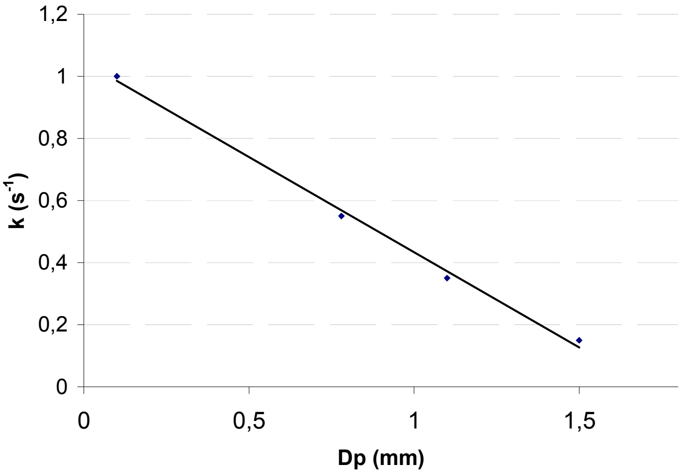

Figure 12: CO_2 transfer coefficient k as a function of dolomite particle diameter.

3.4. Cyclic CO_2 capture/ regeneration tests

The effect of deactivation of dolomite was examined for two of the particle diameters, 0.1 mm and 1.5 mm, by performing ten CO_2 capture experiments, each followed by CaO regeneration at 850°C. These results are shown in Figure 13.

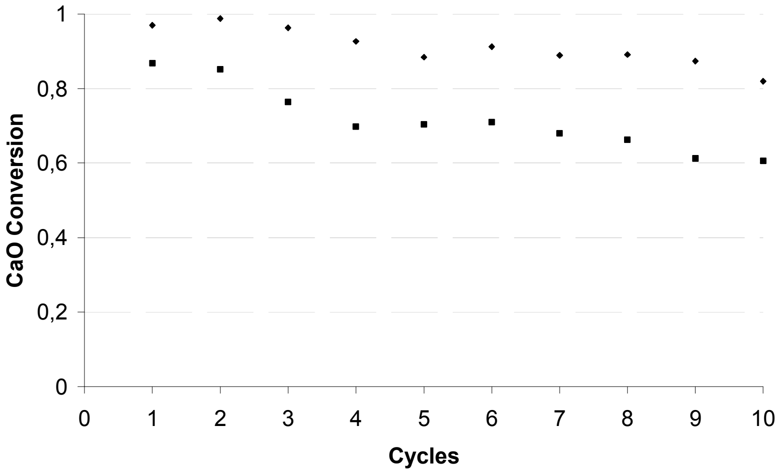

Figure 13: Dolomite deactivation with progressive cycles of CO_2 capture: 1.5 mm dolomite – squares; 0.1 mm dolomite – diamonds.

3.5. Conclusions

An interesting aspect of this work is the manner in which it has proved possible to extract the dynamics of CO_2 capture by the dolomite from the measured response curves in which this key feature is so deeply buried. The fluidized bed itself occupies less than 10% of the total system volume, within which temperatures vary from 650°C to close to ambient. All this would appear to make it virtually impossible to interpret Figures 4 and 7 in any meaningful manner. The analysis has been made possible by the availability of the blank test result – Figure 3. The blank test was performed under conditions matched to those of the CO_2 capture runs, with identical temperature profiles throughout the system and the identical fluidization conditions within the reactor. The model for flow-mixing in the gas phase of the blank system could thus be related to that for the CO_2 capture runs, thereby enabling CO_2 take up by the dolomite to be calculated as described above.

Although the global transfer coefficient k is an empirical parameter, its progressive decrease with increasing dolomite particle diameter suggests strongly the presence of intra-particle diffusional resistances which, as is clear from Figure 12, become quite significant for the larger particle sizes tested.

The reported deactivation of the dolomite with progressive capture/reactivation cycles – measured in terms of CO_2 capture, Figure 13, has been reported by other works on calcium-based sorbents [Hughes *et al.,* 2004], [Silaban *et al.,* 1996], [Lu *et al.,* 2008], [Florin *et al.,* 2008], [Feng *et al.,* 2006], [Lu *et al.,* 2006], [Wang *et al.,* 2005], [Li *et al.,* 2006], [Gallucci *et al.,* 2008], [Pacciani *et al.,* 2008], [Ives *et al.,* 2008]. It has been attributed to modifications of the sorbent particles, in particular due to the loss of pore volume and sintering of the porous calcium oxide [Barker *et al.,* 1973].

Notation

C, C_i	CO_2 gas phase concentration leaving and entering the entire system, mol/NL
C_g, C_s	CO_2 concentration in the gas phase and solid phase of the fluidized bed, mol/l
$C_{s\infty}$	final CO_2 concentrations in the solid phase of the fluidized bed, mol/l
d_p	dolomite particle diameter, mm
H_G, H_S	CO_2 holdup for gas phase and solid phase of entire system, mol
H_T	CO_2 holdup for entire system ($H_G + H_S$), mol
k	global transfer coefficient, 1/s
q	gas flow rate, NL/s
q_{CO_2}	CO_2 flow rate, mol/s
S_{CO_2}	specific volume of CO_2, NL/mol
V_g, V_s	volumes of gas and solid in fluidized bed, l
V_{DT}, V_{MIX}	volumes of dead time and well mixed regions of gas phase of entire system, NL
t	time, s

Bibliography

Abanades J.C., Alvarez D., (2003), Conversion limits in the reaction of CO_2 with lime, Energy & Fuels 17, 308-315.

Barker R. J., (1973), The Reversibility of the Reaction $CaCO_3 \leftrightarrow CaCO+CO_2$, J. Appl. Chem. Biotechnol. 23, 733-742.

Bhatia S.K., Perlmutter D.D., (1983), Effect of the product layer on the kinetics of the CO_2-lime reaction, AIChE J. 29, 79-86.

Feng B., Liu W., Li X., An H., (2006), Overcoming the Problem of Loss-in-Capacity of Calcium Oxide in CO_2 Capture, Energy Fuels 20, 2417-2420.

Florin N.H., Harris A.T., (2008), Enhanced hydrogen production from biomass with in situ carbon dioxide capture using calcium oxide sorbents, Chemical Engineering Science 63, 287-316.

Florin N.H., Harris A.T., (2008), Screening CaO-Based Sorbents for CO_2 capture in Biomass Gasifiers, Energy & fuels 22, 2734-2742.

Gallucci K., Stendardo S., Foscolo P. U., (2008), CO_2 capture by means of dolomite in hydrogen production from syn gas, Int. J. Hydrogen Energy 33, 3049-3055.

Harrison D. P., Harrison D.P., (2008), Sorption-Enhanced Hydrogen Production: A Review, Ind. Eng. Chem. Res. 47, 6486-6501.

Hughes R.W., Lu D., Anthony L.J., Wu Y., (2004), Improved long-term conversion of limestone-derived sorbents for in situ capture of CO_2 in a fluidized bed combustor, Ind. Eng. Chem. Res. 43, 5529-5539.

Ives M., Mundy R.C., Fennell P.S., Davidson J.F., Dennis J.S., Hayhurst A.N., (2008), Comparison of Different Natural Sorbents for Removing CO_2 from Combustion Gases, as Studied in a Bench-Scale Fluidized Bed, Energy Fuels 22, 3852–3857.

Johnsen K., Ryu H.J., Grace J.R., Limb C.J., (2006), Sorption-enhanced steam reforming of methane in a fluidized bed reactor with dolomite as CO_2-acceptor, Chemical Engineering Science 61, 1195-1202.

Li Z., Cai N., Huang Y., (2006), Effect of preparation temperature on cyclic CO2 capture and multiple carbonation-calcination cycles for a new Ca-based CO_2 sorbent, Ind. Eng. Chem. Res. 45, 1911-1917.

Lopez Ortiz A., Harrison D.P., (2001), Hydrogen production using sorption-enhanced reaction, Ind. Eng. Chem. Res. 40, 5102-5109.

Lu D.Y., Hughes R.W., Anthony E.J., (2008), Ca-based sorbent looping combustion for CO2 capture in pilot-scale dual fluidized beds, Fuel Processing Technology 89, 1386-1395.

Lu H., Reddy E.P., Smirniotis P.G., (2006), Calcium Oxide Based Sorbents for Capture of Carbon Dioxide at High Temperatures, Ind. Eng. Chem. Res. 45, 3944-3949.

Marquard-Moellenstedt T., Specht M., Zuberbuehler U., Koppatz S., Pfeifer C., Rauch R., Soukup G., Hofbauer H., Koch M., (2008), Transfer of the absorption enhanced reforming (AER)-process from the pilot scale to an 8 mwth gasification plant in Guessing, Austria, Proceedings of the 14th European Conference on Biomass for Energy Industry and Climate Protection, Valencia, Spain, 02-06 June 2008.

Mess, D., Sarofim, A.F., Longwell, J.P., (1999), Product Layer Diffusion during the Reaction of Calcium Oxide with Carbon Dioxide, Energy &Fuels 13, 999-1005.

Pacciani R., Muller C. R., Davidson J. F., Dennis J. S., Hayhurst A. N., (2008), How does the concentration of CO_2 affect its uptake by a synthetic Ca-based solid sorbent? AIChE J. 54, 3308 - 3311.

Silaban, A., Narcida, M., Harrison, D.P., (1996), Characteristics of the reversible reaction between CO_2 (g) and calcined dolomite, Chemical Engineering Communications 146, 149-162.

Wang J., Anthony E. J., (2005), On the decay behavior of the CO_2 absorption capacity of CaO-based sorbents, Ind. Eng. Chem. Res. 44, 627-629.

CONCLUSIONS

Biomass gasification has been investigated in this work with the aim to optimize catalytic systems for product gas clean-up from its organic vapour phase fraction (tar), at different scales (pilot plant, laboratory scale reactor, micro-reactor). Tests have been performed with or without CO_2 capture, the most important parameter varying in these conditions being temperature, from 650°C to 850°C. Three main catalytic materials have been tested in this work: alkaline earth oxides, nickel based and iron based catalysts. They are list in Table 1, and briefly summarised below.

	Alkaline earth oxides	**Nickel based catalysts**	**Iron based catalysts**
Newly synthesized catalysts	CaO	4, 10% Ni/CaO	1-20% Fe/CaO
	MgO	-	5, 20% Fe/MgO
	(Ca,Mg)O	4, 10% Ni/(Ca,Mg)O	1-20% Fe/(Ca,Mg)O
Commercial catalysts		Pall filter candle	
		Commercial nickel catalyst (Johnson Matthey Plc)	

Table 3: Main catalytic materials tested in this work: the interest of each solid is described in this chapter

2. Alkaline earth oxides

2.1. Tar reforming

Alkaline earth oxides have been tested as catalysts for tar abatement, in a micro-reactor rig, using toluene as model tar compound. Catalytic activity of CaO and MgO has been found to be lower than dolomite, and in addition these materials need an activation time before reaching the maximum plateau of reactivity. Dolomite has been found to be quite active in toluene conversion, but a high carbon deposition is detected on particle surface after catalytic tests.

2.2. CO_2 capture

Plain CO_2 capture tests have been carried out with CaO (micro-reactor) and dolomite (fluidized bed and micro-reactor). The particular sample of CaO used in this work showed a strong reduction in CO_2 capture capacity probably due to particle pore blockage. However, with dolomite, plain CO_2 capture tests have been successfully carried out, and have been used as blank tests for evaluating additional kinetic limitations in metal doped modified dolomites (in the micro-reactor), and as a starting point to elaborate a rigorous model for extracting kinetic data for heterogeneous systems (solid conversion in the fluidized bed). Dolomite has been also used for the combined process of steam reforming and CO_2 capture, coupled with a commercial nickel catalyst (see Section 3.1).

3. Nickel based catalysts

3.1. Tar and methane reforming

Nickel has been found to be very active in tar abatement. A nickel based catalytically activated filter element has been inserted in the freeboard of a pilot plant fluidized bed steam gasifier, and a significant improvement of all relevant performance indicators of a biomass gasification process has been detected.

A commercial nickel catalyst, coupled with dolomite, has been used in a bench scale fluidized bed for the combined process of CO_2 capture and steam reforming of methane, toluene and 1-methyl naphthalene, chosen as gasification key products. The feasibility of simultaneous CO_2 capture and reforming reactions has been therefore demonstrated, and at the same time evidence has been found of improved tar and methane conversion (with a higher H_2/CO ratio in the product gas finally obtained) when dolomite is used as in-bed sorbent.

Newly synthesized nickel based catalysts, 4, 10%Ni/CaO and 4, 10%Ni/(Ca,Mg)O have been characterized and tested as steam reforming catalysts, in a micro-reactor, using toluene and 1-methyl naphthalene as model tar compounds. Both series showed a high tar conversion, and a higher carbon deposition resistance has been detected with respect to raw calcined dolomite. The strong metal-support interaction detected in the Ni/(Ca,Mg)O series has been highlighted as a preferential condition for large scale applications.

3.2. CO_2 capture

Nickel doped dolomite showed a reduced absorption capacity and lower reaction rate than raw calcined dolomite, as evaluated in a micro-reactor rig. However, when the metal content is optimized, the combined process of steam reforming and CO_2 capture in presence of 4%Ni/dolomite showed high values of toluene conversion before saturation of dolomite.

4. Iron based catalysts

4.1. Tar reforming

The potential of iron, a cheap and non toxic metal, as a catalyst for reforming reactions has been also investigated, by deposition on alkaline earth oxides CaO, MgO and dolomite. When CaO is present in the substrate (as lime or calcined dolomite), iron in contact with the reactive atmosphere of toluene steam reforming is preserved mostly as Fe (3+) specie, while it is reduced to Fe (2+) in the Fe/MgO system. Iron has been found to improve catalytic activity of CaO and MgO substrates, rendering them more active than dolomite and making these materials more attractive for scale up applications. Also carbon deposition resistance is improved by adding iron to these raw substrates.

4.2. CO_2 capture

Iron doped dolomite showed a CO_2 absorption capacity decay by increasing the iron amount in the sorbent; however, a high iron content is not required for improving the steam reforming reactions rate. Therefore, dolomite particles containing low iron contents may perform very well both, CO_2 absorption and tar steam reforming reactions. Kinetic limitations in Fe/dolomite systems are less evident with respect to Ni/dolomite, bringing to light the critical role of free MgO in the sorbent matrix on accelerating the rate of CO_2 capture gas-solid reaction.

5. Perspectives

The removal of tar from the product gas of industrial biomass gasifiers, addressed to energy generation and/or fuels synthesis, is of considerable importance to the economic viability of the process. Tar production depends on various factors such as fuel composition, gasifying medium, operating temperature and pressure, gasifier construction, and the type of catalyst employed. The search for new catalytic materials is therefore a worthwhile research activity and one that should focus on realistic features of potential catalysts for commercial exploitation: these should consist of cheap materials so as to minimize manufacturing and final disposal costs. The development of catalysts with such characteristics has been the aim of the research presented in this thesis.

Iron, an appropriately low cost and non-toxic material, has been found to improve the catalytic activity of CaO and MgO substrates, rendering them comparable in activity to dolomite and therefore making them attractive for potential scale up applications.

It has been found that when CaO is present in the substrate (as lime or calcined dolomite) iron may be preserved as the Fe (3+) species, but is reduced to Fe (2+) in Fe/MgO systems. Thus redox behaviour in the product gas atmosphere is strongly dependent on the kind of substrate adopted and the interactions that can take place. Regardless of the fact that Fe (3+) is a thermodynamically unfavoured oxidation state in the presence of steam and carbon dioxide oxidation agents, the $Ca_2Fe_2O_5$ structure enables it to be stabilized.

On the other hand, the Fe (2+) species predicted by thermodynamic evaluation was detected in the Fe-MgO system, stabilized by the FeO-MgO solid solution.

In conclusion, it has been found that both Fe (3+) and Fe (2+), in cooperation with CaO and MgO substrates are active in tar reforming reactions. In view of the fact that raw CaO has been proposed as an ideal additive for biomass gasification applications, the conclusions of this work regarding the improved performance to be expected from the incorporation of iron could be of some significance for further developments.

Concerning nickel based catalysts NiO-CaO and NiO-(CaMg)O, it has been found that they are very active on enhancing tar reforming activity of alkaline earth oxides. However, nickel is toxic so that final disposal and environmental costs are critical. Moreover, it has been found that nickel may reduce CO_2 absorption properties of dolomite, rendering this material less attractive than iron doped sorbents for CO_2 capture applications.

Iron based combined catalysts and sorbents, instead of nickel doped materials, are therefore highly recommended for further investigation and scale-up.

One research approach that can be explored in microreactor scale is the reactivity of these materials with respect to phenol, that has been found to be a very abundant tar specie in the temperature range of interest (650-700°C), and has been found also to be more active than toluene and 1-methyl naphthalene, in order to demonstrate the feasibility of the absorption enhanced reforming process using Fe/dolomite or Fe/CaO.

For pilot or industrial scales biomass gasification applications, in particular the Dual Fluidized Bed technology, one interesting research study that can start from this work is the coupling with Chemical Looping Combustion process. Iron, in fact, is a well known material in the so-called CLC (Chemical Looping Combustion) that is a cyclic process for reduction and oxidation of an OTC (Oxygen Transfer Compound), whereby fuel is consumed and heat can be produced (as explained in the Introduction chapter).

When FICFB (Fast Internally Circulating Fluidised Bed) technique is applied in biomass gasification plants using an iron based catalyst, the basic CLC concepts take place unavoidably in the overall process, even if a gasifying agent is present in the fuel reactor. Iron oxides, together with a sorbent may circulate between a gasifier - CO_2 capture bubbling bed, and a combustor – calciner riser in a continuous process. In the chamber devoted to biomass gasification and CO_2 capture, the reducing conditions force iron oxides (Fe_2O_3) to react with syngas or directly with fuel to form CO_2, steam and the reduced iron oxides (Fe, FeO). On the other hand, in the riser, the thermal loading provided by char may be increased by oxidation of reduced iron or iron oxides that regenerate the OTC (Fe_2O_3).

It may be also of interest to partially recovery the energy stored by the OTC in the gasification reactor, by oxidizing iron with steam (the so-called Steam-Iron process) in a separate reactor, and producing magnetite (Fe_3O_4) and H_2 with high purity. Then magnetite may be transferred in the combustion reactor for recovering heat by $Fe_3O_4 \rightarrow Fe_2O_3$ oxidation, which may be coupled with the exothermic char combustion.

The most recommended substrate for the proposed follow-up study is MgO, because iron can split between FeO-Fe_3O_4 and Fe_2O_3 species, but iron reduction-oxidation behaviour in several cycles has to be investigated.

A last suggestion for the perspectives opened on this Ph. D. work concerns modelistic studies of kinetics of CO_2 capture reaction, using M/substrate (in particular Fe/dolomite) in comparison with raw sorbent, being in this last case the kinetic constant well known in literature (Bhatia S.K., Perlmutter D.D., (1983), AI.Ch.E. J. 29, 79-86). This study should be carried out in different conditions of CO_2 partial pressure, and different temperatures. Also cyclic behaviour on calcination-carbonation of these combined catalysts and sorbents should be envisaged in further investigations based on the present Ph. D. thesis.

Appendix

This chapter shows a report of chemical techniques used for catalytic systems characterization.

X-Ray diffraction

X-ray scattering techniques are a family of non-destructive analytical techniques which reveal information about the crystallographic structure, chemical composition, and physical properties of materials and thin films. These techniques are based on observing the scattered intensity of an X-ray beam hitting a sample as a function of incident and scattered angle, polarization, and wavelength or energy.

Powder X-Ray diffraction is commonly used to identify unknown substances, by comparing diffraction data against a database. It may also be used to characterize heterogeneous solid mixtures to determine relative abundance of crystalline compounds and to determine particles size.

In this work, the crystalline phases contained in the samples and the structural modifications occurring after reduction or catalytic tests were examined by powder X-ray diffraction (XRD) on a Brucker D8 Advance diffractometer using a Ni detector side filtered Cu Kα radiation ($\lambda = 1.5406$ Å).

Temperature Programmed Reduction

Temperature-programmed reduction (TPR) is a technique for the characterization of solid materials and is often used in the field of heterogeneous catalysis to find the most efficient reduction conditions. An oxidized catalyst precursor is submitted to a programmed temperature rise while a reducing gas mixture is flowed over it. A simple container (U-tube) is filled with a solid or catalyst (50 mg of catalyst). This sample vessel is positioned in a furnace with temperature control equipment. A thermocouple is placed near the solid for temperature measurement. To remove the present air the container is filled with an inert gas (argon). Flow controllers are used to add hydrogen. The composition of the gaseous mixture is measured at the exit of the sample container with appropriate detector (thermal conductivity detector, TCD). The maximum of the consumption peaks correspond to the reduction temperature of solids with various oxidation degrees. The surface area of the total signal permits the determination of the total hydrogen consumption and then the percentage of reduction of a given compound. The reductive gas mixture (H_2 = 0.12 L.h^{-1} and Ar = 3 L.h^{-1}) passed through the reactor heated from room temperature to 900°C with a heating rate of 15°C min^{-1} and was then maintained at 900°C until the end of H_2 consumption according to the baseline return.

Temperature Programmed Oxidation

TPO (Temperature Programmed Oxidation) analyses have been carried out after catalytic tests in order to detects the presence of different oxidizable species (different carbon forms) by differences in their oxidization temperatures and rates. CO_2, CO and H_2O formed and O_2 consumed are quantified versus temperature by a mass spectrometer (quadrupole—Pfeiffer). The amount of carbon deposited on different catalysts and oxidized during the analysis was deducted from the amount of carbon-containing products ($CO+CO_2$). The heating program of TPO permits to reach 1000°C with a rate of 15°C/min under a mixture of oxygen (10vol%) in helium.

Mössbauer analysis

Mössbauer spectroscopy is a spectroscopic technique based on the resonant emission and absorption of gamma rays in solids. Mössbauer spectroscopy is sensitive to similar electron-nucleus interactions; due to the high energy and extremely narrow line widths of gamma rays, it is one of the most sensitive techniques in terms of energy resolution.

A solid sample is exposed to a beam of gamma radiation, and a detector measures the intensity of the beam transmitted through the sample. The atoms in the source emitting the gamma rays must be of the same isotope as the atoms in the sample absorbing them (^{57}Fe in our case). In accordance with the Mössbauer effect, a significant fraction of the emitted gamma rays will not lose energy to recoil and thus will have approximately the right energy to be absorbed by the target atoms, the only differences being attributable to the chemical environment of the target, which is what it is envisaged to observe.

In the resulting spectra, gamma-ray intensity is plotted as a function of the source velocity. At velocities corresponding to the resonant energy levels of the sample, some of the gamma-rays are absorbed, resulting in a drop in the measured intensity and a corresponding dip in the spectrum. The number, positions, and intensities of the dips (also called peaks) provide information about the chemical environment of the absorbing nuclei and can be used to characterize the sample.

A major limitation of Mössbauer spectroscopy is finding a suitable gamma-ray source. Usually, this consists of a radioactive parent that decays to the desired isotope. In this work, the source for ^{57}Fe consists of ^{57}Co, which undergoes beta-decay to an excited state of ^{57}Fe and subsequently decays to the ground state emitting the desired gamma-ray.

AKNOWLEDGEMENTS

L. Di Felice was a member of the European Doctoral College of the University of Strasbourg during the preparation of his PhD, from 2006 to 2009, class name Marco Polo. He has benefited from specific financial supports offered by the College and, along with his mainstream research, has followed a special course on topics of general European interests presented by international experts. This PhD research project has been led with the collaboration of two universities: the University of L'Aquila, Italy, and the University of Strasbourg, France.

The financial support of French-Italian University is also gratefully acknowledged for his *co-tutelle* PhD grant